Sustainable Materials from Textile Waste

Department of Civil Engineering and Architecture
DESIGN FOR HERITAGE: KNOWLEDGE AND LANDSCAPE
Ph.D. Program
SSD: ING-IND/11– Building physics and building energy systems

Final Dissertation

Sustainable Materials from Textile Waste

By
Chiara Rubino

Supervisors:

Prof. Marilés Bonet Aracil

Prof. Francesco Martellotta

Prof. Pietro Stefanizzi

Coordinator of Ph.D. Program:
Prof. Carlo Moccia

Course n°33, 14/02/2018-13/07/2021

Acknowledgements

My first thanks go to Pietro Stefanizzi and Francesco Martellotta for their supervision, guidance and huge support in all moments of the PhD. Thanks for teaching me everything I know. In particular, thanks to Pietro Stefanizzi for his patience and constant support during my academic development. Thanks to Francesco Martellotta for his constant availability and for the opportunity to take part in the first international conference of my academic course.

I would like to immensely thank Marilés Bonet Aracil for inviting and supervising me during my wonderful experience in Alcoy. Huge thanks for her welcoming, making me feel in a big family. Also thanks for her precious help to make a part of my PhD work possible and for her availability now I am in Italy.

I would like also to thank the academic staff of the DITEXPA, in particular Eva Bou-Belda, Jaime Gisbert, Pablo Díaz and Ignacio Montava Seguí for making my time in Alcoy special. Also thanks to Manuel Zamorano Cantò for his support in the laboratory.

Thanks to Stefania Liuzzi for being always present in the best and worst moment of my professional and private life. Thanks for being next to me in this challenging years and for helping me every time I needed.

Thanks to my mum and my aunt Anna who always supported me, pushing me to be and do better. Thanks to my husband and my daughter who are my best fans.

Abstract

This thesis shows an experimental investigation carried out on different innovative materials based on pre-consumer textile waste. The research was developed at Polytechnic University of Bari (Department of Civil Engineering and Architecture) in collaboration with the Universitat Politècnica de València (Departamento de Ingeniería Textil y Papelera) and with the support of the private clothing manufacturing company Gordon Confezioni s.r.l. (Bari, Italy).

Three groups of non-woven materials were prepared in laboratory using three different binders (i.e. bi-component fibers, chitosan and gum Arabic) and following two different manufacturing processes (chemically gluing and thermally bonding techniques). All materials were tested from several perspectives and their hygrothermal, acoustic and fire resistance behaviour was discussed and correlated with the physical parameters and the non-acoustic properties of the tested materials. Furthermore, the statistical inference was used as method of comparison, generalizing the information contained in laboratory samples. The achieved scientific results allow to state that the proposed materials may represent a valid alternative for building applications, opening a new research area.

After choosing the best performing mixture, the internal atrium of the Architecture's Building of the Polytechnic University of Bari was selected as case study in order to simulate the effect of different arrangements of the selected material in form of panels. CATT-Acoustic® software and DesignBuilder® software were used to test respectively the acoustic and thermal behaviour of the interested material. Results showed negligible effects on the thermal comfort, but important improvement of the acoustic comfort of the spaces interested by the treatment. Thus, it could be concluded that the conversion of textile residues into secondary raw materials for building components could represent a strategic solution to actualize important circularity objectives, reducing the environmental impacts of the building industry and developing a sustainable management of the textile wastes.

The thesis also includes a part designated to the industrial upscaling of the proposed materials, made possible thanks to the support of the textile machinery manufacturer Cormatex srl (Prato, Italy).

INDEX

Nomenclature

C	specific heat capacity	J/(kg·K)
C	speed of sound in air	m/s
D	thickness	m
d_m	air collision diameter	m
E	error of the sound absorption coefficients	-
F	frequency	Hz
f_V	volume fraction of solid	-
G	gravitational acceleration	m/s^2
H	entalphy	kJ/kg
h_e	external heat exchange coefficients	$W/(m^2 \cdot K)$
h_i	internal heat exchange coefficients	$W/(m^2 \cdot K)$
K	wavenumber	-
k_e	effective bulk modulus	kg/(m·s)
l_m	mean free path	m
M	sample mass	kg
N	refractive index	-
R	radius of the fibers	m
S	shape factor	-
Ω	angular frequency	1/s
A	surface area	m^2
A	acoustic absorbing	m^2
D	thermal diffusivity	m^2/s
G	mass flow rate	kg/s
JND	Just Noticeable Difference	%
H_0	null hypothesis	-
H_a	alternative hypothesis	-
K	air permeability	m^2
L_c	characteristic length	m
$L_{N,A}$	A-weighted ambient noise level	dB
$L_{S,A,r}$	A-weighted sound pressure level at distance r	dB
L_W	source power level	dB

M	mean value of population	-
P	pressure	Pa
R	pressure reflection coefficient	-
R_0	electrical resistivity of the sample	Ω
R_W	electrical resistivity of the conducting flow	Ω
T	temperature	K
T_{30}	reverberation time	s
V	volume	m^3
W	water vapour permeance	$kg/(m^2 \cdot s \cdot Pa)$
Z	surface impedance	Pa·s/m
Zc	characteristic impedance	Pa·s/m

Greek letters

α	significance level	-
α_n	normal sound absorption coefficient	-
β	volumetric thermal expansion coefficient of air	1/K
δ	water vapour permeability	kg/(m·s·Pa)
ε	porosity	-
η	dynamic viscosity	Pa·s
λ	thermal conductivity	W/(m·K)
μ	water vapour resistance factor	-
μ	dynamic viscosity	Kg/(m·s)
ρ	density value	kg/m^3
ρc	volumetric heat capacity	$J/(m^3 \cdot K)$
ρe	effective bulk density	kg/m^3
σ	air flow resistivity	$kN \cdot s/m^4$
σ_s	air flow resistance	$kN \cdot s/m^3$
τ	tortuosity	-
ΔP	vapour pressure gradient	Pa
Λ	viscous characteristic length	m
Λ'	thermal characteristic length	m
ϕ	fibers diameter	m
φ	heat flux	W/m^2

Parameters

Kn	Knudsen number	-
K_B	Boltzmann's constant	J/K
N	Planck number	-
N_p	Prandtl number	-
Ra^*	modified Rayleigh number	-
σ	Stefan-Boltzmann's constant	$W/(m^2 \cdot K^4)$

Subscripts

Air	air value
Bulk	bulk value
Cond	conduction
Conv	convection
E	external air
Eff	effective value
I	internal air
Pores	pores values
Rad	radiation
Se	external surface
Si	internal surface
Solid	solid phase value
Tot	geometrical value
True	true value
CATT	values obtained using CATT-Acoustic software
D&B	values obtained using the Delany-Bazley method
JCA	values obtained using the Johnson-Champoux-Allard method
Lombard	values obtained using Rindel model for verifying the Lombard's effect

Superscripts

*	values obtained using the inverse method

Introduction

The textile industry is the third most profitable manufacturing sector in Italy, where fashion is considered a benchmark of excellence with remarkable revenues. However, at the same time, the textile system is one of the most environmentally impacting activities at global level, both in relation to the processes that characterize the supply chain and to the produced waste (Tedesco and Montacchini, 2020). The current trend of fast fashion stimulates people to buy more clothes and to dispose them in a shorter timeframe, causing not only a growing demand for new apparel, but also a high-volume of textile waste disposal. (Moazzem et al., 2021).

The wastes related to the textile system can be grouped into two sorts: pre-consumer and post-consumer wastes. Pre-consumer wastes are materials produced during the garment manufacturing process. For the most part they consist in fibers, yarns, scraps, clippings, or merchandise harmed amid creation. Post-consumer wastes are any items discarded by the users because they are considered worn out or not fashionable. This type of waste includes towels, sheets and covers, clean clothes and sewing leftovers, table materials, belts, shoes and socks (Rathinamoorthy, 2018). According to Payne (2015), in the apparel context, the pre-consumer offcuts obtained by cutting and sewing clothes represented approximately 15% of the total fabric required to make each garment. Muthu et al., (2012b) estimated the need to recycle at least 75% of pre-consumer waste to obtain a significant lowering of the carbon footprint of a textile product. Therefore, textile and clothing industry is a high-embodied energy system which causes a significant environmental footprint during all stages of the supply-chain, from the synthesis of the fibers to the disposal of the post-consumer wastes (Echeverria et al., 2018).

For a long time, our economy has been a linear model of “take, make and waste”. This means that virgin raw sources were used to make a product which was used until it was discarded as waste. The increasing attention for recycling and reuse activities, has encouraged the governments to apply circular economy principles based on waste management theory of 4 Rs: Reduce, Reuse, Recycle and Recover. As a first step, it is important to prevent or reduce the wastes generation to the possible extent. On the chance

that wastes are created, they ought to be repeatedly reused. If not or after reuse, the wastes can be recycled. Thus, the physical properties of the discarded materials are changed in order to use them as input to make new goods. Throw the recycling process, the leftovers can be converted into something valuable and often beautiful (i.e. the up-cycling); or into low-value items (i.e. the down-cycling). Furthermore, the recycled leftovers can be used as an input into another similar manufacturing process (i.e. open-loop recycling), or became raw materials for a different production process (i.e. close-loop recycling). Finally, the recovery is the conversion of non-recyclable waste materials into useable energy sources i.e. heat, electricity, or fuel (Kirchherr et al., 2017).

Although the long-term goal for the Europe is to reduce wastes and to use them as new resources (COM 666, 2005), textile wastes have not profitable recycling despite their potential (Danihelovà et al., 2019). In 2018, the European community adopted the "Circular economy package" with the aim to impose the textile waste separation by 2025, but the implementation of circular economy in clothing industries of some EU Member States is still very limited. In fact, a large share of textiles is incinerated or landfilled, provoking air and land pollutions. Thus, an alternative solution to disposal could be the inclusion of waste into a new additional market, i.e. the building materials industry. In this way it could be possible to reduce the environmental effects both associated with the textile and the building sectors.

The building sector is responsible for a significant share of the energy consumptions and carbon emissions in Europe. According to some statistical analysis, 40% of the energy consumptions and 36% of the carbon emissions of the European Union could be attributed to the construction sector (European Commission Directorate General of Energy, 2020). Generally, the best strategy to reduce the energy demand of the buildings is to act on their envelope, designing an effective insulating system. Traditional insulation materials entail a wide range of embodied energy per unit volume, including the energy used for raw resource extraction, component assembly and manufacturing, their maintenance and disposal. The development of wastes-based insulation products reduces the use of new raw materials, limiting the energy for their extraction. Furthermore, if made following a

sustainable manufacturing process, they can led to energy savings during their production and can be easily recyclable.

Governments around the world adopted and enforced a variety of financial regulations and incentives to mitigate the impacts of the building industry (Banihashemi et al., 2020). The European Commission introduced the "Green Public Procurement" (GPP), a strategic tool aimed at reaching a more resource-efficient economy, stimulating Public Authorities (who are the major consumers) to use their purchasing power to choose environmentally friendly goods, services and works (COM 400, 2008). In response to the GPP, Italy makes the application of Minimum Environmental Criteria (MEC) compulsory by law, through the Legislative Decree 50, (2016) subsequently amended by Ministerial Decree 56, (2017). The Decree provides some "environmental suggestions" for tenders selecting and tenders calls drafting, aimed at evaluating the most economically advantageous offer, combining the environmental, economic, and social issues. Important MEC about building materials have been established requiring that at least 50% b.w. of the building components must be recyclable or reusable at the end of their life and the total content of recycled and/or recovered sources must be at least 15% b.w. of the all materials used, with at least 5% of non-structural materials. Therefore, eco-compatibility is becoming a strictly necessary quality of building materials, together with their ability to guarantee thermo-hygrometric and acoustic comfort.

The building sector could represent a key partner in the global effort to achieve the 17 Sustainable Development Goals (SDGs) set by the 2030 Agenda. The transition from linear to circular economy through the reuse of waste is one of the strategic way for reaching sustainable cities and communities aimed of realizing the desired world based on the safeguard of the land and water biodiversity. Furthermore, the construction industry could align business strategies with the SDGs and should collaborate with government agencies, industry peers and policymakers to integrate the SDGs into long-term business strategies, providing employment opportunities to eradicate poverty and improve people's standard of living.

Thesis at a glance: motivations and aims

Given the challenges to develop a sustainable management of wastes and to low the environmental impacts of building industry, this thesis investigates the possibility to recycle pre-consumer textile wastes applying an open-loop up-cycling process. The main goal was to convert textile wastes into secondary raw materials for producing building non-wovens with high hygrothermal and acoustic properties. Three mix design were obtained bonding 100% wool waste fibers with gum Arabic, chitosan and copolyester/polyester bi-component fibers. Several samples with different bulk density values were manufactured and tested in order to use them as thermal insulating and/or sound absorbing materials.

The present research work was carried out with the support of the private clothing manufacturing company Gordon Confezioni s.r.l. (Bari, Italy) and with the contribute of the Departamento de Ingeniería TExtil y PApelera (DITEXPA), Universitat Politècnica de València. Gordon Confezioni s.r.l. is a small/medium enterprise which contributed supplying the wool tailored cuttings used as raw materials. Its challenge was the opportunity of a sustainable management of wastes which account of around 30% of its total production. The support of the Department of Textile and Paper Engineering was essential to analyze the microstructure of the fibers and their interaction with the binders. To this purpose, the morphological analysis of the fibers and of the produced final materials (i.e. the Scanning Electron Microscope (SEM) analysis, the infrared spectroscopy analysis and the tortuosity measurements) were carried out in the DITEXPA laboratories. Six months were spent in the company and in the Spanish University.

Three objectives were defined in order to achieve the main scope of producing the innovative woolen materials:

1. the review of the state of the art on use of textile waste in building industry;
2. the analysis and the comparison of the chemically gluing and the thermally bonding techniques;
3. the validation of the best produced materials through its application to a case study and its industrial upscaling.

Objective 1: review of the state of the art on use of textile waste in building industry

Chapter 1 opens with a snapshot of textiles and clothing consumption in Europe and in Italy, useful to quantify the availability of the raw materials. Furthermore, it provides an overview of the most comprehensive scientific research works on the use of textile waste fibers in building sector. In light of the main used non-wovens bonding methods, the chemical and thermal bonding techniques were selected to produce the materials tested in this research work. Furthermore, three different types of binder, two of natural origin, i.e. chitosan and gum Arabic; and the other of synthetic origin, i.e. the bi-component fiber, were proposed.

Objective 2: analysis and the comparison of the chemically gluing and the thermally bonding techniques

Chapter 2 provides a description of the raw materials (i.e. wool, bi-component fibers, chitosan and gum Arabic), including an extensive characterization of their microstructure and thermal behaviour. It also contains an illustration of the mix design and of the two methodologies chosen for preparing samples (i.e. chemically gluing and thermally bonding techniques). Chapter 3 includes the measurements set-up for testing the hygrothermal, acoustic and fire resistance behaviour of the prepared samples. Furthermore, the processing methods and the theoretical acoustic and thermal models used to analyze laboratory data are explained in Chapter 4. In Chapter 5 and Chapter 6, the experimental results are analyzed and compared in order to highlight how the two chosen manufacturing methods have influenced the microstructure of the materials, affecting their hygrothermal and acoustic performances. The results of the flammability tests are also explained. Being the tested materials lightweight, Chapter 7 investigates an alternative mix design which involves the use of phase change materials (PCMs) to improve the thermal energy storage capacity of the samples.

Objective 3: validation of the best produced materials through its application to a case study and its industrial upscaling

Chapter 8 introduces the case study, showing the effects of the application of the most performing tested materials on the acoustic quality of the internal atrium of the Architecture's Building of the Polytechnic University of Bari. The atrium was modeled with CATT-Acoustic® software, simulating and comparing different arrangements of the absorbent materials. In any case, part of the textile non-wovens covered the string course-frames of the buildings surrounding the atrium, modifying the transmittance value of their external walls. Therefore, energy simulations were also carried out using DesignBuilder® software in order to analyze the effects of adding the woolen-based materials on the thermal comfort and on the energy behaviour of the corresponding rooms with atrium view. Some renderings are included in order to represent how the application of the non-woven panels changes the visual perception of the space under study.

Eventually, Chapter 9 discusses some aspects about the environmental sustainability values of the tested materials, summarizes the main findings of this thesis and includes recommendations for future research. In fact, the industrial upscaling of the most performing materials was carried out with the aim of comparing them with laboratory scale samples.

References

Banihashemi, S.A., Khalilzadeh, M., Shahraki, A, Rostami Malkhalifeh, M., Ahmadizadeh, S.S.R., 2021. Optimization of environmental impacts of construction projects: a time–cost–quality trade-off approach. Int. J. Environ. Sci. Te. 18, 631-646. https://doi.org/10.1007/s13762-020-02838-2.

Circular economy package, July 2018. Four legislative proposals on waste. Briefing EU Legislation in Progress, Available at: https://www.europarl.europa.eu/RegData/etudes/BRIE/2018/625108/EPRS_BRI(2018)625108_EN.pdf. (Accessed April 2020).

COM 400, 2008. Communication from the Commission to the Council, the European Parliament, the European Economic and Social Committee and The Committee of the Regions - Public procurement for a better environment. https://eur-lex.europa.eu/legal-content/EN/TXT/?uri=CELEX:52008DC0400. (Accessed April 2021).

COM 666, 2015. Communication from the Commission to the Council, the European Parliament, the European Economic and Social Committee and The Committee of the Regions - Taking sustainable use of resources forward: A Thematic Strategy on the prevention end recycling of waste. http://eur-lex.europa.eu/legal-content/EN/TXT/?uri=CELEX:52005DC0666. (Accessed April 2021).

Danihelová, A., Nemec, M., Gergel', T., Gejdoš, M., Gordanová J., Sˇcensný, P., 2019. Usage of recycled technical textiles as thermal insulation and an acoustic absorber. Sustainability 11(10), 2968. https://doi.org/10.3390/su11102968.

Echeverria, C.A., Handoko, W., Pahlevani, F., Sahajwalla, V., 2019. Cascading use of textile waste for the advancement of fibre reinforced composites for building applications. J. Clean. Prod. 208, 1524-1536. https://doi.org/10.1016/j.jclepro.2018.10.227.

European Commission, 2019. Product Environmental Footprint Category Rules (PEFCRs) for Thermal Insulation. https://ec.europa.eu/environment/eussd/smgp/pdf/Thermal Insulation final-Oct2019.pdf. (Accessed May 2021).

Kirchherr, J., Reike, D., Hekkert, M., 2017. Conceptualizing the circular economy: An analysis of 114 definitions. Resour. Conserv. Recy. 127, 221-232. http://dx.doi.org/10.1016/j.resconrec.2017.09.005.

Legislative Decree, 18 April 2016. Attuazione delle direttive 2014/23/UE, 2014/24/UE e 2014/25/UE sull'aggiudicazione dei contratti di concessione, sugli appalti pubblici e sulle procedure d'appalto degli enti erogatori nei settori dell'acqua, dell'energia, dei trasporti e dei servizi postali, nonché per il riordino della disciplina vigente in materia di contratti pubblici relativi a lavori, servizi e forniture. (GU Serie Generale n.91 del 19-04-2016).

Ministerial Decree, 11 October 2017. Criteri ambientali minimi per l'affidamento di servizi di progettazione e lavori per la nuova costruzione, ristrutturazione e manutenzione di edifici pubblici. (GU Serie Generale n.259 del 06-11-2017).

Moazzem, S., Wang, L., Daver, F., Crossin, E., 2021. Environmental impact of discarded apparel landfilling and recycling. Resour. Conserv. Recy. 166, 105338. https://doi.org/10.1016/j.resconrec.2020.105338.

Muthu, S.S., Li, Y., Hu, J.Y., Ze, L., 2012b. Carbon footprint reduction in the textile process chain: recycling of textile materials. Fiber. Polym. 13(8), 1065-1070. https://doi.org/10.1007/s12221-012-1065-0.

Payne, A., 2015. Open- and closed-loop recycling of textile and apparel products, in:

Muthu, S. (Ed.), Handbook of Life Cycle Assessment (LCA) of textiles and clothing. Woodhead Publishing, Cambridge, United Kingdom, pp. 103-123.

Rathinamoorthy, R., 2018. Sustainable Apparel Production from Recycled Fabric Waste. In: Muthu, S.S. (Ed.), Sustainable Innovations in Recycled Textiles. Springer, Hong Kong, pp. 19-52.

Tedesco, S. and Montacchini, E., 2020. From textile waste to resource: a methodological approach of research and experimentation. Sustainability 12, 10667. https://doi.org/10.3390/su122410667.

Chapter 1

State of the art on textile waste in building industry

This chapter partially reports material from:

- Rubino, C., Liuzzi, S., Martellotta, F., Stefanizzi, P., 2018. *Textile wastes in building sector: A review*. M.M.C._B 87(3), 172-179. https://doi.org/10.18280/mmc_b.870309.
- Rubino, C., Bonet Aracil, M., Liuzzi, S., Martellotta, F., Stefanizzi, P. 2019. *Thermal characterization of innovative sustainable building materials from wool textile fibers waste*. IJES 63 (2-4), 277-283. https://doi.org/10.18280/ti-ijes.632-423.

In textile and clothing sector, the fashion cycle makes the style obsolete before the real end of life of textile products, generating wastes and over consumerist practices which have a serious impact on the environment. In fact, most of these wastes is incinerated or landfills disposed. The inclusion of the textile residues in a new manufacturing process could be a strategy to achieve a sustainable management of wastes, maximizing the added value of new products. The textile leftovers offer many attractive opportunities in different sector, i.e. the automotive industries, the construction industries or the energy sector. The purpose of this Chapter is to provide a snapshot of the textile consumptions and textile wastes management in Europe and in Italy. Furthermore, an overview of the state of the art on the use of recycled fibers in construction materials was carried out.

1.1 Textile consumption in Europe and in Italy

The textile and clothing (T&C) sector is an important branch of the European manufacturing industry, playing a crucial role in the economy and social well-being in many regions of Europe. The sector includes ca. 160,000 companies, employing 1.5 million people and generating a turnover of €162 billion (EURATEX, 2020). The T&C industry accounts for some 5% of employment and 9% of companies in the total EU manufacturing sector, as well as over 4% of total merchandises' exports. As shown in Figure 1.1, a large number of companies are established in Italy and more than half of the EU employment is concentrated in four countries, besides Italy, Romania, Poland and Portugal (EURATEX, 2018).

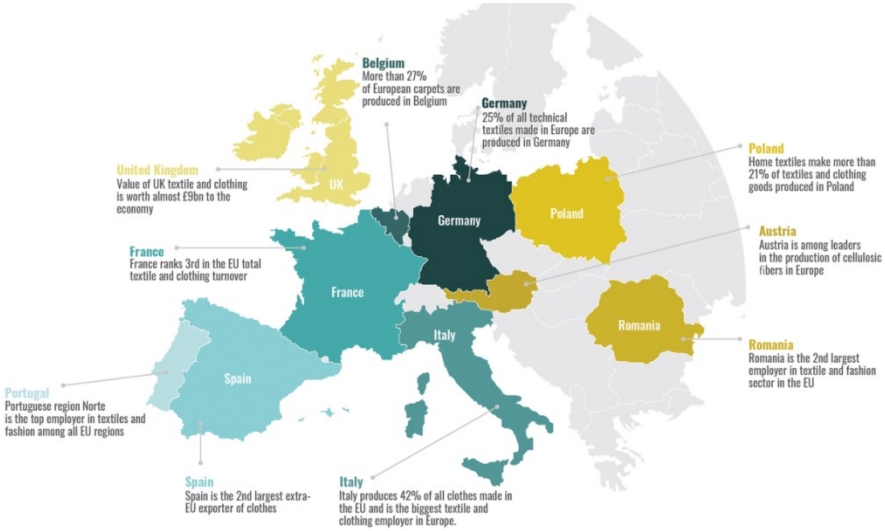

Figure 1.1. Top ten EU textile and clothig producers (Source: https://euratex.eu/infographics/).

Europeans use nearly 26 kilos of textiles and discard about 11 kilos of them every year. Used clothes can be exported outside the EU, but are mostly (87%) incinerated or landfilled and a very low percentage is recycled. Figure 1.2 analyzes the 15 European nations that in 2016 produced the largest amounts of textile wastes, showing that only about 20% of them was used to manufacture new products or new textile items. As it can be seen, although Italy ranked among the leading five textile polluters in the EU, recycled less than one kilogram of textile waste per person.

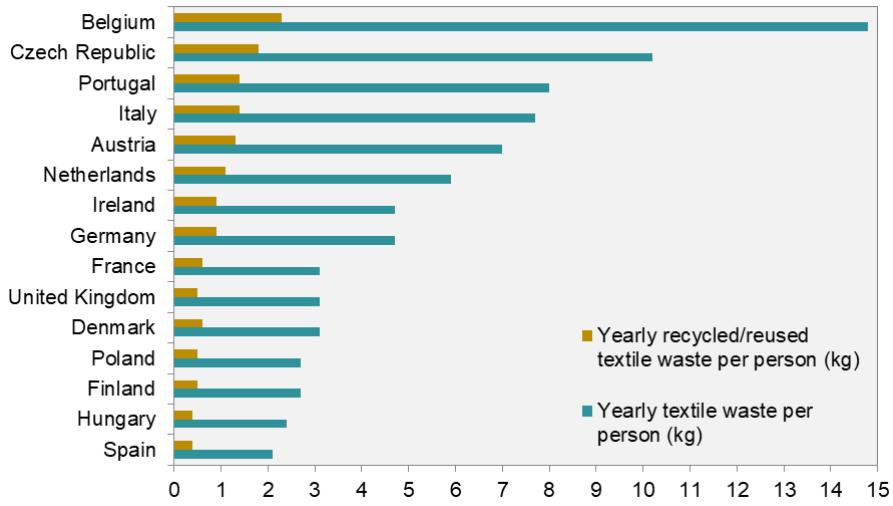

Figure 1.2. Summary of recent trends in textile waste production and recycling in 15 European nations that produce the largest amounts of textile waste each year.

(Source: elaboration of Eurostat data https://appsso.eurostat.ec.europa.eu/nui/submitViewTableAction.do#).

In Italy, post-consumer textiles together with the wood, cellulosic and organic fraction, constitute biodegradable urban wastes (Legislative Decree 152, 2006). As shown in Figure 1.3, in 2018 textiles have covered only 0.8% of separate waste collection, while the cellulosic and organic fraction represented about 60% (Rapporto rifiuti urbani, 2019).

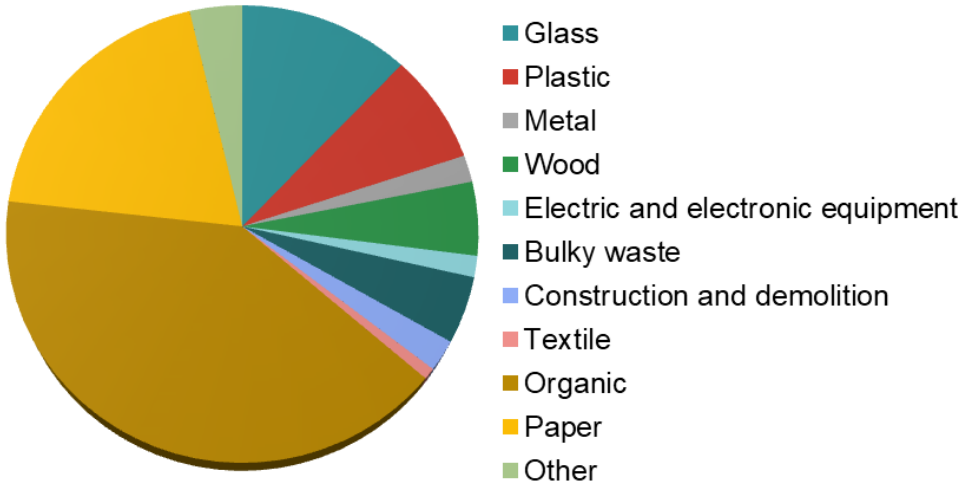

Figure 1.3. Percentage breakdown of separate waste collection.

(Source: elaboration of Rapporto rifiuti urbani (2019) data).

Although the separate textile waste is growing over the years, collection of post-consumer textiles, which is dominated by charities and voluntary take-back campaigns, is still little practiced. Figure 1.4 plots that the separate collection of the post-consumer textile wastes in Italy has grown over the years despite a constant trend during 2016 and 2017. This trend demonstrates an increasingly widespread awareness of the need of wastes recovery in order to limit their negative effects on the environment and on human health.

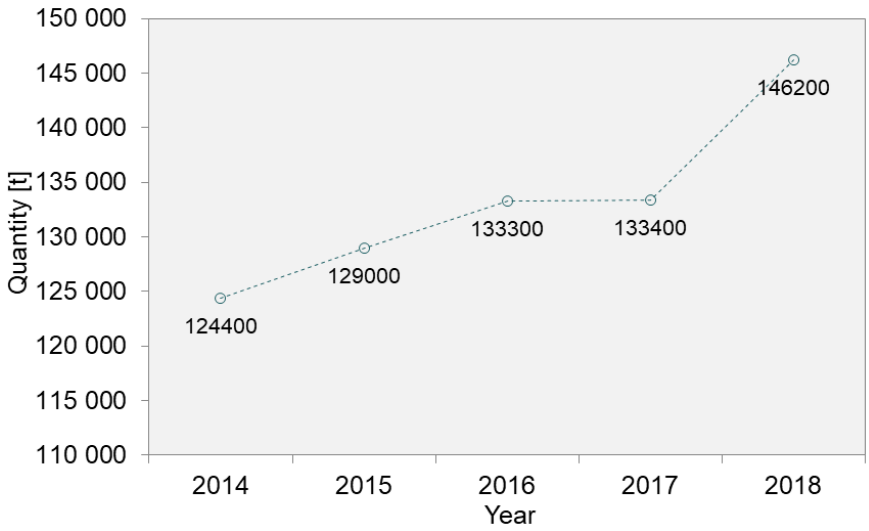

Figure 1.4. Trend of separate collection of the post-consumer textile waste in Italy from 2014 to 2018 (Source: elabooration of ISPRA data https://www.catasto-rifiuti.isprambiente.it/index.php?pg=rs).

According to article 184, sub 3 of the Legislative Decree 152, (2006), the pre-consumer textile wastes are classified as special waste and are reviewed under a special waste management program. Considering their riskiness, they are distinguished in hazardous or non-hazardous waste. Textiles dyes effluents are an example of pre-consumer hazardous waste which are a serious perilous for global environment due to the use of synthetic dyes. Their toxic and non-biodegradable nature pose serious threats to soil fertility, crop production, and human health. For this reason, the attentions have been diverted to bio-dyes or natural dyes (Gulzar et al., 2019).

Cutting fabrics are the most consistent non-hazardous wastes of a textile industry. In 2018 and 2019 about 700,000 ton of dangerous and non-dangerous wastes derived from lather and textile industries and more than 1,500 ton were incinerated (Rapporto rifiuti speciali, 2021). Figure 1.5 shows the incidence percentage of the regional production of the

hazardous and non-hazardous wastes in Italy in 2019. As it can be observed, the Apulia region (the region to which the partners company of this research project belongs) contributes 13% to the production of special hazardous and non-hazardous textile waste in southern Italy.

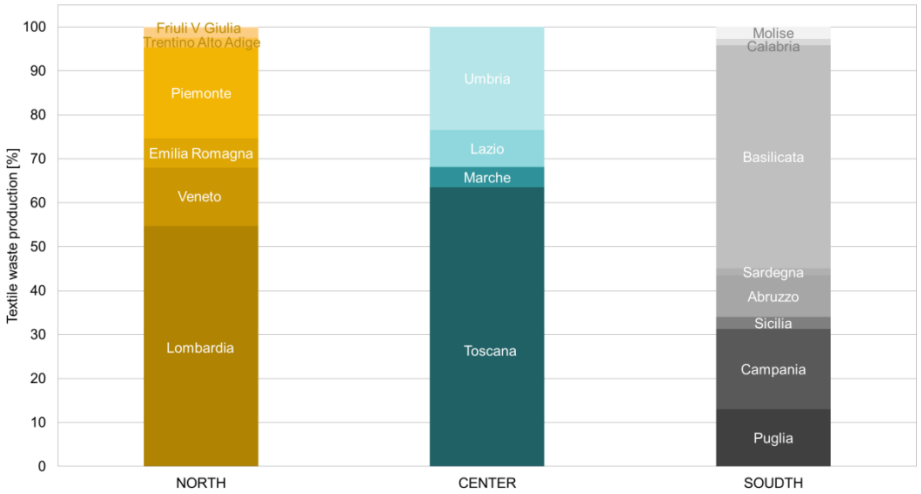

Figure 1.5. Regional production of the hazardous and non-hazardous wastes in Italy in 2019. (Source: Source: elabooration of ISPRA data https://www.catasto-rifiuti.isprambiente.it/index.php?pg=rs).

However, the trend of the hazardous and non-hazardous special textile waste in Apulia region is decreasing, after a peak value recorded in 2017 (Figure 1.6).

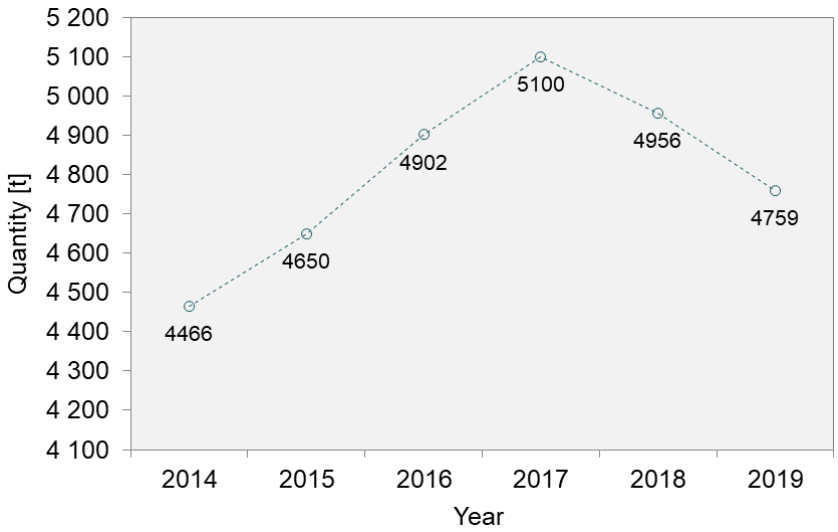

Figure 1.6. Trend of special hazardous and non-hazardous textile wastes in Apulia from 2014 to 2019 (Source: elabooration of ISPRA data https://www.catasto-rifiuti.isprambiente.it/index.php?pg=rs).

1.2 Textile waste as new resource for building materials

In recent years, there have been more and more research studies aimed to use textile wastes as new raw sources in construction sector. The earliest research approaching to the use of textile leftovers for building materials was published in 2003 (Lee and Joo, 2003), meaning that the investigation of this topic is a fairly new activity. A depth analysis of the state of the art was carried out, highlighting the promising use of textile fibers mainly as matrix of panels with good hygrothermal and acoustic performances. However, textile fabrics and threads could be also act as reinforcement for lightweight bricks, or for cement based renders.

1.2.1 Composites, mats and panels

Textile wastes are mostly used to produce innovative heat insulating (Hadded et al., 2015; Gounni et al., 2018) or sound absorbing panels (Segura-Alcaraz et al., 2017); but also to improve the thermal or acoustic performances of conventional materials. Umar et al. 2017 replaced glass fibers with textile waste yarns in door or partitioning panels. Tiuc et al. (2016) investigated the improvement of the Noise Reduction Coefficient (NRC) of rigid polyurethane foam (RPF) by incorporating textile waste (TW). Aghaee et al. (2012, 2013) analyzed the effects of adding a core of textile waste fibers in perlite lightweight concrete panels. The fibers porosity allowed to obtain a thermal conductivity lower than 0.3 W/(m·K). Furthermore, the use of fibers core led to a reduction in the specific weight of the internal partitions by about 20%, reducing the damages and the possibility of collapse of the panels in case of an earthquake.

The production of innovative textile building non-woven mats and panels can be achieved using the fabrics directly, without converting them into fibers (i.e. direct methods); or converting the fabrics into fibers to form batting webs which are tied together by chemically gluing, mechanically entangling, or thermally bonding techniques (i.e. non-wovens).

Several researchers (Jordeva et al., 2014; Trajković et al., 2016) investigated the use of waste fabrics directly for building applications. Jordeva et al. (2014) developed thermal insulation materials by cutting textile wastes and then stabilizing the wastes by stitching.

Trajković et al. (2016) produced a thermal insulating material encasing different fabric mixtures in 100% polypropylene non-woven structure. The mix used were 100% polyester

(blends A and C differing in the size of the waste), polyester/cotton/lycra (blend B: 70/25/5) and polyester/lycra (blend D: 95/5). All tested samples exhibited a thermal conductivity values similar to standard insulation materials, varying between 0.052 and 0.060 W/(m·K). Tests result also showed that the polypropylene structure containing smaller pieces of cutting fabrics exhibited the highest thermal insulation. In addition, the presence of lycra decreased the thermal insulation of the structure. All tested materials exhibited a sound absorption coefficient maximum in the range of 1000-2000 Hz and a Noise Reduction Coefficient value similar to that of other commercial building insulators (NRC was in the range from 0.55 to 0.75).

Briga-Sà et al. (2013) carried out an experimental work to determine the thermal behavior of an external double wall with the air cavity filled with woven fabric wastes (WFW) and wastes of this residue, named woven fabric sub-waste (WFS). The results indicated that the double wall with the air cavity filled with WFW and WFS exhibited a thermal resistance 56% and 30% respectively higher than the double wall with the empty air cavity. The thermal conductivity value of the WFW was similar to the EPS, XPS and mineral wool. WFS showed a thermal conductivity value very close to the granules of clay, vermiculite or expanded perlite.

Concerning the non-wovens method, when dealing with the chemical binding technique, several studies can be found in consequence of the fact that it is the easiest process as it only involves the application of binder dispersions followed by the curing and drying of the impregnated fibers (Wilson, 2006). Different types of agents, mostly epoxy resins (Temmink et al., 2018; Baccouch et al., 2020), have been explored in literature to bind the textile fibers, providing them the structure needed to develop fibrous materials with good thermal, acoustic and mechanical performances. Binici et al. (2014) examined the acoustic performance of new insulation materials produced by grinding and mixing agricultural residues (i.e. sunflower stalks and stubble fibers) and textile waste (i.e. cotton). Two approaches were used: one was by using plaster and another by using epoxy as a binder. The obtained boards were applied on the wall (mud bricks, concrete bricks, and red bricks) of a test room and an improvement of the thermal and sound insulation performances was proved.

A common issue with chemically bonded materials is represented by nature and amount

of the binder which can clearly influence the porosity of the samples (and hence the properties depending on it). It is also important to consider the environmental impact of the binders, which is not always negligible. From this point of view, there is a limited number of scientific studies on the use of natural or biodegradable binding solutions.

Del Mar Barbero-Barrera et al. (2016) tested the use of lime paste as binder to develop building boards made from textile wastes and studied the effects of three different lime-water ratios on the thermal, acoustic and mechanical properties. The results proved that the sound absorption coefficients increased with a higher water to lime ratio, due to the increase in the amount of pores in which sound waves could easily penetrate. A high porosity also meant low hardness and low flexural strengths. Furthermore, the heat insulating performance of the tested boards increased by decreasing the lime past content: the best thermal conductivity of 0.14 W/(m·K) was observed for samples with a density of 716 kg/m^3. These results were comparable with that obtained by Muthuraj et al. (2019) who used the biodegradable poly(butylene adipate-co-terephthalate)/poly(lactic acid) blend binder to develop building panels with a density of 488 kg/m^3 and a thermal conductivity of 0.14 W/(m·K). All the biocomposites showed semi-rigid behaviour with sufficient flexural (0.80-2.25 MPa) and compressive (10-40 MPa) properties.

Lacoste et al. (2017) investigated the adhesive properties of the sodium alginate, a natural polysaccharide derived from seaweed. Wood fibers (W) and recycled cotton fibers (T) were mixed in various proportion to manufacture composites with different softness. The tested wood/textile waste ratios were100/0, 50/50, 60/40, 70/30 and 0/100 in weight. Innovative biocomposites with a thermal conductivity in the range 0.078-0.089 W/m/K for an average density in the range 308-333 kg/m^3 were obtained. The innovative panels were semi-rigid composites, showing a compression strength between 0.40-1.41 MPa and a bending strength between 0.20-0.54 MPa.

Curtu et al. (2012) and Del Rey et al. (2015) focused on the acoustic characterization of innovative textile panels. Curtu et al. (2012) analyzed the effects of different types of binder (acrylic copolymer, clay solved, gypsum solved and formaldehyde) on the acoustic properties of composites produced mixing wood and wool waste. The experimental results pointed out that samples manufactured with acrylic copolymer and gypsum exhibited great sound absorption values at high frequencies; unlike samples produced with formaldehyde performed a not classifiable acoustic behavior, being more reflective due to the flat and

smooth surfaces. Furthermore, samples blended with clay solved in water exhibited a constant sound absorption coefficient in the frequencies range 800-3200 Hz. However, the increase in the density value of the materials produced a decrease in the sound absorption performance.

Del Rey et al. (2015) focused on the characterization of innovative acoustic insulation materials developed from several combination of cotton fibers, polyester fibers and bico PET fibers mixed with phenolic resins or recycled PET fibers. A prototype of a noise absorptive barrier was designed using the new insulation materials as a core of a metal structure with a drilled plate at the side exposed to the noise source. The new fibrous materials barriers exhibited sound absorption coefficients and airflow resistivity values similar to other commercially available absorptive noise barriers.

In order to avoid the environmental impact of the binders, a better alternative might be the mechanical entanglement as the needle punching technique. It consists in a repeated penetration of barbed needles through a preformed dry fibrous carded web (Anand et al., 2006). Materials with different density values could be produced, controlling the density of the final products by varying some needle parameters. Thus, panels with higher density showed better load-bearing properties; whereas materials with less density values favored acoustic absorption and thermal insulation.

El Wazna et al. (2016, 2018) controlled the speed and the thickness of needle, the needle punch depth, the number of barbs and the stitch angle to improve the tortuosity and the porosity of mats made from 100% wool (W) and 100% acrylic (A) fibers. Samples with thermal insulation properties, better than other conventional insulation materials (i.e. glass wool, mineral wool and extruded expanded polystyrene), were developed. The thermal performance of the produced materials was investigated using a numerical model that simulated an external wall exposed to the real climatic conditions. The innovative solution was competitive in terms of annual heating and cooling loads compared to a classic insulation solution (i.e. rock wool and expanded polystyrene).

Patnaik et al. (2015) carried out a research about different type of innovative needle-punched mats suitable for roof ceiling insulation. Two mats were obtained from two type of 100% waste wool fibers (CW and DW), two others mats from the combination of the two type of wool waste and recycled polyester (CWP and DWP), the last one was

manufactured from 100% recycled polyester (RPET). A protective barrier on the wool fibers was created by spraying silicon in order to avoid that an excessive absorption of moisture affected the thermal performances of the samples. Test results showed that all panels exhibited good insulating properties and sound absorption coefficients in the overall frequency range (50–5700 Hz). However, the DWP sample showed a higher sound absorption value due to the rough surface of the wool fibers which improved the friction phenomena by increasing energy losses; and due to the long length of the included fiber which encouraged the sound wave interaction creating a very uniform pore structure.

Seddeq et al. (2012) investigated different non-woven materials containing natural textile fibers (jute, cotton and wool), mechanically connected with synthetic textile fibers (polyester and polypropylene). All tested samples showed higher sound absorption coefficients at mid and high frequencies than at low ones.

Zach et al. (2016) produced thermal and acoustic nonwoven materials from recycled cotton, polyester and flax fibers using the airlay method for web formation. In airlay method, fibers can be separated by suspending them in an air stream, and then blowing the fibers onto a moving belt to form a uniform layer of fiber web. After forming layers of fibers as webs, bonding was done by thermal or mechanical process. Five different mixtures of polyester, flax, cotton, and bi-component fibers were tested. The average thermal conductivity and absorption coefficients values of the produced materials were 0.037–0.049 W/(m·K) and 0.7 to 0.9 (at around 1000 Hz), respectively.

The thermal bonding method involves the use of “base” fibers included in a polymer matrix working as “binder”. A carefully chosen mix of base and binder fibers is heated to melt the thermoplastic polymer and, then is cooled to solidify the bonding area. According to Pourmohammadi (2006), the thermal bonding technique could be considered more economically attractive than chemical one because involved more energy savings as a consequence of less water evaporation during bonding.

Hassanin et al. (2018) used the low-density polyethylene contained in Tetra Pak® waste to develop insulating panels made from wool yarn waste.

Echeverria et al. (2019) proposed fibrillated polypropylene textile waste as thermoplastic matrix to develop load-bearing panel with mechanical strength and moisture absorption performance highest than standard wood-based particleboards.

Several authors (Lin et al., 2016; Zou et al., 2011) proposed the use of polyester (PET) as binder polymer. Nowadays, there is a great recycling of PET from bottles, but recycling of PET from fabrics is still a big challenge. Different methods have been studied to dispose PET fabrics (i.e. PET extraction, or cellulose extraction from cotton/PET blend fabrics, or PET dissolution), but they are unfeasible because of their high cost. Therefore, the use of polyester textile fibers in construction materials could be a sustainable alternative of recycling non-renewable resources, creating a new low cost raw materials.

Palakurthi (2016) developed a composite material from recycled PET and cotton. As the melting temperature of PET (260 °C) is higher than the degradation temperature of cotton (146 °C), she treated PET with plasticizers and alkali to reduce the melting temperature of PET.

Ramamoorthy et al. (2014) also investigated reusing of discarded cotton/PET blend fabrics as reinforcement in building composites. Three compression-molding concepts were discussed and evaluated. In the first method, the melting temperature used was higher than that of polyester fabric with or without using a plasticizer. The result of this method was that cotton fiber degraded due to high temperature. In the second method, a bio-based resin from soybean oil was used as a matrix. Finally, in the third method, a thermoplastic core-sheath bi-component fiber was carded and needle punched to form a nonwoven fabric. The obtained nonwoven was placed between layers of recycled cotton/PET fabrics and subjected to compression molding to form composites. The sheath of the bi-component fiber melts with a temperature lower than that of cotton degradation and acts as a matrix. The using of method two and three allowed to produce a composite successfully, without degrading the cotton fibers. Furthermore, it was observed that the materials produced by the third method showed mechanical properties and tensile strength respectively 4 times and 2.2 times greater than materials obtained from method one and two.

Drochytka et al. (2017) used bi-component fibers to bind polyester waste fibers producing building non-wovens with thermal and acoustic performances comparable to mineral rock wool panels. Samples with three different density values (65, 80, 95 kg/m^3) were produced and a thermal conductivity less than 0.06 W/(m·K) was measured. A sound absorption depending on bulk density was observed in higher frequency range between 1000 and 1600 Hz.

Sedlmajer et al. (2015) used bi-component PES fibers for preparing different insulating

mats. The tested textile waste combinations were cotton pure/recycled PES/bico fibers (40/40/20), recycled PES/bico fibers (80/20), cotton raw/recycled PES/bico fibers (40/45/15 or 45/40/15). Although all materials exhibited good thermal properties, the samples with higher cotton content showed, at the same volume weight, greater performances than the materials with higher proportion of PES fibers.

Several authors used textile wastes to produce innovative sandwich-shaped composites. Ricciardi et al. (2014) evaluated the thermal performances of two types of panels differing in central layer thickness. A core of waste paper was glued and pressed between two layers of polyethylene fibers to reach thicknesses of 7 mm and 15 mm. The mean value of thermal conductivity was varying in 0.034-0.039 W/(m·K) range, with higher performance respect to traditional insulating materials. The NRC of the tested samples varied from 0.25 to 0.40 based on the thickness of the layers.

Binici et al. (2012) investigated new lightweight materials in which a mixture of fly ash, cotton waste and barite was applied between two chipboards. When the content of cotton fibers increased, the thermal and sound insulation performances of the chipboards improved. Furthermore, the use of barite allowed a radioactivity permeability control.

Cosereanu et al. (2012) simulated the thermal behavior of a sandwich wooden wall with a core filled with different textile waste composite materials. By comparing the innovative wall with the brick wall, was concluded that the wooden structure showed a higher thermal resistance than the brick one, at the same thickness.

Figure 1.7 compares the thermal insulation performance of materials previously analyzed. Particularly thermal conductivity was chosen as term of comparison. Not all materials were compared because for some of them density values were not found in the literature. However, thermal insulation properties of the most recycled textile materials resulted comparable with that of commercially available insulation materials, i.e. glass wool, stone wool, expanded polystyrene or extruded polystyrene. Only Del Mar Barbero-Barrera et al. (2016) and Muthuraj et al. (2019) proposed panels with a thermal conductivity above 0.1 W/(m·K) with a density ranged from 500 to 700 kg/m^3. This was maybe due to the used binders, i.e. lime and poly(butylene adipate-co-terephthalate)/poly(lactic acid) blend, which affected the porosity of the materials increasing their thermal conductivity.

As it can be observed in Figure 1.7, Ricciardi et al. (2014) produced panels with promising thermal conductivity values less than 0.04 W/(m·K), despite their density was higher than that of the other materials with similar thermal behaviour. This could be due to the sandwich-shape of the panels which could cause the presence of air between the different layers, allowing to reduce the value of the thermal conductivity.

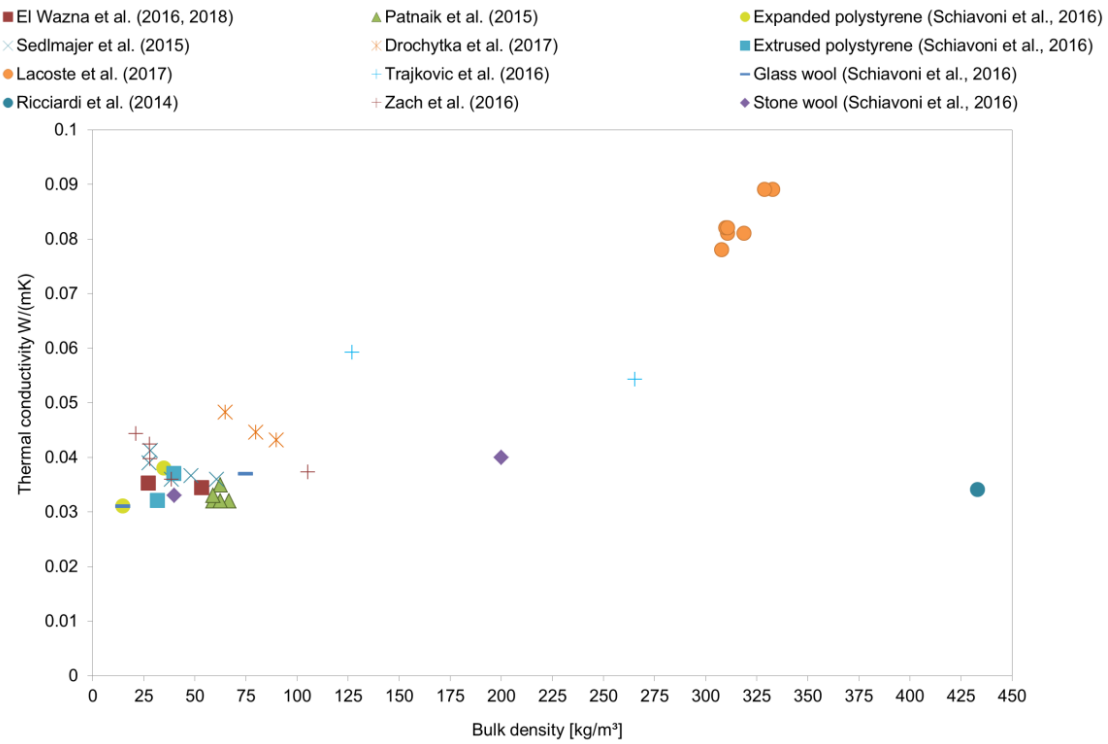

Figure 1.7. Thermal conductivity versus bulk density for insulating materials.

Similar to thermal conductivity, comparison of sound absorption coefficients of different materials are shown in Figure 1.8.

The comparison of acoustic properties is not straightforward like thermal properties, since acoustic properties depend a lot on frequency and on thickness of the samples. Furthermore, not all researchers reported the sound absorption coefficients for each frequency, but an average value for low, medium and high frequency was found (i.e. Patnaik et al., 2015 and Seddeq et al., 2012). However, Figure 1.8 plots the noise reduction coefficient (NRC) for some of materials above analyzed.

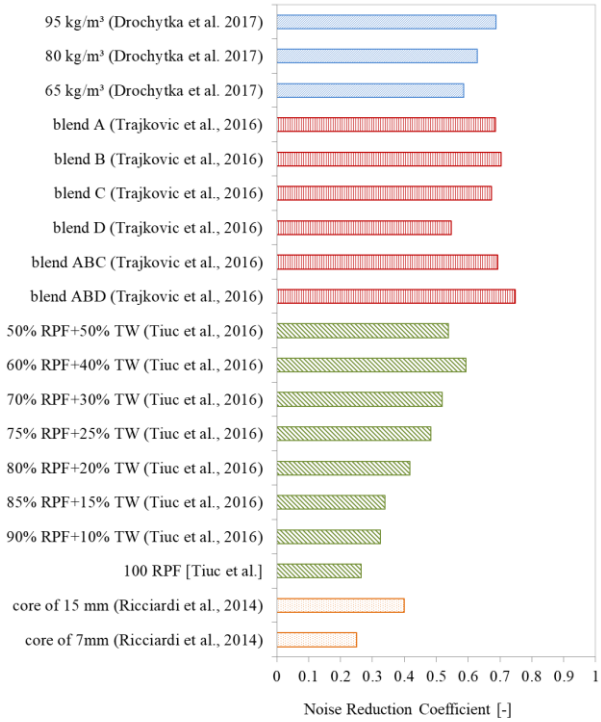

Figure 1.8. Noise reduction coefficient for sound absorbing materials.

1.2.2 Lightweight bricks

Several researches investigated the use of textile fibers to produce lightweight bricks. Rajput et al. (2012) investigated the hygrothermal effects of the addition of different percentages of recycled paper mills waste (PW) and cotton waste (CW) to cement bricks. Results indicated that with the increase of the cotton fibers waste, the porosity increased from 0.18 to 0.29. A more porous structure allowed an improvement of the thermal performance (the thermal conductivity decreased from 0.32 to 0.25 W/(m·K)) and an increase of the water absorption. The amount of fibers also influenced the mechanical properties of the materials due to their nature to be water-absorbent. However, bricks showed good compressive strength (21±1 MPa) to be proposed as not-load bearing partition walls.

Binici et al. (2010) and Binici, and Aksogan, (2015) examined the thermal properties of cement bricks lightened with a combination of cotton waste (CW) and textile fly ash (TW). Two models house were built and monitored in order to compare the thermal insulation properties of the innovative materials with those of control bricks (CB) made without using textile lightening. Being the innovative bricks more lightweight than the control ones, their

thermal conductivity coefficient was 29.3% lower. This reduction explained the rapid increase of the heating temperature of the model house constructed with CW and TW bricks. The water absorption of the tested materials decreased with the increase of the content of cotton fibers. The compressive and flexural strength values also fulfilled the required standards, allowing to use the tested materials for load-bearing walls, reducing their thickness.

Algin et al. (2008) tested lightweight composite materials developed by mixing the cement with different combinations of cotton waste (CW) and limestone powder waste (LPW). The water absorption and the CW percentage content were directly proportional. Substituting of 40% LPW volume with CW, was achieved 27.2% of water absorption b.m. which is a satisfactory value compared to other lightweight building materials. Results proved that with the increase in the CW replacement, the mechanical performances of the analyzed samples decreased. Thus, the bricks with high CW percentages could be used preferably for non-structural applications.

Liu et al. (2017) prepared foamed gypsum blocks from flue gas desulfurization gypsum and textile fiber waste. Results indicated that at 3% of the textile fibers content the samples showed the maximum compressive strength of 1.6 MPa.

Figure 1.9 compares the water absorption values of the bricks produced and tested by Binici et al. (2010) and Algin et al. (2008). As it can be observed, the water absorption decreased with the increase of the content of cotton fibers.

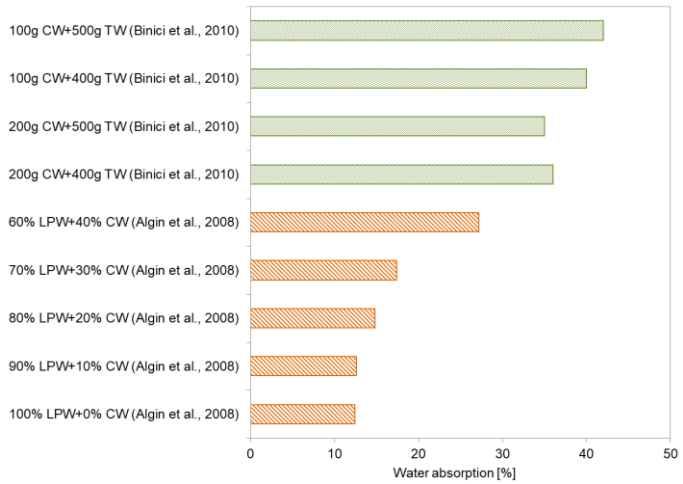

Figure 1.9. Water absorption values for bricks.

1.2.3 Mortar reinforcements

The incorporation of certain types of fibers into the cement matrices improves several characteristics as toughness, energy absorption capacity or post-cracking residual strength. Steel, glass or polymeric fibers have been tested as reinforcement of cement-based matrices. Recently, textile waste fibers have emerged as reinforcement materials able to enhance ductility and cracking control of the cement-based matrices (Sadrolodabaee et al., 2021). Pinto et al. (2013) and Dos Reis et al. (2009) also showed improvement of mechanical properties increasing the fiber content of cement-based renders and polymeric concrete. Kalkan and Gündüz (2016) investigated the hygrothermal benefits of addition of denim powder fibers (DPF) as a new type of reinforcement for perlite and pumice mixtures. They showed that DPF content up to 1.25% allowed to guarantee good hygrothermal properties as well as to improve mechanical performance.

References

Aghaee, K. and Foroughi, M., 2012. Construction of light weight concrete partition using textile waste. International Conference on Sustainable Design, Engineering and Construction, Texas: 793-800.

Aghaee, K. and Foroughi, M., 2013. Mechanical properties of light weight concrete partition with a core of textile waste. Adv. Civ. Eng.: 1-7. https//dx.doi.org/10.1155/2013/482310.

Algin, H.M. and Turgut, P., 2008. Cotton and limestone powder wastes as brick material. Constr. Build. Mater. 22(6): 1074-1080. https//doi.org/10.1016/j.conbuildmat.2007.03.006.

Anand, S.C., Swarbrick, G., Russell, S.J., 2006. Mechanical bonding. In: Russell, S.J. (Ed.), Handbook of Nonwovens. Woodhead Publishing, England, pp. 201e297.

Avcioglu Kalebek, N., Babaarslan, O., 2016. Fiber selection for the production of nonwovens. In: Jeon, H.-Y. (Ed.), Non-woven Fabrics. Intech Open, pp. 1-32.

Baccouch, W., Ghith, A.,Yalcin-Enis, I., Sezgin, H., Miled, W., Legrand, X., Faten, F., 2020. Investigation of the mechanical, thermal, and acoustical behaviors of cotton, polyester, and cotton/polyester nonwoven wastes reinforced epoxy composites. J. Ind. Text. 23: 1-24. https://doi.org/10.1177/1528083720901864.

Binici, H., Gemci, R., Aksogan, O., Kaplan, H., 2010. Insulation properties of bricks made with cotton and textile ash wastes. Int. J. Mater. Res. 101(7): 894-899. https//doi.org/10.3139/146.110348.

Binici, H., Gemci, R., Kucukonder, A., Solak, H.H., 2012. Investigating sound insulation, thermal conductivity and radioactivity of chipboards produced with cotton waste, fly ash and barite. Constr. Build. Mater. 30: 826-832.https://doi.org/10.1016/j.conbuildmat.2011.12.064.

Binici, H., Eken, M., Dolaz, M., Aksogan, O., Kara, M., 2014. An environmentally friendly thermal insulation material from sunflower. Constr. .Build. Mater. 51:24-33. https://doi.org/10.1016/j.conbuildmat.2013.10.038.

Binici, H. and Aksogan, O., 2015. Engineering properties of insulation material made with cotton waste and fly ash. J. Mater. Cycles Waste Manag. 17(1):157-162. https//doi.org/10.1007/s10163-013-0218-6.

Briga-Sá, A., Nascimento, D., Teixeira, N., Pinto, J., Caldeira, F., Varum, H., Paiva, A., 2013. Textile waste as an alternative thermal insulation building material solution. Constr. Build. Mater. 38: 155-160. https//doi.org/10.1016/j.conbuildmat.2012.08.037.

Cosereanu, C., Lăzărescu, C., Olărescu, C., Laurenzi, W., 2012. Ecological solutions for low energy building walls. Pro Ligno 8(1): 28-34. http://www.proligno.ro/ro/articles/2012/1/cosereanu_full.pdf.

Curtu, I, Stanciu, M.D., Coereanu, C., Ovidiu, V., 2012.Assessment of acoustic properties of biodegradable composite materials with textile inserts. Mater. Plast. 49(1): 68-72. http://www.revmaterialeplastice.ro/pdf/CURTU%20IOAN%201%2012.pdf.

Del Mar Barbero-Barrera, M., Pombo, O., Navacerrada, M., 2016.Textile fibre waste bindered with natural hydraulic lime. Compos. Part B 94: 26-33. https://doi.org/10.1016/j.compositesb.2016.03.013.

Del Rey, R., Bertó, L., Alba, J., Arenas, J.P., 2015. Acoustic characterization of recycled textile materials used as core elements in noise barriers. Noise Control Eng. J. 63(5): 439-447. https//doi.org/10.3397/1/376339.

Dos Reis, J.M.L., 2009. Effect of textile waste on the mechanical properties of polymer

concrete. Mater. Res. 12(1): 63-67. https//doi.org/10.1590/S1516-14392009000100007.
Drochytka, R., Dvorakova, M., Hodna, J., 2017. Performance evaluation and research of alternative thermal insulation based on waste polyester fibers. Procedia Eng 195: 236-243. https://doi.org/10.1016/j.proeng.2017.04.549.
Echeverria, C. A., Handoko, W., Pahlevani, F., Sahajwalla, V., 2019. Cascading use of textile waste for the advancement of fibre reinforced composites for building applications. J. Clean. Prod. 208: 1524-1536. https://doi.org/10.1016/j.jclepro.2018.10.227.
El Wazna, M., El Fatihi, M., El Bouari, A., Cherkaoui, O., 2016. Thermo physical characterization of sustainable insulation materials made from textile waste. J. Build. Eng. 12: 196-201. https://doi.org/10.1016/j.jobe.2017.06.008.
El Wazna, M., Gounni, A., El Bouari, A., El Alami, M., Cherkaoui, O., 2018. Development, characterization and thermal performance of insulating nonwoven fabrics made from textile waste. J. Ind. Text. 6. https://doi.org/10.1177/1528083718757526.
EURATEX Report: Facts & Figures of the European textile and clothing industry, June 2020. https://euratex.eu/facts-and-key-figures/, (Accessed March 2021).
EURATEX Report: Annual Report, 2018. https://euratex.eu/about-euratex/annual-reports/, (Accessed March 2021).
Gounni, A., El Wazna, M., El Alami, M., El Bouari, A., 2018a. Thermal performance evaluation of textile waste as an alternative solution for heat transfer reduction in buildings. J. Sol. Energy Eng. 140(2). https://doi.org/10.1115/1.4038786.
Gounni, A., Tahar Mabrouk, M., Elwazna, M., Kheiri, A., El Alami, M., El Bouari, A., Cherkaoui, O., 2018b. Thermal and economic evaluation of new insulation materials for building envelope based on textile waste. Appl. Therm. Eng. 149: 475-483. https://doi.org/10.1016/j.applthermaleng.2018.12.057.
Gulzar, T., Farooq, T., Kiran, S., Ahmad, I., Hameed, A., 2019. Green chemistry in the wet processing of textiles. In: Shahid-ul-Islam and B.S. Butola (Eds.), The Impact and Prospects of Green Chemistry for Textile Technology. Woodhead Publishing, England, pp. 1-20.
Hadded, A., Benltoufa, S., Fayala, F., Jemni, A., 2015.Thermo physical characterization of recycled textile materials used for building insulating. J. Build. Eng. 5: 34-40. https://doi.org/10.1016/j.jobe.2015.10.007.
Hassanin, A.H., Candan, Z., Demirkir, C., Hamouda, T., 2018. Thermal insulation properties of hybrid textile reinforced biocomposites from food packaging waste. Journal of Industrial Textiles 47(6):1024-1037. https://doi.org/10.1177/1528083716657820.
Jordeva, S., Tomovska, E., Trajković, D., Zafirova, K., 2014. Textile waste as a thermal insulation material. Tekstil 63(5-6): 174-178. https://hrcak.srce.hr/index.php?show=clanak&id_clanak_jezik=210294.
Kalkan, S.O. and Gündüz L., 2016. A study on the usage of denim waste as reinforcement element in composite mortars on exterior building application. 12 International congress on advances in civil engineering, Istanbul 1-7.
Lacoste, C., El Hage, R., Bergeret, A., Corn, S., Lacroix, P.,2017. Sodium alginate adhesives as binders in wood fibers/textile waste fibers biocomposites for building insulation. Carbohydr. Polym. 184: 1-8. https://doi.org/10.1016/j.carbpol.2017.12.019.
Lee, Y. and Joo, C., 2003. Sound absorption properties of recycled polyester fibrous assembly absorbers. Autex Res. J. 3(2): 78-84. http://www.autexrj.com/articles/33/118.
Legislative Decree 152, 2006. Norme in material ambientale. (G.U. n. 88 del 14-04-2006).

Liu Y, Zhang Y, Guo Y, Chu PK, Tu S., 2017. Porous materials composed of flue gas desulfurization gypsum and textile fiber wastes. Waste Biomass Valor 8(1): 203-207. https//doi.org/10.1007/s12649-016-9617-y.

Lin, J.H., Li, T.T., Lou, C.W., 2016. Puncture-resisting, sound-absorbing and thermal-insulating properties of polypropylene-selvages reinforced composite nonwovens. J. Ind. Text. 45, 1477–1489. https://doi.org/10.1177/1528083714562088.

Mochizuki, M. and Matsunaga, N., 2016. Bicomponent polyester fibers for nonwovens. In: The society of fiber science and techno J. (Eds), High-performance and specialty fibers. Springer, Tokyo, pp. 395-408.

Muthuraj, R., Lacoste, C., Lacroix, P., Bergeret, A., 2019. Sustainable thermal insulation biocomposites from rice husk, wheat husk, wood fibers and textile waste fibers: Elaboration and performances evaluation. Ind. Crop. Prod. 135: 238-245. https://doi.org/10.1016/j.indcrop.2019.04.053.

Naeimirad, M., Zadhoush, A., Kotek, R., Neisiany, R.E., Khorasani, S.N., Ramakrishna, S., 2018. Recent advances in core/shell bicomponent fibers and nano fibers: a review. J. Appl. Polym. 135(21): 46265. https://doi.org/10.1002/ app.46265.

Palakurthi, M., 2016. Development of Composites from Waste PET-Cotton Textiles. University of Nebraska – Lincoln. http://digitalcommons.unl.edu/cgi/viewcontent.

Patnaik, A., Mvubu, M., Muniyasamy, S., Botha, A., Anandjiwala, R.D., 2015. Thermal and sound insulation materials from waste wool and recycled polyester fibers and their biodegradation studies. Energy Build. 92: 161-169. https://doi.org/10.1016/j.enbuild.2015.01.056.

Pinto, J., Peixoto, A., Vieira, J., Fernandes, L., Morais, J.,Cunha, V.M.C.F., Varum, H., 2013. Render reinforced with textile threads. Constr. Build. Mater. 40 :26-32. https//doi.org/10.1016/j.conbuildmat.2012.09.099.

Pourmohammadi, 2006. Thermal bonding. In: Russell, S.J. (Ed.), Handbook of Nonwovens. Woodhead Publishing, England, pp. 298-329.

Ramamoorthy, S.K., Persson, A., Skrifvars, M., 2014. Reusing textile waste as reinforcements in Composites. J. Appl. Polym. Sci. 131(17): 1-16. https://doi.org/10.1002/APP.40687.

Rajput, D., Bhagad, S.S., Raut, S.P., Ralegaonkar, R.V.,Mandavgane, S.A., 2012. Reuse of cotton and recycle paper mill waste as building material. Constr. Build. Mater. 34: 470-475. https//doi.org/10.1016/j.conbuildmat.2012.02.035.

Rapporto rifiuti speciali, 2021. ISPRA - Istituto Superiore per la Protezione e la Ricerca Ambientale.

Rapporto rifiuti urbani, 2019. ISPRA - Istituto Superiore per la Protezione e la Ricerca Ambientale.

Ricciardi, P., Belloni, E., Cotana, F., 2014. Innovative panels with recycled materials: thermal and acoustic performance and life cycle assessment. Appl. Energy 134: 150-162. https://doi.org/10.1016/j.apenergy.2014.07.112.

Sadrolodabaee, P., Claramunt, J., Ardanuy, M., de la Fuente, A., 2021. Characterization of a textile waste nonwoven fabric reinforced cement. Constr. Build. Mater. 276: 122179. https://doi.org/10.1016/j.conbuildmat.2020.122179.

Seddeq, H.S., Aly, N.M., Marwa, A.A., Elshakankery M.H., 2012. Investigation on sound absorption properties for recycled fibrous materials. J. Ind. Text. 43(1): 56-73. https//doi.org/10.1177/1528083712446956.

Sedlmajer, M., Zach, J., Hroudova, J., 2015. Possibilities of development of thermal insulating materials based on waste textile fibers. Adv. Mat. Res. 1124: 183 188.

https://doi.org/10.4028/www.scientific.net/AMR.1124.183.

Segura Alcaraz, M.P., Bonet-Aracil, M., Segura Alcaraz, J.G.,Seguí, I.M., 2017. Sound absorption of textile material using a microfibers resistive layer. IOP Conference Series: Materials Science and Engineering 254. https//doi.org/10.1088/1757-899X/254/7/072022.

Schiavoni, S, D'Alessandro, F, Bianchi, F, Asdrubali, F., 2016. Insulation materials for the building sector: A review and comparative analysis. Renew Sust. Energ. Rev 62: 988-1011. https://doi.org/10.1016/j.rser.2016.05.045.

Temmink, R., Baghaei, B., Skrifvars, M., 2018. Development of biocomposites from denim waste and thermoset bioresins for structural applications. Compos. Part A 106: 59-69. https//doi.org/10.1016/j.compositesa.2017.12.011.

Tiuc, A.E., Vermeşan, H., Gabor, T., Vasile, O., 2016. Improved sound absorption properties of polyurethane foam mixed with textile waste. Energy Procedia 85: 559-565. https//doi.org/10.1016/j.egypro.2015.12.245.

Trajković, D., Jordeva, S, Tomovska, E., Zafirova, K., 2016. Polyester apparel cutting waste as insulation material. J. Text. I. 108 (7): 1238-1245. https://doi.org/10.1080/00405000.2016.1237335.

Umar, M., Shaker, K., Ahmad, S., Nawab, Y., Umair, M., Maqsood, M., 2017. Investigating the mechanical behavior of composites made from textile industry waste. J. Text. I. 108(5): 835-839. https//doi.org/10.1080/00405000.2016.1193.

Wilson, A., 2006. Development of the nonwovens industry. In: Russell, S.J. (Ed.), Handbook of Nonwovens. Woodhead Publishing, England, pp. 1e15.

Zach, J., Hroudová, J., Korjenic, A., 2016. Environmentally efficient thermal and acoustic insulation based on natural and waste fibers. J. Chem. Technol. Biotechnol. 91, 2156–2161. https://doi.org/10.1002/jctb.4940.

Zou, Y., Reddy, N., Yang, Y., 2011. Reusing polyester/cotton blend fabrics for composites Compos.B Eng.42(4):763770.https//doi.org/10.1016/j.compositesb.2011.01.022.

Chapter 2

Materials chosen for the study

This chapter partially reports material from:

- Rubino, C., Bonet Aracil, M., Liuzzi, S., Stefanizzi, P., Martellotta, F., 2021. *Wool waste used as sustainable non-woven for building applications*. J. Clean. Prod. 278, 123905. https://doi.org/10.1016/j.jclepro.2020.123905.

This Chapter characterizes the raw materials and the methods selected to produce the tested samples. A brief description of the polymers used as base matrix (i.e. wool) and binding agents (i.e. bi-component fibers, chitosan and gum Arabic) is reported with the aim of analyzing their origin and their previous use in construction field. The characterization of the microstructure and the thermal behaviour of the raw materials are included. In fact, a Scanning Electron Microscope (SEM) analysis of the wool and of the bi-component fibers, in addition to a Differential Scanning Calorimetry (DSC) analysis of the all used raw materials were carried out. The examination of the SEM and DSC results were useful for choosing the best procedure for samples preparing (i.e. the chemical and thermal bonding techniques), of which a detailed illustration is provided.

2.1 Description of raw materials

In light of the considerations about the main non-wovens bonding methods included in the previous Chapter, the chemical and thermal bonding techniques were selected to produce the materials tested in this research work. The chosen methods resulted easily reproducible at laboratory scale and were able to ensure the suitable acoustic and hygrothermal properties of the final products.

Wool fibers, 100% recycled, obtained from tailored cuttings produced by the Italian clothing company Gordon Confezioni srl., were used as base fibers.

Regarding the chemical bonding technique, two different environmental friendly binders were chosen: one of vegetable origin, i.e. gum Arabic; and the other of animal origin, i.e. chitosan. Although these two materials were already examined in literature successfully, they have never been tested as adhesives for construction materials made from textile fibers. In fact, as will be better explained in the next "Chitosan" and "Gum Arabic" Sections, they were mainly used for bonding agricultural wastes or natural fibers. Furthermore, the number of systematic studies on the thermal and sound absorbing properties of the produced materials resulted limited. Concerning the thermal bonding technique, a polyester/copolyester (Co PET/PET) sheath-core bi-component fibers were explored as thermoplastic material. The purpose was to use a working temperature able to avoid side effects such as yellowing or chemical degradation of the wool matrix.

Gum Arabic used in the present research was purchased from Lana y Telar company; whereas chitosan of medium molecular weight and acetic acid to solubilize it, were supplied respectively by Sigma-Aldrich and Panreac. The bi-component fiber was supplied by FiberVision company.

2.1.1 Wool

Wool is an animal protein fiber with a complex and sophisticated structure characterized by numerous ordered layers. The outermost layer (the cortex) represents about 90% of the fiber weight and is covered with thin and flat overlapping scaly ‘‘cuticle cells’’ arranged in the direction of the fiber axis (Figure 2.1).

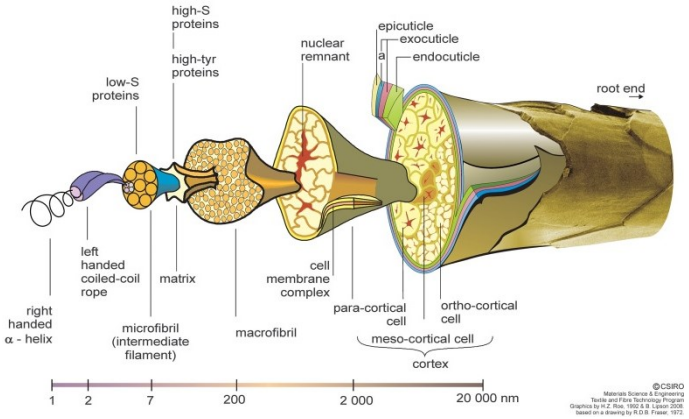

Figure 2.1. Structure of a Merino wool fiber (Source: http://www.scienceimage.csiro.au/image/7663//large).

Although the waxy coating on the cuticle cells makes them water repellant, they are able to absorb water vapor, playing an important role in the hygric behaviour of wool. Furthermore, the high nitrogen and water content makes wool flame retardant (Baker, 2018). These characteristics, in addition to the intertwining ability, allow to choose wool as matrix of construction materials. In fact, during repeated mixing and pressing actions, the scales edges became curved favoring the entanglement of the fibers and enabling a good cohesion of the resulting fibrous matrix (Tridrico, 2009).

2.1.2 Bi-component fibers

The bi-component fibers are defined as “extruding two polymers from the same spinneret with both polymers contained within the same filament” (Avcioglu Kalebek and Babaarslan, 2016). The two polymers can be extruded with different cross-section shapes in order to obtain several configurations i.e. sheath/core, side by side, or island in the sea (Figure 2.2).

The main objective of producing this type of fibers is to combine properties which could only be found individually in different materials. In fact, during heating, one polymer works as low melting component, softening to form the bond; while the other works as high melting component, maintaining its shape and its structural integrity (Mochizuki and Matsunaga, 2016). Therefore, the bi-component fibers are usually applied for self-bonding in non-woven materials with the aim of using lower temperatures than the usual thermal molding process (Naeimirad et al, 2018).

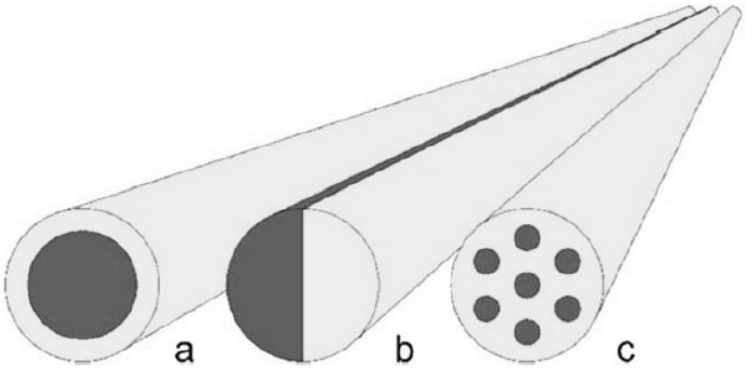

Figure 2.2. Schematic illustration of cross section of bi-component fibers: sheath/core (a),side by side (b), or islands in the sea (c) (Source: Naeimirad et al., 2018).

As analyzed in the previous Chapter, the bi-component fibers have been gaining wide application in several fields other than constructions materials sector, where they can be used combined with both vegetable and textile fibers (Korjenic et al., 2011; Zach et al., 2016). Recently, Dieckmann et al. (2019) used polyethylene/polypropylene bi-component fibers to bind feather and cotton wastes producing materials for automotive and sustainable packaging applications.

2.1.3 Chitosan

Chitosan is the second most abundant bio-polymer after cellulose. It consist of β-(1→4)-2-acetamido-D-glucose and β-(1→4)-2-amino-D-glucose units obtained after a deacetylation of chitin, a cell wall component of fungi and a skeletal component of shrimp and other crustaceans (Figure 2.3).

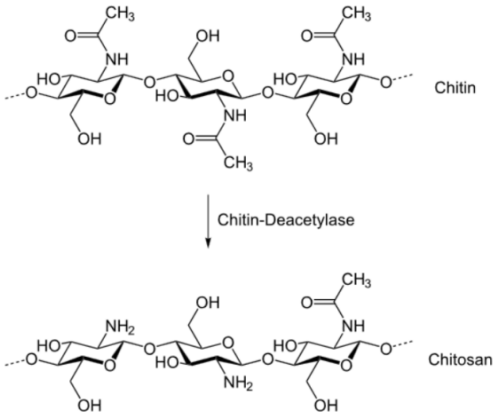

Figure 2.3. Structure of chitin and chitosan (Source: Nilsen-Nygaard et al., 2015).

Chitosan has always attracted attention as a multifunctional polymer applicable to various purposes. Thanks to its antimicrobial action, it is suitable for food and pharmaceutical industries, or medical applications (Bakshi et al., 2020).

The literature review also revealed about the possibility of using it in sustainable constructions field, thanks to properties such as biodegradability, antibacterial activity and non-toxicity. Aguilar et al. (2016) investigated the feasibility of using chitosan biopolymer as an admixture or as an external coating for earthen constructions. Results pointed out that the use of low concentrations of chitosan could be a promising treatment for new or existing constructions, leading to a significant improvement of water and mechanical resistances.

Chitosan is soluble in aqueous acidic conditions (pH < 6.5), while it is insoluble in organic solvents and in water. The low surface tension and the viscosity make it suitable as liquid adhesive solution (Mati-Baouche et al., 2014a). In this regard, Mati-Baouche et al. (2014b, 2016) used a chitosan solution to bond shredded sunflowers stalks producing bio-based construction materials with a good thermal insulating behaviour (thermal conductivity of 0.056 W/(m K)). Martellotta et al. (2018) also explored the binding capability of chitosan, investigating the acoustic behaviour of panels produced from olive tree pruning waste and chitosan solution as binder. Experimental results showed a promising sound absorbing behaviour with absorption coefficients as high as 0.9 above 1 kHz using a 50 mm sample.

2.1.4 Gum Arabic

Gum Arabic is a biopolymer obtained as an exudate from mature Acacia senegal and Acacia seyal trees widespread in the African district of the Sahel in Sudan. In fact, in the semi-arid regions, shrubs and trees produce a plastic aqueous sealant as a natural defense mechanism to plug cracks naturally formed in the bark, preventing infection and dehydration of the plant (Figure 2.2 (a)). When this plastic material is in contact with air and sunlight, it dries leading to the formation of hard, glasslike spherical nodules that can be easily collected (Figure 2.2 (b)) (Verbeken et al., 2003).

(a) (b)

Figure 2.4. Gum Arabic on Acacia senegal tree shoot (a) and hard glasslike lumps of gum Arabic (b) (Source: Mariod, 2018).

Gum Arabic is a group of polysaccharides with an important mineralizing ability thanks to its rich content of calcium, magnesium and potassium salts. It is water soluble, and its solution gives a slight yellow to reddish color (Mariod, 2018). According to Ahmed (2018), the attendance of tannins in the gum Arabic plant is the main reason of the antibacterial potentiality of the biopolymer.

Gum Arabic is used for a great number of purposes, mainly in food sector. However, there are also considerable non-food applications. In the last few years, gum Arabic has been gaining wide application in the construction industry, especially as water-reducing able to improve the physical and mechanical properties of the cement pastes (Elinwa, 2018). Mohamed et al. (2020), evaluated the positive effects of the inclusion of gum Arabic biopolymer on the durability of concrete in aggressive ambient. In fact, cement samples incorporating the biopolymer showed better resistance to the acid attack, achieving lower mass lost than samples without it. Zhao et al. (2015) showed that 0.3 wt% of gum Arabic was the optimum dosage to achieve the best dispersion effects and the best holding capacity during hydration in Portland cement.

The bio-adhesive capacity of the gum Arabic has been also investigated. Abuarra et al. (2014) studied the effects of the gum Arabic addition in particleboards made from stems of a typical mangrove tree of the tropical and subtropical coasts regions. Panels with smooth surface, rigid texture and good internal bonding strength were obtained. Dieye et al. (2019) investigated the thermal properties of innovative boards made from a mixture of powder Typha leaves and gum Arabic, observing a promising thermal insulating behaviour.

2.2 Preliminary characterization of raw materials

Raw materials characterization is the most important step of any high quality production process. The aim is to acquire a deep knowledge of the used resources, in order to determine their impact on performance of the final products and to allow the manufacturer to make critical decisions about the procedures to be used.

2.2.1 Morphological analysis

Scanning Electron Microscope (SEM) is a technique able to produce images of a sample by scanning it with a beam of electrons. The electrons interact with the different atoms of the sample surface, producing various signals that reveal information on the sample surface morphology and composition.

In this work, a Scanning Electron Microscope ZEISS, model ULTRA 55 was used in order to carry out a microstructure analysis of the fibers used as raw materials. The samples were prepared by cutting small slices of the testing materials onto an adhesive carbon tab, attached to an aluminum stub. In order to observe the cross section of the bi-component fibers, they were cut after freezing in liquid nitrogen for a few minutes to reduce the possibility of deformation when they were broken. All fractured surfaces were sputter-coated with gold for about 15 min before testing.

Figure 2.5 and Figure 2.6 show the SEM images of the wool and the bi-component fibers.

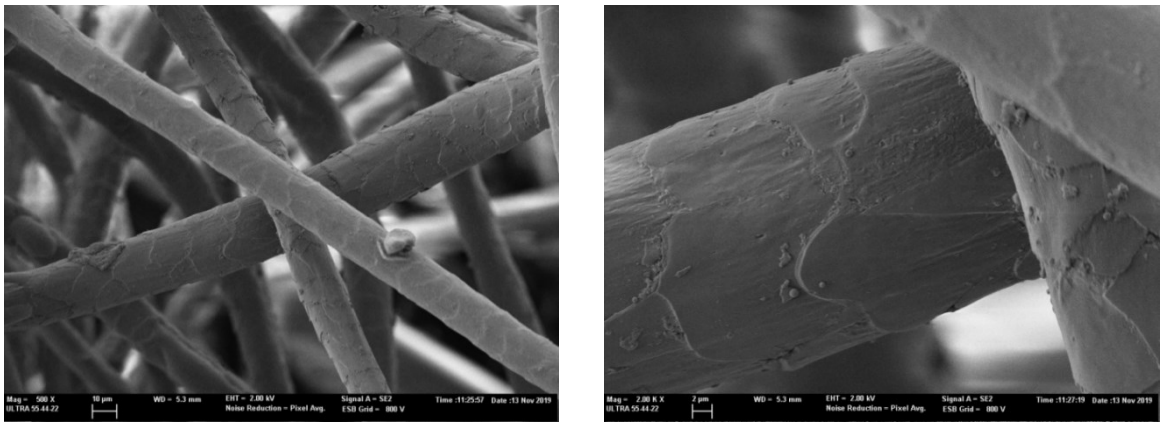

(a) (b)

Figure 2.5. SEM micrographs of wool at 500X (a) and 2000X (b).

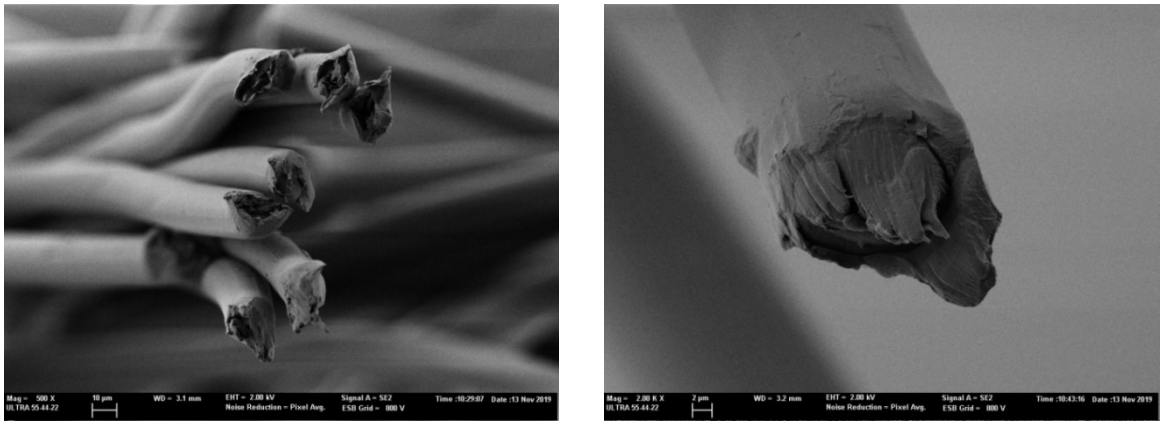

(a) (b)

Figure 2.6. SEM micrographs of Co-PET/PET bi-component fibers at 500X (a) and 2000X (b).

Fiber diameters is considered an important factor that affects the acoustic properties of the materials. Thus, several SEM images were analyzed using a Matlab® script and, considering the different sources of the used fibers, a population of 300 wool fibers was chosen in order to determine a distribution of their diameters. As shown in the bar chart in Figure 2.7, fiber diameters ranged from 8 to 34 µm (with a mean value of 19 µm and a standard deviation of 7 µm). The diameters distribution of the bi-component fibers was also analyzed. They were characterized by a nearly constant diameter around of 22 µm, as a consequence of their fabrication process. As will be better explained in Chapter 4, although the mean diameters values of the wool and PET/CoPET fibers were very close, their distribution allowed to obtain high porous structure with positive effects on the hygrothermal and acoustic performances.

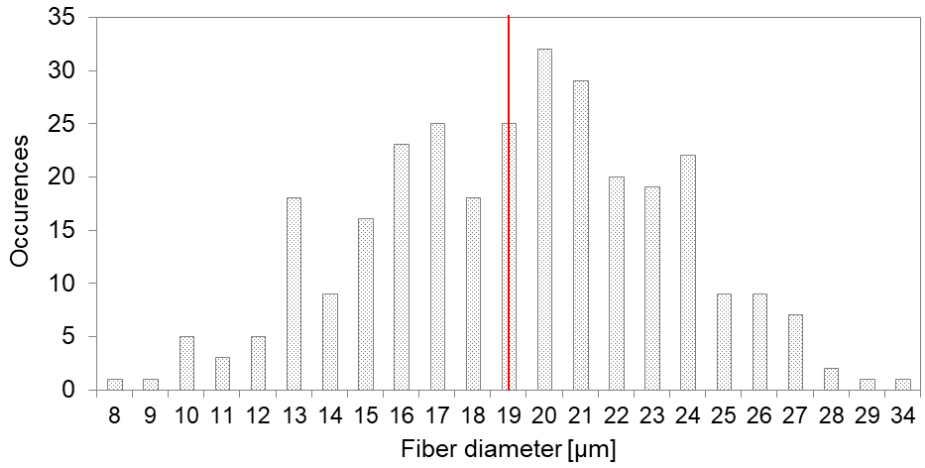

Figure 2.7. Distribution of diameters of wool fibers. In red, the average fiber diameter value.

2.2.2 Thermal analysis

Differential Scanning Calorimetry (DSC) analysis was performed in order to characterize the thermal behaviour of the base fibers and the binder agents. DSC is one of the most frequently used techniques for thermal characterization of materials. It consists in measuring the heat flow associated with phase transitions in material as a function of temperature and time, when the material is subjected to a controlled heating program under an inert gas purge. Such measurements provide quantitative and qualitative information about physical and chemical changes that include endothermic/exothermic processes or changes in heat capacity.

The Differential Scanning Calorimetry analysis was carried out by using a DSC 1 Star System Mettler Toledo device, according to ISO 11357-1 (2016). The aim was to choose the suitable working temperature to produce the final products, while avoiding the decomposition of the wool base polymer and ensuring the effectiveness of the binder ones. Accurately weighted samples (2 mg each) were placed into aluminum pans and then crimped closed. A small hole was done on the top of the assembly allowing the release of water. An empty aluminum pan was used as a reference. During the experiments, the samples were heated from 30 °C to 500 °C for chitosan, gum Arabic and wool; whereas from 30 °C to 350 °C for the bi-component fibers. The temperature was increased at a heating rate of 30 °C/min and nitrogen was used as the purge gas at 50 ml/min.

As observed in Figure 2.8(a), the DSC curve of wool fibers showed two endothermic processes. The first endothermic process was noted from 106.68 °C to 132.83 °C, with a peak temperature of 115.22 °C. According to (Zargarkazemi et al., 2015), it could be explained by the vaporization of the water as a consequence of the increasing temperature. A second endothermic heat transfer was observed from 253.57 °C to 426.32 °C. This baseline shift was consequence of a decomposition process characterized by the α-keratin denaturation with the relative cleavage of the helical hydrogen bonds and the melting of the ordered regions of the wool. During this process, the breakdown of the disulfide bonds also occurred, causing the release of numerous volatiles i.e. hydrogen sulfide and sulfur dioxide (Forouharshad et al., 2011).

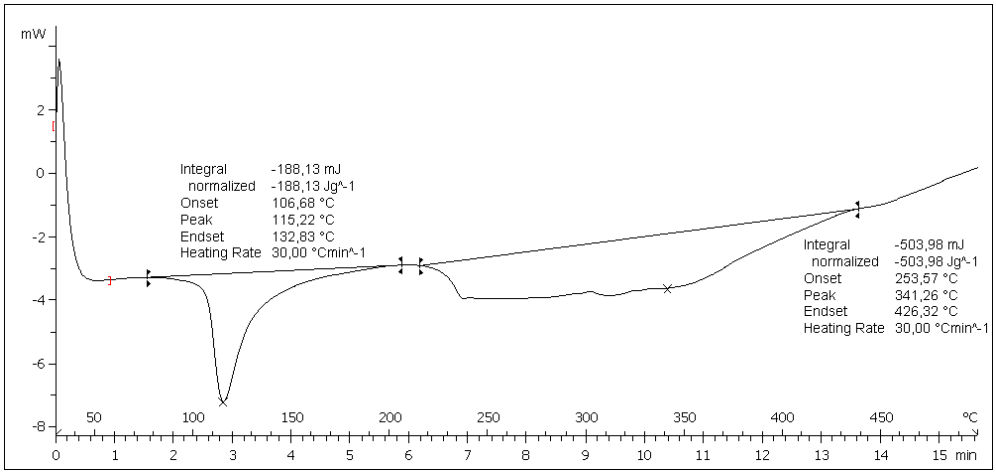

(a)

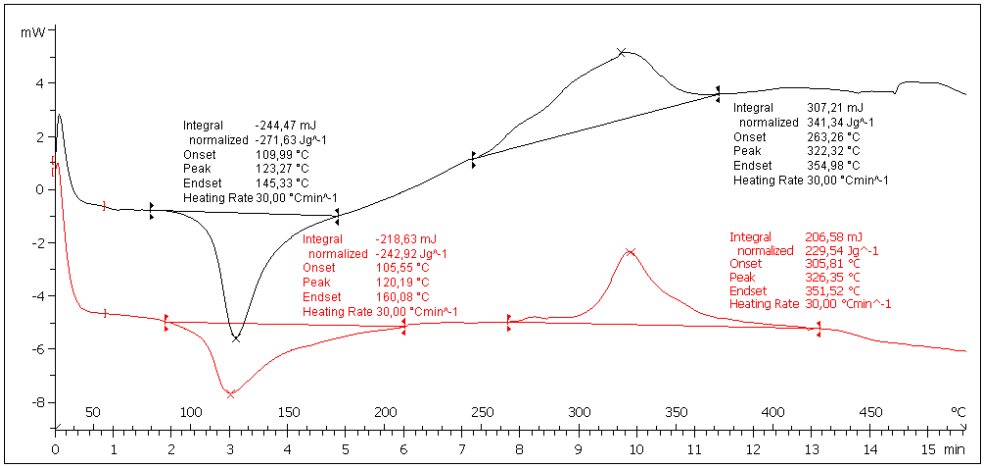

(b)

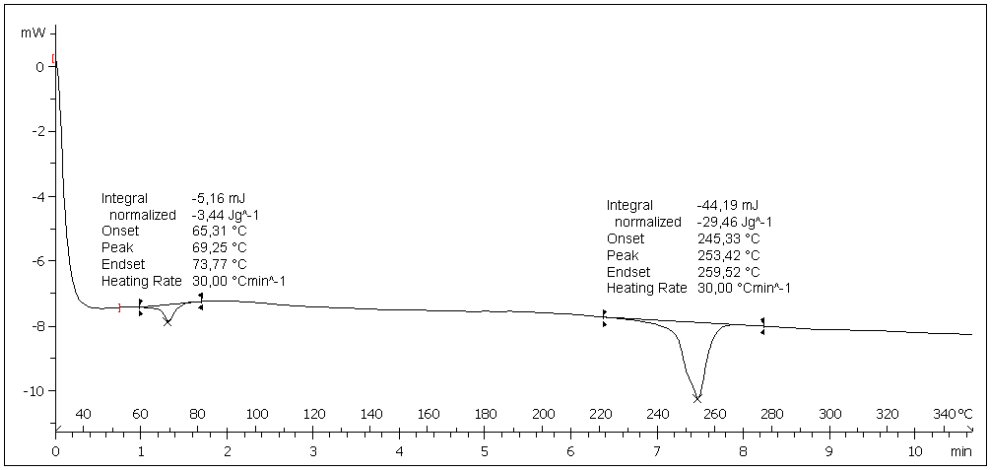

(c)

Figure 2.8. DSC curve of 100% wool fibers (a), chitosan (in red) and gum Arabic (in black) (b) and copolyester/polyester sheath-core bi-component fibers (c).

As observed in Figure 2.8(b), chitosan and gum Arabic show two similar DSC curves characterized by one endothermic shift followed by an exothermic one. According to Neto et al. (2005) and Osman et al. (2006), the first stage was related to the loss of water. A closer observation of Figure 2.8(b) reveals very small differences in the endotherm area and peak position of the two materials suggesting their similar water holding capacity and strength of water-polymer interaction. In fact, the first endothermic transition was from 109.99 °C to 145.33 °C, with a peak temperature of 123.27 °C for chitosan and from 105.55 °C to 160.08 °C, with a peak temperature of 120.19 °C for gum Arabic. The second exothermic stage it could be assigned to a decomposition process. Approximately around 326 °C, chitosan was subjected to a thermal and oxidative degradation of the main chain, characterized by vaporization and elimination of volatile products. As with most polysaccharides, pyrolysis of chitosan starts with a random split of the glycosidic bonds, followed by a release of acetic, butyric and a series of lower fatty acids (Neto et al., 2005). According to Osman et al. (2006), the exothermic transition observed around 322 °C for gum Arabic was attributed to a dehydration, depolymerization, recrystallization, and pyrolytic decomposition resulting in the formation of H_2O, CO_2, and CH_4.

Figure 2.8(c) shows the DSC curve of the synthetic fibers in which the two endothermic baseline shifts proved the presence of the two polymers. According to Brydon and Pourmohammadi (2006) the crystallites of the polyester melt at about 250 °C and there are polymers such as poly (ethylene sebacate) which have a melting temperature centered around 69.5 ºC (Wunderlich, 1980). Thus, it can be concluded that the first peak of the curve at 69.25 °C corresponded to the melting temperature of the copolyester polymer and the second peak at 253.42 °C was the melting temperature of the polyester.

2.2.3 Infrared spectroscopy analysis

The Fourier Transform Infrared Spectrum (FTIR) analysis was conducted to support the SEM and DSC analysis in verifying the fibers composition. FTIR spectroscopy uses the mid-infrared energy to identify the chemical structure and the functional groups of the fibers. The infrared light is absorbed at specific frequencies related to the vibrational bond energies of the functional groups present in the molecule. Thus, a characteristic pattern of bands is formed, where the position and the intensity of each band provide a fingerprint of the molecular structure.

Figure 2.9 shows the FTIR spectra for wool, CoPET/PET fiber and a standard Polyethylene terephthalate (PET). PET fiber was used as term of comparison in order to better highlight the main characteristics of the wool and the bi-component fibers.

A JASCO FTIR 4700 equipped with an Attenuated Total Reflectance (ATR) was used to scan samples with resolution of 4 cm^{-1}, 256 scans/minute. The spectrums were observed from 400 to 4000 cm^{-1}. It could be clearly appreciated the difference between wool and polyesters. However, when the focus was placed on polyester, only slight differences could be observed between CoPET/PET fiber and a standard PET. Those alterations might be attributed to the differences due to the new monomer included to obtain the copolymer CoPET. Table 2.1 reports the frequencies and the assignments of the bands in the FTIR for wool and polyester fibers.

Wool characteristic structure is the cysteine S-S bond; the S-S stretching vibration shows a characteristic band in the region 560 - 480 cm^{-1} (Wojciechowska et al., 2004). The N-H group, also characteristic from wool, can be appreciated on the bands around 3290 cm^{-1}, 1638 cm^{-1} and 1515 cm^{-1} (Pielesz et al., 2003).

Whereas the most characteristic peaks for PET are centered around 2874 cm^{-1} due to -CH_2- groups; 1717 cm^{-1} due to carbonyl C=O stretching vibration; 1242, 1120 and 1096 cm^{-1} due to C-O vibration; and between 900 - 640 cm^{-1} due to benzene rings (Li and Ding, 2007; Zhang et al., 2008; Bozaci et al., 2012).

The comparison between CoPET/PET and PET fibers through the FTIR analysis confirmed the composition of the used bi-component fibers. Normally, considering the bi-component fibers, the co-polymer shows a melting temperature close to the main polymer. Thus, the analyzed fiber it could be considered a monomeric PET fiber and the first endothermic shift resulting from the DSC analysis around 70°C (Figure 2.8) it could be due to the possible moisture presence. The slight difference between the FTIR spectra of CoPET/PET and PET fibers dispelled any doubt, proving the bi-component characteristics of the synthetic fibers.

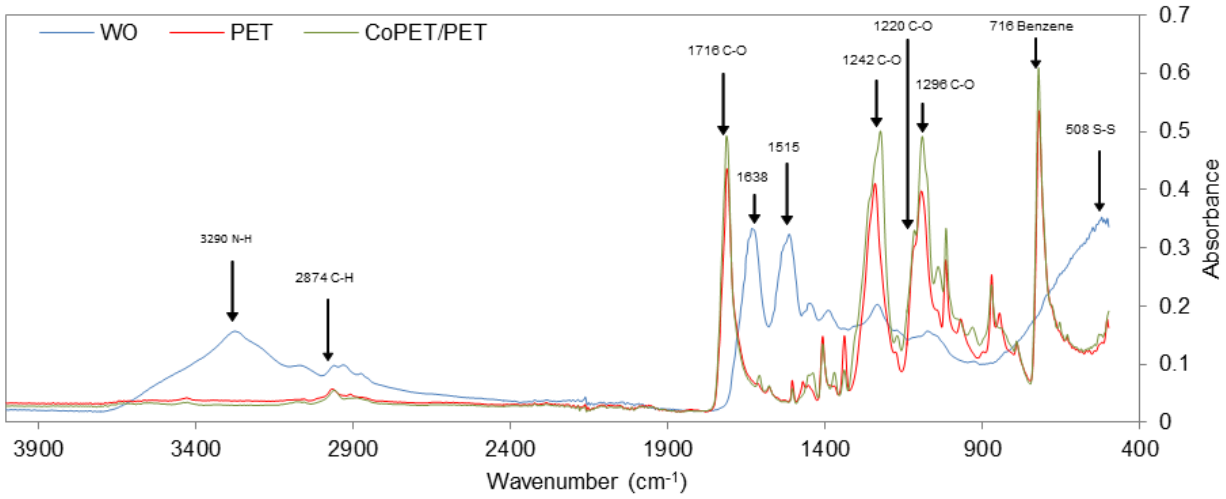

Figure 2.9. FTIR analysis applied to the wool, PET and CoPET/PET fibers.

Table 2.1. Frequencies and assignments of bands identified in the FTIR spectra for PET and wool.

Frequency [cm^{-1}]	Assigment	Fibre
508	S-S Stretching vibration	Wool (Wojciechowska et al. 2004, Pielesz et al., 2003)
1096	-C-O- vibration	PET (Li and Ding. 2007, Bozaci et al., 2012)
1120	-C-O- vibration	Wool and PET (Li and Ding. 2007, Bozaci et al., 2012)
1242	-C-O- vibration	PET (Li and Ding. 2007, Bozaci et al., 2012)
1515	-NH	Wool (Wojciechowska et al. 2004, Pielesz et al., 2003)
1638	-NH	Wool (Wojciechowska et al. 2004, Pielesz et al., 2003)
1717	-C=O stretching vibration	PET (Li and Ding. 2007, Bozaci et al., 2012)
2874	$-CH_2-$ stretching vibration	Wool and PET (Li and Ding. 2007, Bozaci et al., 2012)
3290	-NH	Wool (Wojciechowska et al. 2004, Pielesz et al., 2003)

2.3 Mix design and samples preparation

The tested materials were prepared by using 100% Merino wool fibers initially available in the form of cut fabrics. Then, a soft wool batting was obtained by manually carding and scouring the fibers. As previously anticipated, wool wastes were used as base matrix, whereas gum Arabic, chitosan and CoPET/PET bi-component fibers were used as binder materials, following two different methods.

In order to produce the thermally bonded non-woven materials, a hydraulic press built by Dupra SL company was used. The device was optimized by adjusting concentric metal cylinders on the two pressing plates (Figure 2.10). In detail, a hollow cylinder working as mold was fixed on the lower plate and another solid cylinder working as press was hooked on the upper plate. Molds with different diameters were used in order to prepare samples with adequate sizes for the subsequent tests. The compression molding process was applied at 100 °C for 1 hour, then the samples were cooled in desiccators containing silica gel.

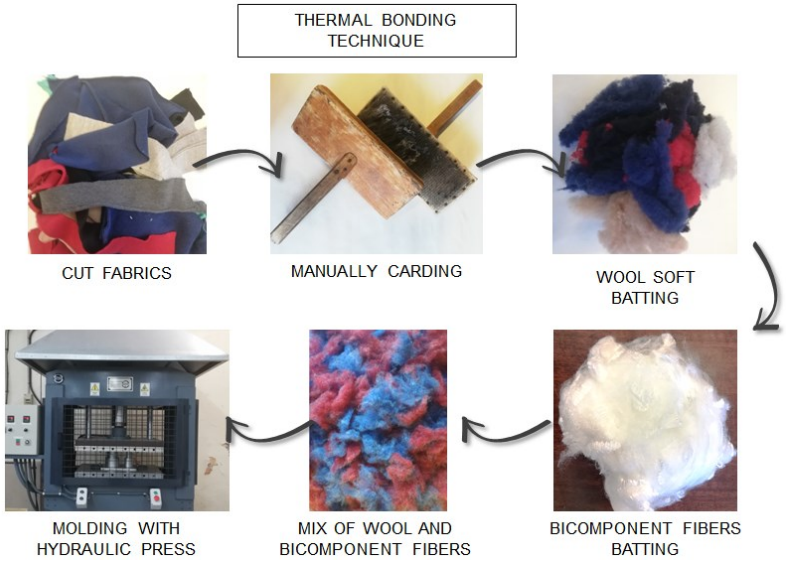

Figure 2.10. Main steps of the thermal bonding process.

Defined proportions of wool and bi-component fibers were uniformly mixed, after being carded together. Then, several samples were prepared casting the fibrous blend in the cylindrical mold and pressing it by lowering the top plate up to a chosen height depending on the thickness needed for the final samples.

As shown in Table 2.2, five types of non-wovens (subsequently referred as “BICO”)

with different bulk density values were manufactured. Bulk density values are given as mean values among six measurements with its measurement uncertainty expressed as the standard deviation of the mean (ISO/IEC Guide 98-3, 2008).

The binder fibers content was chosen after producing samples having a fixed bulk density (0.51 kg/m^3) and bi-component fibers varying between 15 and 50% in mass. In fact, the amount of the binder fibers to produce nonwoven materials usually varies from 5 to 50% in mass, depending on the physical requirements. According to Pourmohammadi et al., (2006), a binder content of 50% of the total mass of the fibers causes a reinforced plastic nonwoven material. Reducing the binder content to 10-20% allows to obtain a porous and flexible structure resulting in lower thermal conductivity and greater sound absorption capacity. As shown in Table 2.2, the percentage of 20% in mass was finally selected as it offered the best balance between porous structure and compactness of the skeleton.

Table 2.2. Sample ID, binder/base fibers percentage and density of the samples.

Sample ID	Bulk density [kg/m^3]	Base fibers [%]	Binder fibers [%]
BICO-1	167±6	80	20
BICO-2	136±1	80	20
BICO-3	115±1	80	20
BICO-4	90±2	80	20
BICO-5	51±1	80	20

A three steps process was followed to produce textile samples using chitosan and gum Arabic. First, the wool batting was soaked in the binding solution to let the fibers get fully impregnated. Then, the excess amount of liquid was removed by squeezing, mostly to avoid the exceeding binder, that once solid, might compromise a homogeneous distribution of porosity in the final specimen (e.g., by creating surface crusts). In the third step, the achieved mix was compressed into PVC molds to form cylindrical samples. Finally, the samples were dried in an oven at 100 °C, for 1 h and, after drying, they were left in desiccators containing silica gel, under controlled conditions to reach their mass stabilization before testing (Figure 2.11).

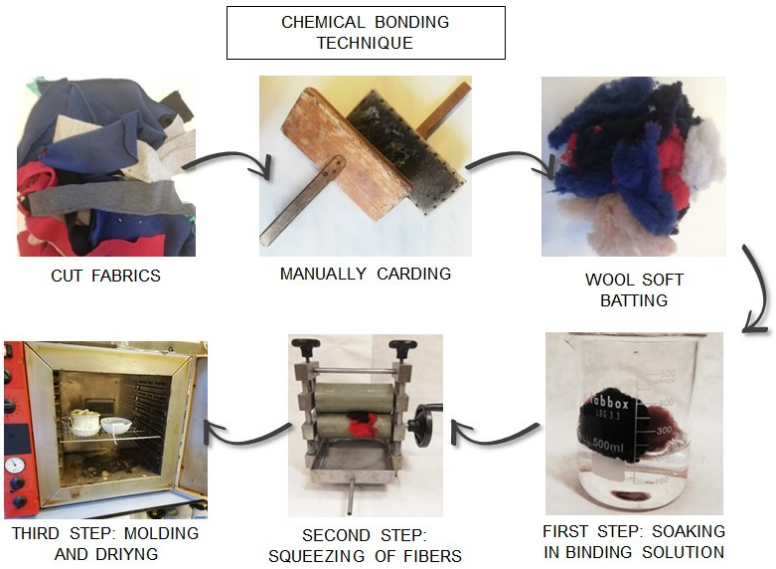

Figure 2.11. Main steps of the chemical bonding process.

The two binding solutions were achieved by dissolving different amounts of chitosan and gum Arabic, as outlined in Table 2.3. Both blends were mixed in a magnetic stirrer, at room temperature and relative humidity, for about 1 h. The concentration of solutes was chosen, after several attempts, in order to obtain the best combination of porosity and compactness.

Table 2.3. Mixing ratio of binding solutions.

Solution	Solute [g]	Water [g]	Acetic acid [g]
Chitosan	15	1000	5
Gum Arabic	200	1000	-

Two different groups of final composites were produced: the first one based on textile wastes bonded with chitosan solution was referred to as “CH”; the second type prepared by binding textile wastes with the gum Arabic solution was referred to as “GA”.

For each group, several mixes with different bulk densities and the same percentages of binder and fibrous matrix were prepared (Table 2.4). The fiber dosing of each specimen was controlled in terms of density. The aim was to produce samples with density values comparable with the samples prepared with bi-component fibers, in order to compare the results. In Table 2.4, binder concentration is expressed both as a percentage in wet mass

(obtained by weighing the fibers before soaking and after removing the excess binder), and in dry mass (obtained by weighing the final products, after drying them in the oven). Bulk density values are given as mean values among six measurements with its measurement uncertainty expressed as the standard deviation of the mean (ISO/IEC Guide 98-3, 2008).

Table 2.4. Sample ID, binder/fibrous matrix percentage (in wet and dry mass) and density of the samples.

Sample ID	Bulk density [kg/m^3]	Fibrous matrix [wet %]	Binder [wet %]	Fibrous matrix [dry %]	Binder [dry %]
CH-1	197±2	40	60	95	5
CH-2	145±2	40	60	95	5
CH-3	122±1	40	60	95	5
CH-4	80±1	40	60	95	5
GA-1	177±3	40	60	78	22
GA-2	143±2	40	60	78	22
GA-3	93±1	40	60	78	22

The choice of using a temperature of 100 °C as working temperature was a consequence of the DSC results (Figure 2.9(b-c)). In this way, the chemical decomposition of wool, chitosan and gum Arabic was avoided and the best combination of the two synthetic polymers behaviors (i.e. polyester and copolyester) was performed. In fact, during heating, the copolyester worked as low melting component and softens to form the bond; while the polyester worked as higher melting component maintains its shape and its structural integrity.

Figures 2.12, 2.13 and 2.14 show the SEM images of the CH, GA and BICO samples obtained after applying respectively the chemical and thermal bonding techniques.

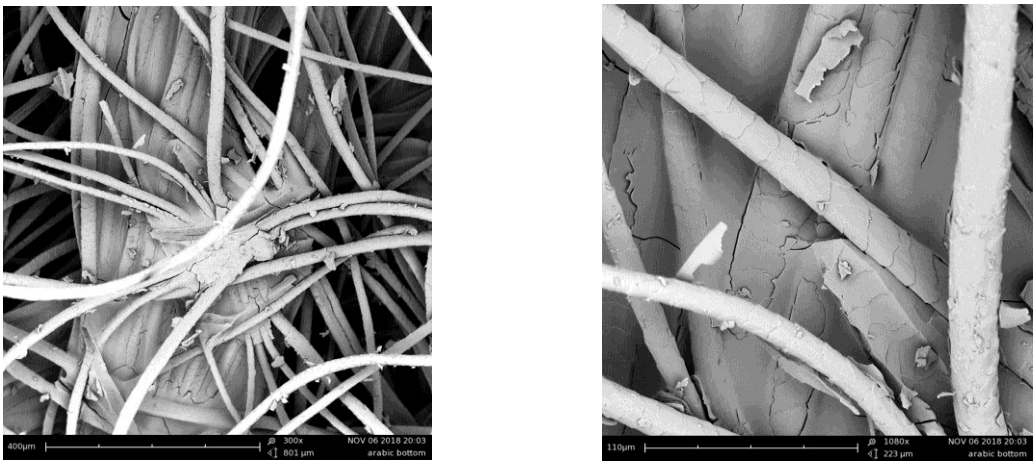

(a) (b)

Figure 2.12. SEM micrographs of GA samples at 300X (a) and 1000X (b).

(a) (b)

Figure 2.13. SEM micrographs of CH samples at 300X (a) and 1000X (b).

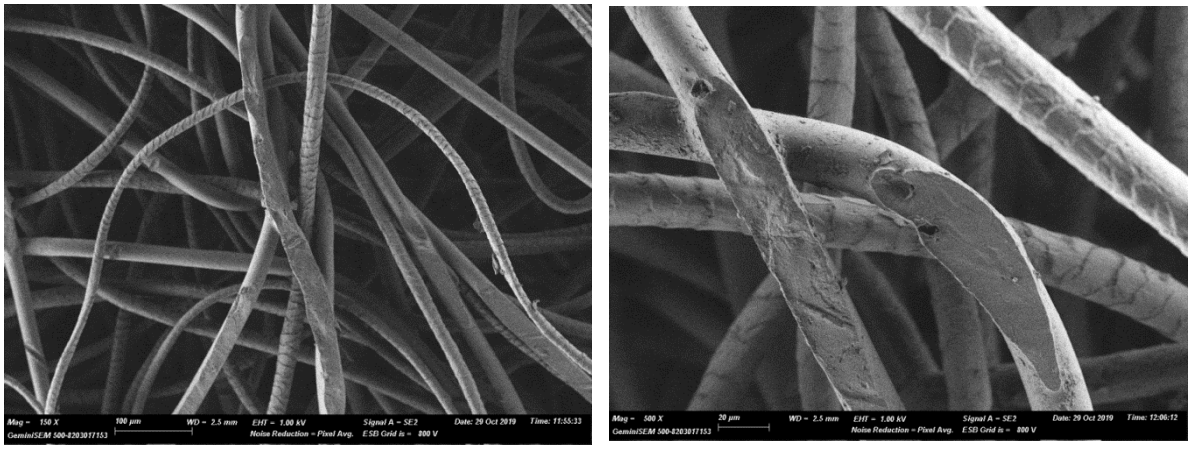

(a) (b)

Figure 2.14. SEM micrographs of BICO samples at 150X (a) and 500X (b).

The resulting materials were characterized by fibers distributed more or less randomly in plane. As observed in Figure 2.12 and 2.13, when the chemical agents were used, the fibers intertwined creating a network of tiny air pockets with a random distribution. A closer observation of Figure 2.14 allowed to distinguish the surface scale pattern of the wool fibers from the smooth surface of the man-made polymers, highlighting that the last one was not completely melted, but only the copolymer sheath melted creating bonding points among wool and bi-component fibers. At this early morphological stage, it could be concluded that both binding methods allowed to join the fibers preserving a high void fraction in the microstructure of the final products.

Figure 2.15 shows some samples prepared to test materials from different perspectives.

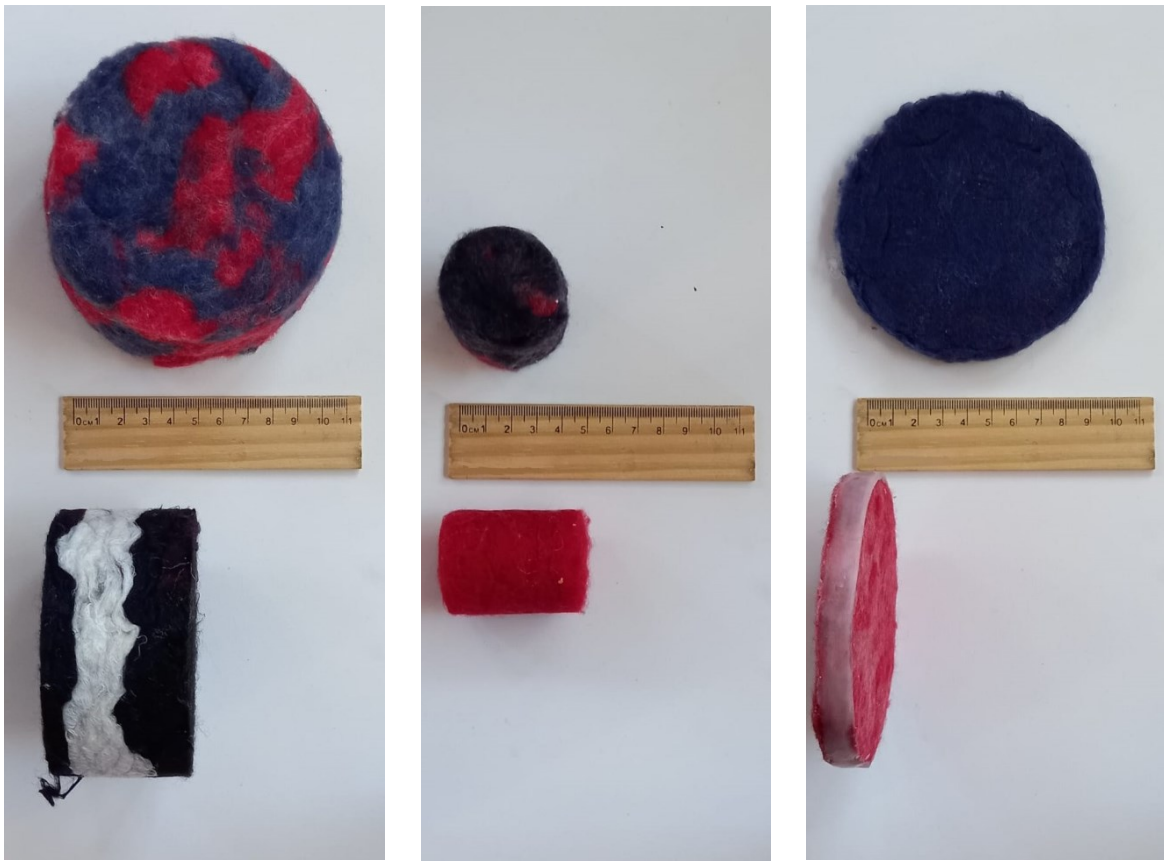

(a) (b) (c)

Figure 2.15. Samples prepared to measure thermal properties and sound absorption coefficients at medium-low frequencies (a), non-acoustic properties and sound absorption coefficients at high frequencies (b) and hygric properties (c).

Five cylindrical specimens with a diameter of 10 cm were prepared for each type of binder and for each density value. Three were prepared 5 cm thick to measure thermal properties and normal incidence sound absorption coefficient at medium-low frequencies. The remaining two samples were prepared in 1 cm thick to measure the hygric properties. Furthermore, three specimens in 4 cm diameter and 5 cm thick were prepared to measure the normal incidence absorption coefficient at high frequencies and non-acoustic properties. Table 2.5 summarizes the thickness and the diameters of the samples used to test the different behaviours of the studied materials.

Table 2.5. Size of the tested samples.

Size [cm]	Tested properties					
	Thermal	Hygric	Flammability	Acoustic	Acoustic	Non-acoustic
Thickness	5	1	1	5	5	5
Diameter	10	10	10	10	4	4

References

Abuarra, A., Hashim, R., Bauk, S., Kandaiya, S., Tousi, E. T., 2014. Fabrication and characterization of gum Arabic bonded Rhizophora spp. Particleboards. Mater. Des., 60: 108-115. http://dx.doi.org/10.1016/j.matdes.2014.03.032.

Aguilar, R., Nakamatsu, J., Ramírez, E., Elgegren, M., Ayarza, J., Kim, S., Pando, M.A., Ortega-San-Martin, L., 2016. The potential use of chitosan as a biopolymer additive for enhanced mechanical properties and water resistance of earthen construction. Constr. Build. Mater. 114, 625-637. https://doi.org/10.1016/j.conbuildmat.2016.03.218.

Ahmed, A.A., 2018. Health benefits of gum arabic and medical use, in: Mariod A.A. (Ed), Gum Arabic_Structure, Properties, Application and Economics. Academic press, United Kingdom, pp.183-210.

Avcioglu Kalebek, N. and Babaarslan, O., 2016. Fiber selection for the production of non-wovens, in: Jeon, H.-Y. (Ed), Non-woven fabrics. IntechOpen, pp. 1-32.

Baker, I, 2018. Wool, in Fifty Materials That Make the World. Springer, New York, NY, USA, pp. 261–265.

Bakshi, P.S., Selvakumar, D., Kadirvelu, K., Kumar, N.,S., 2020. Chitosan as an environment friendly biomaterial – a review on recent modifications and applications. Int. J. Biol. Macromol., 150, 1072-1083. https://doi.org/10.1016/j.ijbiomac.2019.10.113.

Bozaci, E., Arik, B., Demir, A., Özdoğan, E., 2012. Potential use of new methods for identification of hollow polyester fibers. Tekstil ve Konfeksiyon, 22, (4), 317-323.

Brydon, A.G. and Pourmohammadi, A., 2006. Dry-laid web formation, in: Russell, S.J. (Ed), Handbook of non-wovens. Woodhead Publishing, England, pp. 16-111.

Dieckmann, E., Eleftheriou, K., Audic, T., Lee, K-Y., Sheldrick, L., Cheeseman, C., 2019. New sustainable materials from waste feathers: properties of hot-pressed feather/cotton/bicomponent fibre boards. SM&T 20, e00107. https://doi.org/10.1016/j.susmat.2019.e00107.

Dieye, Y., Toure, P.M., Gueye, P.M., Sambou, V., Bodian, S., Tigampo, S., 2019. Thermomechanical Characterization Of Particleboards From Powder Typha Leaves. J Sustain. Construct. Mater. Technol., 4(1), 306-317.

Elinwa, A., U., Abdulbasir G., Abdulkadir G., 2018. Gum Arabic as an admixture for cement concrete production. Constr. Build. Mater., 176, 201-212. https://doi.org/10.1016/j.conbuildmat.2018.04.160.

Forouharshad, M., Montazer, M., Moghadam, M.B., Saligheh, O., 2011. Preparation of flame retardant wool using zirconium acetate optimized by CCD. Thermochim. Acta 520 (1-2), 134-138. https://doi.org/10.1016/j.tca.2011.03.029.

ISO 11357-1, 2016. Plastics Differential Scanning Calorimetry (DSC) Part 1: general principles. https://www.iso.org/standard/70024.html (Accessed April 2020).

ISO/IEC Guide 98-3, 2008. Uncertainty of Measurement – Part 3: Guide to the expression of Uncertainty in Measurement (GUM:1995). https://www.iso.org/sites/JCGM/GUM-JCGM100.htm, (Accessed April 2020).

Korjenic, A., Petránek, V., Zach, J., Hroudová, J., 2011. Development and performance evaluation of natural thermal-insulation materials composed of renewable resources. Energ. Buildings 43(9), 2518-2523. https://doi.org/10.1016/j.enbuild.2011.06.012.

Li, W.D. and Ding E.Y., 2007. Preparation and Characterization of Poly(ethylene terephthalate) Fabrics Treated by Blends of Cellulose Nanocrystals and Polyethylene Glycol. J. Appl. Polym., 105, 373-378. https://doi.org/10.1002/app.26098.

Mariod A.A., 2018. Chemical Properties of Gum Arabic in: Mariod A.A. (Ed), Gum Arabic_Structure, Properties, Application and Economics. Academic press, United Kingdom, pp. 113-123.

Martellotta, F., Cannavale, A., De Matteis, V., Ayr, U., 2018. Sustainable sound absorbers obtained from olive pruning wastes and chitosan binder. Appl. Acoust. 141, 71-78. https://doi.org/10.1016/j.apacoust.2018.06.022.

Mati-Baouche, N., Elchinger, P.-H., de Baynast, H., Pierre, G., Delattre, C., Michaud, P., 2014a. Chitosan as an adhesive. Eur. Polym. J60, 198-212. https://doi.org/10.1016/j.eurpolymj.2014.09.008.

Mati-Baouche, N., de Baynast, H., Lebert, A., Sun, S., Sacristan Lopez-Mingo, C.J., Leclaire, P., Michaud, P., 2014b. Mechanical, thermal and acoustical characterizations of an insulating bio-based composite made from sunflower stalks particles and chitosan. Ind. Crop. Prod. 58, 244-250. https://doi.org/10.1016/j.indcrop.2014.04.022.

Mati-Baouche, N., de Baynast, Michaud, P., Dupont, T., Leclaire, P., 2016. Sound absorption properties of a sunflower composite made from crushed stem particles and from chitosan bio-binder. Appl. Acoust. 111, 179-187. https://doi.org/10.1016/j.apacoust.2016.04.021.

Mohamed, A., M., Ariffin, M., A., M., Smaoui, H., Osman, M., H., 2020. Performance evaluation of concrete with Arabic gum biopolymer. Mater. Today, In press. https://doi.org/10.1016/j.matpr.2020.04.576.

Mochizuki, M. and Matsunaga, N., 2016. Bicomponent Polyester Fibers for Non-wovens, in: The society of fiber science and techno, Japan (Ed), High-performance and specialty fibers: concepts, technology and modern applications of man-made fibers for the future, Springer, Tokyo, pp. 395-408.

Naeimirad, M., Zadhoush, A., Kotek, R., Neisiany, R.E., Khorasani, S.N., Ramakrishna S., 2018. Recent advances in core/shell bicomponent fibers and nanofibers: A review. J. Appl. Polym. 135 (21), 46265. https://doi.org/10.1002/app.46265.

Neto, C.G.T., Giacometti, J.A., Job, A.E., Ferreira, F.C., Fonseca, J.L.C., Pereira, M.R., 2005. Thermal analysis of chitosan based networks. Carbohydr. Polym. 62, 97-103. doi: https://10.1016/j.carbpol.2005.02.022.

Nilsen-Nygaard, J., Strand, S.P., Vårum, K.M., Draget, K.I., Nordgård, C.T., 2015. Chitosan: gels and interfacial properties. Polymers 7, 552-579. https://doi:10.3390/polym7030552.

Osman, B.I., Hussein, M.A., Elfatih A. Hassan, Mohamed E. Osman, Mahiran Basri, 2006. Gravimetric and calorimetric analysis of some sudanese acacia exudate gums, in: Mariod A.A. (Ed), Gum Arabic_Structure, Properties, Application and Economics.

Academic press, United Kingdom, pp 171-190.

Pielesz, A., Freeman, H.S., Wesełucha-Birczyńska, A., Wysocki, M., Włochowicz, A., 2003. Assessing secondary structure of a dyed wool fibre by means of FTIR and FTR spectroscopies. J. mol. Struct. 651, 405-418. https://doi.org/10.1016/S0022-2860(03)00210-2.

Pourmohammadi, A., 2006. Thermal bonding in: Russell, S.J. (Ed), Handbook of nonwovens. Woodhead Publishing, England, pp. 298-329.

Tridico, S.R. 2009. Natural animal textile fibers: Structure, characteristics and identification, in: Houck, M.M. (Ed), Identification of Textile Fibers. Woodhead Publishing in Textiles, New York, pp. 27-67.

Verbeken D, Dierckx S, Dewettinck, 2003. Exudate gums: occurrence, production, and applications. Appl. Microbiol. Biotechnol., 63(1): 10–21. https://doi.org/10.1007/s00253-003-1354-z.

Wunderlich, B, 1980. Macromolecular physics, volume 3 - crystal melting. Academic press, New York.

Wojciechowska, E., Rom, M., Włochowicz, A., Wysocki, M., Wesełucha-Birczyńska, A., 2004. The use of Fourier transform-infrared (FTIR) and Raman spectroscopy (FTR) for the investigation of structural changes in wool fibre keratin after enzymatic treatment. J. Mol. Struct., 704 (1-3), 315-321. https://doi.org/10.1016/j.molstruc.2004.03.044.

Zach, J., Slávik, R., Novák, V., 2016. Investigation of the process of heat transfer in the structure of thermal insulation materials based on natural fibers. Procedia Eng. 151, 352-359. https://doi.org/10.1016/j.proeng.2016.07.389.

Zargarkazemi, A., Sadeghi-Kiakhani, M., Arami, M., Bahrami, S.H., 2015. Modification of wool fabric using prepared chitosan-cyanuric chloride hybrid. J Text I 106 (1), 80-89. https://doi.org/10.1080/00405000.2014.906097.

Zhang, W., Yi, X., Sun, X., Zhang, Y., 2008. Surface modification of non-woven poly (ethylene terephthalate) fibrous scaffold for improving cell attachment in animal cell culture. J. Chem. Technol. Biotechnol., 83, 904-911. https://doi.org/10.1002/jctb.1890.

Zhao, C, Zhao, Q., Zhang, Y., Zhou M., 2015. The Effect of Gum Arabic on the Dispersion of Cement Pastes. In: Dong F. (Eds) Proceedings of the 11th International Congress for Applied Mineralogy (ICAM). Springer, Cham.

Chapter 3

Measurement methods and data analysis

This chapter partially reports material from:

- Rubino, C., Bonet Aracil, M., Liuzzi, S., Stefanizzi, P. and F. Martellotta, 2021. *Wool waste used as sustainable non-woven for building applications*. J. Clean. Prod. 278, 123905. https://doi.org/10.1016/j.jclepro.2020.123905.
- Rubino, C., Bonet-Aracil, M., Gisbert-Payá, J., Liuzzi, S., Zamorano Cantó, M., Martellotta, F., Stefanizzi, P., 2019. *Composite eco-friendly sound absorbing materials made of recycled textile waste and biopolymers*. Materials 12 (23), 4020. https://doi.org/10.3390/ma12234020.

An experimental investigation was carried out with the aim of testing the behaviour of the produced woolen building materials as thermal insulators and sound absorbing non-wovens. For this purpose, the Chapter illustrates the standardized procedures useful for measuring the thermal properties (i.e. the thermal conductivity, the thermal diffusivity, and the volumetric heat capacity) and the hygric ones (i.e. the water vapour permeability and the water vapour diffusion resistance factor). The experimental methods followed to measure the acoustic parameters (i.e. the sound absorption coefficients) and the non-acoustic parameters (i.e. the porosity, the tortuosity and the air flow resistivity) are explained. Furthermore, the Chapter describes the standard procedure to evaluate the fire resistance behaviour of the tested samples.

Each measurement result is given together with its uncertainty value expressed as the standard deviation of the mean. About this, the Chapter reports some indications about the approach chosen for determining the measurement uncertainty which express the quality of the experimental results.

Lastly, the statistical inference is discussed as method of comparison for drawing valid conclusions on the sample data collected in the laboratory.

3.1 Measurements set-up and procedures

To achieve a satisfactory quality of buildings it is necessary to consider a set of aspects that are interconnected and influence each other. The choice of an adequate wall layers structure should increase the thermal and acoustic building performances, guaranteeing its energy efficiency as well as its sustainability. Thus, an experimental program was planned to measure the behavior of the tested materials as thermal insulators and sound absorbing non-wovens.

Usually, referring to building materials, their hygrothermal behaviour is defined as the simultaneous and inter-dependent occurrence of absorption and release of heat, and absorption and release of vapour (Hall, 2010(a)). For this reason, the thermal properties (i.e. thermal conductivity λ, thermal diffusivity D, and specific heat capacity c) and the hygric properties (i.e. water vapour permeability δ and water vapour diffusion resistance factor μ) of the studied materials were experimentally evaluated. Furthermore, their sound absorption efficiency was analyzed measuring the normal incidence sound absorption coefficients α_n.

Both the hygrothermal and the acoustic performances of building materials are strongly affected by their macroscopic (or non-acoustic) properties. Thus, the bulk porosity ε, the tortuosity τ and the airflow resistance σ_s were measured in laboratory.

The heat or vapour transfer in a porous medium can be attributed to a wide range of parameters such as the total volume of void space (i.e. bulk porosity); the complex spatial connectivity of the pores, including their irregular shape and their non-uniform distribution (i.e. the tortuosity); as well as minor factors such as the roughness of void interior surfaces. For example, tortuosity values greater than one result in long flow paths and turbulence due to increased changes in flow direction and variation in voids diameters which prevent the passage of heat and steam through the material (Hall, 2010(b)).

Similar considerations could be valid for sound which travels through a porous medium. The sound absorption occurs in the network of interconnected pores as a consequence of viscous and thermal effects that cause the dissipation of the acoustic energy. Sound velocity and attenuation in fibrous materials are determined by their air flow resistance which depends on the fibers morphology, size, and arrangements. The air flow resistance reflects the air permeability of a porous material (high airflow resistance value is an

indication of the low permeability of the material) and is usually referred to a unit material thickness, obtaining the air flow resistivity σ.

The behavior of materials under fire may be responsible of serious safety issues. Several studies (Stamyr et al., 2012) proved that toxic fumes are the most important causes in fire deaths. For this reason, the fire resistance behaviour of the prepared samples was tested paying attention to the possible smoke or droplets production.

3.1.1 Thermal properties

The thermal insulation properties of the all prepared mix were experimentally investigated by means of the transient plane source device Isomet 2104 (Applied Precision Ltd). The advantage of this technique is the possibility to perform rapid measurements on relatively small samples.

(a) (b)

Figure 3.1. Samples (a) and apparatus for testing thermal properties (b).

The tests were carried out at laboratory conditions of 21±2 °C and 45±5% RH, after oven drying the specimens (10 cm diameter and 5 cm tick) to constant mass at 105°C. Thermal conductivity λ, thermal diffusivity D, and volumetric heat capacity ρc were provided from the analysis of the temperature response of the material as a consequence of an heat flow impulse (Log and Gustafsson, 1995). The heat flow was induced by electrical heating of the resistor inserted in the surface probe in direct contact with the tested specimen (Figure 3.1). The error in the measurement of thermal conductivity, thermal

diffusivity, and volumetric heat capacity is estimated to be within 4%, 5%, and 7%, respectively (Bouguerra et al., 2001). The specific heat capacity *c* was calculated from the measured volumetric heat capacity and bulk density.

3.1.2 Hygric properties

The water vapour diffusion behaviour of the prepared samples was determined according to the EN 12086 (2013). The dry cup method was followed. The 1 cm thick cylindrical samples were wax sealed on the top of PVC cups in which a relative humidity of 0÷4% was set by using a calcium chloride desiccant (Figure 3.2(a)). The assemblies were then conditioned in the Angelantoni DY340 climatic chamber (Figure 3.2(b)) at relative humidity of 50% and 23 °C and were daily weighed by a Mettler Toledo PB3002 (±0.01 g accuracy).

(a) (b)

Figure 3.2. Specimens sealed on the top of PVC cups (a) and their conditioning in the climatic chamber (b).

The mass variations of the cups were recorded until mass rate change *G* stabilization. The mass rate change was determined by plotting mass gain versus time. This was in order to calculate the water vapour permeance *W* which represents the ability of the different materials to transfer moisture due to a vapour pressure gradient ΔP between the two specimen faces.

$$W = \frac{G}{A \cdot \Delta P} \quad [3.1]$$

where A is the exposed area of the sample.

Thus, the water vapour permeability δ and the water vapour diffusion resistance factor μ which are the commonly properties used to characterize the hygric behaviour of a building materials, were calculated as follows:

$$\delta = W \cdot d \quad [3.2]$$

$$\mu = \frac{\delta_{air}}{\delta} \quad [3.3]$$

where d is the sample thickness and δ_{air} is the water vapour permeability of air.

The term $\delta_{air} = 1.95 \cdot 10^{-11}\ \mathrm{kg/(m \cdot s \cdot Pa)}$ was calculated according to the Schimer's formula:

$$\delta_{air} = \frac{0.083}{R_D \cdot T} \cdot \frac{P_0}{P} \cdot \left(\frac{T}{273}\right)^{1.81} \quad [3.4]$$

where $R_D = 462 \cdot 10^{-8}\ Nm/(mg \cdot K)$ is the gas constant of water vapour, T is the test temperature, P and P_0 are respectively the air pressure and the test pressure.

3.1.3 Acoustic properties

The normal incidence sound absorption coefficients α_n were measured by means of a two microphones impedance tube, usually referred as Kundt's tube. According to ISO 10534-2 (1998), the transfer function method was performed to acquire the pressures produced by the sound source at two fixed microphones positions on the tube wall. A plane wave propagates down the tube before reflecting from the sample. The impedance of the sample alters how sound is reflected and, by measuring the resulting pressure, it is possible to calculate the normal incidence absorption coefficients. The combination of measurement results derived from two different tube configurations (of different diameters and length) allowed to obtain the absorption coefficients in a wide frequency range (125 Hz ÷ 5000 Hz). Each configuration consisted of two methacrylate parts: a tube with built-in loud speaker and a sample holder (Figure 3.3). The first configuration considered the use of tubes with 10 cm inner diameter, with two different microphone spacing equal to 6 cm and 20 cm, respectively characterized by a low frequency limit of 400 and 50 Hz. The second configuration is the same used for flow resistance measurements and involved the use of two tubes with 4 cm inner diameter. In this case, the microphone spacing was 3 cm

resulting in a frequency range spanning between 200 Hz and 5 kHz. The whole system was controlled by a Matlab® graphic user interface which generated and played a 5 s linear sweep from 70 Hz to 3 kHz, used in combination with the largest tube, and from 500 Hz to 5 kHz in combination with the smallest tube.

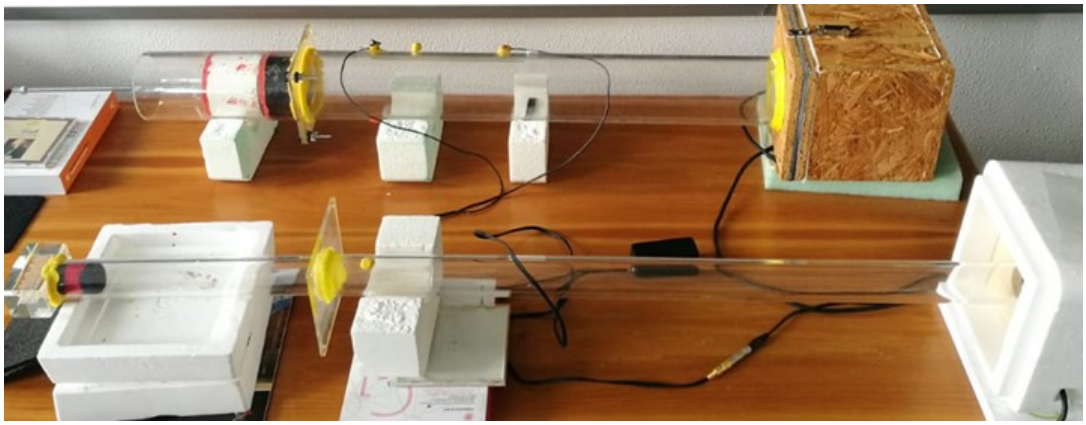

Figure 3.3. Standing wave tubes used for sound absorption at low and medium frequencies (top), and at high frequencies (bottom).

3.1.4 Non-acoustic properties

According to ASTM D4892 (2019), the true density ρ_{true} of the specimens was measured by a ULTRAPYC 1200-e Quantachrome Helium gas Pycnometer (Figure 3.4(a)) in order to determine the open bulk porosity ε as follows:

$$\varepsilon = 1 - \frac{\rho_{bulk}}{\rho_{true}} \quad [3.5]$$

where ρ_{bulk} is the bulk density value, based on the geometrical volume V_{tot} of the sample and including pores and interparticle voids which characterized the matrix of the tested material.

The pycnometer is equipped with two chambers of known volume (a sample holder with volume V_1 and a reference chamber with volume V_2) connected in series to the helium source. The true volume V_{true}, i.e. the volume of the sample excluding the volume V_{pores} of any open pores, was provided by the pycnometer after recording the pressure measured when the gas was allowed to expand into the holder containing a 4 cm diameter sample (P_1), and when the same amount of gas was allowed to expand into the reference empty chamber (P_2):

$$V_{true} = V_1 + \frac{V_2}{1 - \frac{P_1}{P_2}} \quad [3.6]$$

Then, the true density ρ_{true} excluding pores and interparticle voids was calculated as follows:

$$\rho_{true} = \frac{m}{V_{tot} - V_{pores}} = \frac{m}{V_{true}} \quad [3.7]$$

where m is the mass of the sample.

For a non-conducting porous absorber, the tortuosity can be measured following a method proposed by Brown (1980), based on an electroacoustic analogy. According to Pfretzschner and Rodriguez (1999), cylindrical samples 4 cm thickness were soaked in a 10% copper sulfate solution ($CuSO_4$) for 24 hours and the electrical resistivity R_0 was determined after applying them an electrical current with a voltage variable from 1 to 8 voltage (Figure 3.4(b)). The electrical resistivity of the conducting fluid R_W was also measured. The tortuosity was given by:

$$\tau = \varepsilon \cdot \frac{R_0}{R_w} \quad [3.8]$$

where ε is the bulk porosity of the sample.

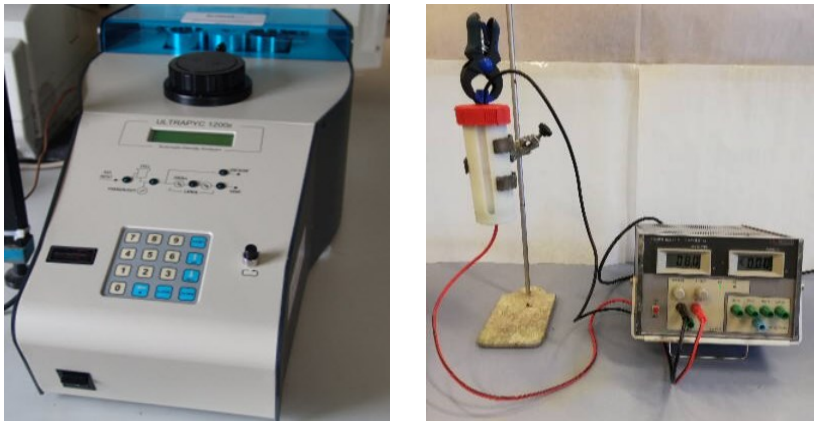

(a) (b)

Figure 3.4. Helium pycnometer for porosity measurement(a) and apparatus for tortuosity measurement (b).

The air flow resistance σ_s of the investigated materials was experimentally evaluated according to the method proposed by Ingard and Dear (1985). Although this procedure

could not be considered as steady as the standardized approach, del Rey et al. (2013) proved that it was scientifically accurate when adopted for thin or scarcely resistive samples, as occurs in the present research.

The measurement set up consisted in two methacrylate tubes of 4 cm inner diameter and 85 cm long, between which the tested sample was adjusted. The tube had two different terminations: a 5 cm loudspeaker (Visaton FRS 5) with a frequency response spanning from 150 Hz to 20 kHz at one end and a rigid termination made by 5 cm thick methacrylate at the other end. The pressure drop of the fluid flow through the sample was extrapolated by acoustic measurements carried out using two microphones (Core Sound) with a flat frequency response from 20 Hz to 20 kHz and properly calibrated in amplitude and phase. The microphones were excited using an exponential sine sweep and located in front of the sample and in front of the rigid termination end.

3.1.5 Fire resistance properties

An ignitability test was carried out, as far as possible according to ISO 11925-2 (2010). The major non-standard compliant element was represented by the shape and dimension of the sample that, for this batch, was only produced in cylindrical molds having 10 cm diameter and 5 cm thickness. Thus, an “edge exposed” test was carried out, with a 15 s flame application, on two different samples of the selected typology. A reference sample, made of pressed wool fibers (3 cm thick) was used as a reference for comparison purposes.

3.2 Analysis of uncertainty in measurement

When reporting the result of a measurement of a physical quantity, it is recommended to provide some quantitative indication of the quality of the result in order to assess its reliability. Without such information, measurement results cannot be compared, either among themselves or with reference values given in a specification or a standard.

The procedure chosen for characterizing the quality of the measurement results of the present research study is the approach commonly referred to as “GUM”. The Guide to the expression of Uncertainty in Measurements (GUM) presents a widely applicable method for evaluating and expressing uncertainty in measurements (ISO/IEC Guide 98-3, 2008).

In general, a measurement has imperfections that give rise to an error in the result. Traditionally, an error is viewed as having two components: a random component due to

the random variations of the observations and a systematic component due to a recognized effect of an influence quantity on a measurement result. Being the exact values of the contributions to the error unknown and unknowable, the uncertainties *u* associated with the random and systematic effects that give rise to the error can be evaluated. If uncertainty is referred to repeated measurement results, it is evaluated by the application of standard statistical methods to a series of the observations. Particularly, when there are *n* observations of the same variable *Y* (i.e. the measurand), it would be possible to determine the mean *y* of the *n* values (which is regarded as the "best estimate") and the standard deviation of the mean (referred to in many textbooks as the "standard error of the mean") (Kirkup, 2002). The standard deviation of the mean is referred to in GUM as "standard uncertainty obtained by a type A evaluation" and it is used in this research work to better express the quality of the experimental results.

Supposing that *y* is an estimate of the value of a particular quantity *Y* and it is calculated using estimates x_1, x_2, …, x_n of the values of quantities X_1, X_2, …, X_n, respectively, the relationship between *Y* and X_1, X_2, …, X_n is written most generally as $Y = f(X_1, X_2, \dots, X_n)$. It is commonplace to calculate a combined standard uncertainty u_c of *y* in which the uncertainties of various quantity x_1, x_2, …, x_n are brought together:

$$u_c(y) = \sqrt{\sum_{i=1}^{n} \left(\frac{\partial f}{\partial x_i} \cdot u(x_i) \right)^2} \qquad [3.9]$$

where the partial derivatives $\frac{\partial f}{\partial x_i}$ are equal to $\frac{\partial f}{\partial X_i}$evaluated at $X_i = x_i$, $u(x_i)$ is the standard uncertainty of x_i obtained through type A evaluations.

3.3 The statistical inference as method of comparison

Every data analysis begins with their exploration and illustration using numerical and graphical summaries which are the base of the descriptive statistic. Often, the ultimate purpose of an experimental research project is a statistical investigations aimed to go beyond a set of data, generalizing the information contained in random samples to the population to which the samples belong. This part of the statistic theory is known as statistical inference and its goal is the knowledge of the parameters that characterize a specific population. The estimation of the exactly true values of these parameters is

subjected to sampling uncertainty. Thus, the mostly chosen language to make an inference from a sample to a population is the probability theory, particularly the "interval estimation" and the "hypothesis testing". Although the differences between these two procedures, there is a very close connection between them (Miller and Freund, 1985).

The interval estimation consists in identifying an interval which contains the true value of the parameter of interest with a reasonable degree of certainty. An interval of this kind is referred as a confidence interval having $(1-\alpha)\cdot 100\%$ degree of confidence and its endpoints confidence limits are obtained used sample data.

Hypothesis testing uses data obtained from a sample to decide whether to accept or reject a statement about the parameter of one population. Particularly, the null hypothesis H_0 is the hypothesis under test which specifies an exact value of the parameter and the alternative hypothesis H_a will be accepted in case of rejection of the null one. The decision to accept or reject H_0 statement is a result of the comparison between the test statistic and the critical value. The test statistic is obtained from sample data, assuming the null hypothesis is true; whereas the critical value is determined by statistical software or tables, depending on the stated significance level and the sampling distribution. Rejecting the null hypothesis H_0 when it is true is defined as a type I error, also known as significance level α. The construction of testing criteria involves the choose between a one-tailed or two-tailed method. In both cases, the critical value is the cutoff between retaining or rejecting the null hypothesis as it distinguishes the acceptance area (i.e. the white region of the bell curves in Figure 3.5) to the critical one (i.e. the blue region of the bell curves in Figure 3.5).

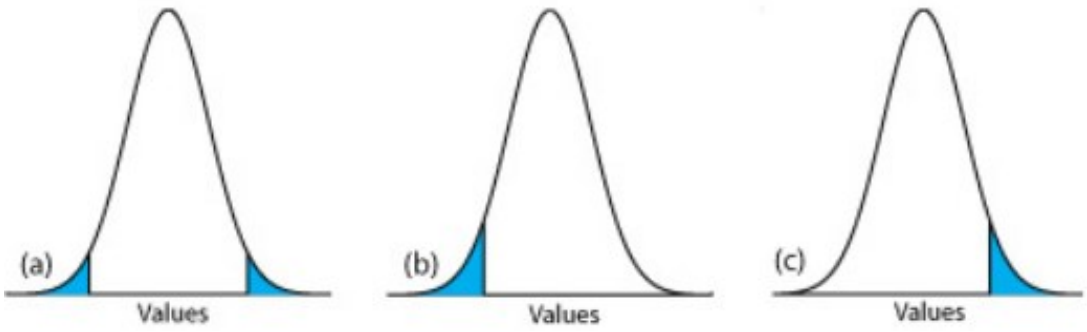

Figure 3.5. Difference between two tailed and one tailed significance tests (Source: https://community.asdlib.org/imageandvideoexchangeforum/files/2013/07/Figure4.13.jpg).

When a two-tailed test is performed, half of α is allotted to test the statistical significance in one direction and half to test statistical significance in the other direction. This means that the null hypothesis is rejected if the test statistic value is either in the lower tail or in the upper one (Figure 3.5(a)), resulting larger than the absolute critical value. For a negative one-tailed test, the null hypothesis is rejected if the test statistic value is smaller than the critical one or is in the lower tail (Figure 3.5(b)); whereas for a positive one-tailed test, the null hypothesis is rejected if the test statistic value is larger than the critical one or is in the upper tail (Figure 3.5(c)).

Usually, the significance level α is set to 0.05. This allows to identify a confidence interval which contains the hypothesized parameter with 95% degree of certainty and a hypothesis test with 5% probability of rejecting the null hypothesis if it is true.

3.3.1 The *t*-distribution

The most frequent eventuality when a researcher collects laboratory data is that the sample size n is small and population variance S^2 (i.e. the measure of how far a set of data is spread out) and population mean M are unknown. In this case, the *t*-distribution (usually refers as Student's *t*-distribution) instead of the standard normal distribution is considered to compute the statistical analysis.

The *t* distribution was introduced in 1908 by William Sealy Gosset, better known by his pseudonym "Student", who claimed that when the number of experiments is small, there could be two source of uncertainty: the mean of the experiments can deviate more or less widely from the mean of the population and the sample size is not sufficiently large to determine what is the law of distribution of individuals (Student, 1908). Thus, in order to determine the probability that the mean of the population lies within a given distance of the mean of the sample, a *t*-statistic t_M, following a *t*-distribution, was introduced:

$$t_M = \frac{\widehat{M} - M}{\frac{\hat{S}}{\sqrt{n}}} \qquad [3.10]$$

where M is the population mean and $\widehat{M}$, n and $\hat{S}$ are respectively the mean, the size and the standard deviation of the samples.

The *t*-distribution is similar to the standard normal distribution with the difference of

using the sample standard deviation instead of the population standard deviation to calculate $\hat{S}/\sqrt{n}$ standard error of $\widehat{M}$. This makes the statistic t_M following a *t*-distribution with $(n-1)$ degrees of freedom. In Figure 3.6, the shapes of *t*-distribution for different degrees of freedom are related with the normal distribution shape. As it can be observed, when the sample size increases, the *t*-distribution becomes more similar to a normal distribution and, above 30 degrees of freedom, roughly matches the normal one. Furthermore, the *t*-distribution has heavier tails which result in more probability. However, both curves are symmetric and unimodal and the maximum ordinate value is reached when the mean is equal to zero (Montgomery et al., 2002).

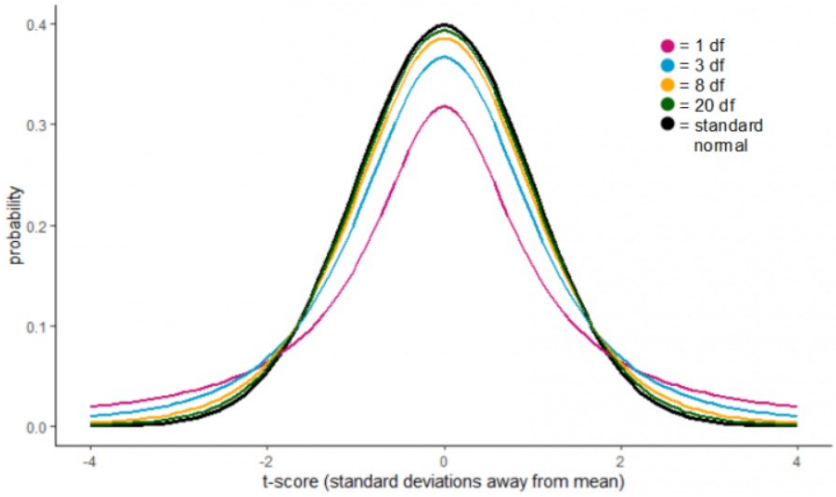

Figure 3.6. Probability density as function of t-score for the normal distribution and the t-distributions for different degrees of freedom (df) (Source: https://cdn.scribbr.com/wp-content/uploads/2020/08/t_distribution_comparisons-768x448.png).

3.3.2 Use of *t*-distribution for a difference in means

According to Andrade and Estévez-Pérez (2014), the "two samples *t*-test" is the most frequently method used to compare the means of two data sets sampled from two different populations and to evaluate the significance of this difference. Let be n_1 and n_2 the sizes of two independent data sets coming from normal populations with unknown means M_1 and M_2 and unknown variances S_1^2 and S_2^2, the simultaneously estimation of these parameters it could be difficult due to the very limited number of laboratory experimental data. Thus, common practice involves the application of the two samples Student's *t*-test, assuming that both data groups are sampled from populations with equal variances $S_1^2 = S_2^2 = S^2$

(i.e. homoscedasticity assumption). Being $\widehat{S_1^2}$ and $\widehat{S_2^2}$ the sampling variances estimating the same quantity S^2, it seems reasonable to combine them in a weighted average estimator S_{pool}:

$$S_{pool} = \frac{(n_1 - 1) \cdot \widehat{S_1^2} - (n_2 - 1) \cdot \widehat{S_2^2}}{(n_1 + n_2 - 1)} \quad [3.11]$$

The null hypothesis $H_0: M_1 - M_2 = 0 \leftrightarrow M_1 = M_2$ is tested against to the alternative one $H_a: M_1 - M_2 \neq 0 \leftrightarrow M_1 \neq M_2$ and, after choosing the significance level α, the *t*-statistic is computed as follows:

$$t_{M_1 - M_2} = \frac{\left(\widehat{M_1} - \widehat{M_2}\right) - (M_1 - M_2)}{S_{pool} \cdot \sqrt{\frac{1}{n_1} + \frac{1}{n_2}}} \quad [3.12]$$

where $\widehat{M_1}$ and $\widehat{M_2}$ are the means of the two data sets.

The *t*-statistic value is compared with the *t*-critical one and the null hypothesis is rejected if $\left|t_{M_1 - M_2}\right| > t_{\alpha/2, n_1 + n_2 - 2}$, being $t_{\alpha/2, n_1 + n_2 - 2}$ the *t*-critical value with $(n_1 + n_2 - 2)$ degrees of freedom, when a two-tailed test is performed.

The equality of the population variances is verified by the Fisher–Snedecor's *F*-test. It is an hypothesis test with the aim of comparing the standard deviations of two sample groups and checking their variability. Being $\widehat{S_1^2}$ and $\widehat{S_2^2}$ the variances of two independent random data sets sampled from two normal populations with variances S_1^2 and S_2^2, the test consists of calculating the *F*-statistic value following an *F*-distribution with $(n_1 - 1)$ numerator degrees of freedom and $(n_2 - 1)$ denominator degrees of freedom:

$$F_{M_1 - M_2} = \frac{\widehat{S_1^2} / S_1^2}{\widehat{S_2^2} / S_2^2} \quad [3.13]$$

The null hypothesis $H_0: S_1^2 = S_2^2$ is rejected with respect to the alternative one $H_a: S_1^2 \neq S_2^2$ if $F_{M_1 - M_2} > F_{\alpha, n_1 - 1, n_2 - 1}$, being $F_{\alpha, n_1 - 1, n_2 - 1}$ the *F*-critical value with $(n_1 - 1)$ numerator degrees of freedom and $(n_2 - 1)$ denominator degrees of freedom, when a one-tailed test is performed (Montgomery et al., 2002).

3.3.3 Use of *t*-distribution in linear regression model

The linear regression technique attempts to model the relationship between two variables, i.e. the dependent variable *Y* and the independent variable *x*, by fitting a linear equation to observed data. The best-fitting line is calculated by minimizing the sum of the squares of the vertical deviations of each data point to the line. Thus, the least-squares regression line $\hat{Y} = \widehat{\beta_0} + \widehat{\beta_1}x + \hat{e}$ is obtained. The latter equation represents an estimation of the population true regression line $Y = \beta_0 + \beta_1 x + e$ which describes how the mean response *Y* changes with *x*.

An important step to assess the adequacy of a linear regression model is testing statistical hypotheses about the model parameters identifying certain confidence intervals. According to Ortiz et al. (2009), it is possible to conduct the hypothesis *t*-test to determine whether there is a significant linear relationship between the independent variable *x* and the dependent variable *Y*. The test focuses on the slope of the regression line and consists in assuming a two-sided alternative, verifying the null hypothesis $H_0: \beta_1 = 0$ versus the alternative hypothesis $H_a: \beta_1 \neq 0$. If there is a significant linear relationship between the two variables *x* and *Y*, the slope will not equal zero and the null hypothesis will be rejected. After choosing the significance level α, the *t*-statistic t_{β_1} following $(n-2)$ degrees of freedom is computed:

$$t_{\beta_1} = \frac{\widehat{\beta_1} - \beta_1}{S_{\widehat{\beta_1}}} \qquad [3.14]$$

where $\widehat{\beta_1}$ and β_1 are respectively the slope of the regression line of the sample and of the population, and $S_{\widehat{\beta_1}}$ is the standard error of the sample regression slope which represents the average distance that the observed values deviate from the regression line.

Thus, the *t*-statistic value is compared with the *t*-critical one and the null hypothesis is rejected if $\left|t_{\beta_1}\right| > t_{\alpha/2,n-2}$, being $t_{\alpha/2,n-2}$ the *t*-critical value with $(n-2)$ degrees of freedom, when a two-tailed test is performed.

In addition to the analysis of the slope, it is important to estimate the confidence interval of the regression line in order to evaluate the overall quality of the model. A (1-α)·100% confidence interval about the mean response *Y* for $x = x_0$ is computed as follows:

$$\hat{Y} - t_{\alpha/2,n-2} \cdot \sqrt{\widehat{S_{yx}^2} + \frac{1}{n} + \frac{(x_0 - x_m)^2}{\sum_{i=1}^{n}(x_i - x_m)^2}} < Y < \hat{Y} + t_{\alpha/2,n-2} \cdot \sqrt{\widehat{S_{yx}^2} + \frac{1}{n} + \frac{(x_0 - x_m)^2}{\sum_{i=1}^{n}(x_i - x_m)^2}} \quad [3.15]$$

where $t_{\alpha/2,n-2}$ is the *t*-critical value with $(n-2)$ degrees of freedom when a two-tailed test is performed; $\sqrt{\widehat{S_{yx}^2} + \frac{1}{n} + \frac{(x_0 - x_m)^2}{\sum_{i=1}^{n}(x_i - x_m)^2}}$ is the standard error of the fit which depends on the variance of the estimated residual error $\widehat{S_{yx}^2}$, on the sample size *n*, on how far in squared units the estimated value x_0 is from the average of the estimated values x_m or $(x_0 - x_m)^2$ and on the sum of the squared distances of the estimated values x_i from the average of the estimated values x_m or $\sum_{i=1}^{n}(x_i - x_m)^2$. The term $\widehat{S_{yx}^2} = \frac{\sum_{i=1}^{n}(y_i - y_m)^2}{n-2}$ represents the population regression variance in which the numerator indicates how far each response is from its estimated mean and the denominator divides the sum by $(n-2)$ degrees of freedom because two parameters (i.e. β_0 and β_1) are unknown Ortiz et al. (2009).

Assuming two independent sets of data of size n_1 and n_2, sampled from two normal population, it's possible to compare the corresponding two population regression lines $Y_1 = \beta_{0_1} + \beta_{1_1}x + e_1$ and $Y_2 = \beta_{0_2} + \beta_{1_2}x + e_2$ applying a Student's *t*-test statistic similar to Equation [3.14] and verifying the null hypothesis $H_0: \beta_{1_1} - \beta_{1_2} = 0 \leftrightarrow \beta_{1_1} = \beta_{1_2}$ (Andrade and Estévez-Pérez, 2014). As a consequence of the difficult simultaneous estimation of the unknown regression parameters β_0 and β_1, the equality of the residual variances of the two population is assumed ($S_{yx_1}^2 = S_{yx_2}^2 = S_{yx}^2$). Being $\widehat{S_{yx_1}^2}$ and $\widehat{S_{yx_2}^2}$ the sampling residual variances which estimate the same quantity represented by the populations residual variance S_{yx}^2, it seems reasonable to combine them in a unique estimator $S_{yx,pool}^2$ which is a weighted average of the two sample variances:

$$S_{yx,pool}^2 = \frac{(n_1 - 2) \cdot \widehat{S_{yx_1}^2} - (n_2 - 2) \cdot \widehat{S_{yx_2}^2}}{(n_1 + n_2 - 4)} \quad [3.16]$$

Therefore, after choosing the significance level α, the *t*-statistic $t_{\beta_{1_1} - \beta_{1_2}}$ is computed as follows:

$$t_{\beta_{1_1}-\beta_{1_2}} = \frac{\left(\widehat{\beta_{1_1}} - \widehat{\beta_{1_2}}\right) - \left(\beta_{1_1} - \beta_{1_2}\right)}{\sqrt{S^2_{yx,pool} \cdot \left(\frac{1}{\sum_{x=1}^{n_1}\left(x_{i_1} - x_{m_1}\right)^2} + \frac{1}{\sum_{x=1}^{n_2}\left(x_{i_2} - x_{m_2}\right)^2}\right)}} \qquad [3.17]$$

where $\widehat{\beta_{1_1}}$, $\widehat{\beta_{1_2}}$ and β_{1_1}, β_{1_2} are respectively the regression lines slopes of the two samples and of the two populations; whereas $\sum_{x=1}^{n_1}\left(x_{i_1} - x_{m_1}\right)^2$ and $\sum_{x=1}^{n_2}\left(x_{i_2} - x_{m_2}\right)^2$ are the sum of the squared distances of the estimated values x_i from the average of the estimated values x_m ,respectively from the data sets of size n_1 and n_2.

The *t*-statistic value is compared with the *t*-critical one and the null hypothesis it could be rejected if $\left|t_{\beta_{1_1}-\beta_{1_2}}\right| > t_{\alpha/2,n_1+n_2-4}$, being $t_{\alpha/2,n_1+n_2-4}$ the *t*-critical value with $(n_1 + n_2 - 4)$ degrees of freedom when a two-tailed test is performed.

As previously anticipated, the equality of the residual regression variances $S^2_{yx_1}$ and $S^2_{yx_2}$ of the two populations was assumed and verified using the *F*-test. For this purpose, the ratio of the estimated residual variances $\widehat{S^2_{yx_1}}$, and $\widehat{S^2_{yx_2}}$ is calculated to obtain the *F*-statistic $F_{\beta_{1_1}-\beta_{1_2}}$ value which has an F_{n_1-2,n_2-2} distribution. The null hypothesis is rejected if $F_{\beta_{1_1}-\beta_{1_2}} > F_{\alpha,n_1-2,n_2-2}$ being F_{α,n_1-2,n_2-2} the *F*-critical value with $(n_1 - 2)$ numerator degrees of freedom and $(n_2 - 2)$ denominator degrees of freedom when a one-tailed test is performed (Montgomery et al., 2002).

References

Andrade, J.M. and Estévez-Pérez, M.G., 2014. Statistical comparison of the slopes of two regression lines: A tutorial. Anal. Chim. Acta 838, 1-12. http://dx.doi.org/10.1016/j.aca.2014.04.057.

ASTM D4892 – 14, 2019. Standard Test Method for Density of Solid Pitch (Helium Pycnometer Method). https://www.astm.org/Standards/D4892.htm, (Accessed October 2020).

Bouguerra, A., Aït-Mokhtar, A., Amiri, O., Diop, M.B., 2001. Measurement of thermal conductivity, thermal diffusivity and heat capacity of highly porous building materials using transient plane source technique. Int. Commun. Heat Mass 28, 1065–1078. https://10.1016/S0735-1933(01)00310-4.

Brown, R.J.S., 1980. Connection between formation factor for electrical resistivity and fluid-solid coupling factors in Biot's equations for acoustic waves in fluid filled porous media. Geophysics 45 (8), 1269e1275. https://doi.org/10.1190/1.1441123.

Del Rey, R.; Alba, J.; Arenas, J.P.; Ramis, J., 2013. Evaluation of two alternative procedures for measuring air flow resistance of sound absorbing materials. Arch. Acoust. 38 (4), 547–554. https://doi.org/10.2478/aoa-2013-0064.

EN 12086, 2013. Thermal Insulating Products for Building Applications Determination of Long Term Water Absorption by Diffusion. http://store.uni.com/catalogo/uni-en-12088-2013. (Accessed April 2020).

Hall, M.R., 2010(a). Hygrothermal materials for heat and moisture control in buildings. In: Hall, M.R. (Ed.), Material for energy efficiency and thermal comfort in building. Woodhead publishing limited, Oxford., pp. 345-364.

Hall, M.R., Allinsons, D., 2010(b). Heat and mass transport processes in building materials, in: Hall, M.R. (Ed.), Material for energy efficiency and thermal comfort in building. Woodhead publishing limited, Oxford., pp. 1-53.

ISO 10534-2, 1998. Acoustics e determination of sound absorption coefficient and impedance in impedance tubes-Part 2: Transfer-function method. https://www.iso.org/standard/22851.html. (Accessed April 2020).

ISO/IEC Guide 98-3, 2008. Uncertainty of Measurement – Part 3: Guide to the expression of Uncertainty in Measurement (GUM:1995). https://www.iso.org/sites/JCGM/GUM-JCGM100.htm, (Accessed April 2020).

ISO 11925-2, 2010. Reaction to fire tests—ignitability of products subjected to direct impingement of flame—Part 2: Single-Flame Source Test. (Accessed April 2020).

Ingard, U.K. and Dear, T.A., 1985. Measurement of acoustic flow resistance. J. Sound Vib. 103(4), 567–572. https://doi.org/10.1016/S0022-460X(85)80024-9.

Kirkup, L., 2002. A guide to GUM. Eur. J. Phys. 23(5), 483–487. https://doi.org/10.1088/0143-0807/23/5/305.

Log, T. and Gustafsson, S.E., 1995. Transient plane source (TPS) technique for measuring thermal transport properties of building materials. Fire Mater. 19, 43-49. https://doi.org/10.1002/fam.810190107.

Miller, I. and Freund, J.R., 1985. Probability and statistics for engineers, third Ed. Prentice hall international, New Jersey.

Montgomery, D.C. and Runger G.C., 2002. Applied statistics and probability for engineers, third Ed. J. Wiley, USA.

Ortiz, M.C., Sánchez, S., Sarabia, L., 2009. Quality of analytical measurements: univariate regression, in: S.D., Brown, R., Tauler, B., Walczack (Eds.), Comprehensive chemometrics: chemical and biochemical data analysis, vol. 1, Amsterdam, pp. 128-168.

Pfretzschner, J. and Rodriguez, R.M., 1999 Acoustic properties of rubber crumbs. Polym. Test. 18(2), 81–92. https://doi.org/10.1016/S0142-9418(98)00009-9.

Stamyr, K., Thelander, G., Ernstgård, L., Ahlner, J., Johanson, G., 2012. Swedish forensic data 1992–2009 suggest hydrogen cyanide as an important cause of death in fire victims. Inhal. Toxicol 24(3), 194-9. https://doi.org/10.3109/08958378.2012.660285.

Student, 1908. The probable error of a mean. Biornetrika 6(1), 1–25. https://doi.org/10.2307/2331554.

Chapter 4

Analytical models of selected physical properties

This chapter partially reports material from:

- Rubino, C., Bonet Aracil, M., Liuzzi, S., Stefanizzi, P. and F. Martellotta, 2021. *Wool waste used as sustainable non-woven for building applications*. J. Clean. Prod. 278, 123905. https://doi.org/10.1016/j.jclepro.2020.123905.
- Rubino, C., Bonet-Aracil, M., Gisbert-Payá, J., Liuzzi, S., Zamorano Cantó, M., Martellotta, F., Stefanizzi, P., 2019. *Composite eco-friendly sound absorbing materials made of recycled textile waste and biopolymers*. Materials 12 (23), 4020. https://doi.org/10.3390/ma12234020.
- Rubino, C., Bonet Aracil, M., Liuzzi, S., Martellotta, F., Stefanizzi, P. 2019. *Thermal characterization of innovative sustainable building materials from wool textile fibers waste*. IJES 63 (2-4), 277-283. https://doi.org/10.18280/ti-ijes.632-423.

The experimental measurement of the non-acoustic properties of the produced samples (i.e. the porosity, the tortuosity and the air flow resistivity) allowed to characterize their microstructure for better investigating their thermal and acoustic behaviour also through theoretical models.

Since a fibrous material is a multiphase system, all the thermal transfer processes (i.e. conduction, convection and radiation) become possible, depending on the construction and environmental conditions. Therefore, the effective thermal conductivity of the tested materials was evaluated using existing analytical models, according to which the porosity mostly plays an important role in the heat transfer.

All the non-acoustic parameters were also necessary to perform the acoustic prediction models proposed to validate the experimental data. In fact, the Chapter provides a detailed illustration of how the Delany-Bazley and Johnson-Champoux-Allard theories allowed to model the sound absorption of the textile tested materials, starting from their microstructural characteristics.

4.1 Evaluation of conductive, convective and radiative contributions in fibrous materials

The large majority of the building insulation materials belongs to the family of fibrous media, as the woolen composite investigated in the present study. Fibrous materials are made of a solid matrix consisting of fibers and a gas phase formed by air. Therefore, the heat transfer can occur in three different ways: conduction (λ_{cond}) through the fibrous solid matrix and through the gas medium, i.e. the air trapped within the pores; natural convection (λ_{conv}) due to the movement of the air between fibers, and radiation (λ_{rad}). The effective thermal conductivity λ_{eff} is used to encompass all these phenomena with a single variable:

$$\lambda_{eff} = \lambda_{cond} + \lambda_{conv} + \lambda_{rad} = \lambda_{solid} + \lambda_{air} + \lambda_{conv} + \lambda_{rad} \quad [4.1]$$

where λ_{solid} and λ_{air} are the conduction terms due to solid fibers and air, respectively.

The λ_{eff} of a fibrous material is one of the most difficult physical quantities to investigate because it depends not only on the porosity, but also on the macroscopic structure of the materials such as the distance between fibers and their directions (Tilioua et al., 2018). In fact, the way the solid components are connected developing a three-dimensional shape plays an important role for heat transfer (Miettinen et al., 2012).

Usually, the effective thermal conductivity can be modeled using existing fundamental structural models. In this work, the novel effective medium theory proposed by Gong et al. (2014) was used. This model considers the solid and gas phases which constitute the materials as small spheres dispersing into an assumed uniform medium which has the thermal conductivity λ_m. Five basic structural models, including the Series, Parallel, Maxwell–Eucken (two forms) and EMT models for a two-component system are unified in a single equation:

$$(1-\varepsilon)\cdot\frac{\lambda_{solid}-\lambda_{eff}}{\lambda_{solid}+2\cdot\lambda_m}+\varepsilon\cdot\frac{\lambda_{air}-\lambda_{eff}}{\lambda_{air}+2\cdot\lambda_m} \quad [4.2]$$

where λ_m is a variable value. The equation can adapt to various models by simply changing values of λ_m. When $\lambda_m = \lambda_{eff}$, the above equation is the EMT model. When $\lambda_m = \lambda_{solid}$, (or $\lambda_m = \lambda_{air}$), the equation is the Maxwell–Eucken (two forms, respectively). When

$\lambda_m = 0$ the equation is the Series model, and when $\lambda_m = \infty$ the equation is the Parallel model.

4.1.1 Conduction in gas medium

Gases in which the ratio of the mean molecular spacing and the mean molecular diameter is less than 7 can be described as being dense gases; conversely they can be considered dilute gases (Barber and Emerson, 2006). The rarefaction degree of air trapped in the pores of a porous material plays an important role to evaluate the contribution of the gas to heat conduction. In a dilute gas, the intermolecular forces can be neglected, and the molecules spend most of their time in free flight between successive collisions. Therefore, a dilute gas contribute to heat conduction less than a dense gas.

The rarefaction effect in microsystems is attributed to the mean free path of the gas and it can be related to the Knudsen number *Kn*. The Knudsen number is the characteristic dimensionless parameter for the theory of collisions and it is defined as the ratio of the mean free path of the gas molecules l_m to the characteristic length L_C:

$$Kn = \frac{l_m}{L_C} \qquad [4.3]$$

The mean free path l_m is the length that a molecule can travel before a collision event with a second molecule, and it is given by:

$$l_m = \frac{K_B \cdot T}{\sqrt{2} \cdot \pi \cdot d_m^2 \cdot P} \qquad [4.4]$$

where K_B is the Boltzmann's constant, T and P are the temperature and the pressure of air, and d_m is the air collision diameter defined as the diameter of the circular area around an air particle in which the center of another particle must be for a collision to occur.

The characteristic length L_C in a fibrous material is defined as the mean distance between the fibers and it can be calculated by an empirical formulation that assumes the fibers as a three-dimensional matrix:

$$L_C = \frac{3\pi}{5} \cdot \frac{\phi}{f_V} \qquad [4.5]$$

where ϕ is the diameter of the fibers and $f_V = 1 - \varepsilon$ is the volume fraction of solid (being ε

the porosity of the samples).

Depending on the value of Knudsen number, different flow regimes take place. As *Kn* number increases, the degree of rarefaction becomes more significant and the continuum assumption breaks down (Zhang et al., 2012). The subdivision of the flow regimes is very important in order to choose the empirical model to apply for characterizing the gas heat conduction (Tugnoli et al., 2019).

4.1.2 Convection

According to Incropera et al. (2002), for natural convection to take place in a fibrous medium, the buoyancy forces must overcome viscous resistance caused by the fibers. This assumption could be justified by evaluating the modified Rayleigh number *Ra** which is a dimensionless number associated with buoyancy-driven flow. According to Silberstein and Langlais (1990), the sensibility of porous materials to convection is also strongly linked to their air permeability. Consequently, the modified Rayleigh number *Ra** was calculated as follows:

$$Ra^* = \frac{g \cdot \beta_{air} \cdot \rho_{air}^2 \cdot c_{air} \cdot d \cdot \Delta T}{\mu_{air} \cdot \lambda} \cdot K \qquad [4.6]$$

where g is the gravity acceleration, c_{air}, β_{air}, ρ_{air} and μ_{air} are respectively the specific heat capacity, volumetric thermal expansion coefficient, density, and dynamic viscosity of air; K, λ and d are respectively the air permeability, thermal conductivity and thickness of the material, and ΔT is the temperature difference between the two sides of the sample.

The values of air permeability K could be calculated according to the Davies's empirical correlation (Jackson and James, 1986):

$$K = \frac{1}{16 f_V^{1.5} \cdot (1 + 56 f_V^3)} \cdot r^2 \qquad [4.7]$$

where f_V is the volume fraction of solid and r is the mean radius of the fibers.

4.1.3 Radiation

Thermal radiation heat transfer that takes place between two distant bodies depends on the difference of the fourth power of their absolute temperatures (Howell et al., 2010).

Therefore, the radiative contribution of the fibers in an insulating material may be particularly significant at high temperatures, while it can be neglected at temperatures around 293 K. According to Lux et al. (2006), the importance of radiative contribution could be evaluated by calculating the Planck number *N*:

$$N = \frac{\lambda}{4n^2 \cdot \sigma \cdot T^3 \cdot l_m} \qquad [4.8]$$

where λ is the experimental thermal conductivity, n is the refractive index of air, σ is the Stefan-Boltzmann's constant, T is the temperature and l_m is the mean free path of photons.

4.2 Acoustic prediction models

The non-acoustic properties, i.e. the porosity ϵ, tortuosity τ and air flow resistance σ_s or its value referred to the unit material thickness (the air flow resistivity σ), are important not only to characterize the microscopic structure of the materials, but also allow to predict their acoustic response by the use of appropriate theoretical models. In this work, the empirical D&B approach proposed by Delany and Bazley (Delany and Bazley, 1970) and later improved by Miki (1990), and the phenomenological JCA model formulated by Johnson et al. (1987) and subsequently refined by Allard and Champoux (1992) offered a good balance between ease of use and prediction accuracy.

4.2.1 Delany-Bazley model

The D&B model involves the computation of the propagation wavenumber k and the characteristic impedance Zc to obtain the absorption coefficients. The latter parameter determines how much sound will be transmitted and reflected when the wave encounters a boundary with another material. When the air flow resistance value is too high, the impedance mismatch between the air and the absorbent causes the reflection of the sound from the surface of the material and the reduction of its absorption. If the air flow resistance is too small, the acoustic energy attenuation caused by internal friction decreases and the absorption effect is poor. (Peng, 2017).

The empirical model proposed by Delany and Bazley is considered the simplest approach to predict the acoustic behaviour of porous materials because it just links the

sound absorption coefficients to the air flow resistivity σ of the materials. Thus, to solve the D&B equations only one non-acoustic property was used to calculate the parameter $X = \frac{\rho_{air} \cdot f}{\sigma}$ (f being the frequency and ρ_{air} being the density of the air), needed to determine the characteristic impedance Zc and the propagation wavenumber k:

$$Z_c = \rho_{air} \cdot c_{air} \cdot (1 + 0.057X^{-0.754} - j0.087X^{-0.732}) \quad [4.9]$$

$$k = \frac{\omega}{c_{air}}(1 + 0.0978X^{-0.700} - j0.189X^{-0.595}) \quad [4.10]$$

where c_{air} is the speed of sound in air, ω is the angular frequency and j is the complex unit.

The D&B equations can be considered valid only in a defined frequency range given by $0.01 < X < 1.0$, and for σ values below 50 kN·s/m^4 (Cox and D'Antonio, 2017).

Once the characteristic impedance Zc and wavenumber k of the material are known, it is necessary to convert them to the surface impedance and then to the absorption coefficients. Considering a single layer of the absorber with a rigid backing, the impedance at the backing is taken to be infinite. Thus, the impedance Z of the surface of the absorbent is:

$$Z = -jZ_c \cdot cotg(k \cdot d) \quad [4.11]$$

where j is the complex unit and d is the sample thickness.
So that, the absorption coefficient α_n may be calculated according to the usual formula:

$$\alpha_n = 1 - |R|^2 \quad [4.12]$$

where $R = \frac{Z - Z_{air}}{Z + Z_{air}}$ is the pressure reflection coefficient which gives the ratio of the reflected and incident pressure; $Z_{air} = \rho_{air} \cdot c_{air}$ is the impedance of the air with c_{air} and ρ_{air} representing the speed of sound in air and the density of air, respectively.

4.2.2 Johnson-Champoux-Allard model

Although the D&B empirical model has been successfully tested over a variety of fibrous materials having porosity close to unity (similar to those under investigation), it nonetheless neglects the important effects that other structural parameters of the materials may have to influence their acoustic performance. For this reason, the JCA model was also

considered. In fact, although there are more complex phenomenological models, their additional variations are typically small and refer only to low frequencies.

According to JCA equations, Z_C and k are expressed as a function of the effective (or dynamic) bulk density ρ_e and bulk modulus k_e:

$$Z_c = (k_e \cdot \rho_e)^{0.5} \quad [4.13]$$

$$k = \omega \cdot (\frac{\rho_e}{k_e})^{0.5} \quad [4.14]$$

The effective bulk density is based on the work by Johnson et al. (1987), where visco-inertial dissipative effects inside the porous media are described. The word "effective" is used to signify that ρ_e is the density experienced by the acoustic waves rather than the more normal definition of mass divided by volume. The effective bulk density is computed as follows:

$$\rho_e = \tau\rho_{air} \cdot \left[1 + \frac{\sigma\varepsilon}{j\omega\rho_{air}\tau} \cdot \sqrt{1 + j \cdot \frac{4\tau^2\eta\rho_{air}\omega}{\sigma^2\Lambda^2\varepsilon^2}}\right] \quad [4.15]$$

where ρ_{air}=1.21 kg/m^3 is the density of the air, τ is the tortuosity, σ is the flow resistivity, ε is the porosity, ω is the angular frequency, η_{air}=1.846x10^{-5} Pa·s is the dynamic viscosity of air, Λ is the viscous characteristic length and j is the complex unit.

The work by Allard and Champoux (1992) is used to describe the thermal dissipative effects and calculate the dynamic bulk modulus according to the formula:

$$k_e = \frac{\gamma P_{air}}{\gamma - (\gamma - 1)\Big/\left(1 + \frac{8\eta}{j\Lambda'^2 N_p\rho_{air}\omega} \cdot \sqrt{1 + j \cdot \frac{\Lambda'^2 N_p\rho_{air}\omega}{16\eta}}\right)} \quad [4.16]$$

where γ=1.4 is the ratio of the specific heat capacities, P_{air} is the atmospheric pressure, N_p is the Prandtl Number and Λ' is the thermal characteristic length.

Starting from the values of the characteristic impedance Zc and wavenumber k, it is possible to determine the absorption coefficients α_n following the Equation [4.11, 4.12] previously illustrated for the Delany-Bazley model.

As suggested by the JCA Equations [4.15, 4.16], in order to evaluate the thermal and viscous effects in pores, additional non-acoustic properties, i.e. the viscous Λ and thermal Λ' characteristic lengths, were estimated. These parameters are strictly related to the geometric structure of pores by means of the pores shape factor s.

The dissipation of acoustical energy through a porous material involves thermal and viscous-inertial dissipation effects. The thermal dissipation effect exists when there is significant heat exchange between air particles and pores walls, creating a thermal boundary layer. In fact, a thermal wave is created as a result of successive compression and dilatation when sound waves propagate through the porous medium (Otaru, 2019). The viscous-inertial dissipation effect results from the friction of air particles with the pores walls.

The characteristic length Λ is a weighted ratio of the volume to surface area of the pores. It is weighted according to the squared modulus of the microscopic velocity evaluated including the effects of viscosity. It can be found for simple pore shapes using the following formulation:

$$\Lambda = \frac{1}{s} \cdot \sqrt{\frac{8\eta_{air}\tau}{\varepsilon\sigma}} \qquad [4.17]$$

where s is the pore shape factor, η_{air} is the viscosity of air, τ, ε and σ are respectively the tortuosity, bulk porosity and airflow resistivity of the material.

The shape of the pores influences the sound propagation and hence its absorption, causing different thermal and viscous effects. Therefore, for materials with a complicated internal structure the thermal characteristic length Λ' is also introduced:

$$\Lambda' = \frac{2V_{pores}}{A_{pores}} \qquad [4.18]$$

where V_{pores} and A_{pores} are the surface area and the volume of the pores respectively.

The determination of the pores structure is so complex that usually is considered the ratio of the characteristic lengths instead of their empirical measurements. In general $\Lambda' \geq \Lambda$ and to a first approximation $\Lambda' = 2\Lambda$ (Cox and D'Antonio, 2017).

4.2.3 Parameters to feed the theoretical models

As it was impossible to measure all the input parameters required by JCA model, an inverse method (Atalla and Panneton, 2005) was used to estimate the missing ones. Taking advantage of measured absorption coefficients, the values of the physical properties (i.e. viscous and thermal lengths ratio and shape factor) and of the directly measured ones (porosity, tortuosity and air flow resistivity), were determined by means of optimization techniques. A search algorithm was developed using the Matlab® software, in order to find the set of parameters which allowed the best match between measurements and predictions. The algorithm explored properties which were not measurable over the entire range of possible values, while for measured parameters the range was chosen considering their average values and taking into account their uncertainty.

In particular, for the shape factor (on which the viscous characteristic length is directly dependent), values between 1 and 3 were explored, while the ratio of the characteristic lengths varied between 1 and 2.5. The cost function minimized by the search algorithm was the mean absolute error between measured and predicted one-third octave absorption coefficients in the range from 100 Hz to 3150 Hz. As the porosity and tortuosity were characterized by very low uncertainty, their measured values were directly used as input data of the JCA model, allowing to speed up calculations. For GA samples tortuosity could not be measured because gum Arabic is soluble in water and this would have prevented a suitable placement of the sample in the measurement equipment. Thus, the value estimated according to the inverse method was used to run the JCA model. All the remaining input parameters, including air flow resistivity, which showed significant variations during measurements, were consequently estimated by the search algorithm. The air flow resistivity values resulting from the inverse method were also used to feed the Delany-Bazley model in order to get the best fit between measured and predicted absorption coefficients curves.

References

Allard, J.F., Champoux, Y., 1992. New empirical equation for sound propagation in rigid frame fibrous material. J. Acoust. Soc. Am. 91, 346-3353. https://doi.org/10.1121/1.402824.

Atalla, Y. and Panneton, R., 2005. Inverse acoustical characterization of open cell porous media using impedance tube measurements. Can. Acoust. 33(1), 11-24. //jcaa.caa-aca.ca/index.php/jcaa/article/view/1711.

Barber, R.W., Emerson D.R., 2006. Challenges in Modeling Gas-Phase Flow in Microchannels: From Slip to Transition. Heat Transfer Eng. 27(4): 3-12. https://doi.org/10.1080/01457630500522271.

Berryman, J.G, 1980. Confirmation of Biot's theory. Appl. Phys. Lett. 37, 382-384. https://doi.org/10.1063/1.91951.

Carosio, F., Alongi, J., 2018. Flame retardant multilayered coatings on acrylic fabrics prepared by one-step deposition of chitosan/montmorillonite complexes. Fibers 6(2), 36. https://doi.org/10.3390/fib6020036.

Cox, T.J., D'Antonio, P.K., 2017. Acoustic Absorbers and Diffusers, Theory, Design and Application; Spon Press: London, UK.

Delany, M.E., Bazley, E.N., 1970. Acoustical properties of fibrous materials. Appl. Acoust. 3 (2), 105e116. https://doi.org/10.1016/0003-682X(70)90031-9.

Howell, J.R., Siegel, R., Menguc, M.P., 2010. Thermal radiation heat transfer. Fifth Edition, CRC Press, NewYork.

Incropera, F.P., Frank, P., DeWitt, D.P., 2002. Fundamentals of heat and mass transfer. J. Wiley, NewYork.

Jackson, G.W. and James, D.F., 1986. The permeability of fibrous porous media. Can. J. Chem. Eng. 64: 364-374. https://doi.org/10.1002/cjce.5450640302.

Johnson, D.L., Koplik, J., Dashen, R., 1987. Theory of dynamic permeability and tortuosity in fluid-saturated porous media. J. Fluid Mech. 176, 379e402. https://doi.org/10.1017/S0022112087000727.

Koponen, A., Kataja, M., Timonen, j., 1998. Simulations of single-fluid flow in porous media. Int. J. Mod. Phys. C 9(8), 1505-1521. https://doi.org/10.1142/S0129183198001369.

Lux, J., Ahmadi, A., Gobbé, C., Delisée, C., 2006. Macroscopic thermal properties of real fibrous materials:Volume averaging method and 3D image analysis. Int. J.Heat Mass Transf. 49(11-12), 1958-1973. https://doi.org/10.1016/j.ijheatmasstransfer.2005.09.038.

Matyka, M., Khalili, A., Koza, Z., 2008. Tortuosity–porosity relation in the porous media flow. Phys. Rev. E 78, 026306. https://doi.org/10.1103/PhysRevE.78.026306.

Miki, Y., 1990. Acoustical properties of porous materials-Generalizations of empirical models. J. Acoust. Soc. Jpn. 11, 19–24. https://doi.org/10.1250/ast.11.25.

Miettinen, L, Kekalainen, P, Turpeinen, T, Hyvaluoma, J, Merikoski, J, Timonen, J., 2012. Dependence of thermal conductivity on structural parameters in porous samples. AIP Adv 2(1). 021101. https://doi.org/10.1063/1.3676435.

Otaru, A.J., 2019. Review on the acoustical properties and characterisation methods of sound absorbing porous structures: a focus on microcellular structures made by a replication casting method. Met. Mater. Int. 26, 915–932. https://doi.org/10.1007/s12540-019-00512-y.

Peng, L., 2017. Sound absorption and insulation functional composites, in: Fan, M. and Fu, F. (Eds.), Advanced high strength natural fibre composites in construction, Woodhead publishing, Oxford, pp. 333-373.

Pisani, L.,2011. Simple expression for the tortuosity of porous media. Transport Porous Med. 88 (2), 193-203. https://doi.org/10.1007/s11242-011-9734-9.

Silberstein, A., Langlais, C., 1990. Natural convection in light fibrous insulating materials with permeable interfaces: onset criteria and its effect on the thermal performances of the product. Journal of thermal insulation 14(1), 22-42. https://doi.org/10.1177/109719639001400104.

Tilioua, A., Libessart, L., Lassue, S., 2018. Characterization of the thermal properties of fibrous insulation materials made from recycled textile fibers for building applications: Theoretical and experimental analyses. Appl Therm. Eng. 142, 56–67. https://doi.org/10.1016/j.applthermaleng.2018.06.071.

Tugnoli, A., Moricone, R., Scarponi, G.E., Cozzani, V., 2019. Effective thermal conductivity of fibrous fireproofing materials. Int J Therm. Sci. 136, 107–120. https://doi.org/10.1016/j.ijthermalsci.2018.09.035.

Zhang W.M., Meng G., Wei X., 2012. A review on slip models for gas microflows. Microfluid Nanofluid 13(6), 845–882. https://doi.org/10.1007/s10404-012-1012-9.

Chapter 5

Analysis of the hygrothermal and fire resistance experimental results

This chapter partially reports material from:

- Rubino, C., Bonet Aracil, M., Liuzzi, S., Stefanizzi, P. and F. Martellotta, 2021. *Wool waste used as sustainable non-woven for building applications*. J. Clean. Prod. 278, 123905. https://doi.org/10.1016/j.jclepro.2020.123905.
- Rubino, C., Bonet-Aracil, M., Gisbert-Payá, J., Liuzzi, S., Zamorano Cantó, M., Martellotta, F., Stefanizzi, P., 2019. *Composite eco-friendly sound absorbing materials made of recycled textile waste and biopolymers*. Materials 12 (23), 4020. https://doi.org/10.3390/ma12234020.
- Rubino, C., Bonet Aracil, M., Liuzzi, S., Martellotta, F., Stefanizzi, P., 2019. *Thermal characterization of innovative sustainable building materials from wool textile fibers waste*. IJES 63 (2-4), 277-283. https://doi.org/10.18280/ti-ijes.632-423.
- Rubino, C., Bonet Aracil, M., Liuzzi, S., Martellotta, F., 2019. *Preliminary investigation on the acoustic properties of absorbers made of recycled textile fibers*. Proceedings of the 23rd International Congress on Acoustic, 9-13 September, Aachen, Germany.

This Chapter includes the results of the hygrothermal and of the fire resistance experimental measurements. All tested non-wovens might represent a valid alternative for building applications, showing hygrothermal performances well comparable to materials currently available on the market, i.e. a thermal conductivity between 0.044 and 0.060 W/(m K) and a water vapour permeability close to $2 \cdot 10^{-11}$ kg/(m·s·Pa). Furthermore, the followed production techniques negligibly affected the thermal behaviour of the samples, but had a more evident influence on the hygric behaviour. This was due to the effect of the manufacturing techniques on the microstructure of the materials, especially on tortuosity and porosity values, as will be better explained in the next Chapter.

Lastly, good fire resistance properties were found for the three typologies of material in light of the possibility of improving their behaviour with additives.

5.1 The hygrothermal properties

Thermal conductivity is an important parameter for expressing the material's insulation property, as well as thermal diffusivity and specific heat capacity are useful for performing dynamic thermal comfort analysis of buildings. Therefore, Table 5.1 summarizes the experimental mean values of thermal conductivity λ, thermal diffusivity D and specific heat capacity c, given together with their measurement uncertainty expressed as the standard deviation of the mean (ISO/IEC Guide 98-3, 2008).

Table 5.1. Thermal properties of BICO, CH and GA materials by varying their density values ρ_{bulk}: mean values of thermal conductivity λ, thermal diffusivity D, specific heat capacity c and their standard deviation of the mean.

Sample code	ρ_{bulk} [kg/m^3]	λ [W/(m·K)]	D [10^{-7}m^2/s]	c [J/(kg·K)]
BICO-1	167±6	0.057±0.0008	1.83±0.003	1863±22
BICO-2	136±1	0.054±0.0004	1.86±0.001	2148±6
BICO-3	115±1	0.052±0.0002	1.85±0.002	2459±7
BICO-4	90±2	0.050±0.0003	2.00±0.004	2770±10
BICO-5	51±1	0.044±0.0004	2.46±0.010	3544±13
CH-1	197±2	0.060±0.0005	1.77±0.005	1726±21
CH-2	145±2	0.055±0.0007	1.96±0.005	1929±19
CH-3	122±1	0.052±0.0006	1.98±0.002	2156±6
CH-4	80±1	0.049±0.0005	2.17±0.009	2792±17
GA-1	177±3	0.059±0.0012	1.66±0.003	2020±19
GA-2	143±2	0.056±0.0006	1.95±0.007	2024±24
GA-3	93±1	0.050±0.0005	2.08±0.006	2624±16

The achieved results could be considered satisfactory, being in agreement with those obtained for bio-based insulating materials with similar density values, like panels made from hemp fibers and shives bonded with bi-component fibers (λ=0.044÷0.048 W/(m·K), ρ_{bulk}=33.1÷111.6 kg/m^3) or PLA (λ=0.037÷0.040 W/(m·K), ρ_{bulk}=40÷100 kg/m^3) and boards produced using a liquid glass to bind moss, rye straw and reed (λ=0.037÷0.056 W/(m·K), ρ_{bulk}=156÷191 kg/m^3) (Korjenic et al. 2016, Kremensas et al., 2017, Bakatovich et al., 2019). The experimental thermal conductivity values were also similar to those of thermal insulators based on mineral fibers (λ=0.054÷0.048 W/(m·K), ρ_{bulk}=40÷150 kg/m^3), cork (λ=0.043 W/(m·K), ρ_{bulk}=110÷160 kg/m^3) or perlite (λ=0.048 W/(m·K),

ρ_{bulk}=80÷120 kg/m^3) (UNI 10351, 2015).

The properties which characterize the hygric behaviour of the BICO, CH and GA non-wovens are shown in Table 5.2. The water vapour permeability δ and the water vapour resistance factor μ are given as mean values of experimental results, together with measurement uncertainty expressed as the standard deviation of the mean value (ISO/IEC Guide 98-3, 2008).

Table 5.2. Hygric properties of tested BICO, CH and GA materials by varying their density values ρ_{bulk}: mean values of water vapour permeability δ and water vapour resistance factor μ expressed with the standard deviation of the mean.

Sample code	ρ_{bulk} [kg/m^3]	δ [10^{-11} kg/(m·s·Pa)]	μ [-]
BICO-1	167±6	1.90±0.08	10.3±0.4
BICO-2	136±1	2.15±0.68	9.1±2.9
BICO-3	115±1	2.20±0.27	8.9±1.1
BICO-4	90±2	2.00±0.53	9.8±2.6
BICO-5	51±1	2.20±0.17	8.9±0.7
CH-1	197±2	2.67±0.26	7.4±0.7
CH-2	145±2	2.32±0.33	8.5±1.2
CH-3	122±1	2.56±0.23	7.8±0.7
CH-4	80±1	2.44±0.08	8.0±0.3
GA-1	177±3	2.32±0.12	8.5±0.4
GA-2	143±2	2.27±0.16	8.6±0.6
GA-3	93±1	2.52±0.26	7.8±0.8

The hygric results were compared with those obtained for construction materials characterized by similar density values. The produced samples showed μ coefficients in agreement with sustainable insulators based on natural materials as wood (μ=9.06, ρ_{bulk}=117 kg/m^3) or cork (μ=5÷10, ρ_{bulk}=100÷220 kg/m^3) (Cetiner and Shea., 2018, Pfundstein, 2008) and with felts produced from mineral rocks (μ=12, ρ_{bulk}=40÷150 kg/m^3) (UNI 10351, 2015).

5.1.1 Effective thermal conductivity for tested fibrous materials

Fibrous materials can be considered as heterogeneous systems and analysis of their responses to external disturbances depends on the interactions between their components. For example, textile non-wovens are a mixture of fibers and air and the behaviour of both components influences the thermal performance of the whole in terms of effective thermal conductivity λ_{eff}.

As anticipated in Section 4.1, three dimensionless number, i.e. the Knudsen number *Kn*, the modified Rayleigh number *Ra** and the Plank number *N*, were computed to evaluate λ_{eff} of the tested materials.

Knudsen number was calculated in order to evaluate the contribution of the air trapped in the pores to heat conduction. Table 5.3 shows *Kn* number for BICO, CH and GA samples, calculating by assuming the air collision diameter d_m=0.369×10^{-9} m at 293 K (Glassman and Harris, 1952). The Boltzmann's constant was K_B=1.3807×10^{-23} J/K; while the mean density of wool fibers ϕ was about 1300 kg/m^3 (Baker, 2018) and their mean diameter was assumed to be 19 μm, as previously shown in Figure 2.7. As it can be observed, the Knudsen number was less than 0.01 for all the tested samples. This means that the characteristic length was larger than the mean free path of the gas molecules. No slip between the wall of the pores and the air was considered because of the thermal equilibrium achieved between the pore walls and nearby fluid (Zhang et al., 2012). Therefore, the fluid was treated in a continuum regime, dominated by intermolecular collisions and was assumed λ_{air}=0.026 W/(m·K).

Taking into account that the very small dimensions of the voids between the fibers make air movement negligible, heat transfer due to convection was likely to be insignificant and could be ignored without affecting accuracy. To better demonstrate this, the modified Rayleigh number *Ra** computed assuming ΔT=20 K and samples thickness *d*=0.05 m was evaluated (Table 5.3). *Ra** was less than 40 which represents the critical value below which there is no fluid motion and heat transfer is by conduction rather than convection. Thus, in the all cases, convection might be neglected (Tilioua et al., 2018).

Finally, the Planck number was calculated by assuming the mean free path of photons l_m equivalent to the mean fibers distance L_C computed to calculate the Knudsen number. Being N>10 for all samples, the contribution of radiation could be neglected.

Table 5.3. Knudsen number *Kn*, modified Rayleigh number *Ra** and Plank number *N* for BICO, CH and GA samples.

Sample code	*Kn* [-]	*Ra** [-]	*N* [-]
BICO-1	2.225×10^{-4}	0.7	74
BICO-2	1.812×10^{-4}	1.1	57
BICO-3	1.532×10^{-4}	1.3	47
BICO-4	1.199×10^{-4}	2.0	35
BICO-5	6.796×10^{-5}	3.8	18
CH-1	2.625×10^{-4}	0.5	92
CH-2	1.932×10^{-4}	0.9	62
CH-3	1.626×10^{-4}	1.3	49
CH-4	1.066×10^{-4}	2.6	30
GA-1	2.359×10^{-4}	0.6	81
GA-2	1.906×10^{-4}	1.0	62
GA-3	1.239×10^{-4}	2.1	36

As a result of the negligible convective and radiative contribution to the effective conductivity, the heat transfer in the fibrous woolen materials under test was fundamentally due to conduction in solid and gas phases. Considering sample CH-2, a value of λ_{air}=0.026 W/(m·K) was estimated by exploring several values for the variable λ_m, in order to identify which value minimized the standard deviation between the experimental values and those estimated by the model. The best agreement between the model and the experimental values was obtained when $\lambda_m \to \infty$, so that the Equation [4.2] became:

$$\lambda_{eff,est} = (1-\varepsilon)\cdot\lambda_{solid} + \varepsilon\cdot\lambda_{gas} \qquad [5.1]$$

Comparing the estimated effective conductivity $\lambda_{eff,est}$ yielded by Equation [5.1], with the measured one λ, the relative error $\frac{\lambda-\lambda_{eff,est}}{\lambda}\cdot 100$ was computed and given in Figure 5.1. As it can be observed, the highest error was observed for the lightest samples BICO-5, CH-4 and GA-3. This could be due to a less negligible contribution of convection and

radiation heat transfer when the porosity increases. This result was confirmed by the highest modified Rayleigh number and the lowest Planck number previously calculated for these samples (i.e. $Ra^*_{BICO} = 3.8$, $Ra^*_{CH} = 2.6$, $Ra^*_{GA} = 2.1$; $N_{BICO} = 18$, $N_{CH} = 30$, $N_{GA} = 36$).

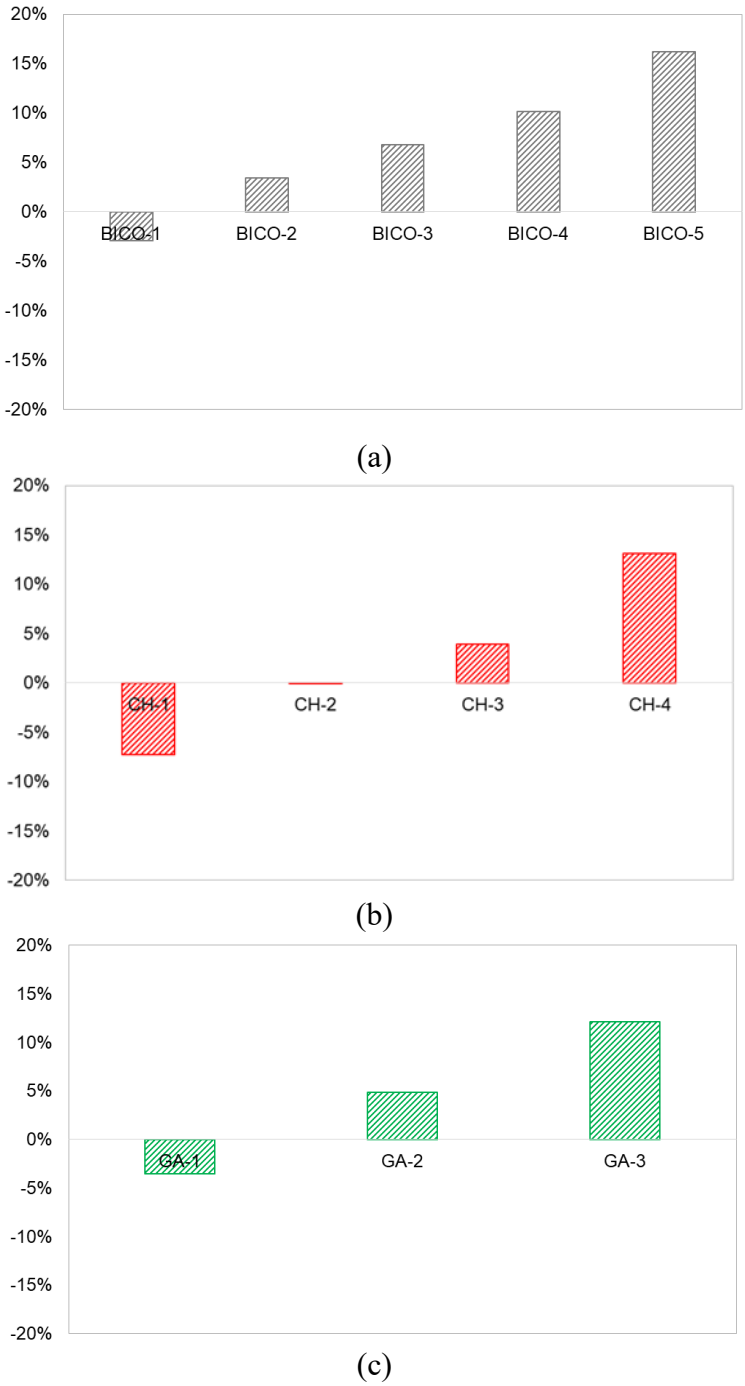

Figure 5.1. Relative error of estimated respect to measured effective conductivity for BICO (a), CH (b) and GA (c) samples.

In conclusion, although the most significant heat transfer mode in the studied materials was the conduction in the solid and gas phases, the analysis showed that the error in estimating the effective thermal conductivity could become unacceptable when porosity increases and convection and radiation became important ways of heat transfer.

5.1.2 Comparison of BICO, CH and GA samples using statistical inference

The experimental results of the hygric and thermal properties previously individually displayed for BICO, CH and GA samples were compared through a statistical analysis, in order to study how the manufacturing processes affected the performances of the final products.

In Figure 5.2, a linear correlation between conductivity and density can be noted for all the compared materials. A regression analysis was performed to evaluate the statistical significance of the linear relationship between λ and ρ_{bulk}. For this reason, assuming a significance level $\alpha = 0.05$ and the relevant number of observations n for BICO, CH and GA samples ($n_{BICO} = 5$, $n_{CH} = 4$ and $n_{GA} = 3$), a two tailed hypothesis test of the slope β_1 of the regression lines was applied using the Student's t distribution.

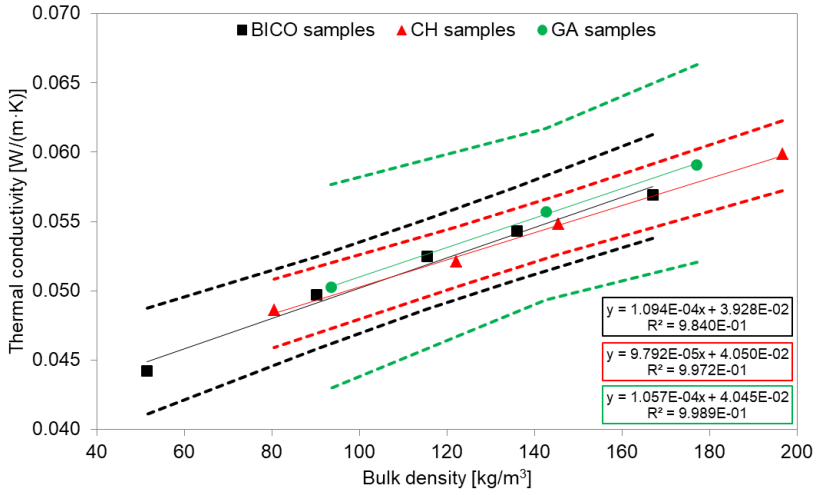

Figure 5.2. Thermal conductivity λ vs. bulk density ρ_{bulk} for samples produced using bi-component fibers, chitosan and gum Arabic solution as binder. Dashed curves represent confidence intervals at 95%.

As anticipated in Section 3.3, the comparison between the statistic absolute values t_{β_1} and the associated critical ones $t_{\alpha/2,n-2}$ (with $n-2$ degrees of freedom) was carried out to test the null hypothesis $H_0: \beta_1 = 0$ versus the alternative one $H_a: \beta_1 \neq 0$. The t_{β_1} values computed for BICO, CH and GA samples were respectively 13.58, 26.82 and 29.89; while the associated critical values $t_{\alpha/2,n-2}$ were 4.18, 6.21 and 25.45. Being $\left|t_{\beta_1}\right| > t_{\alpha/2,(n-2)}$ for each type of material, the null hypothesis was rejected at significance level α. Thus, a statistically significantly linear correlation between the independent variable ρ_{bulk} and the dependent variable λ was found for the three types of materials.

Following the previous analysis, Figure 5.2 also shows, in addition to regression lines, the corresponding 95% confidence intervals plotted as the upper and lower dotted lines. These confidence regions were useful in establishing the accuracy of the estimated regression lines. A narrow range of the confidence region was found for BICO and CH samples, while for GA it was quite larger. This was clearly influenced by the greater number of observations *n* for BICO and CH materials than for GA.

Statistical methods were used to verify whether the rate of change of λ was the same when data sets of different materials were compared. The slopes of the regression lines estimated for CH and GA samples were then compared and the null hypothesis $H_0: \beta_{1_{CH}} = \beta_{1_{GA}}$ was verified applying the Student t-test, with $\alpha = 0.05$. The statistic $t_{\beta_{1_{CH}} - \beta_{1_{GA}}}$ absolute value was 1.36 and resulted to be less than the critical one $t_{\alpha/2,(n_{CH}+n_{GA}-4)} = 4.18$. Thus, the null hypothesis was accepted at significance level α and the slope $\beta_{1_{CH}}$ and $\beta_{1_{GA}}$ were considered comparable, meaning that in statistical terms the two slopes should be considered the same. Assuming $\beta_{1_{CH}} = \beta_{1_{GA}}$, the CH samples were chosen to compare the materials prepared using Co-PET/PET fibers as binder and those produced using bio-binders. The null hypothesis $\beta_{1_{CH}} = \beta_{1_{BICO}}$ was tested at significance level $\alpha = 0.05$. Being $\left|t_{\beta_{1_{CH}} - \beta_{1_{BICO}}}\right| = 1.20$ lower than $t_{\alpha/2,(n_{CH}+n_{BICO}-4)} = 3.16$, even in this case the null hypothesis was accepted and the slopes of the regression lines of BICO, CH and GA samples were considered comparable. As a consequence of comparable β_1 parameters, the changes in the bulk densities of the three types of materials affected thermal conductivity values in the same way, regardless of the different fabrication techniques.

In order to compute the statistics $t_{\beta_{1_{CH}} - \beta_{1_{GA}}}$ and $t_{\beta_{1_{CH}} - \beta_{1_{BICO}}}$, the equality of the

estimated residual variances of the CH and GA samples and of the CH and BICO samples was verified applying the *F*-test. The $F_{\beta_{1CH}-\beta_{1GA}}$ and $F_{\beta_{1CH}-\beta_{1BICO}}$ were respectively 2.13 and 5.37, resulting lower than the associated critical values $F_{\alpha,(n_{CH}-2,n_{GA}-2)}$ and $F_{\alpha(,n_{CH}-2,n_{BICO}-2)}$ which were 19.95 and 19.16. Thus, for each type of material, the equality of the residual variances were verified at significance level $\alpha = 0.05$.

The result of the statistical tests could be expected due to the similar porosity values shown by the compared materials. In fact, as will be better illustrated in the next Chapter, the molding process and the chemical binding technique used to interlock together the wool fibers produced several groups of samples with a void fraction close to 90%.

Furthermore, as previously explained in Section 5.1.1, the thermal conductivity is mainly the result of the heat conduction transfer through the solid and air phases. The air entrapped within the pores affects the thermal behaviour of a fibrous material more than the fibrous matrix, because of its thermal conductivity coefficient with an order of magnitude lower than that of the solid matrix. Thus, being the porosity value exhibited by the same-density BICO, CH, and GA samples close to 0.9, the three materials showed comparable λ values and similar rate of variation.

In Figure 5.3, the distribution of the water vapour permeability values as a function of the bulk density for BICO samples is compared with that for CH and GA samples.

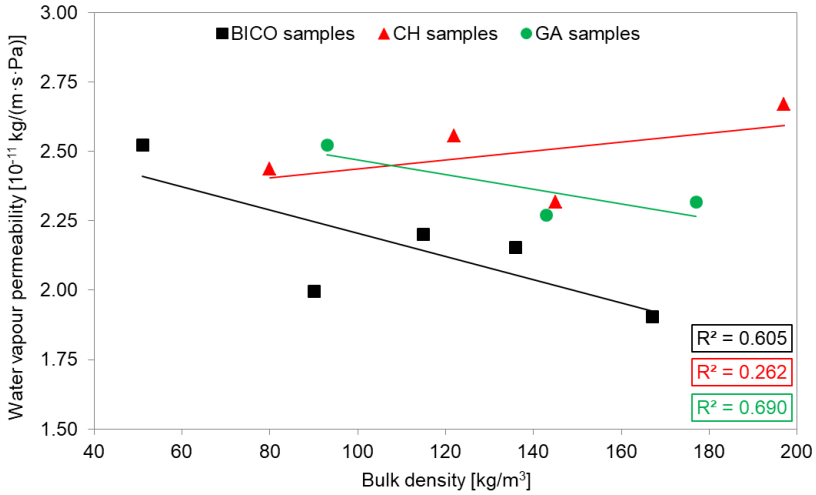

Figure 5.3. Water vapour permeability δ vs. bulk density ρbulk for samples produced using bi-component fibers, chitosan and gum Arabic solution as binder. The solid lines represent the regression lines.

For the three types of materials the coefficient of determination R^2, less than 0.7 for each sample, showed a non-significant linear correlation existing between the independent variable ρ_{bulk} and the dependent variable δ. Similar result was further proved by applying a hypothesis test to compare the slope parameter β_1 of the three regression lines. Particularly, the Student's t-test was performed to verify the null hypothesis $\beta_1 = 0$ at significance level $\alpha = 0.05$. The statistic t_{β_1} absolute values computed for BICO, CH and GA samples were respectively 2.14, 0.84 and 1.46; whereas the associated $t_{\alpha/2,(n-2)}$ values were respectively 4.18, 6.21 and 25.45. The $\left|t_{\beta_1}\right|$ values resulted to be less than $t_{\alpha/2,(n-2)}$ ones; thus the null hypothesis $\beta_1 = 0$ was accepted in support of the alternative one $\beta_1 \neq 0$. Consequently, no statistically significant relationship was found between ρ_{bulk} and δ whatever the material considered and, in any case, the relations were substantially the same for each subset of values.

Therefore, in order to better investigate the hygric behaviour of the studied samples, the mean values of the distribution of the three data sets δ were compared. Assuming $\overline{\delta_{BICO}}$, $\overline{\delta_{CH}}$ and $\overline{\delta_{GA}}$ as the average values of the δ data sets of BICO, CH and GA samples, a two samples Student's *t*-test was applied to study whether the difference among the three values could be statistically zero. First, the null hypothesis $\overline{\delta_{CH}} - \overline{\delta_{GA}} = 0$ was tested at significance level $\alpha = 0.05$. Since $|t_{calc}| = 1.13$ was less than $t_{\alpha/2,(n_{CH}+n_{GA}-2)} = 3.16$, the null hypothesis was accepted and the magnitude of the difference between the two mean values was assumed statistically insignificant. As a consequence, CH and GA samples were considered belonging to the same group of materials characterized by a mean water vapour permeability value $\overline{\delta_{CH+GA}} = 2.44 \times 10^{-11}$ kg/(m · s · Pa). Finally, the null hypothesis $\overline{\delta_{CH+GA}} - \overline{\delta_{BICO}} = 0$ was tested at significance level $\alpha = 0.05$. Being $\left|t_{\overline{\delta_{CH+GA}}-\overline{\delta_{BICO}}}\right| = 2.68$ greater than $t_{\alpha/2,(n_{CH+GA}+n_{BICO}-2)} = 2.63$, the null hypothesis was rejected, although the difference between the *t* values was marginal. Therefore, the two means $\overline{\delta_{CH+GA}} = 2.44 \times 10^{-11}$kg/(m · s · Pa) and $\overline{\delta_{BICO}} = 2.16 \times 10^{-11}$kg/(m · s · Pa) were assumed as different, concluding that the samples with bi-component fibers and natural solutions as binder belong to different groups of materials, although by a statistically marginal amount.

In order to compute the statistic value $t_{\overline{\delta_{CH+GA}}-\overline{\delta_{BICO}}}$, the equality of the estimated variances of the CH+GA and BICO samples was verified applying the *F*-test. The

$F_{\overline{\delta_{CH+GA}}-\overline{\delta_{BICO}}}$ was 3.20, resulting lower than the associated critical values $F_{\alpha,n_{CH+GA}-1,n_{BICO}-1}$ which was 4.53. Thus, the equality of the variances was verified at significance level $\alpha = 0.05$.

The difference between the two mean values $\bar{\delta}$ was a consequence of the effects of the thermal and chemical manufacturing process on the tortuosity values of the final products. In fact, the geometry of the pores plays an important role in describing the water vapour transfer in fibrous materials (Collet et al, 2011). As will be better illustrated in the next Section 6.1, the BICO samples showed higher tortuosity values than the CH and GA ones, allowing a more complex vapour flow path and consequently a lower water vapour permeability.

A box plot (Figure 5.4) was used to provide a visual summary of the distribution of δ data sets of the two groups of materials; i.e. non-wovens obtained using Co-PET/PET fiber as binder and non-wovens prepared with chitosan and gum Arabic binding solutions. As it can be observed, the distribution of the observations belonging to the two sub-sets presents a certain overlapping. However, according to statistical tests mean values can be nonetheless considered as independent.

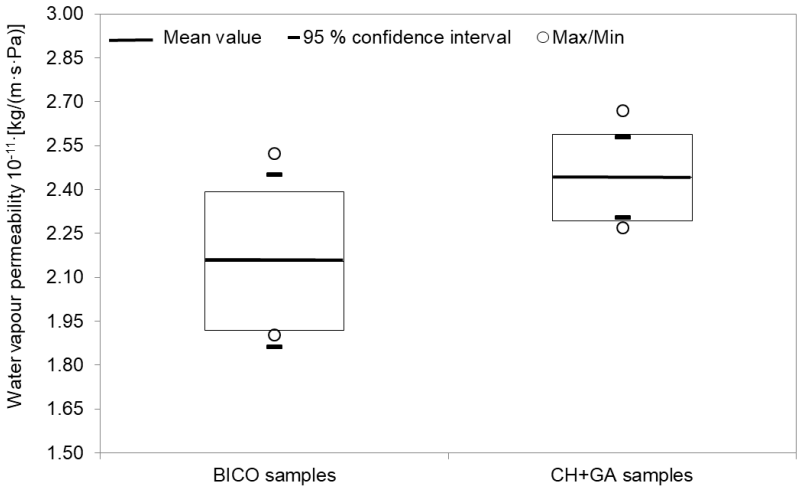

Figure 5.4. Box plot of water vapour permeability data sets of BICO, CH and GA samples. Bold line corresponds to mean value, boxes correspond to standard deviations, whiskers to 95% confidence intervals and dots represent the maximum and minimum values.

5.2 Fire resistance properties

Results of the ignitability test are given in Figure 5.5 and show some interesting differences. It can be observed that pressed wool (Figure 5.5(a,e)) presented the best behavior, with a very limited flame propagation on the flat face (not exceeding 60 mm from ignition point), some smoke, and no droplets of melted material. Flame extinguished immediately after the burner was retracted. Such good results it could be expected as wool is known to outperform any other textile fiber (both natural and synthetic) in terms of fire resistance. In fact, it has a very high ignition temperature of 570–600 °C combined with a high limiting oxygen index (that measures the amount of oxygen needed to sustain combustion) and low combustion heat. Thus, in the light of the above features it is self-extinguishing. In addition, wool does not melt and fibers swell when heated, creating a tighter layer that prevents flame from spreading.

Samples with chitosan binder (Figure 5.5(b,f)) showed a quite different behavior, with a flame spreading up to the topmost part of the sample, limited smoke, and no droplets. The flame extinguished as soon as the burner was retracted, but very small carbonized portions kept burning for about 5 s, with smoke production.

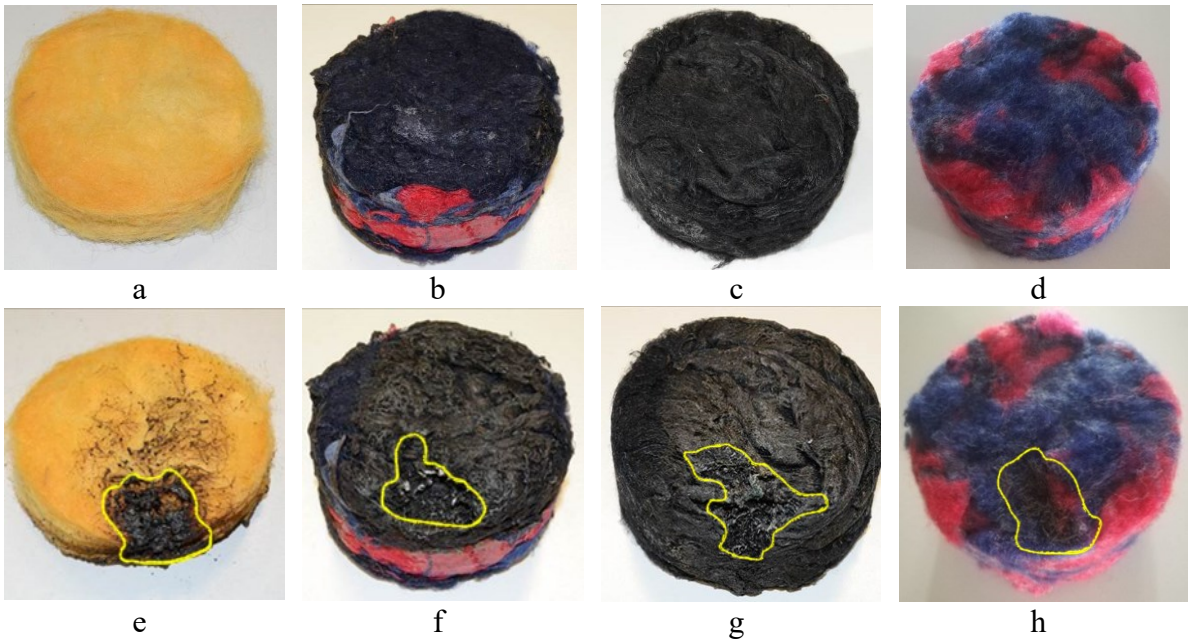

Figure 5.5. Samples used during ignitability test before (a-d) and after (e-h) flame application: pressed wool fibers without binders (a,e), recycled wool with chitosan binder (b,f), recycled wool fibers with gum Arabic binder (c,g), and recycled wool with bi-component fibers (d,h). In yellow, the propagation of flame on the flat samples surface is represented.

As shown in Figure 5.5(c,g), samples with gum Arabic binder showed a limited flame spreading on the flat surface (not exceeding 80 mm from the ignition point), copious smoking, and no droplets. No flaming and smoking was observed after the burner was retracted.

Finally, samples with bi-component fiber as binder (Figure 5.5(d,h)) showed a limited flame spreading on the flat face (not exceeding 60 mm from ignition point), limited smoke and not droplets of melted materials. Furthermore, it was clear that the synthetic fibers burnt before the wool ones. In fact, after the burner was retracted, flame extinguished immediately but the synthetic fibers continued to melt for about 5 s, without smoke.

Thus, some differences that are worth being further investigated were observed. However, results were promising, also in the light of potentially improving this behavior by means of additives (Carosio and Alongi, 2018).

References

Bakatovich, A., Gaspar, F., 2019. Composite material for thermal insulation based on moss raw material. Constr. Build. Mater., 228, 116699. https://doi.org/10.1016/j.conbuildmat.2019.116699.

Baker, I., 2018. Wool, in: Fifty materials that make the world, Springer, New York, NY, USA, pp. 261-265.

Cetiner, I. and Shea, A.D., 2018. Wood waste as an alternative thermal insulation for buildings. Energ. Buildings 168, 374-384. https://doi.org/10.1016/j.enbuild.2018.03.019.

Collet, F., Achchaq, F., Djellab, K., Marmoret, L., Beji, H., 2011. Water vapor properties of two hemp wools manufactured with different treatments. Constr. Build. Mater., 25, 1079-1085. https://doi.org/10.1016/j.conbuildmat.2010.06.069.

Glassman, I., and Harris, B. L., 1952. Collision diameters of some gases as a function of temperature. J. Phys. Chem. 56 (6), 797-799. https://doi.org/10.1021/j150498a036.

ISO/IEC Guide 98-3, 2008. Uncertainty of Measurement – Part 3: Guide to the expression of Uncertainty in Measurement (GUM:1995). https://www.iso.org/sites/JCGM/GUM-JCGM100.htm, (Accessed April 2020).

Korjenic, A., Zach, J., Jitka, J., 2016. The use of insulating materials based on natural fibers in combination with plant facades in building constructions, Energy Build. 116, 45–58. http://dx.doi.org/10.1016/j.enbuild.2015.12.037.

Kremensas., A., Stapulionienė., R., Vaitkus., S., Kairytė., A., 2017. Investigations on physical-mechanical properties of effective thermal insulation materials from fibrous hemp. Procedia Eng. 172, 586-594. https://doi.org/10.1016/j.proeng.2017.02.069.

Pfundstein, M., Gellert, R., Spitzner, H.M., Rudolphi, A., 2008. Properties of insulating materials. In: Schulz, C., (Ed), Insulation Materials: Principles, Materials, Applications. Birkhauser, Basel, pp. 8-15.

Tilioua, A., Libessart, L., Lassue, S., 2018. Characterization of the thermal properties of fibrous insulation materials made from recycled textile fibers for building applications: Theoretical and experimental analyses. Appl. Therm. Eng. 142, 56-67. https://doi.org/10.1016/j.applthermaleng.2018.06.071.

UNI 10351, 2015. Building materials and products - Hygrothermal properties - Procedure for determining the design values. http://store.uni.com/catalogo/index.php/uni-10351-2015, (Accessed April 2020).

Zhang, WM, Meng, G, Wei, X. (2012). A review on slip models for gas microflows. Microfluid Nanofluid 13(6): 845-882. https://doi.org/10.1007/s10404-012-1012-9.

Chapter 6

Analysis of the acoustic experimental results

This chapter partially reports material from:

- Rubino, C., Bonet Aracil, M., Liuzzi, S., Stefanizzi, P. and F. Martellotta, 2021. *Wool waste used as sustainable non-woven for building applications*. J. Clean. Prod. 278, 123905. https://doi.org/10.1016/j.jclepro.2020.123905.
- Rubino, C., Bonet-Aracil, M., Gisbert-Payá, J., Liuzzi, S., Zamorano Cantó, M., Martellotta, F., Stefanizzi, P., 2019. *Composite eco-friendly sound absorbing materials made of recycled textile waste and biopolymers*. Materials 12 (23), 4020. https://doi.org/10.3390/ma12234020.
- Rubino, C., Bonet Aracil, M., Liuzzi, S., Martellotta, F., 2019. *Preliminary investigation on the acoustic properties of absorbers made of recycled textile fibers*. Proceedings of the 23rd International Congress on Acoustic, 9-13 September, Aachen, Germany.

This Chapter includes the analysis of the experimental measurements of the no-acoustic and acoustic properties of the tested samples.

As well as the hygrothermal behaviour, also the acoustic results were very promising. All the samples showed absorption coefficients that, for 50 mm thick, were higher than 0.5 from 500 Hz on, and higher than 0.9 from 1 kHz on. As previously anticipated, a deeper statistical analysis of the laboratory measurements showed that the manufacturing processes especially affected the tortuosity values of the samples with consequent implications on their air flow resistivity, thus on their acoustic performance.

Comparison with theoretical models showed that the approach proposed by Johnson, Champoux and Allard predicted the measured acoustic coefficients better than the theory formulated by Delany and Bazley. This was due to the possibility of the phenomenological model of considering the microstructure of the materials.

6.1 Non-acoustic properties

Table 6.1 outlines the non-acoustic properties resulting from the experimental measurements: the mean values of porosity ε, tortuosity τ and air flow resistivity σ are reported together with their measurement uncertainty expressed as the standard deviation of the mean (ISO/IEC Guide 98-3, 2008).

As it can be observed, all materials were characterized by a porosity close to 0.9, regardless of the nature of the binder. This was in agreement with the porosity values of felts and mineral fiber materials ranging respectively from 0.83 to 0.95 and from 0.92 to 0.99 (Mechel, 2008). A void fraction close to 90% was expected in light of the microstructural analysis carried out in Section 2.2.

With reference to tortuosity, although samples under test should have a tortuosity value close to the unity, complying with the idea of a fibrous structure (Willie and Spangles, 1952), some significant differences could be observed especially for BICO samples. Table 6.1 shows the tortuosity values τ directly measured for BICO and CH samples; while tortuosity could not be measured for GA samples. As it can be observed, τ values of BICO samples varied from 1.09 to 2.55; whereas CH samples were characterized by τ values slightly higher than one (τ varied from 1.11 to 1.23). Such results suggested that the different process used to produce the materials could largely affect the geometric complexity of their fibrous microstructure. Likely, when the wool batting was soaked in the chitosan solution and then squeezed, the air trapped in the voids was eliminated and the fibers tended to align. Therefore, samples with a network of pores interconnected following a preferential direction were obtained. Conversely, the richly entangled microstructure resulting from wool carding was better preserved when bi-component fibers were hot molded. An agreement with some vegetal woolen building materials showing high porosity and a tortuosity of about one (Piégay et al., 2018 and Glé et al., 2018) was observed for CH samples.

Table 6.1. Non-acoustic properties of BICO, CH and GA samples resulting from the experimental measurements: mean values of porosity ε, tortuosity τ and air flow resistivity σ expressed with the standard deviation of the mean.

Sample code	ρ_{bulk} [kg/m^3]	ε [-]	τ [-]	σ [kN·s/m^4]
BICO-1	167±6	0.88±0.0005	2.55±1.17	76.8±16.8
BICO-2	136±1	0.90±0.0006	1.82±0.81	69.4±10.7
BICO-3	115±1	0.91±0.0003	2.16±0.37	59.3±10.5
BICO-4	90±2	0.93±0.0004	1.09±0.11	44.9±12.0
BICO-5	51±1	0.95±0.0008	1.32±0.66	23.6±2.2
CH-1	197±2	0.86±0.0028	1.23±0.07	66.3±7.8
CH-2	145±2	0.89±0.0008	1.11±0.05	46.0±9.1
CH-3	122±1	0.91±0.0013	1.12±0.05	16.5±2.7
CH-4	80±1	0.94±0.0016	1.20±0.18	11.7±2.2
GA-1	177±3	0.87±0.0014	-	44.7±5.0
GA-2	143±2	0.90±0.0003	-	23.6±2.5
GA-3	93±1	0.93±0.0004	-	14.4±2.3

As anticipated in Section 4.2, although the non-acoustic parameters of the produced samples were experimentally measured, the inverse method was also used to estimate them. In Table 6.2, the parameters obtained by the inverse characterization for each type of materials (i.e. the tortuosity τ*, the air flow resistivity σ*, the shape factor s* and the characteristic length ratio Λ/Λ'*) are marked with a star.

A comparison between measured and estimated tortuosity values (respectively τ and τ*), both available for CH samples, was carried out. As it can be observed in Tables 6.1 and 6.2, τ* values resulted underestimated respect to τ values with differences between 11% and 19%. Therefore, in light of the above mentioned effect of the manufacture procedure of materials on their microstructure and being CH and GA samples produced following a similar process, similar differences between τ and τ* might be expected. On the contrary, the tortuosity values estimated for BICO samples didn't take into account the effect of the manufacture method on the microstructure of the materials. In fact, τ* values were close to unity, resulting similar to CH and GA samples. However, tortuosity values higher than one for denser BICO samples were verified by their air flow resistivity values which were higher than those of CH and GA materials with comparable density.

Table 6.2. Non-acoustic properties of BICO, CH and GA samples resulting from the inverse characterization: values of tortuosity τ^*, air flow resistivity σ^*, shape factor s^* and characteristic lengths ratio Λ/Λ'^*.

Sample code	ρ_{bulk} [kg/m^3]	τ^* [-]	σ^* [kN·s/m^4]	s^* [-]	Λ/Λ'^* [-]
BICO-1	167±6	1.30	86.0	1.35	1.00
BICO-2	136±1	1.30	54.1	1.32	1.00
BICO-3	115±1	1.00	48.6	1.95	1.00
BICO-4	90±2	1.30	33.2	1.40	1.00
BICO-5	51±1	1.30	23.4	1.50	1.20
CH-1	197±2	1.90	78.2	0.80	2.00
CH-2	145±2	1.30	48.8	2.00	2.00
CH-3	122±1	1.00	19.5	3.00	2.00
CH-4	80±1	1.00	13.8	2.00	2.00
GA-1	177±3	1.00	50.1	1.50	2.00
GA-2	143±2	1.00	27.8	2.50	2.00
GA-3	93±1	1.00	15.3	2.00	2.00

Figure 6.1 compares the values of the air flow resistivity obtained from the laboratory measurements and from the inverse algorithm.

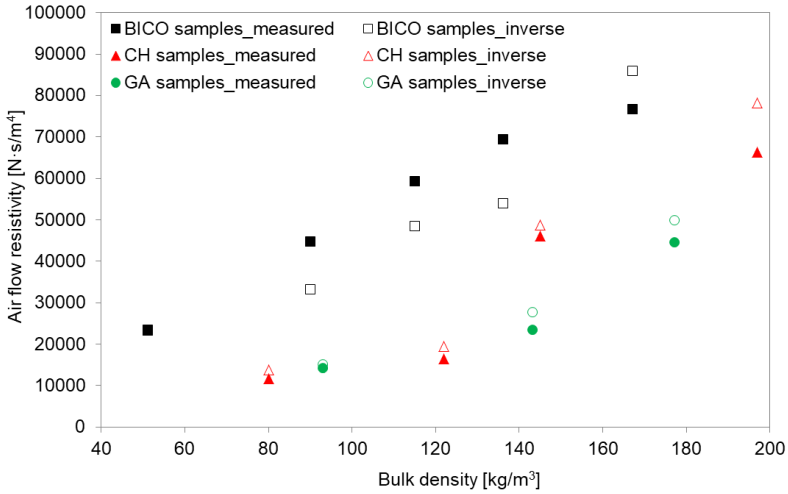

Figure 6.1. Measured and inverse air flow resistivity values, σ and σ*, vs. bulk density ρbulk for samples produced using bi-component fibers, chitosan and gum Arabic solution as binder.

As it can be observed, σ values measured for BICO samples resulted higher than those measured for CH and GA samples. Such result could be explained by the tortuosity measurements. In fact, higher tortuosity values measured for BICO samples implied more

intricate flow paths, resulting in less air permeability. However, air flow resistivity for all tested materials was below 100 kN·s/m^4 which is the limiting value for a material to be considered as an impervious layer, as reported by del Rey et al (2015).

The comparison between the measured and the inverse values shows that the difference was up to 15% for CH and GA samples and up to about 22% for BICO ones.

6.2 The acoustic properties

The acoustic behaviour was evaluated comparing the sound absorption curves of the different mix prepared for each type of material. The air flow resistivity obtained from the inverse algorithm σ* was considered for comparison because σ showed significant variations during measurements.

Figure 6.2(a) plots the mean sound absorption coefficients values resulting from the impedance tube measurements for BICO non-wovens. As it can be seen, the acoustic behaviour of the samples changed according to their air flow resistivity values, providing sound absorption curves with different trends. The BICO-1 sample, having $\sigma^* = 86.0\ \mathrm{kN \cdot s/m^4}$, exhibited a sound absorption curve without evident peaks due to its high air flow resistivity value which reflected the low air permeability of the material.

Conversely, the sample BICO-5 showing a $\sigma^* = 23.4\ \mathrm{kN \cdot s/m^4}$, proved to be more permeable to air and showed a sound absorption curve with a peak moving towards medium and high frequencies; while its absorption in the low frequency range became weaker than BICO-1.

The remaining samples, characterized by σ* value between 54.1 and 33.2 kN·s/m^4, showed intermediate acoustic behaviours between that of BICO-1 and BICO-5 samples.

The BICO-4 sample, having $\sigma^* = 33.2\ \mathrm{kN \cdot s/m^4}$, exhibited a behaviour similar to that of BICO-5, with sound absorption coefficients which sharply increased at medium and high frequencies. However, some differences in the location of the first peak of the two materials could be noticed. For BICO-4, the first peak appeared at 1000 Hz, with α rising up to almost 0.9; while for sample BICO-5 the first peak appeared at 1250 Hz, with α rising up to almost the unity.

At the same frequencies, lower sound absorption properties were observed for the samples BICO-2 and BICO-3 which exhibited α coefficients almost overlapped at all

frequencies as a consequence of their comparable σ* values (i.e. 54.1 kN·s/m^4 for BICO-2 and 48.6 kN·s/m^4 for BICO-3). For both samples, α was equal to about 0.8 at 1000 Hz and just over 0.8 at 1250 Hz. The sound absorption coefficients trend of the samples BICO-2 and BICO-3 could be considered similar to that of BICO-1 sample due to their sound absorption curves shifted towards low frequencies, with α values higher than BICO-4 and BICO-5 samples up to 400 Hz. However, starting from 500 Hz, the sound absorption coefficients of the BICO-2 and BICO-3 samples were about 0.1 higher than BICO-1 sample, without showing evident peaks.

Figure 6.2(b) plots the absorption coefficients obtained from the experimental measurements for CH samples. A comparison among all the investigated materials pointed out that the samples CH-4 and CH-3 showed a sound absorption coefficients trend in accordance with the acoustic behavior of mats with higher absorbent performance. This was due to their low air flow resistivity values (13.8 kN·s/m^4 for CH-4 and 19.5 kN·s/m^4 for CH-3) and their surface impedance values as close as possible to the wave impedance of the air, allowing sound wave to easily penetrate the material. Although the sound absorption curves of the two samples were very similar up to 315 Hz, some differences in the location of the first peak could be noticed. For CH-4 sample, a first peak appeared at 1250 Hz, with α raising up to almost the unity; while for CH-3 sample, a first peak appeared at 1000 Hz, with α raising up to 0.92.

The sound absorption capability of the CH-1 and CH-2 mix decreased in the mid and high frequency ranges and increased at low frequencies. At 1250 Hz, α was around 0.73 for sample CH-1 and 0.86 for sample CH-2, against 0.92 for sample CH-3 and 0.99 for sample CH-4. This was because the high air flow resistivity values of the samples CH-1 and CH-2 (78.2 kN·s/m^4 and 48.8 kN·s/m^4, respectively) increased the viscous and thermal interaction inside the micro pores forming the material, but at the same time, the surface impedance also increased.

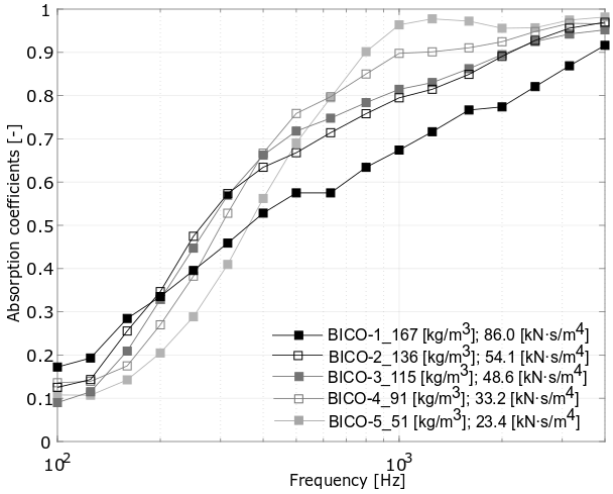

(a)

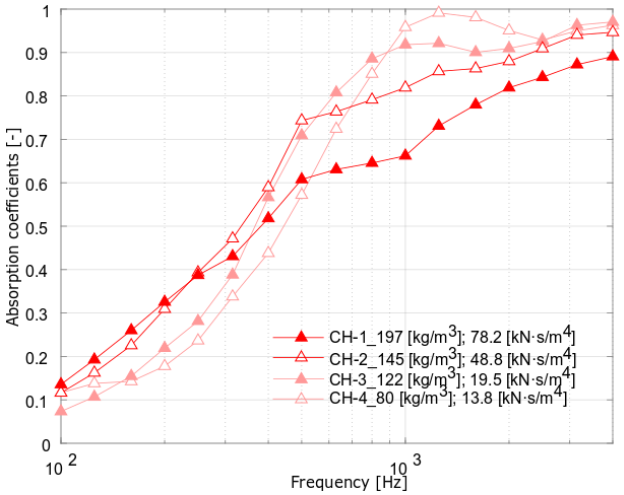

(b)

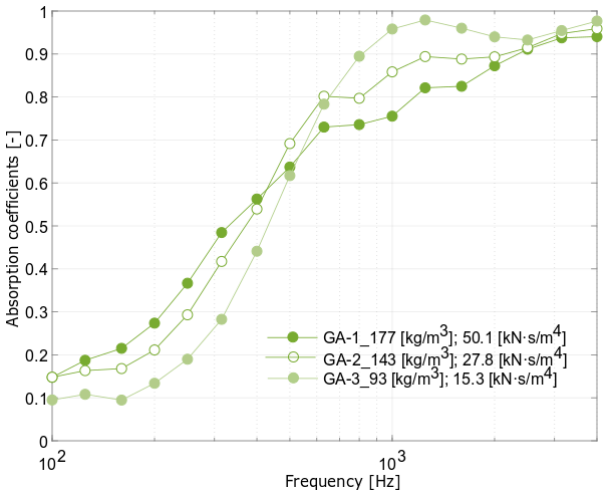

(c)

Figure 6.2. Mean measured normal incidence sound absorption coefficients of BICO (a), CH (b) and GA (c) samples.

In Figure 6.2(c), the experimental sound absorption coefficients measured for GA samples are shown. As observed for the two groups of samples previously analyzed, the different values of the air flow resistivity allowed to distinguish different trends of the acoustic behaviour for samples GA-1 (50.1 kN·s/m^4) and GA-3 (15.3 kN·s/m^4); whereas an intermediate behaviour was observed for sample GA-2 (27.8 kN·s/m^4).

The GA-1 sample showed absorption coefficients that increased more sharply than GA-3 until 500 Hz, where α was about 0.6 for both mix. Then, a change in the trend of the sound absorption curves was observed with α values higher for GA-3 than GA-1 sample.

An intermediate behaviour was observed for sample GA-2 due to its intermediate air flow resistivity value. For example, at 315 Hz, α was about 0.5 for GA-1 sample versus 0.3 for GA-3 samples and 0.4 for GA-2 sample. At 1250 Hz, where GA-3 sample raised up a peak of about 0.9, α was 0.9 for GA-2 sample and 0.8 for GA-1.

6.2.1 Comparison of BICO, CH and GA samples

The sound absorption curves of BICO, CH and GA samples individually evaluated in the above Section, were compared in order to provide a complete analysis of the possible effects of the manufacturing processes on the sound absorption behaviour of the tested materials. The air flow resistivity obtained from the inverse algorithm σ^* was considered for comparison.

A comparison between BICO and CH samples shows that materials with different bulk densities were characterized by a similar sound absorbent behaviour. As it can be observed in Figure 6.3(a), the absorption curves of the samples BICO-1 and CH-1 were almost overlapped. Furthermore, BICO-1 mix showed an air flow resistivity value 9% higher than CH-1, despite was 15% lighter. Likewise, CH-2 and BICO-3 materials were characterized by similar air flow resistivity values, resulting in almost overlapped sound absorption curves, although BICO-3 sample was 21% lighter than CH-3 one (Figure 6.3(b)). This could be explained due to the tortuosity value which was 2.55 for BICO-1 sample versus 1.23 for CH-1 sample; while τ was 2.16 for BICO-3 sample versus 1.11 for CH-2 one. The high τ value led to more intricate microscopic air flow paths in the BICO samples which resulted less permeable than CH ones, despite their lower bulk densities.

Similar consideration could be made when BICO and GA materials were compared, despite no direct measure of tortuosity was available for GA samples (Figure 6.3(c)). BICO-2 sample showed sound absorption coefficients comparable to GA-1 sample and an air flow resistivity value 7% higher, although its density value was about 23% lower. Considering valid the tortuosity values obtained from inverse algorithm for GA sample, the higher air flow resistivity of BICO sample could be ascribe to its tortuosity value higher than GA sample. In fact, τ^* was 1 for GA-1 sample; whereas τ was 1.82 for BICO-2 sample.

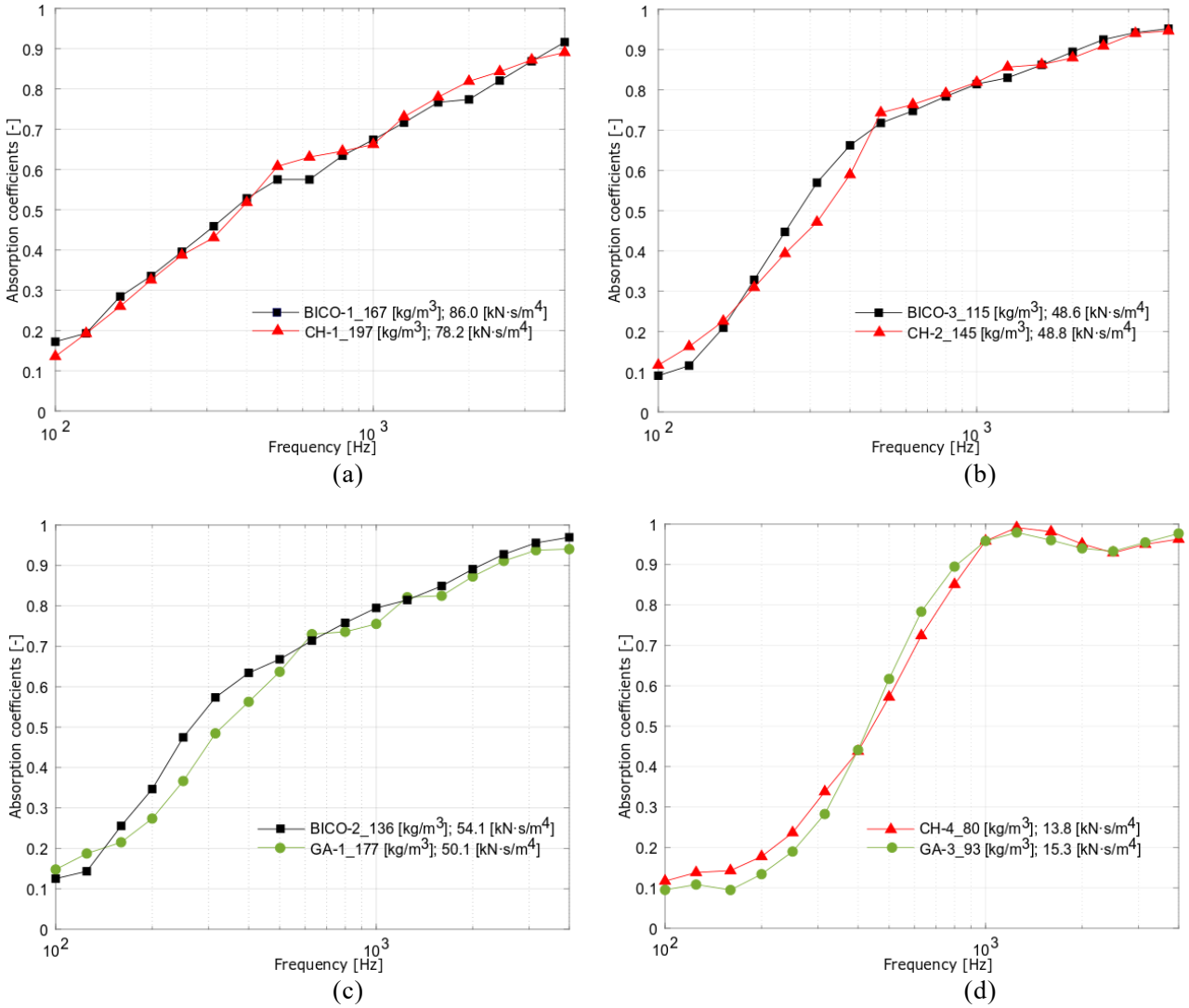

Figure 6.3. Comparison of the sound absorption curves of samples BICO-1 and CH-1 (a), BICO-3 and CH-2 (b), BICO-2 and GA-1 (c), CH-4 and GA-3 (d).

Taking into account comparison between CH and GA materials, Figure 6.3(d) displays that samples CH-4 and GA-3 samples showing absorption curves perfectly overlapped at all frequencies as a consequence of their similar bulk density and air flow resistivity values.

6.2.2 Comparison with the acoustic prediction models

The acoustic behaviour of the investigated samples was discussed by comparing the sound absorption curve resulting from the impedance tube measurements with values predicted by Delany-Bazley and Johnson–Champoux–Allard theoretical models.

Following the previously described determination of the non-acoustic parameters according to both direct measurement and inverse method (Chapter 3), the subsequent discussion was referred to predictions based on the "optimized" parameters and, for comparison purposes, on the measured values. The absolute error expressed as a mean value of the absolute difference between the sound absorption coefficients predicted by the theoretical models and those resulting from the experimental measurements was used to test the accuracy of the predicted sound absorption curves.

As previously mentioned in Section 4.2, JCA models was fed using the directly measured values of porosity ε and tortuosity τ; while the values of the characteristic physical properties (Λ/Λ'* and s*) and the air flow resistivity σ* were estimated by the inverse algorithm. Taking into account the D&B model, the "inverse" value of the air flow resistivity was used.

Table 6.3 shows the mean absolute errors ($e_{D\&B}$ and e_{JCA}) of the sound absorption coefficients when the measured air flow resistivity values were used to fed the JCA and D&B models and the mean absolute errors ($e_{D\&B}$* and e_{JCA}*) obtained using the estimated air flow resistivity values. As it can be observed, the use of optimization techniques allowed to significantly reduce the error values $e_{D\&B}$ and e_{JCA}.

Table 6.3. The mean absolute errors $e_{D\&B}$ and e_{JCA} of the sound absorption coefficients when the measured air flow resistivity values are used to fed the JCA and D&B models and the mean absolute errors $e_{D\&B}$* and e_{JCA}* obtained using the estimated air flow resistivity values in the JCA and D&B.

Tested materials	$e_{D\&B}$ [-]	$e_{D\&B}$* [-]	e_{JCA} [-]	e_{JCA}* [-]
BICO-1	0.0345	0.0475	0.0297	0.0186
BICO-2	0.0870	0.0564	0.0494	0.0273
BICO-3	0.0686	0.0468	0.0480	0.0292
BICO-4	0.0600	0.0464	0.0465	0.0267
BICO-5	0.0323	0.0325	0.0161	0.0159
CH-1	0.0249	0.0357	0.0172	0.0167
CH-2	0.0407	0.0405	0.0240	0.0171
CH-3	0.0604	0.0489	0.0295	0.0246
CH-4	0.0443	0.0340	0.0334	0.0284
GA-1	0.0297	0.0251	0.0307	0.0164
GA-2	0.0540	0.0396	0.0304	0.0288
GA-3	0.0306	0.0306	0.0263	0.0247

Figure 6.4 displays the sound absorption coefficients measured and predicted for the BICO samples. Particularly, Figure 6.4(a) compares measured and predicted sound absorption coefficients of BICO-1 sample. The comparison with the theoretical curves pointed out that the D&B empirical model gave rise to significant discrepancies, despite the σ* value was used to implement the model. On the contrary, the JCA model almost perfectly predicted the trend of the experimental absorption coefficients of the sample.

A similar result was observed when the experimental and the theoretical sound absorption curves of the samples BICO-2 and BICO-3 were compared (Figure 6.4(a)). The JCA model predicted the measured values of the two materials better than the D&B one. Although significant discrepancies appeared from 250 Hz to 400 Hz, the phenomenological model allowed a rather precise estimation of the absorption coefficients fluctuations starting from 800 Hz.

Figure 6.4(c-d) plot the acoustic behaviours of the samples BICO-4 and BICO-5. It can be noted that the phenomenological approach allowed a rather good estimation of first peak location, its maximum-minimum fluctuations and values of absorption coefficients for both materials. However, slightly larger discrepancies between measurements and

predictions could be appreciated for BICO-4 sample in the medium frequencies range from 250 to 500 Hz, where the JCA model slightly underestimated the measured absorption coefficients. D&B model predicted the acoustic behaviour of both BICO-4 and BICO-5 samples better than of the remaining three materials. Possibly, this occurs because BICO-4 and BICO-5 were the only samples having air flow resistivity lower than 50 kN·s/m^4, which is the upper limit for a safe application of the empirical model.

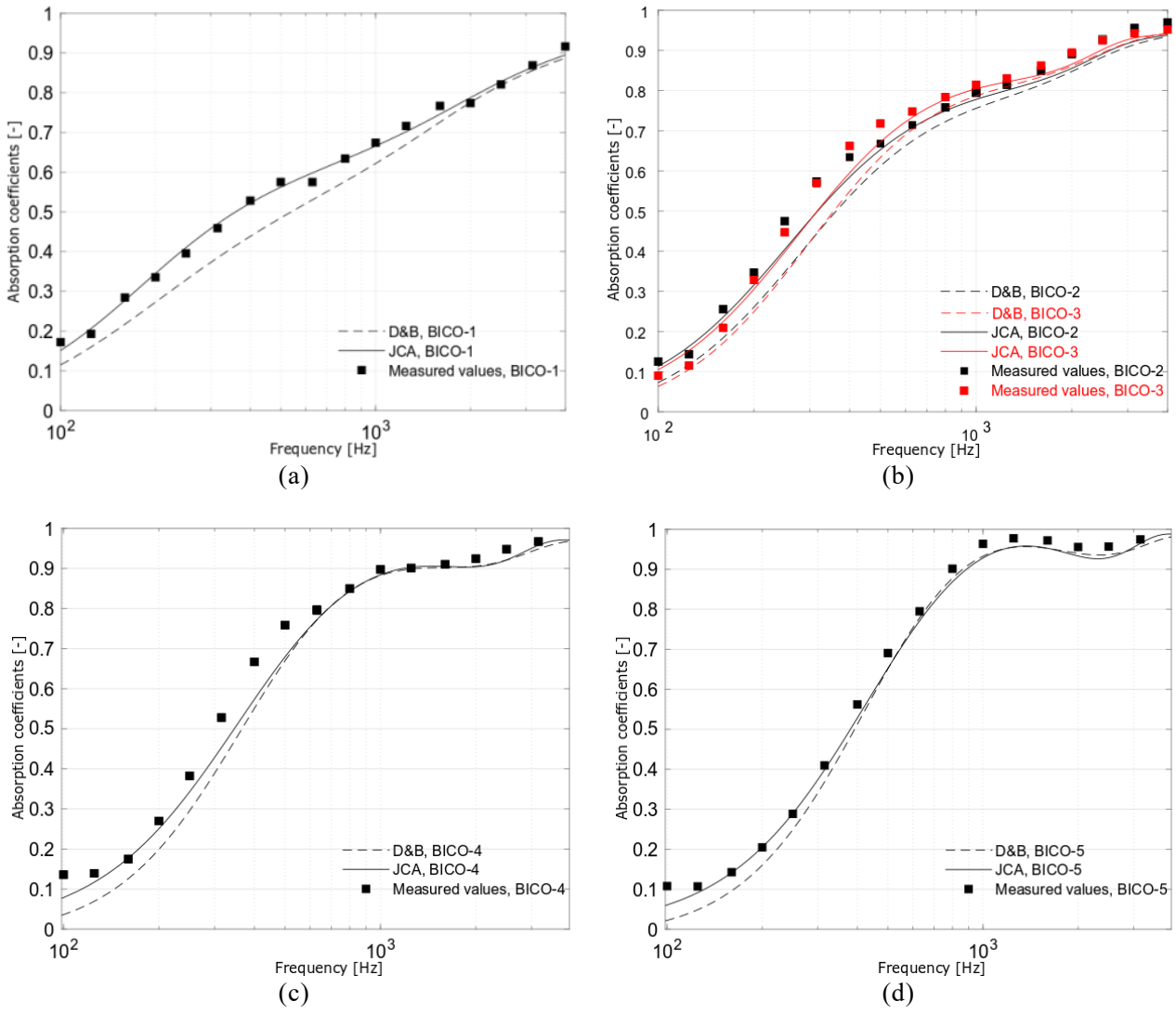

Figure 6.4. Comparison between mean measured normal incidence sound absorption coefficients and those predicted by the D&B and JCA model for BICO-1 sample (a), BICO-2 and BICO-3 samples (b), BICO -3 sample (c) and BICO-4 sample (d).

As observed for the BICO samples, the phenomenological model outperformed the empirical model in comparison with measured absorption coefficients of the CH samples too (Figure 6.5). Figure 6.5(a) compares measured and predicted sound absorption coefficients of CH-1 and CH-2 samples. The JCA model predicted better than the D&B one the acoustic behaviour of the two samples. In fact, the JCA curves almost overlapped the experimental ones with some discrepancies around 500 Hz.

In Figure 6.5(b), it can be observed that the phenomenological model perfectly predicted the acoustic behaviour of the CH-3 sample up to 500 Hz. Starting from 630 Hz some discrepancies appeared in the estimation of the peak fluctuations. However, the first peak predicted by JCA model was almost aligned to the measured one, although overestimated. Conversely, the D&B model predicted the first peak at 1250 Hz instead of 1000 Hz, with α close to unity. Considering the CH-4 material, the phenomenological model allowed a rather precise estimation of the first peak appearing around 1250 Hz with α close to unity and the following drop around 2500 Hz. On the contrary, the empirical model predicted the first peak at 1600 Hz and the following drop at 3150 Hz.

Figure 6.6 compares measured and predicted sound absorption coefficients of GA samples. As it can be observed in Figure 6.6(a), both phenomenological and empirical models estimated the acoustic behavior of the GA-1 sample almost with the same good accuracy.

Similar consideration could be made for GA-3 sample (Figure 6.6(b)), although JCA model predicted the fluctuations at high frequencies better than D&B one, allowing a precise estimation of the first peak followed by a drop. Possibly, the accuracy of the empirical model for GA-1 and GA-3 samples was due to their air flow resistivity, lower the upper limit for a safe application of the empirical model (i.e. 50 kN·s/m^4). On the contrary, taking into account the GA-2 material, a poor correspondence was verified between the predicted and the measured curves, despite the low air flow resistivity value of the sample. Significant discrepancies appeared between 600 and 1600 Hz, where measured values were lower than expected according to the models, and apparently no combination of parameters could return a similar behavior. Thus, the discrepancy should suggest that some anomalous

behavior took place with GA-2 samples. In fact, both phenomenological and empirical models didn't estimate the first peak at 630 Hz and the second one at 1250 Hz.

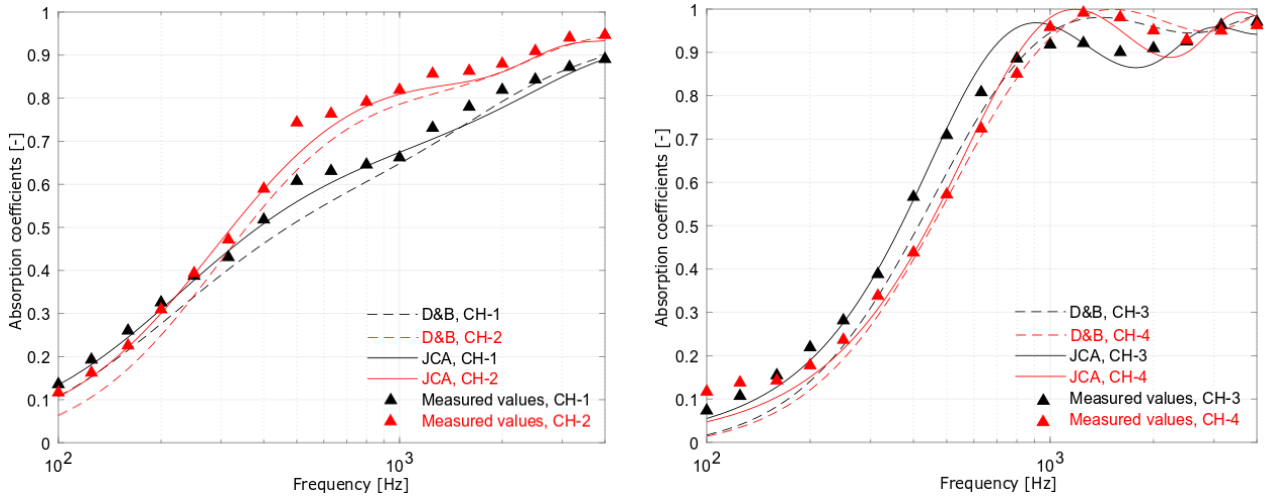

(a) (b)

Figure 6.5. Comparison between mean measured normal incidence sound absorption coefficients and those predicted by the D&B and JCA model for CH-1 and CH-2 samples (a) and CH-3 and CH-4 samples (b).

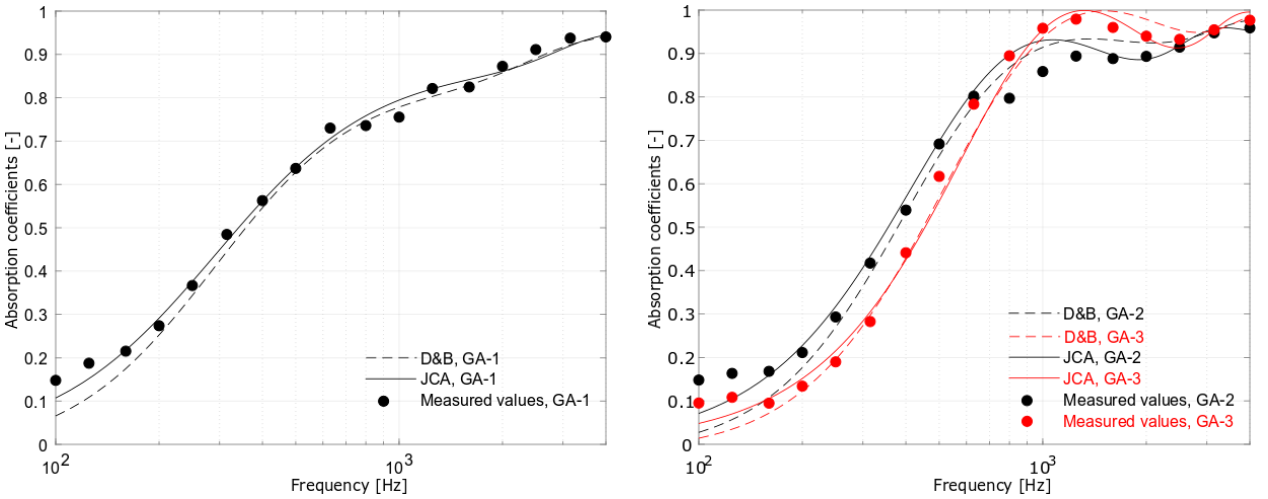

(a) (b)

Figure 6.6. Comparison between mean measured normal incidence sound absorption coefficients and those predicted by the D&B and JCA model for GA-1 sample (a) and GA-2 and GA-3 samples (b).

References

Del Rey, R., Bertó, L., Alba, J., Arenas, J.P., 2015. Acoustic characterization of recycled textile materials used as core elements in noise barriers. Noise Control Eng. J., 63(5), 439-447. http://dx.doi.org/10.3397/1/376339.

Glé, P., Blinet, T., Guigou-Carter, C., 2018. Acoustic performance prediction for building elements including biobased fibrous materials. In: Proceedings of the Euronoise 2018, Crete, Greece, 27–31.

ISO/IEC Guide 98-3, 2008. Uncertainty of Measurement – Part 3: Guide to the expression of Uncertainty in Measurement (GUM:1995). https://www.iso.org/sites/JCGM/GUM-JCGM100.htm, (Accessed April 2020).

Mechel, F.P., 2008. Porous Absorbers, in: Formulas of Acoustics, Mechel, F.P., Ed. Springer, New York, USA. pp. 348–402.

Piégay, C., Glé, P., Gourdon, E., Gourlay, E., Marceau, S., 2018. Acoustical model of vegetal wools including two types of fibers. Appl. Acoust., 129, 36–46. https://doi.org/10.1016/j.apacoust.2017.06.021.

Willie, M.R.J. and Spangles, M.B., 1952. Application of electrical resistivity measurements to problem of fluid flow in porous media. Am. Assoc. Pet. Geol. Bull, 36 (2), 359-403. https://doi.org/10.1306/3D934403-16B1-11D7-8645000102C1865D.

Chapter 7

Alternative mix design to improve the thermal behaviour of the samples

This chapter partially reports material from:

- Rubino, C., Liuzzi, S., Martellotta, F., Stefanizzi, P., Straziota, P., 2021. *Nonwoven textile waste added with pcm for building applications* Appl. Sci. 11, 1262. https://doi.org/10.3390/app11031262.

As previously explained, the buildings and the construction sectors are responsible for the use of large amounts of energy. Most of the energy used in buildings is aimed to maintain adequate indoor conditions in terms of thermal comfort. Therefore, the development of new materials with the purpose of increasing the buildings thermal efficiency is becoming imperative. In response to this need, as the tested materials are lightweight, part of this research was designated to investigate how the integration of Phase Change Materials (PCMs) in the tested non-woven samples could improve their thermal energy storage capacity. Particularly, the behaviour of the samples produced using gum Arabic as binding agent was studied due to the easier and greater economic availability of this binder on the market. At the beginning, the basic thermodynamics characteristics of the used PCMs resulting from the DSC test are reported. Then, the thermal properties of the samples containing PCMs are investigated in order to demonstrate their energy storage capacity in comparison with a reference sample without PCMs. The Chapter closes with an analysis of the heat flux exchanged through the internal and the external surfaces of the samples in a Hot Box test. The study of the flux as a function of time and temperature proved that the addition of the PCMs microcapsules improved the ability of materials in reducing the temperature fluctuations and shifting the temperature peaks.

7.1 Materials and methods

The latent thermal energy storage is a useful tool for improving energy efficiency and increasing energy savings in buildings ensuring, at the same time, the improvement of the users comfort. Phase change materials (PCMs), in liquid or powdered form, are largely used for their considerable energy storage capacity, as they are able to absorb and release energy from/in the environment, leading to a reduction of the temperature fluctuations. The working principle of PCMs takes advantages of changing their state due to temperature variations: as the temperature increases, the PCMs melt absorbing thermal energy from the environment; conversely, when the temperature decreases, they solidify releasing the previously stored energy (Frigione et al. 2019). Once the melting point is reached, the PCMs will maintain a slightly constant temperature for a more or less significant period depending on their amount. In fact, all the absorbed thermal energy is used to break the chemical bonds and to make the phase change take place. The melting heat is called "latent heat of fusion" and is strictly correlated to the thermal storage capacity of PCMs (Socaciu, 2012).

Phase change materials can be included in building components through different ways i.e., direct incorporation, immersion, micro and macro encapsulation, and stabilization. Among all these potential techniques, encapsulation is the most frequently used method because it involves the incorporation of PCMs in capsules with a protective shell able to prevent material leakage during the phase transition. Furthermore, in this way the PCMs can be directly used in the mixing process of the construction materials (da Cunha and de Aguiar, 2020). The micro-encapsulation leads to several advantages over the macro-encapsulation procedure (Abokersh et al., 2017). It involves the use of small PCM particles, ranging from 0.1 μm to 1 mm,. providing a high rate of heat transfer due to a large surface area per unit volume. The micro-encapsulation technique also improves chemical stability and thermal reliability (the latter representing the capability to repeat many times the melt/freeze cycle without the occurrence of degradation phenomena) (Hassan et al., 2016). These listed aspects contribute to expand the possibilities of integration of PCMs microcapsules in construction materials (Riffat ey al. 2015).

Not all existing phase change materials can be used for thermal storage in building applications; but the selection of the appropriate PCM for a specific construction material

could start from the analysis of its properties as the melting temperature and the latent heat (Pasupathy et al., 2008). Referring to the melting temperature, materials with a melting/freezing temperature between 18 °C and 40 °C are particularly suitable for application in construction sector. According to the literature (Whiffen and Riffat, 2013 and Kamali, 2014), the temperature of PCM phase transition should be very close to the human comfort one (i.e., 22–26 °C). Nevertheless, phase change materials that fall within three temperature ranges have been suggested for use in buildings: up to 21 °C PCMs are suitable for cooling applications; from 22 °C to 28 °C for reaching optimal human comfort; from 29 °C to 60 °C for hot water applications, such as in the case of radiant floors with water it could be combined with PCMs (Cabeza et al., 2011).

The PCMs incorporation in materials employed on the internal side of buildings appears the most attractive solution in order to minimize the massive energetic consumption related to building conditioning. The aim is to regulate the temperature inside buildings through latent heat energy storage, reducing the use of heating and cooling energy. Furthermore, it is with low thermal mass materials that PCMs prove to be more effective. Therefore, the most frequent use of PCMs involves their incorporation in mortar and concrete, in which the efficiency of the treatment is improved due to the large heat exchange area surface. In recent years, several researches (Serrano et al., 2015 and Toppi and Mazzarella, 2013) has been focused on the easy incorporation of cheap microcapsules filled with paraffin, into gypsum-based plasters paste for internal walls or plasterboard panels.

In addition to improving the thermal behaviour of the building materials, the phase change materials led advantages in terms of low environmental impact. In fact, they can be classified in organic PCMs (i.e. paraffin and fatty acids) which are biodegradable, inorganic PCMs (i.e. salt hydrates) which are innocuous and eutectic ones (combination of two or more substances, either organic, inorganic, or both). At the end of their useful life, most PCMs can be recycled, being more sustainable than conventional construction materials (Baldassarri et al., 2017).

7.1.1 Description and characterization of used PCMs

In order to test the effects of adding phase change materials on the thermal behaviour of the gum Arabic-based non-woven, Micronal® DS 5001 X produced by the German company BASF was chosen as organic paraffin-based PCM. It is a dry powder PCM, microencapsulated with highly cross-linked polymethylmethacrylate polymer wall, formaldehyde-free. The particle size varies from 0.1 to 0.3 mm, with a bulk density ranging from 250 to 350 kg/m^3. Its 26 °C melting temperature falls within the range of average working temperatures that characterize a Mediterranean climate, making the Micronal® DS 5001 X suitable for construction applications through direct incorporation into building materials for the purpose of improving interior comfort conditions. The latent heat of fusion for selected PCMs is about 110 kJ/kg, with an overall storage capacity of 145 kJ/kg in temperature range 10÷30 °C. More detailed information about the properties of the Micronal® DS 5001 X (i.e. the phase-change temperature between 26.09 °C and 27.81 °C, the melting enthalpy between 114.98 kJ/kg and 142.55 kJ/kg, and the solidification enthalpy between 117.85 kJ/kg and 137.85 kJ/kg) are given by Giro-Paloma et al. (2013).

A dynamic Differential Scanning Calorimetry (DSC) analysis with constant heating rates of 0.5 °C/min was performed in order to characterize the thermal behavior of the chosen PCMs (Figure 7.1). The analysis was carried out on 5.5 mg sample of material, following the methods previously illustrated in Section 2.2.

As it can be observed in Figure 7.1, the DSC curve shows two endothermic processes. The first process was noted from -2.74 °C to 1.79 °C, with a peak temperature of -0.31 °C. This baseline shift it could be due to the phase change of the water within the sample; therefore it was not taken into account. The second endothermic transformation referred exclusively to Micronal® DS 5001 X. The process was observed from 24.72 °C to 33.71 °C, with a peak of 29.19 °C. The area of the transformation was 632.09 mJ and the melting enthalpy was 114.93 kJ/kg, resulting complies with the manufacturer specifications on the technical data sheet (i.e. 110 kJ/kg).

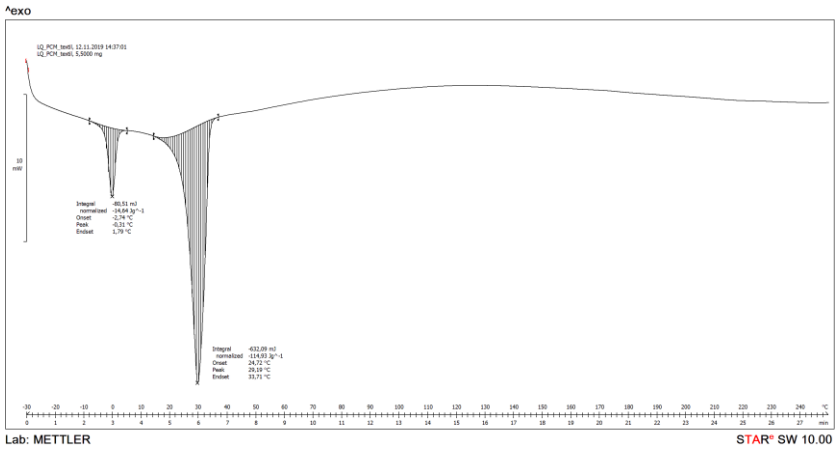

Figure 7.1. DSC curve of Micronal® DS 5001 X PCM.

On the contrary, the peak temperature and the nominal value of the melting temperature of 26 °C differed of about 3 °C from the manufacturer specifications. This discrepancy could be due to the measurement conditions, including heating speed and mass of the sample. In fact, the peak temperature is not an intrinsic value of the material and it is generally unreliable for comparison purposes (Giro-Paloma et al., 2013).

The DSC test was useful to determine the enthalpy-temperature function, an important characteristic of phase change materials related to their heat storage capacity. As shown in Figure 7.2, the first and the last slopes of the curve represent the specific heat capacity of the solid and the liquid phases of the PCM, respectively. The phase change enthalpy variation corresponds to the central slope of the curve and resulted not attributed to a single temperature, but to a broadened melting range.

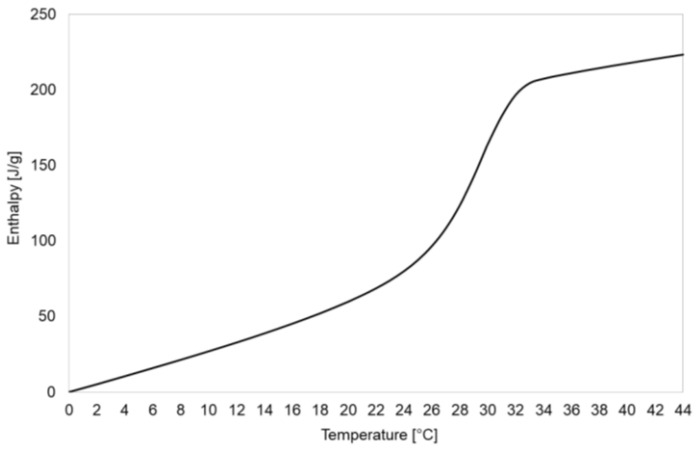

Figure 7.2. Enthalpy variation with temperature for Micronal® DS 5001 X.

7.1.2 Samples preparation

The three steps chemical bonding method explained in Section 2.3 (Figure 2.11) was followed to produce non-wovens similar to GA materials previously tested, but with the addition of PCMs. After squeezing the excess of gum Arabic-based binder, tufts of batting fibers were placed in cylindrical molds 5 cm thick and 10 cm in diameter, alternating wool and PCM powder. This latter was homogeneously added between the various layers, so that the PCMs remained trapped between the meshes of the sample. Finally, the samples were dried in an oven for about 12 h at 60 °C. As shown in Figure 7.3, three specimens were prepared: one without PCM which was used as reference and was referred as "PCM-00"; the other two were produced using different percentages of phase change materials (i.e. 26% and 41%) and were respectively referred as "PCM-26" and "PCM-41".

Figure 7.3. From left to right: PCM-00, PCM-26, PCM-41.

Tables 7.1 outlines the quantity expressed in grams of raw materials used to produce the tested samples.

Table 7.1. Quantity of materials used to prepare the samples.

Sample ID	Wool [g]	Gum Arabic [g]	Water [mL]	PCM [g]
PCM-00	25	20	100	/
PCM-26	25	20	100	12.50
PCM-41	25	20	100	25

Table 7.2. shows the percentages of wool fibers, gun Arabic solution and PCM resulted in each sample, after squeezing the excess of binder.

Table 7.2. Weight percentage of materials used.

Sample ID	Wool [%]	Gum Arabic [%]	PCM [%]
PCM-0	73.19	26.81	40.72
PCM-26	52.55	21.17	18.57
PCM-41	25	26.28	40.72

The morphological analysis of the prepared samples was carried out using the Scanning Electron Microscope (SEM), as previously explained in Section 2.2. Figure 7.4 shows the interaction between the wool fibers, the binder and the PCM microcapsules whose surfaces look compact without any deformations.

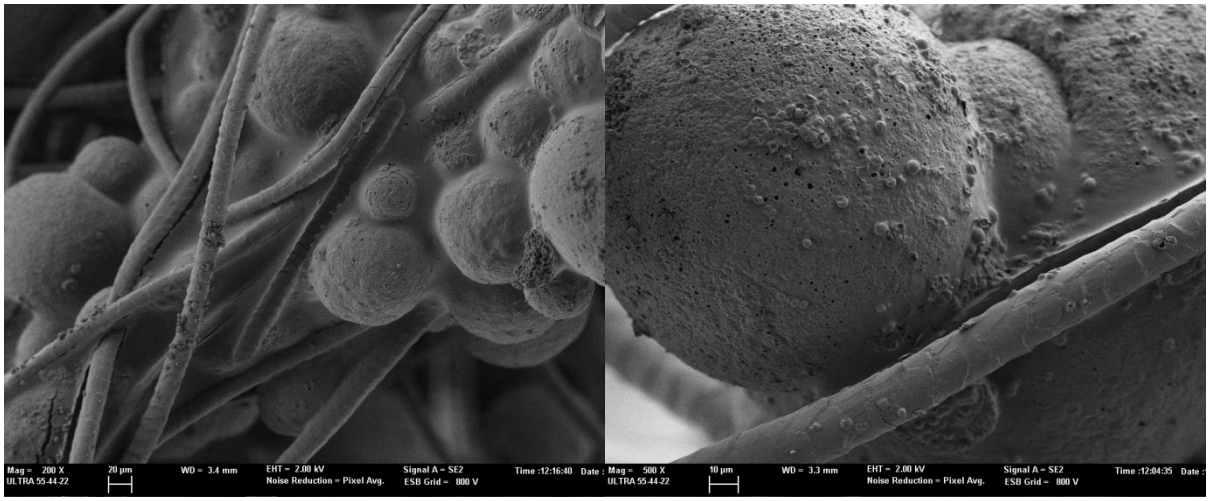

(a) (b)

Figure 7.4. SEM micrographs of wool at 500X (a) and 2000X (b).

As it can be observed, the microcapsules often tended to cluster rather than being uniformly distributed among the fibers, with possibly implications on making phase change less efficient due to smaller surface area versus volume.

7.2 Measurements set-up

The thermal properties of the sample PCM-00 without phase change materials were tested by means of the transient plane source device Isomet 2104 (Applied Precision Ltd), as previously explained in Section 3.1.1. The same method was followed for samples containing PCMs, after their conditioning in the climatic chamber Angelantoni DY340 set

to temperature values far from the phase change ones. Figure 7.5 shows the difference between the measurement set-up for samples without PCMs (Figure 7.5(a)) and samples with PCMs which were tested while were conditioned (Figure 7.5(b-c)). Measurements under controlled hygrothermal conditions allowed to overcome the drawback that when the probe of the Isomet device generated a heat flow around 26 °C, it would cause a phase change in the PCM, without any change in temperature; thereby biasing the measurement. Two measurement configurations were chosen: 16 °C and 50% RH, and 36 °C and 50% RH. The test started when in the climatic chamber were reached constant values of temperature and relative humidity.

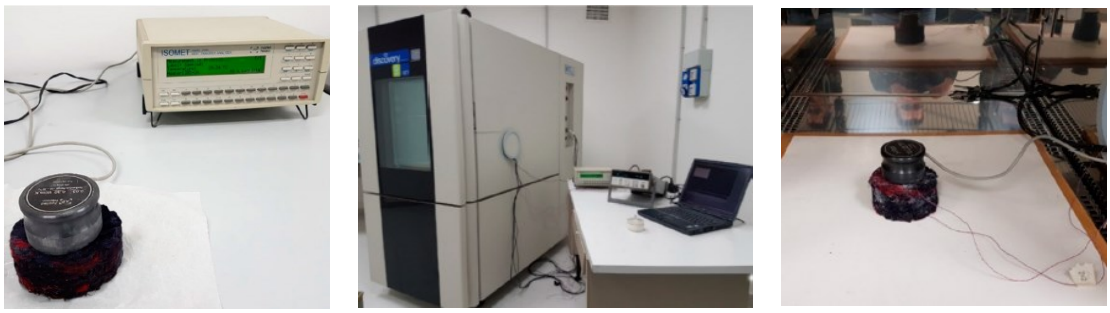

(a) (b) (c)

Figure 7.5. Measurements set-up for samples without (a) and with (b-c) PCMs.

Furthermore, in order to consider the thermal energy exchanged by PCMs during their change of state, the enthalpy variation for the three different samples was determined according to the following equation:

$$h(T) = f_w \cdot c_w(T) \cdot T + f_{PCM} \cdot h_{PCM}(T) \quad [7.1]$$

where *fw* is the weight percent fraction of the mixture wool-gum arabic PCM-00, *cw* is the specific heat capacity of the PCM-00 sample, f_{PCM} is the weight percent fraction of PCM and $h_{PCM}(T)$ is the enthalpy vs temperature of the pure PCM as obtained from the DSC diagram (Figures 7.1 and 7.2).

The thermal behaviour of the specimens under dynamic regime was also investigated carrying out a Hot Box test. A small parallelepiped Hot Box (40x40x53 cm) characterized by a metal frame was used (Figure 7.6). Each side of the Hot Box was outfitted with six polystyrene panels 4.85 cm thick, with a thermal conductivity of 0.035 W/(m·K). In the

center of three of the four vertical side surfaces were cut three circular holes with 10 cm diameter in which were put in the three tested samples. For each specimen, two T-type thermocouples were used for monitoring the internal and external surface temperatures, while two more thermocouples were used for monitoring the internal and external air temperature. The external air conditions corresponded to the laboratory ones; whereas a simple 28 W halogen bulb was used as internal heat source. All the thermocouples were connected to an Agilent 34970A data acquisition multiplexer which, through its proprietary software (Agilent BenchLink Data Logger), scanned and recorded the temperature values read by each thermocouple at regular intervals of 10 s. The test lasted about 5 hours and was divided into two heating cycles (60 minutes each) and two cooling cycles (90 minutes each).

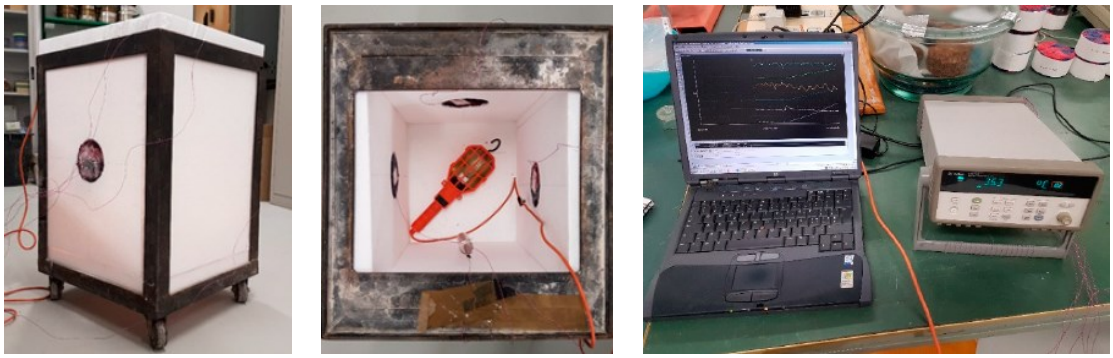

(a) (b) (c)

Figure 7.6. Outside (a) and inside (b) view of Hot Box and data acquisition set-up (c).

A further temperatures measurement lasted about 20 minutes was carried out under quasi steady-state conditions, in order to estimate the internal and the external heat exchange coefficients, respectively h_i and h_e. They were supposed to be equal on the surfaces of the polystyrene panels and of the woolen samples and were determined as follows:

$$h_i = \frac{\varphi}{(T_i - T_{si})} \qquad [7.2]$$

$$h_e = \frac{\varphi}{(T_{se} - T_e)} \qquad [7.3]$$

were T_i and T_e are respectively the internal and the air external temperature, T_{si} and T_{se} are respectively the temperature of the internal and the external surfaces of the samples, φ is the heat flux exchanged through the wall of the Hot Box.

The flux φ was calculated according to the Equation [7.4], being λ the thermal conductivity of the polystyrene panels, d their thickness and T_{si} and T_{se} the internal and the external temperatures of their surfaces:

$$\varphi = \frac{\lambda}{d} \cdot (T_{si} - T_{se}) \qquad [7.4]$$

7.3 Results

Table 7.3 summarizes the experimental values of the mean temperature T, the thermal conductivity λ, the thermal diffusivity D and the specific heat capacity c obtained for the tested samples. The "mean temperature" T is reported in order to monitor the temperature that occurred at the interface between the probe and the specimen surface during the test.

As it can be observed, thermal conductivity increased with increasing temperature. This was a predictable result, considering that air filling pores increases its own conductivity by about 6% from 20 to 40 °C. Similarly, thermal conductivity increased with increasing the amount of PCM. This was due to more connections among fibers and less volume of pores occurred when PCM microcapsules were added. The latter consideration is clearly supported also by higher density values of PCM-26 and PCM-41 samples respect to PCM-00 ones.

Taking into account the specific heat capacity data, the experimental values resulted much greater than the literature ones. The wool sample PCM-00 showed a density of 104 kg/m^3 and a specific heat capacity of about 3000 J/(kg·K) which was higher than the value of 1800 J/(kg·K) reported by Schiavoni et al. (2016) for sheep's wool with a density of 20 kg/m^3.

Table 7.3. Thermal properties of PCM-00, PCM-26 and PCM-41: mean values of temperature *T*, thermal conductivity λ, thermal diffusivity *D* and specific heat capacity *c*.

Sample code	ρ_{bulk} [kg/m^3]	*T* [°C]	λ [W/(m·K)]	*D* [10^{-7}m^2/s]	*c* [J/(kg·K)]
PCM-00	104	27.3	0.053	1.72	2962
PCM-00	104	37.8	0.069	1.91	3936
PCM-26	137	19.8	0.060	2.09	2100
PCM-26	137	39.4	0.064	1.60	2941
PCM-41	173	19.5	0.077	2.26	1970
PCM-41	173	37.7	0.085	1.91	2576

The enthalpy variation as a function of temperature was determined according to the Equation [7.1]. The specific heat capacity of PCM-00 sample $c_w(T) = 92.827 \cdot T + 427.5\ \mathrm{J/(kg \cdot K)}$ was obtained with a linear interpolation of the values reported in Table 7.3. The enthalpy vs temperature *h(T)* resulting for the three mixtures are plotted in Figure 7.7, where the grey zone shows the temperature range in which the phase change took place.

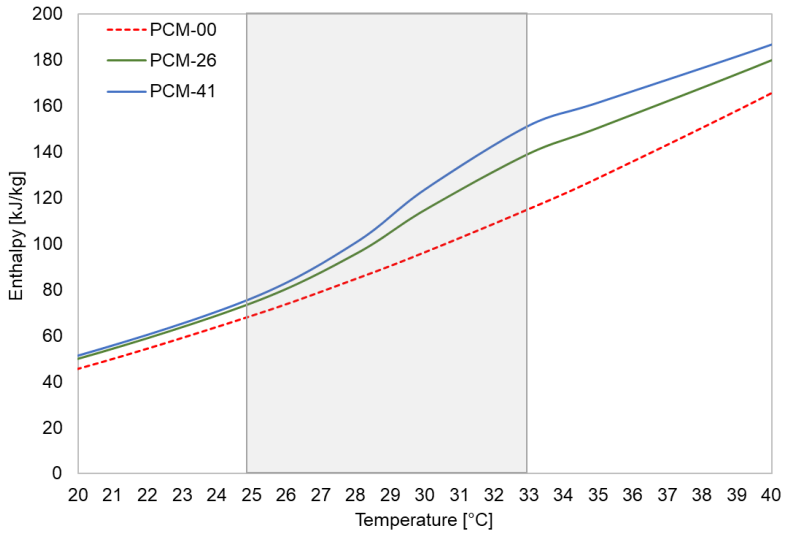

Figure 7.7. Entalphy variation as a function of temperatures for different mixtures.

The analysis of the temperatures resulting from the Hot Box test shows that the samples PCM-26 and PCM-41 exhibited a temperature variation on the interior surface much slower than PCM-00, with instantaneous differences up to 2 °C (Figure 7.8). During heating cycle, both samples containing PCMs showed lower temperatures than the

reference sample, suggesting a clear energy storage capacity. Similarly, during cooling, the storage energy was unloaded resulting in temperatures of samples with PCMs higher than the reference sample and the air.

Differences between the three samples were even more emphasized when temperature values on the outside surfaces were considered. As it can be observed in the topmost part of Figure 7.8, the addition of PCMs microcapsules allowed to shift the temperature peaks during heating and cooling cycles.

The surface heat exchange coefficients were estimated according to Equations [7.2] and [7.3]. As it can be seen in Figure 7.9, the values of the heat exchange coefficient on the internal surface was lower than the one on the external surface (i.e. the mean values were $h_i = 2.8\ \mathrm{W}/(m^2 \cdot K)$ and $h_e = 7.6\ \mathrm{W}/(m^2 \cdot K)$). This was due to the negligible contribution of the heat exchange by radiation through the internal surfaces of the Hot Box which could be considered almost isothermal. Furthermore, the value of h_i was very close to that calculated following the ASHRAE (2016) formula for natural convection heat flux between a heated or cooled wall panel surface and indoor air, for a vertical surface with height $H = 0.53\ m$:

$$h_i = 1.87 \cdot (T_i - T_{si})^{0.32} \cdot H^{-0.55} \qquad [7.5]$$

Figure 7.10 shows time variation of heat flux on the internal and the external faces of the specimens. As it can be observed, the addition of phase change materials resulted in a time shift of the heat flux peaks on the external surface of the samples with PCM compared to the reference sample. The Figure clearly shows that the sample PCM-41 with the most content of PCM produced the longest time shift of the peaks.

The PCM influence is more evident in Figure 7.11, where the difference between the heat flow entering and exiting respectively through the internal and the external faces is shown as a function of the mean temperature (average between the internal surface temperature and the external surface one). The PCMs addition make the heat flow imbalance about four times greater than the sample without PCMs, with a peak shifts to the temperature range typical of the phase change. The apparent hysteresis shown by the materials with PCM, where the unloading cycle did not perfectly resume the initial

conditions of the loading one, could be explained due to the solidification process not completed before starting the new heating cycle. As a consequence the thermal storage capacity of the PCMs were reduced. However, according to Soares (2016), a different storage capacity in heating or in cooling conditions it could be also explained by the characteristic latent heat of the used PCM which it could be different during solidification and liquefaction phases.

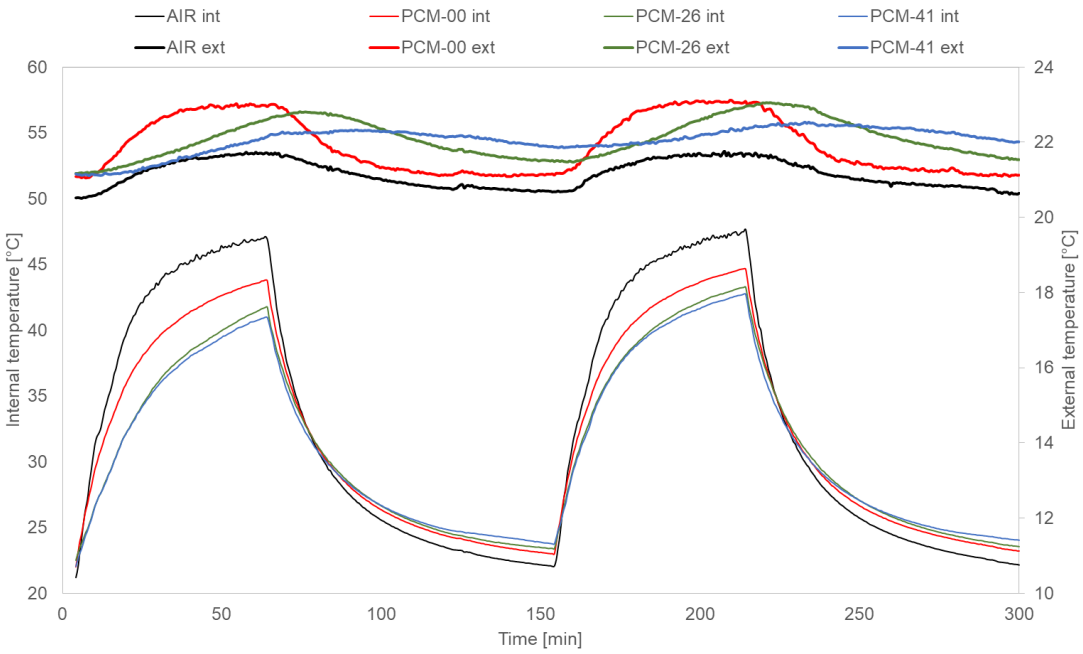

Figure 7.8. Air and surface temperatures in the Hot Box: Internal side (bottom) and external side (top).

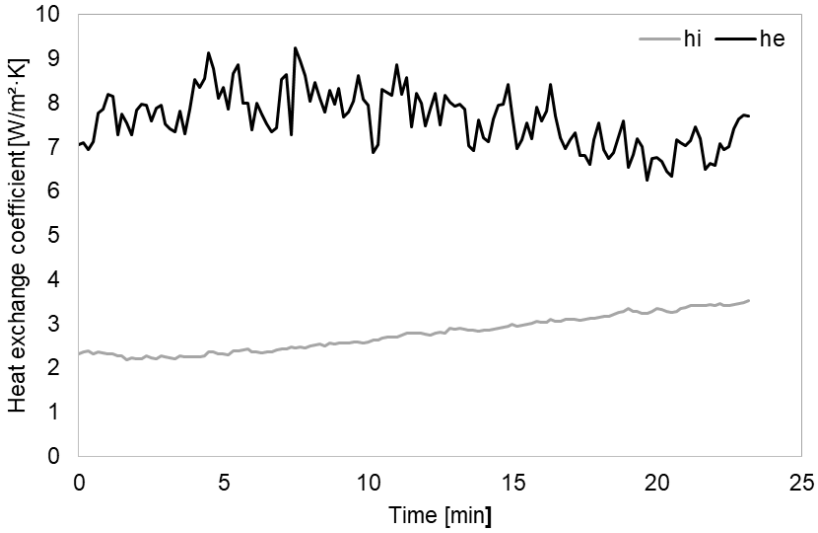

Figure 7.9. Internal (*hi*) and external (*he*) surface heat exchange coefficients.

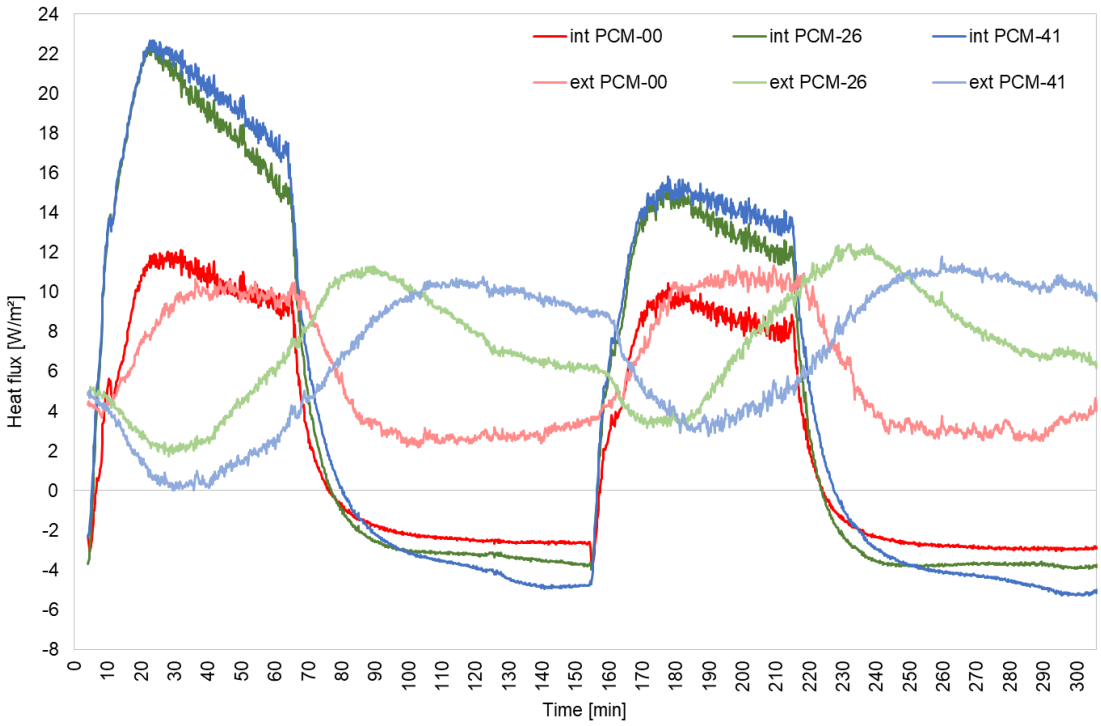

Figure 7.10. Specific heat flux through the internal (int) and external (ext) specimen side.

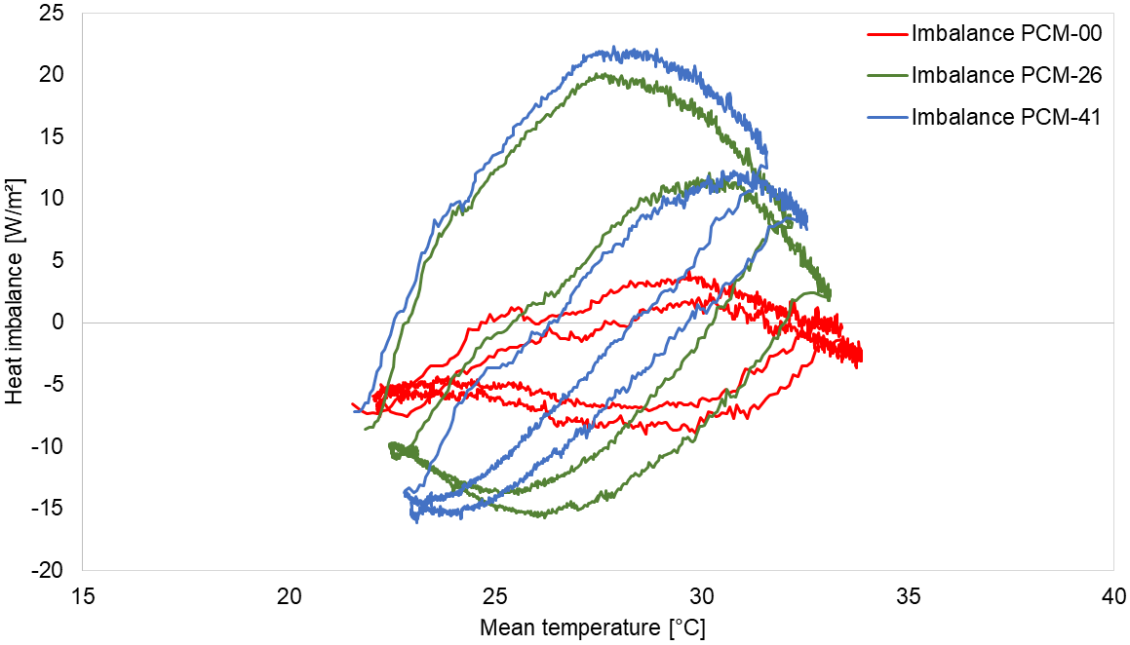

Figure 7.11. Heat flux imbalance vs the mean temperature of the different samples.

References

Abokersh, M.H., Osman, M., El-Baz, O., El-Morsi, M., Sharaf, O., 2017. Review of the phase change material (PCM) usage for solar domestic water heating systems (SDWHS). Int. J. Energy Res. 42, 329-357. https://doi.org/10.1002/er.3765.

ASHRAE. ASHRAE Handbook–HVAC Systems and Equipment; ASHRAE: Peachtree Corners, GA, USA, 2016.

Baldassarri, C., Sala, S., Caverzan, A., Lamperti Tornaghi, M., 2017. Environmental and spatial assessment for the ecodesign of a cladding system with embedded Phase Change Materials. Energy Build. 156, 374–389. https://doi.org/10.1016/j.enbuild.2017.09.011.

Cabeza, L.F., Castell, A., Barreneche, C., de Gracia, A., Fernández, A.I., 2011. Materials used as PCM in thermal energy storage in buildings: A review. Renew. Sustain. Energy Rev. 15, 1675-1695. https://doi.org/10.1016/j.rser.2010.11.018.

da Cunha, S.R.L. and de Aguiar, J.L.B. Phase change materials and energy efficiency of buildings: A review of knowledge. J. Energy Storage 2020, 27, 101083. https://doi.org/10.1016/j.est.2019.101083.

Feldman, D., Banu, D., Hawes, D., Ghanbari, E., 1991. Obtaining an energy storing building material by direct incorporation of an organic phase change material in gypsum wallboard. Sol. Energy Mater. 22, 231-242. https://doi.org/10.1016/0165-1633(91)90021-C.

Frigione, M., Lettieri, M., Sarcinella, A., 2019. Phase Change Materials for Energy Efficiency in Buildings and Their Use in Mortars. Mater. 12, 1260. https://doi.org/10.3390/app11031262.

Giro-Paloma, J., Oncins, G., Barreneche, C., Martínez, M., Fernández, A.I., Cabeza, L.F., 2013. Physicochemical and mechanical properties of microencapsulated phase change material. Appl. Energy 109, 441–448. https://doi.org/10.1016/j.apenergy.2012.11.007.

Hassan, A., Shakeel Laghari, M., Rashid, Y., 2016. Micro-Encapsulated Phase Change Materials: A Review of Encapsulation, Safety and Thermal Characteristics. Sustainability 8, 1046. https://doi.org/10.3390/su8101046.

Kamali, S., 2014. Review of free cooling system using phase change material for building. Energy Build. 80, 131-136. https://doi.org/10.1016/j.enbuild.2014.05.021.

Pasupathy, A., Velraj, R., Seeniraj, R.V., 2008. Phase change material-based building architecture for thermal management in residential and commercial establishments. Renew. Sustain. Energy Rev. 12, 39-64. https://doi.org/10.1016/j.rser.2006.05.010.

Peippo, K., Kauranen, P., Lund, P.D., 1991. A multicomponent PCM wall optimized for passive solar heating. Energy Build. 17, 259-270. https://doi.org/10.1016/0378-7788(91)90009-R.

Riffat, S., Mempouo, B., Fang, W., 2015. Phase change material developments: A review. Int. J. Ambient Energy 36, 102–115. https://doi.org/10.1080/01430750.2013.823106.

Serrano, S., Barreneche, C., Rincón, L., Boer, D., Cabeza, L.F., 2013. Optimization of three new compositions of stabilized rammed earth incorporating PCM: Thermal properties characterization and LCA. Constr. Build. Mater. 2013, 47, 872–878. https://doi.org/10.1016/j.conbuildmat.2013.05.018.

Soares, N.M.L., 2016. Thermal Energy Storage with Phase Change Materials (PCMs) for the Improvement of the Energy Performance of Buildings. Ph.D. Thesis, Mechanical Engineering Deptartment, University of Coimbra, Coimbra, Portugal.

Socaciu, L.G., 2012. Thermal energy storage with phase change material. Leonardo Electron. J. Pract. Technol. 11, 75-98.

Schiavoni, S., D'Alessandro, F., Bianchi, F., Asdrubali, F. 2016. Insulation materials for the building sector: A review and comparative analysis. Renew. Sustain. Energy Rev. 62, 988-1011. https://doi.org/10.1016/j.rser.2016.05.045.

Serrano, S., Barreneche, C., Inés Fernández, A., Farid, M.M., Cabeza, L.F., 2015. Composite gypsum containing fatty-ester PCM to be used as constructive system: Thermophysical characterization of two shape-stabilized formulations. Energy Build. 86, 190-193. https://doi.org/10.1016/j.enbuild.2014.10.015.

Toppi, T., Mazzarella, L, 2013. Gypsum based composite materials with micro-encapsulated PCM: Experimental correlations for thermal properties estimation on the basis of the composition. Energy Build. 57, 227-236. https://doi.org/10.1016/j.enbuild.2012.11.009.

Whiffen, T.R., Riffat, S.B., 2013. A review of PCM technology for thermal energy storage in the built environment: Part I. Int. J. Low-Carbon Technol. 8, 147-158. https://doi.org/10.1093/ijlct/cts021.

Chapter 8

From theory to practice: application of the proposed materials to a real case study

In order to prove the potential of the investigated non-wovens, the atrium of the Department of Architecture was taken into account as it offered the opportunity to investigate both acoustic and thermal insulating effects. In fact, the atrium is used as a semi-open space for students, so application of sound absorbing treatments might significantly improve acoustic comfort. Meanwhile, application of treatments on the wall might also contribute to improve thermal insulation of walls and, therefore, reduce the energy demand needed to heat/cool the spaces facing the atrium.

CATT-Acoustic® software was used to test different arrangements of the BICO-5 material in form of panels. In addition, as part of them was applied on the opaque walls surrounding the atrium, energy simulations were also carried out using DesignBuilder® software, in order to analyze the effects of adding the panels on the thermal behaviour of the relevant rooms. Results demonstrated the potential application of the BICO-5 panels might led to a reduction of the A-weighted ambient noise level in the atrium. Conversely, in terms of energy saving implications, only small variations were found in the yearly sensible heating and cooling loads.

8.1 Case study

The atrium of the Architecture's Building of the Polytechnic University of Bari was chosen as a case study (Figure 8.1). The aim was to optimize the acoustic characteristics of this semi-outdoor space in order to make it suitable for using by students while reducing noise exposure of the rooms facing the atrium. A targeted distribution of the acoustic absorption was planned to keep low the background noise level from speech and to control the reverberation phenomenon. At the same time, application of panels on the walls also affected the energy consumptions of the interior spaces. Consequently, implications on thermal and energetic behaviour of such spaces were also investigated.

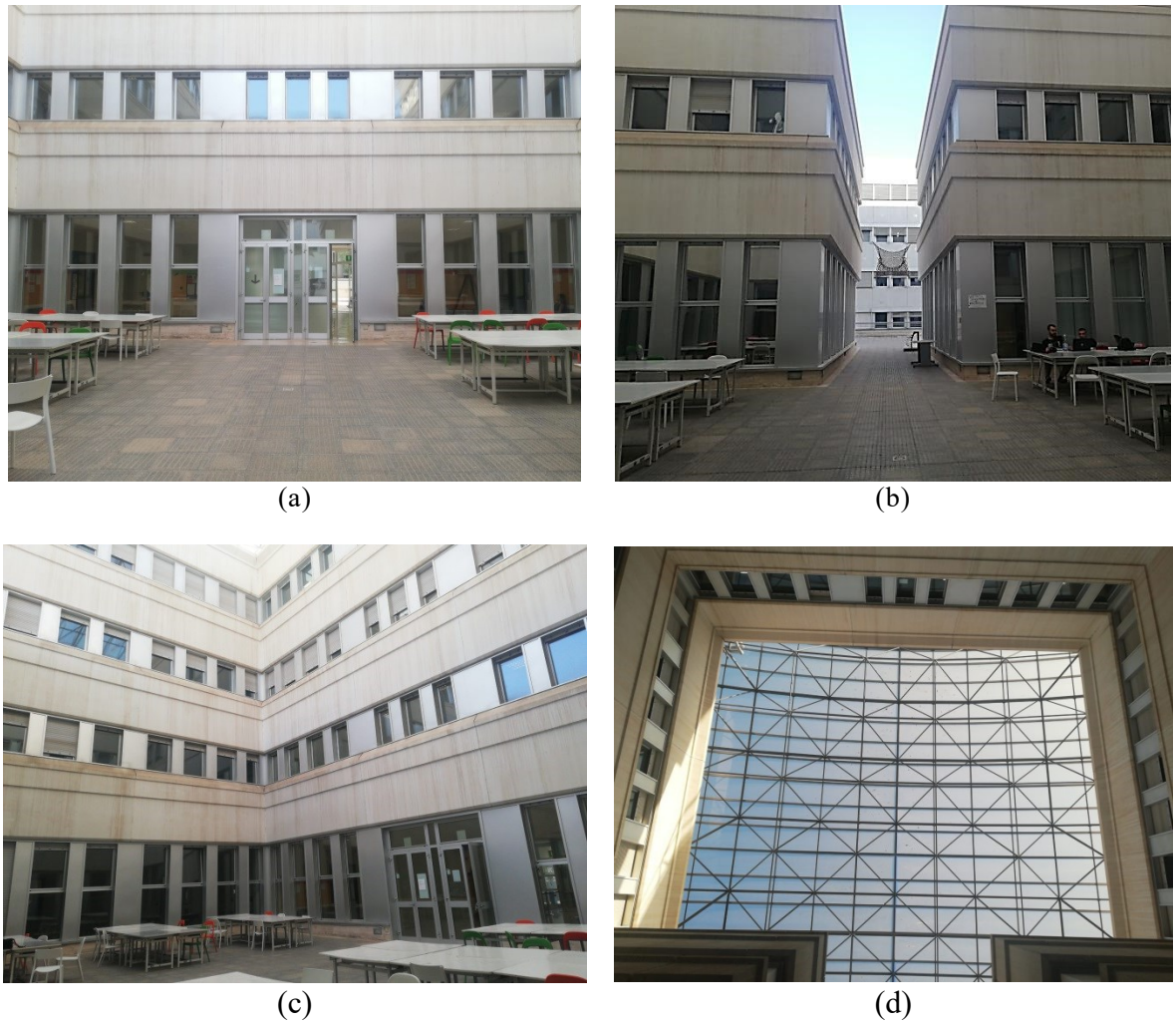

(a) (b)

(c) (d)

Figure 8.1. Atrium of of the Architecture Building: long side (a), long side with passageway (b), short side (c) and Plexiglas covering (d).

The atrium is rectangular in square, approximately 11 m × 15 m. On three sides, it is surrounded by buildings with four floors above ground (i.e. on one long side and on the two short ones). On the other long side, it is surrounded by two buildings with two floors above ground, divided by a passageway about 3 m wide and 12 m long. Strip windows create horizontal stripes across the facade of these buildings. The rhythm of the openings repeats in the same way on all the floors and it is underlined by large plastered string course-frames. The rectangular space and the passageway have a Plexiglas covering at approximately 21 m high (Figure 8.1). In the layout in Figure 8.2, the passageway and the atrium are highlighted in grey. As it can be seen, the passageway connects the atrium with an uncovered larger space.

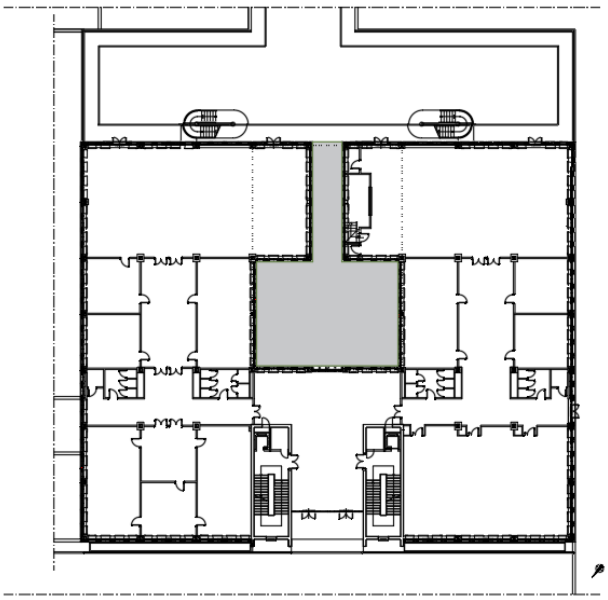

Figure 8.2. Layout of the atrium of the Architecture's Building.

Different arrangements of the absorbing material were simulated and compared with the current condition, in order to identify the best configuration for improving the acoustic quality of the analyzed space. In any case, part of them was applied on the opaque portions of the wall of the buildings surrounding the atrium, modifying their envelope. Therefore, energy simulations were also carried out in order to analyze the effects of adding the panels on the energy behaviour of the corresponding rooms. The BICO-5 mix was chosen for the acoustic optimization because, as previously analyzed in Section 6.2, it showed the best compromise in terms of sound absorption coefficients among the entire spectrum.

8.2 Overview of comfort factors affected by proposed materials

Thermal and acoustic comfort are important aspects of the environmental quality due to their influences on well-being, people's performance and building energy requirements. For many years these two aspects have been studied separately having effects on the space design strategies and on the chosen materials. Only in recent year, application of the ergonomics principles stated the need to use materials able of maximizing the hygrothermal and the acoustic performances at the same time. In this way, it could be possible to control both the acoustic and thermal comforts of the occupants or to apply a treatment that can benefit two adjacent spaces for two different perspectives, as in the examined case study.

8.2.1 Acoustic comfort in large spaces

Acoustic comfort is the perceived state of well-being and satisfaction with the acoustical conditions in an environment and the sound pressure level is one of the main acoustical factors that affects comfort (Azar et al., 2020). According to the theory of sound propagation in enclosed rooms (Marshall, 2014), if the absorption is uniformly distributed and if the sound field is diffuse, the sound pressure level $L_{S,A,}r$ at a point at a distance r from the source assumed to be omnidirectional is:

$$L_{S,A,r} = L_W + 10log\left(\frac{1}{4\pi r^2} + \frac{4}{A}\right) \quad [8.1]$$

where L_W is the sound power level of the source and A is the total acoustic absorbing area including both wall absorption and air absorption. The latter term A it could be expressed as a function of the reverberation time T_0 and of the room volume V by means of Sabine's equation:

$$A = \frac{0.16 \cdot V}{T_0} \quad [8.2]$$

The reverberation time is an important acoustic parameter which characterizes the rate of sound decay. Thus, it also plays a crucial role in the ability of understanding speech in a given space as long reverberation time will cause a buildup of the noise level in a space (Levy, 2011). In this situation, the occupants may leave the place with a feeling of exhaustion due to the difficulty in understanding what is the important message to hear

compared to the unwanted ambiance that gets in the way. The open spaces are generally characterized by a long reverberation time for which noise travels and bounces for too long before it dissipates.

Noise from people speaking in large open spaces is a well-known and wide spread problem. Because of the noise, everyone raises the voice, which again leads to a higher ambient noise level. The spontaneous increase of the vocal effort induced by the increase of the ambient noise level is called "Lombard effect". It was introduced in 1909, after the French otolaryngologist Étienne Lombard (1869–1920) observed and reported that people with normal hearing raised their voice when subjected to noise (Rindel, 2010). The vocal effort under different conditions has been studied by several authors and is also reported in ISO 9921 (2004), where is objectively defined in terms of equivalent continuous A-weighted sound pressure level of the direct sound in front of a male speaker in a distance of 1 m from the mouth (in symbol $L_{S,A,1m}$). Thus, according to Lombard effect, $L_{S,A,1m}$ increases as a function of the A-weighted ambient noise level $L_{N,A}$ as follows:

$$L_{S,A,1m} = 55 + c \cdot (L_{N,A} - 45) \qquad [8.3]$$

where c is the Lombard slope. As it can be observed in Figure 8.3, the valid range for this relationship is limited to speech levels above 55 dB, assuming a linear relationship for noise levels above 45 dB.

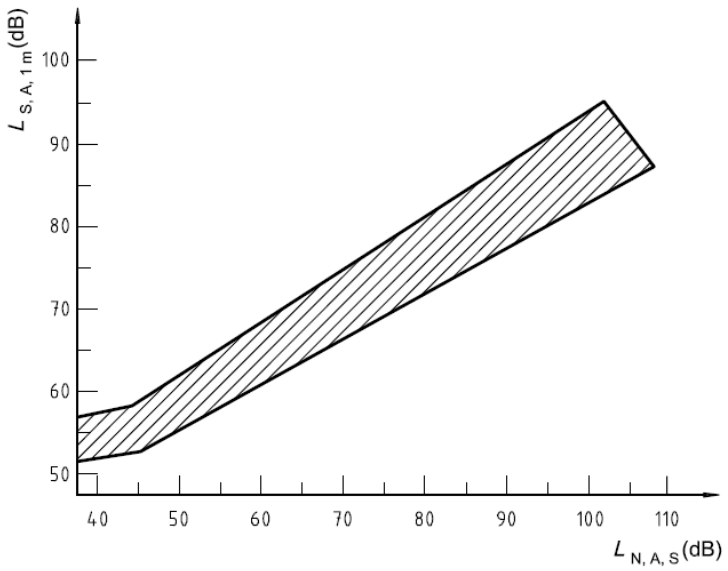

Figure 8.3. Relation between the range of vocal effort $L_{S,A,1m}$ and the ambient-noise level at the speaker's position $L_{N,A,S}$ (Source: ISO 9921 (2004)).

Values of c ranging from 0.5 to 0.7 dB/dB have been suggested in literature (Lazarus, 1986). Rindel (2012), after comparing the data measured in eating establishments for a wide range of customers, found that the Lombard slope $c = 0.5$ made a reasonable agreement with the measured data. This meant that the A-weighted sound power level of speech was assumed to increase by 0.5 dB when the ambient noise level increased by 1 dB. The same slope was already found in 1962 by Webster and Klumpp (1962) and again by Gardner (1971) in several cases, including dining rooms, auditoriums and theaters, studying a large number of individuals in each facility.

Generally, noise from speech cannot be predicted with a high accuracy simply because there are unknown parameters related to individual differences and how much people actually want to talk. This may depend on the type of gathering, which can be more or less lively, how well people know each other and other social circumstances. However, Equation [8.4] suggests a prediction model to estimate the expected ambient noise level $L_{N,A}$ in a space with the equivalent absorption area A_0 and a number N_S of simultaneously speaking people (Rindel, 2010):

$$L_{N,A} = \frac{1}{(1-c)} \cdot \left(69 - c \cdot 45 - 10\log\frac{A_0}{N_S}\right) \qquad [8.4]$$

If the studied space has a volume V, with a reverberation time T_0 in unoccupied state and under diffuse sound field, the Sabine's equation [8.2] gives the following estimate of the equivalent absorption area, including the contribution from N people:

$$A_0 = \frac{0.16 \cdot V}{T_0} + A_P \cdot N \qquad [8.5]$$

where A_P is the sound absorption per person that can be estimated according to Rindel (2010).

Introducing the group size g, defined as the average number of people per speaking person $g = \frac{N}{N_S}$, Equation [8.4] becomes as follows:

$$L_{N,A} = \frac{1}{(1-c)} \cdot \left[69 - c \cdot 45 - 10\log\left(\mathrm{g} \cdot \left(\frac{0.16 \cdot V}{T_0 \cdot N} + A_P\right)\right)\right] \qquad [8.6]$$

The g value may usually varies between 2 and 4 in eating courts and canteens, but higher values may occur in places with little verbal communication (Rindel, 2010).

Thus, according to Equation 8.6, in order to reduce the ambient noise level $L_{N,A}$ it's possible to modify three different factors: reducing the number of people N, reducing the reverberation time T_0, or increasing the volume of the interesting space V.

8.2.2 Thermal comfort in air conditioned spaces

Thermal comfort is an important environmental parameter strongly affecting human well-being. The ASHRAEE 55 (2017) standard defines the thermal comfort as a condition of mind that expresses satisfaction with the thermal environment. Human physiological and psychological variations result in different specific environmental conditions that are required for individual thermal well-being.

Various thermal comfort indices have been proposed over the years, but the most used is Predicted Mean Vote (PMV) introduced by Fanger in 1970 (Fanger, 1970). PMV allows to check whether a given thermal environment complies with comfort criteria by calculating the mean value of the votes of a large group of people on the seven-points thermal sensation scale where neutrality corresponds to thermal comfort. In particular, Fanger adapted the results of the heat balance of the body so that its result numerically corresponded to the sensation scale, to make an easier interpretation of the results. (i.e. +3: hot, +2: warm, +1: slightly warm, 0: neutral, -1:slightly cool, -2:cool, -3: cold). The thermal comfort equation of Fanger [8.7] assumes that people feel comfortable when the internal heat production in the body is equal to the loss of heat to the environment:

$$M-W=C+R+E \qquad [8.7]$$

where M (W/m^2) is metabolic rate; W (W/m^2) is the effective mechanical power by movement; C (W/m^2) is the convection heat transfer rate; R (W/m^2) is radiation heat transfer rate and E (W/m^2) is the total heat dissipation by evaporation of sweat and exhalation of water vapour.

Therefore, in order to specify the combination of activity, clothing and environment parameters useful to define thermal comfort conditions, six factors should be addressed: metabolic rate, clothing insulation, air temperature, radiant temperature, air speed and humidity. The first two factors depend on of the occupants, while the remaining four depend on of the thermal environment. The thermal insulation provided by garments and clothing is one of the most important thermal comfort adjustments available to building

occupants. For near sedentary activity, where the metabolic rate is approximately 1.2 met, the effect of changing clothing insulation on the optimum operative temperature is approximately 6 °C/clo (Lee and Schiavon, 2014). In most building energy simulations, thermal comfort condition is calculated based on the assumption that the clothing insulation is equal to a constant value of 0.5 clo during the cooling season and 1.0 clo during the heating season (Lee and Schiavon, 2014).

A specific combination of the six thermal comfort parameters are required to prevent local thermal discomfort due to draft, vertical air temperature difference between head and ankle, warm or cold floors and radiant temperature asymmetry (Khovalyg et al., 2020). Mainly people performing light sedentary activity are sensitive to local discomfort because the body as a whole is in a neutral thermal state (PMV is close to neutral). At higher activity levels, people are less thermally sensitive and, consequently, the effect of local discomfort could be insignificant.

The standard ISO 7730 (2006) establishes three classes of satisfaction on the base of the PMV value:

class A when $-0.2 < PMV < 0.2$, represents the highest satisfaction to the environment;

class B when $-0.5 < PMV < 0.5$, is the moderate satisfaction level;

class C when $-0.7 < PMV < 0.7$, is minimum requirement for thermal comfort.

In a thermally moderate environment, the human thermoregulatory system will automatically attempt to modify skin temperature and sweat secretion to maintain heat balance.

8.3 Acoustic analysis

CATT-Acoustic® software, with two different calculation engines, i.e. CATT-Acoustic v.9.0a and CATT TUCT v.1, was used for acoustic simulations. This software adopts the principles of the geometrical acoustics and uses a hybrid calculation, combining the image source method with the ray-tracing method. The diffuse part of each reflection is treated deterministically for reflections up to a certain order that can be chosen by the user. Above that limit, diffuse reflections are simply randomized speeding up the calculations (Alvarez-Morales and Martellotta, 2015). In order to obtain the best results when applying acoustical treatments to a space, it is important to first “calibrate” the model against acoustical measurements carried out in the real space (Bork, 2000; Katz et al., 2018). Thus, the

preliminary acoustic properties assigned to all surfaces of the model were modified in order to obtain the best fit between measurements and simulated results for reverberation time, as will be better explained later.

8.3.1 In situ measurements

Measurements of the impulse response were carried out in the empty atrium in order to characterize the sound field of the space, obtaining its reverberation time. A balloon burst was used as a source and a binaural microphone was used for recording the variation in sound pressure over time. The measurements were carried out following the ISO 3382–2 (2009) standard. The source (A0) was located in the middle of the atrium and 4 positions were established for the receivers (01 to 04): three within the largest rectangular covered area and one located in the covered passageway (Figure 8.4). As the balloon burst was used as a source, each measurement was repeated at least twice.

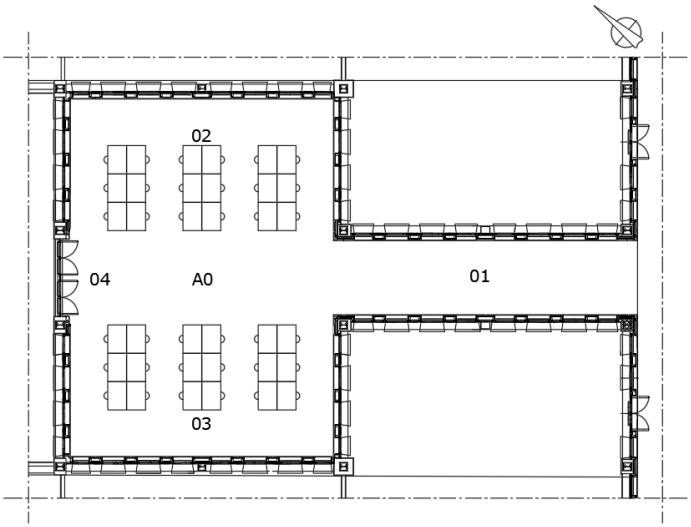

Figure 8.4. Source and receivers positions for in situ measurements of the impulse response.

The environmental conditions were monitored and a temperature of 13.8 °C and a relative humidity of 56.6% were recorded.

After getting the impulse response, the reverberation time T_{30} was obtained by using the Schroeder's backwards integration method (Schroeder, 1965). Figure 8.5 represents the decay of the sound pressure level in the atrium as a function of time after balloons burst.

According to ISO 3382-1, (2009) Standard, the T_{30} was considered as the signal-to-noise level was more than 35 dB.

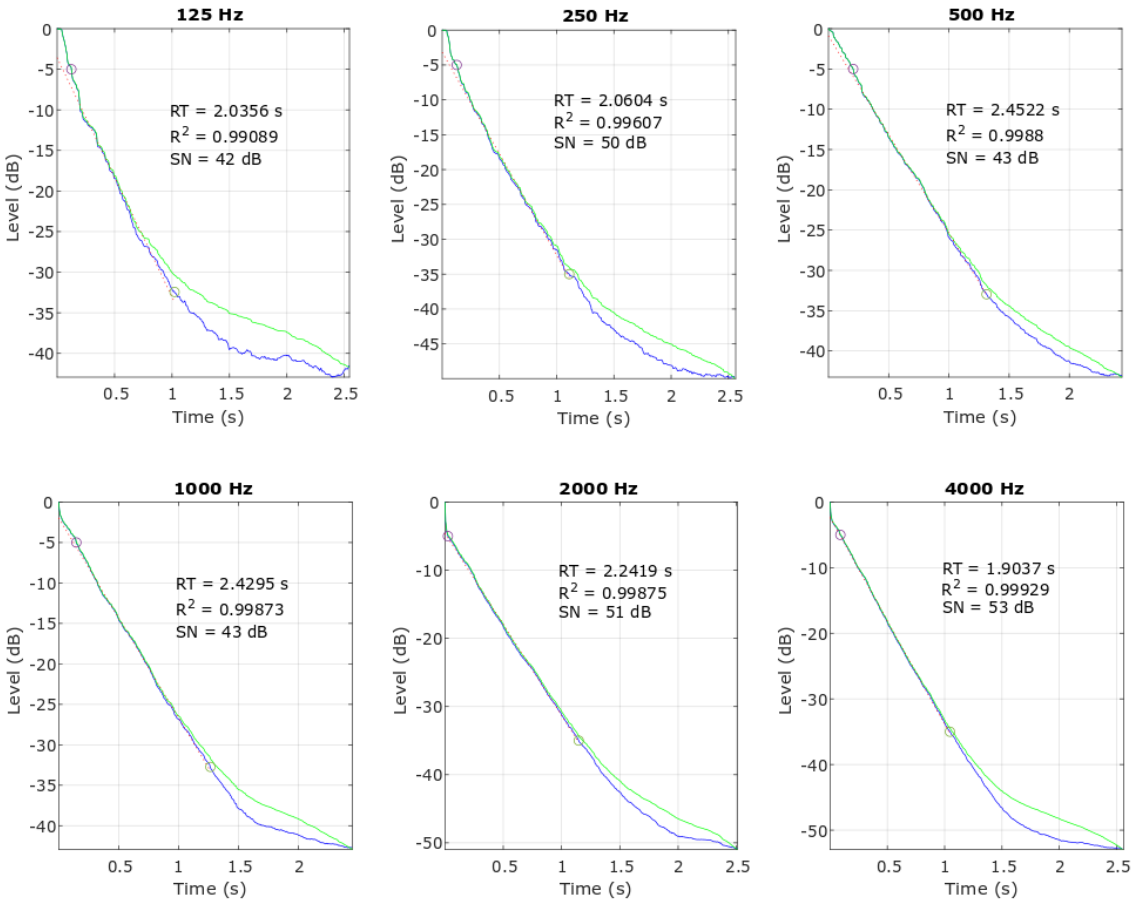

Figure 8.5. Decay curves for the six octave bands 125 to 4k Hz.

8.3.2 Implementation and calibration of the model

The geometry of the atrium and the passageway was modeled with SketchUp® v.8 software and then exported to CATT-Acoustic® via a SU^{2}Catt plugin. The model simplified the tested space, eliminating the smallest elements, since an exhaustive geometric definition was not the most decisive factor in ensuring adequate results. In fact, the acoustic properties (absorption and diffusion) of the surfaces that delimited the space were more decisive for obtaining good results and very detailed models are known to largely increase computation time without improving results accuracy (Vorländer, 2011; Alberdi et al., 2021). Table 8.1 shows the materials of the atrium model, their location, surface and percentage with respect to the total.

Table 8.1. Materials, location, surface and percentage of surface.

Materials	Location	Surface [m^2]	Surface [%]
Plaster	String course-frames	742.3	27.1
Plexiglas	Atrium and passageway roof	484.3	17.7
Aluminum	Space between windows	466.0	17.0
Glass	Windows	290.8	10.6
Concrete tiles	Atrium floor	211.9	7.7
Concrete	Roof floor of lower two buildings	139.8	5.1
Marble	Baseboard	38.2	1.4

The initial input values of the sound absorption coefficients of the different surfaces were selected from literature data (Cox Cox and D'Antonio, 2017). Then, the assigned absorption and scattering coefficients were adjusted starting from the materials with the highest uncertainty, in order to have a reverberation time as close as possible to the measured ones. The reverberation time calculated with the acoustic software considered the same source and receivers locations used in situ measurements chain. The differences between measured and predicted reverberation time are usually evaluated in terms of Just Noticeable Difference (JND) which for this parameter corresponds to 5%, as reported in ISO 3382-1, (2009) Standard. However, in the present case, when possible, smaller differences were achieved. Table 8.2 reports the difference between the T_{30} values resulted from the in situ measurements (i.e. measured values) and the values obtained after little adjustments to the sound absorption and scattering coefficients (i.e. calibration values), showing their percentage difference.

Table 8.2. Spatially averaged reverberation time T30: measured values, calibration values, and their percentage difference.

	125 Hz	250 Hz	500 Hz	1k Hz	2k Hz	4k Hz
Measured values [s]	2.09	2.35	2.63	2.40	2.21	1.86
Calibration values [s]	2.08	2.27	2.52	2.42	2.32	1.80
Percentage difference[%]	0.47	3.40	4.18	0.82	4.74	3.22

In Table 8.3 are reported the calibration values of the sound absorption coefficients expressed in % for the six octave bands from 125 to 4 kHz. As it can be observed, the scattering coefficients following the Lambert model were considered for the aluminum

surfaces between the windows and for the concrete tiles floor. This was for taking into account the protrusion due to different planes of windows and aluminum surfaces and the effect of the worktable usually placed in the atrium. Scattering coefficients were assigned starting from 15% at 125 Hz and increasing of 5% for each octave bands. Table 8.3 also reports the sound absorption coefficients of the BICO-5 mix illustrated in Section 6.2.

The environmental conditions, i.e. humidity and temperature, recorded during the in situ measurements were used in the model.

Table 8.3. Final values of the sound absorption coefficients expressed in % for the six octave bands 125 to 4k Hz.

Materials	125 Hz	250 Hz	500 Hz	1 kHz	2 kHz	4 kHz
Plaster	1	2	4	6	6	6
Plexiglas	18	15	10	8	4	4
Aluminum	30	20	10	8	6	3
Glass	18	12	6	5	4	3
Concrete tiles	2	2	2.7	4	4	4
Concrete	1.5	1.5	2.5	3	3	4
Marble	1	1	1.5	1.5	2	2
BICO-5	14	38	76	90	92	96

8.3.3 Results of acoustic simulations

TUCT provides several algorithms, that differ in the way rays are treated when they interact with surfaces, and that may be more or less suitable depending on the characteristics of the model. In the present case, as the model is open the recommended Algorithm is the second, that was used with a total of 1000,000 rays and a truncation time of 2500 ms. Based on the above considerations about acoustic comfort in open spaces, the A-weighted ambient noise level L_{N,A_CATT} obtained from the CATT-Acoustic simulations was considered as index value to evaluate the acoustic quality of the space. The L_{N,A_CATT} value was calculated in different points (to account for the non-ideally diffuse behaviour of the space) and then averaged. Six simultaneous people, one person sitting at each worktable were assumed as sources. Figure 8.6 shows the position of the receivers R and of the six sources from S1 to S6.

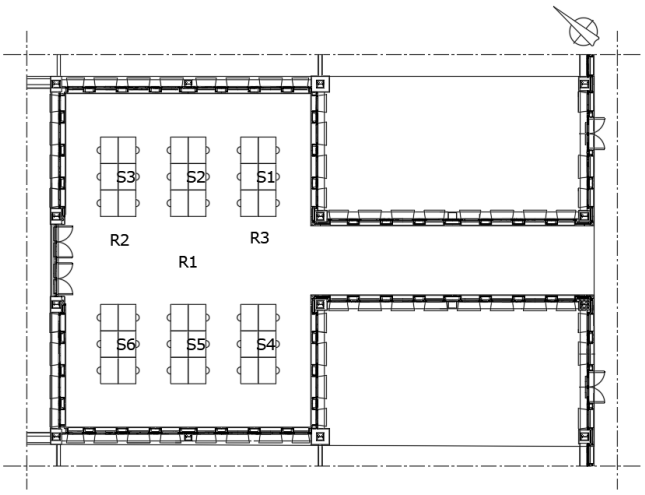

Figure 8.6. Receiver and sources positions for simulating of L_{N,A_CATT}.

The sources were supposed directive and a directivity curve “singer down” (Meyer J., 2009) was selected from the source directivity library-files of CATT-Acoustic software. Figure 8.7 shows the directivity curves at different frequencies.

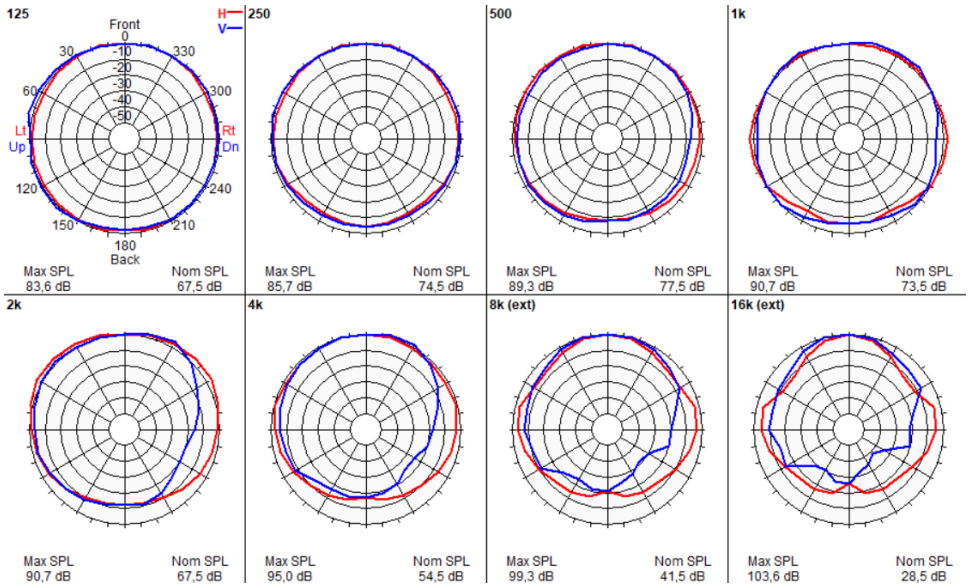

Figure 8.7. Directivity curves of the source.

In addition, the A-weighted ambient noise level $L_{N,A\_Lombard}$, calculated according to the model proposed by Equation [8.3], was used for comparison and to discuss the simulation results, assuming the Lombard’s slope $c = 0.5$.

As previously anticipated, several scenarios with different arrangements of the same surface area of BICO-5 panels were simulated. In each solution part of the absorbing

materials were used to create a covering over the atrium; part was applied on the concrete walls at the first and the second floors of the building surrounding the atrium and as baffles between the worktables.

The simulated scenarios differed in type of covering (i.e. continuous, baffle, and with flat and baffle elements) and in arrangements of baffles between the worktables: in scenarios named "a" no baffles were interposed between sources and receivers respect to the configurations named "b". The amount of absorbing panels which in scenarios "b" behaved as barriers cutting the line of sight between the sources and the receivers was integrated in covering in scenarios "a", in order to ensure the same quantity of absorption in both solutions.

Figures 8.8(a-g) plots software outputs rendering in which the arrangements of the panels are represented in red. Figure 8.8(a) shows a rendering of the current situation, i.e. scenario 0, without acoustic treatment. The scenarios 1a and 1b (Figures 8.8(b, c)) considered an arrangement of BICO-5 panels aimed to delimit the volume of the atrium, creating a continuous covering. The scenario 1 resulted to be an intuitive solution as a consequence of the dependence of the reverberation time to the volume of the space, but it did not have so good architectural value because destroyed the quality of the space, reducing the brightness and the openness of the atrium. Therefore, the scenarios 2 and 3 were proposed with the aim to converge the acoustic and the architectural characteristics. In fact, in scenario 2 (Figure 8.8(d, e)) a baffle covering was created, while a covering with both flat and baffle elements was supposed for scenario 3 (Figure 8.8(f, g)).

A pre-dimensioning of the absorbing panels need was carried out in order to halve the reverberation time $T_{30} = 2.5\ s$ measured at mid frequencies (500–1000 Hz) in the current condition. The quantity of 600 m^2 of BICO-5 panels was estimated with reference to scenario 1a, according to Sabine's Equation [8.2], thus supposing a diffuse sound field. Although the arrangements of material influenced the reverberation time in the atrium in different ways, the surface pre-dimensioning allowed to reach the best compromise between reducing the reverberation time and respecting the atrium concept. In fact, as previously explained, the aim was to achieve both the acoustic and the architectural qualities. Table 8.4 reports T_{30} values corresponding to the reverberation time at mid frequencies (500–1000 Hz), calculated with the acoustic software, for each scenario, considering the same source and receivers locations used in situ measurements chain.

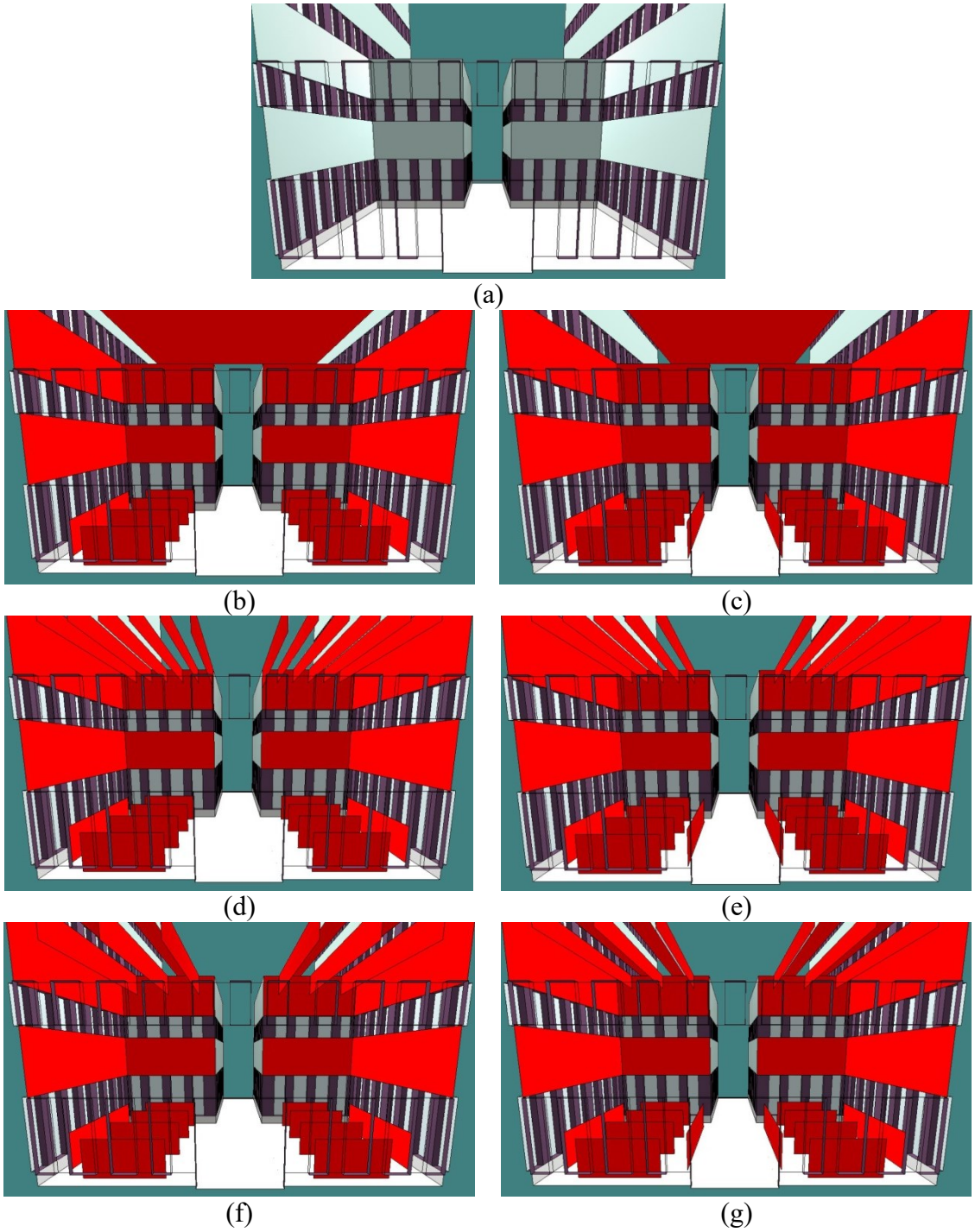

Figure 8.8. Different scenarios of simulation investigated with CATT-Acoustic: scenario 0 without panels (a); scenario 1 with continuous covering, without (b) and with (c) baffles between sources and receivers; scenario 2 with baffle covering, without (d) and with (e) baffles between sources and receivers; scenario 3 with flat and baffle elements for covering, without (f) and with (g) baffles between sources and receivers.

The simulations were firstly carried out assuming sources with a normal speech spectrum defined by ANSI S3.79 (1993) Standard as spectral densities at the center frequencies and as an average from males and females. The corresponding A-weighted sound pressure level at 1 m distance was $L_{S,A,1m} = 59.5\ dB$ and the corresponding power source level was $L_W = 67.5\ dB$. In order to verify the Lombard effect, the $L_{S,A,1m}$ values were then iteratively modified to achieve the correspondence between L_{N,A_CATT} and $L_{N,A\_Lombard}$ values.

Table 8.4 compares the $L_{N,A\_CATT\ 0}$ values obtained considering $L_{S,A,1m} = 59.5\ dB$ and the $L_{N,A_{CATT}*}$ values obtained using $L_{S,A,1m*}$ resulting from the iteration process.

Table 8.4. A-weighted ambient noise level $L_{N,A\_CATT\ 0}$ values obtained from CATT-Acoustic simulations using $L_{S,A,1m}$ and A-weighted ambient noise level L_{N,A_CATT*} obtained using the $L_{S,A,1m*}$ resulting from the iteration process. T_{30} values represent the reverberation time at mid frequencies (500–1000 Hz) obtained from CATT-Acoustic simulations.

Scenario	T_{30} [s]	$L_{S,A,1m}$ [dB]	$L_{N,A\_CATT\ 0}$ [dB]	$L_{S,A,1m*}$ [dB]	$L_{N,A\_CATT\ *}$ [dB]
0	2.50	59.5	58.0	63.5	62.0
1a	1.15	59.5	53.6	59.5	54.0
1b	0.94	59.5	47.3	52.5	40.0
2a	1.81	59.5	53.4	58.5	52.0
2b	1.70	59.5	45.5	50.5	36.0
3a	1.61	59.5	53.5	59.5	54.0
3b	1.75	59.5	47.5	53.5	42.0

As it can be observed, in the current situation (i.e. the scenario 0 in Figure 8.8(a)), the correspondence between L_{N,A_CATT0} and $L_{N,A\_Lombard}$ values occurred for $L_{S,A,1m*} = 63.5\ dB$. This means that the occupants of the atrium raised their vocal efforts of 4 dB more than the normal vocal spectrum, as a consequence of the Lombard effect.

Taking into account the scenarios "a" without baffles interposed between sources and receivers (Figure 8.8(b, d, f)), the A-weighted sound pressure level at 1 m distance $L_{S,A,1m*}$ which gave back the correspondence between L_{N,A_CATT} and $L_{N,A\_Lombard}$ values were 59.5 dB for solutions 1a and 3a and 58.5 dB for solution 2a. Therefore, the application of the BICO-5 panels made it possible to reduce the vocal effort of the occupants of the atrium by at least 4 dB compared to the current situation, while maintaining the normal speech level.

Considering the scenarios “b”, acoustic comfort conditions were achieved as a consequence of the baffles which cut the line of sight between the sources and the receivers. In fact, the L_{N,A_CATT*} values were less than 55 dB for each solution (i.e. 40.0, 36.0 and 42.0 dB respectively for 1b, 2b and 3b solutions) with a speech level lower than that corresponding to a normal vocal effort. Therefore, according to Equation [8.3], no Lombard effect occurred, being L_{N,A_CATT*} less than 45 dB.

8.4 Energy performance and thermal comfort analysis

DesignBuilder® software v.6.1.3 was used to evaluate if the application of panels on the concrete string course-frames affected the energy performance and the thermal comfort in the corresponding rooms which overlook the atrium. The DesignBuilder® software is an advanced graphical user interface for EnergyPlus® dynamic thermal simulation engine, useful to model building heating, cooling, lighting, ventilating, and other energy flows.

8.4.1 Implementation of the model

All geometric characteristics of rooms, envelope features, and Heating, Ventilation and Air Conditioning (HVAC) details were entered into DesignBuilder® software to perform an hourly dynamic simulation of the interested spaces. The input data were conveniently chosen considering the simulated spaces belonging to Category II which is usually refers to new buildings and renovations with normal level of expectation (EN 15251, 2008).

The geometry of the whole Architecture’s Building was modeled, but only some rooms at ground, first and second floors were considered as thermal zones for energy simulations. Figure 8.9 plots the layouts of the ground and the second floors where the thermal zones are highlighted in grey. Only one layout is reported for ground and first floor because they perfectly correspond. As it can be observed, the surface area of each zone is reported; however the simulated zones covered about a total surface of 300 m^2 at ground and first floors and of 200 m^2 at second floor.

Two different models were implemented in DesignBuilder® software in order to simulate the configurations without and with treatment. Figure 8.10 shows software outputs rendering in which the simulated zones are represented in detail respect to the rest of the building and the BICO-5 panels are highlighted in red.

The internal walls and the ceilings were considered adiabatic, being all the spaces of the building roughly at the same thermal conditions. Thus, mostly the external wall played an important role for heat exchange between thermal zones and outside.

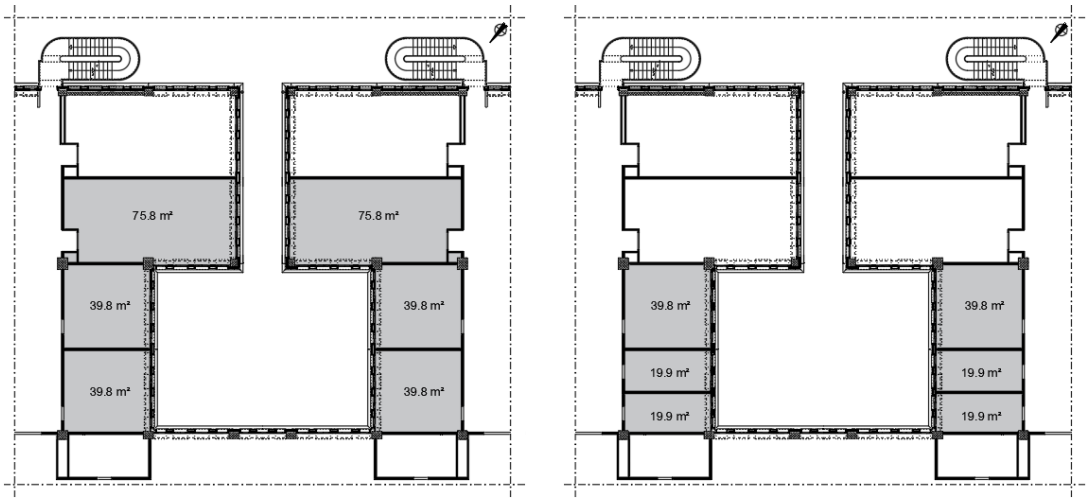

(a) (b)

Figure 8.9. Layout of the simulated thermal zones at ground floor which correspond with first one (a) and at second floor (b).

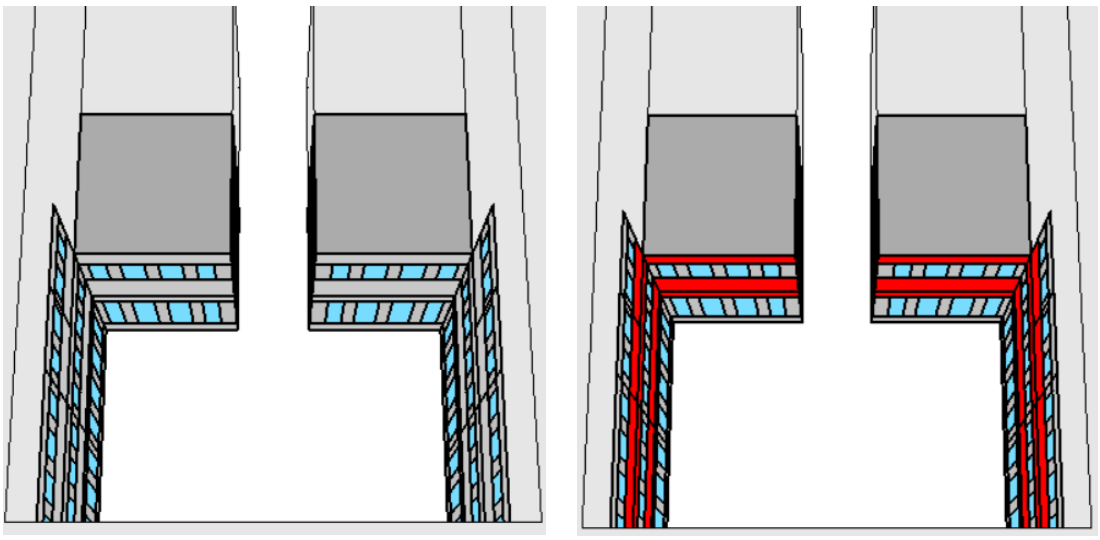

(a) (b)

Figure 8.10. Model implemented with DesignBuilder® software to simulate the thermal behaviour without (a) and with (b) BICO-5 panels.

The façades were characterized by a window-to-wall ratio of about 35%. Clear strip windows, double glazed (6 mm glass/13mm air/6 mm glass), with a thermal transmittance $U = 2.70\ W/m^2K$ were considered.

The external wall was made of five layers for a total of 56 cm. The last layer was constituted by cement boards where were applied the BICO-5 panels. The Building was built before 2015, in fact thermal transmittance of wall envelope was $U = 0.43\ W/m^2K$, resulting higher than the Italian legislation limits (Ministerial Decree, 15 July 2015). However, the addition of 5 cm thick BICO-5 panels allowed to reduce the transmittance value which became $U = 0.29\ W/m^2K$, resulting within the limits for the considered climatic zone (Bari belongs to the climatic zone C). Table 8.5 shows the details of the wall layers of the external wall from outer to inner layer.

All zones were equipped with an HVAC system of fan-coil units powered by an air cooled chiller. The heat pump was characterized by a coefficient of performance (COP) of 3.00, with an inlet temperature of 35 °C and a target temperature of 20 °C; whereas the energy efficiency ratio (EER) was 3.00, with an inlet temperature of 10 °C and a target temperature of 25 °C. According to the Heating and cooling systems were set for ten hours daily, respectively from 15 November to 31 March (Decree of President of the Republic 412, 1993) and from 15 May to 31 October, excluding the month of August. The temperature set points were fixed at 20°C for heating seasons and at 26°C for cooling seasons, according to the recommendations of EN 16798-1 (2019) Standard for offices and spaces with similar activities (sedentary activity of 1.2 met) belonging to Category II.

Table 8.5. Layers of the external wall from outside to inside.

Layer	Material	d [m]	ρ [kg/m^3]	λ [W/(m·K)]	c [J/(kg·K)]
1	Cement board	0.020	1860	0.720	840
2	Air gap	0.350	-	-	-
3	Stone wool	0.050	40	0.038	1400
4	Hollow brick	0.120	520	0.200	840
5	Cement plaster	0.020	1920	0.720	840

No mechanical ventilation and domestic hot water were considered, but only natural ventilation with a minimum fresh air of 7 l/s per person in compliance with the ventilation rates data recommended by EN 16798-1 (2019) for Category II buildings.

Internal loads included only the loads from occupants, considering a density of 0.1 person/m^2. The clothing resistance value was assumed to be 1 clo and 0.5 clo, respectively for winter and for summer seasons; while the metabolic rate was set at 1.2 met.

Whether data for Bari (Bari-Plaese Macchie) were used, considering a Mediterranean climate characterized by hot-dry summers and cool-wet winters.

8.4.2 Results of energy simulations

The yearly sensible heating and cooling loads were considered as index for evaluating the behaviour of the thermal zones. Results showed that the adding of the panels allowed to reduce the heating winter loads of 10%; whereas a slight increase of cooling summer loads (i.e. 4%) was observed. In fact, as previously explained, the increase of the insulation allowed to reduce the transmittance value of the external walls of the simulated rooms, reducing their rate of heat loss. The reduction of the heat flux exchanges led to advantages during the winter seasons avoiding the heat diffusion. At the same time, it made more difficult the exchange of heat during the fresh hours of the summer seasons, having influences on the cooling summer loads.

Figure 8.11 shows the sensible heating and cooling loads during the crucial months of January and July for both simulated solutions with and without BICO-5 panels. Figure 8.11(a), compares the two curves of the sensible heating loads during January, showing the energy improvement due to the application of the insulating panels. In fact, the dotted red curve referred to the solution with BICO panels shows lower peaks than the continuous blue curve referred to the solution without insulation. Otherwise, Figure 8.11(b) shows that no significant changes could be observed between the scenario before and after the walls treatment during July. In fact, the curves of the cooling loads were almost overlapped.

In order to support the results on the energy behaviour of the considered rooms, data about the thermal comfort of the occupants were also analyzed. Particularly, the occupant's thermal satisfaction was evaluated through the PMV data provided by the software. Figure 8.12 illustrates the PMV values during January and July in terms of frequency distribution, for scenario with and without BICO-5 panels. As it can be expected, the application of panels had only negligible effects on the thermal comfort of the occupants of the simulated rooms during the periods in which air conditioning is turned on. In fact, as previously explained, the thermal comfort is influenced by some environmental factors (i.e. the temperature, the humidity and the speed of the air) which mainly depend on the HVAC system setting parameters. Being the HVAC system the same in both solutions with and

without BICO panels, the insulating treatment of walls didn't have significant effects on the PMV values.

Figure 8.12 (a) shows that -0.7<PMV<0.2 during January, with most of the values distributed around PMV=0.3. Thus, as previously explained in Section 8.2.2 acceptable comfort levels were achieved most of the working time. Figure 8.12 (b) plots the PMV during July, showing that -0.3<PMV<1.2 , with the most frequent values being around PMV=0.7. Thus, during summer seasons, minimum requirements for thermal comfort were verified most of the time.

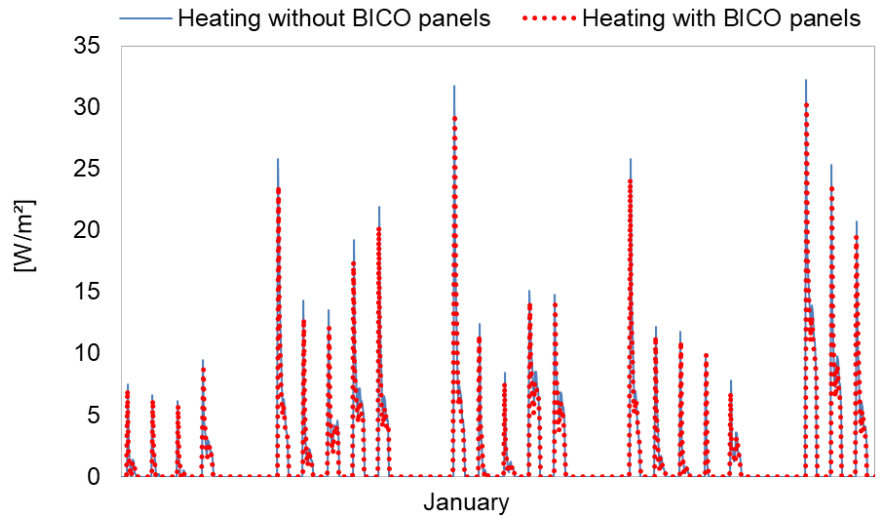

(a)

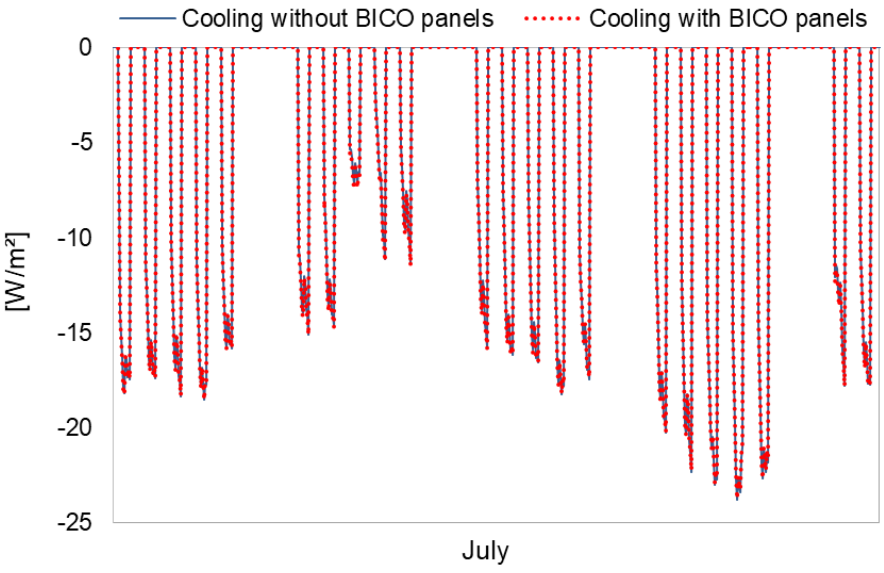

(b)

Figure 8.11. Sensible heating and cooling loads in scenario without and with BICO-5 panels, during January (a) and July (b).

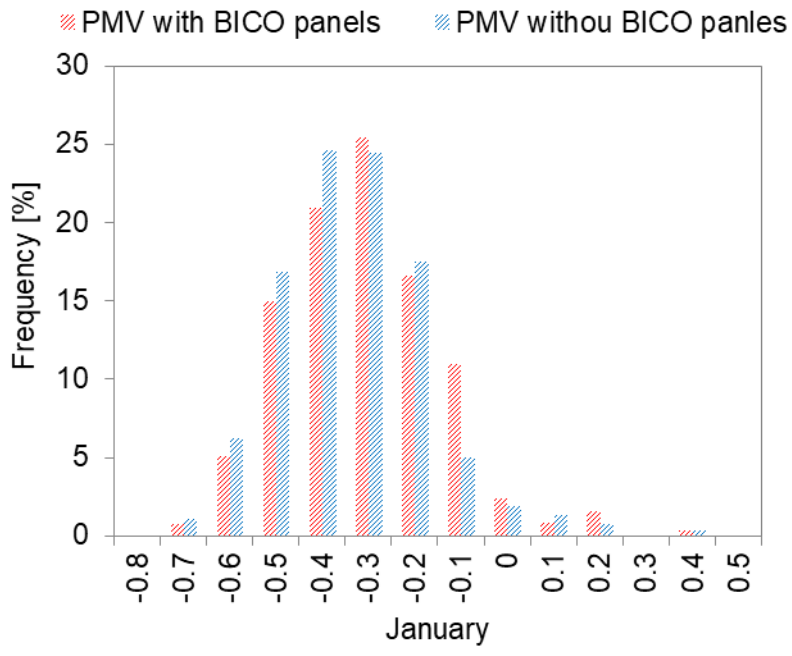

(a)

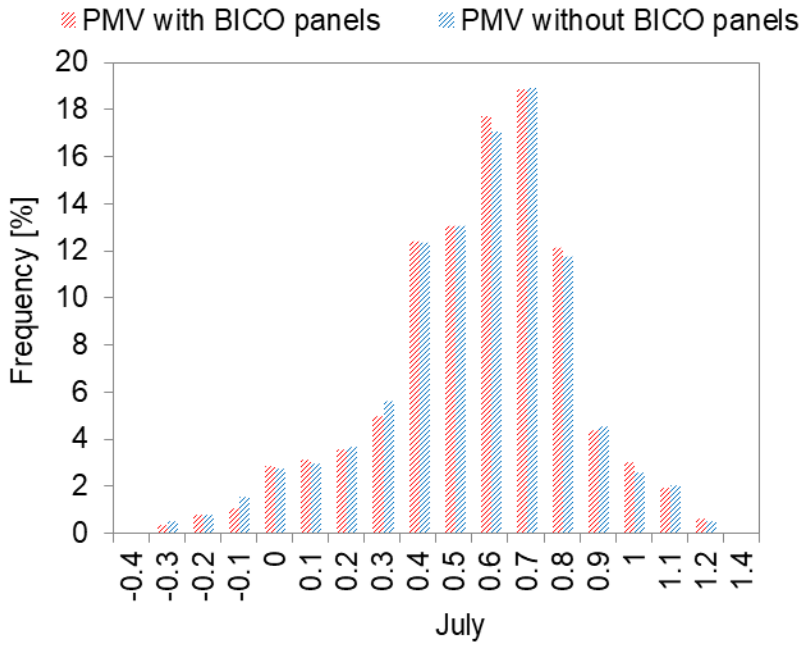

(b)

Figure 8.12. PMV values in scenario without and with BICO-5 panels, during January (a) and July (b).

8.5 The proposed solution in practice

Some renderings were carried out to get a realistic idea of how the application of the panels can change the perception of the atrium space (Figures 8.13-8.19). As a consequence of the analysis of the effects of the different panels arrangements on the acoustic quality of the atrium, it was chosen to represent the scenario characterized by flat and baffles element as covering. In fact, this solution allowed to converge acoustic and architectural perspectives.

As it can be observed in Figures 8.13-8.19, it was imagined to cover the panels with a sound-transparent fabric covering. The idea was to create a "play of colors" aimed at making the treatment pleasing to the eye. Furthermore, the use of a textile covering highlighted the fabric origin of the wastes used as base matrix of the panels.

A metallic grid of "C" section bars was imagined to fix the panels (250×90 cm) applied on the opaque walls of the buildings surrounding the atrium. A color similar to that of the other plastered opaque walls was chosen in order to emphasize the horizontal stripes created by strip windows across the façade of the building surrounding the atrium.

Gradual nuances of green and blue were selected for the baffles between the worktables and for the elements of the covering which were arranged following an alternate rhythm. The aim was to include elements which discontinue the regular harmony of the atrium space where all the elements repeats in the same way on the all floors, i.e. the horizontal strip windows, the opaque plaster walls with the same width and the vertical aluminum elements which divides the façades of the building in similar rectangular partitions. Panels with variable height (i.e. 150, 160 and 170 cm) and constant width (i.e. 30 cm) were used as baffles between worktables; whereas panels 100×120 cm, 80×120cm or 70×120cm were used as flat elements and baffles for atrium covering.

However, the quantity of absorbing material supposed to be used for the treatment was about 600 m^2, coinciding with that calculated for acoustic simulation previously analyzed.

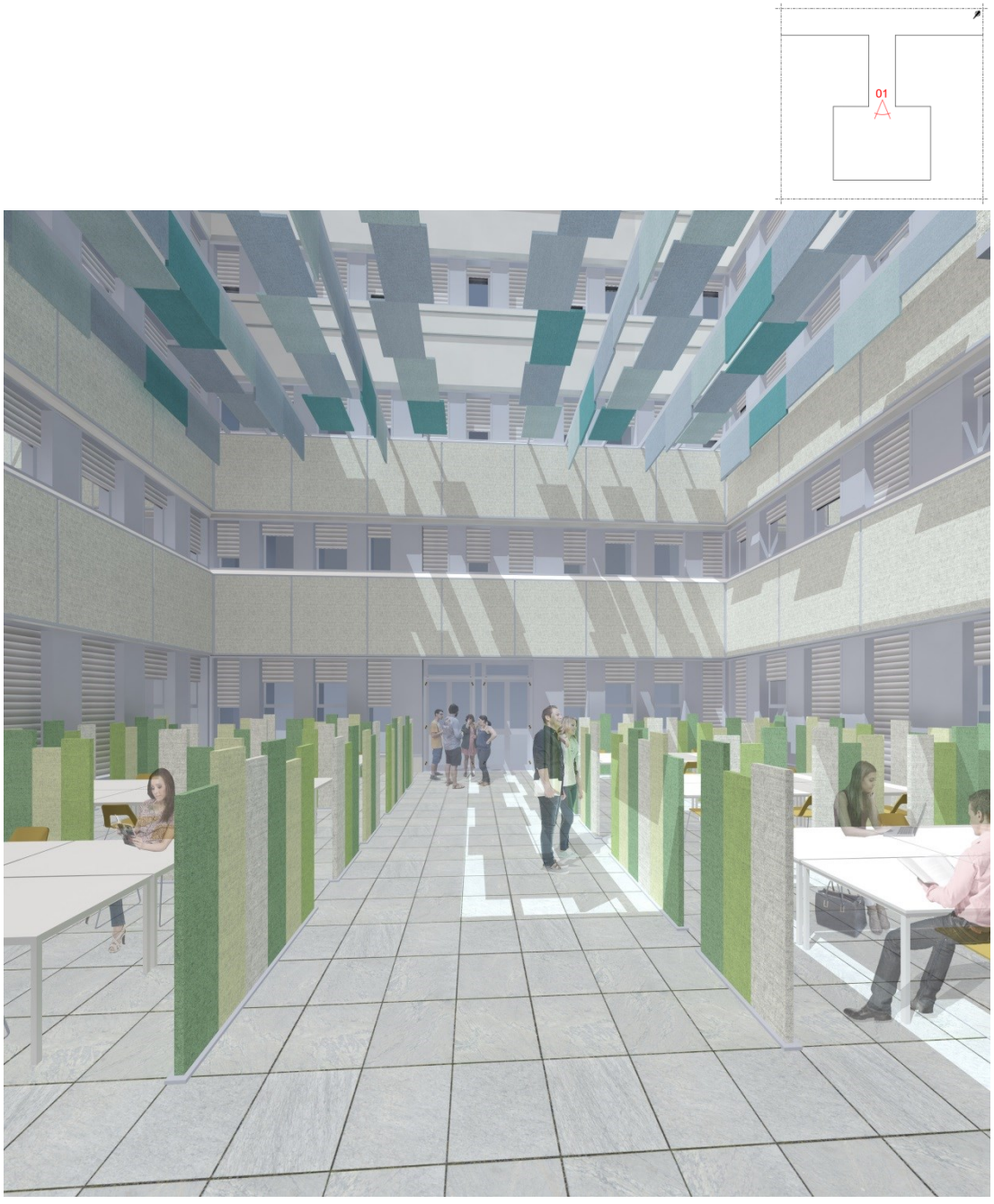

Figure 8.13. Rendering of the atrium:view 01.

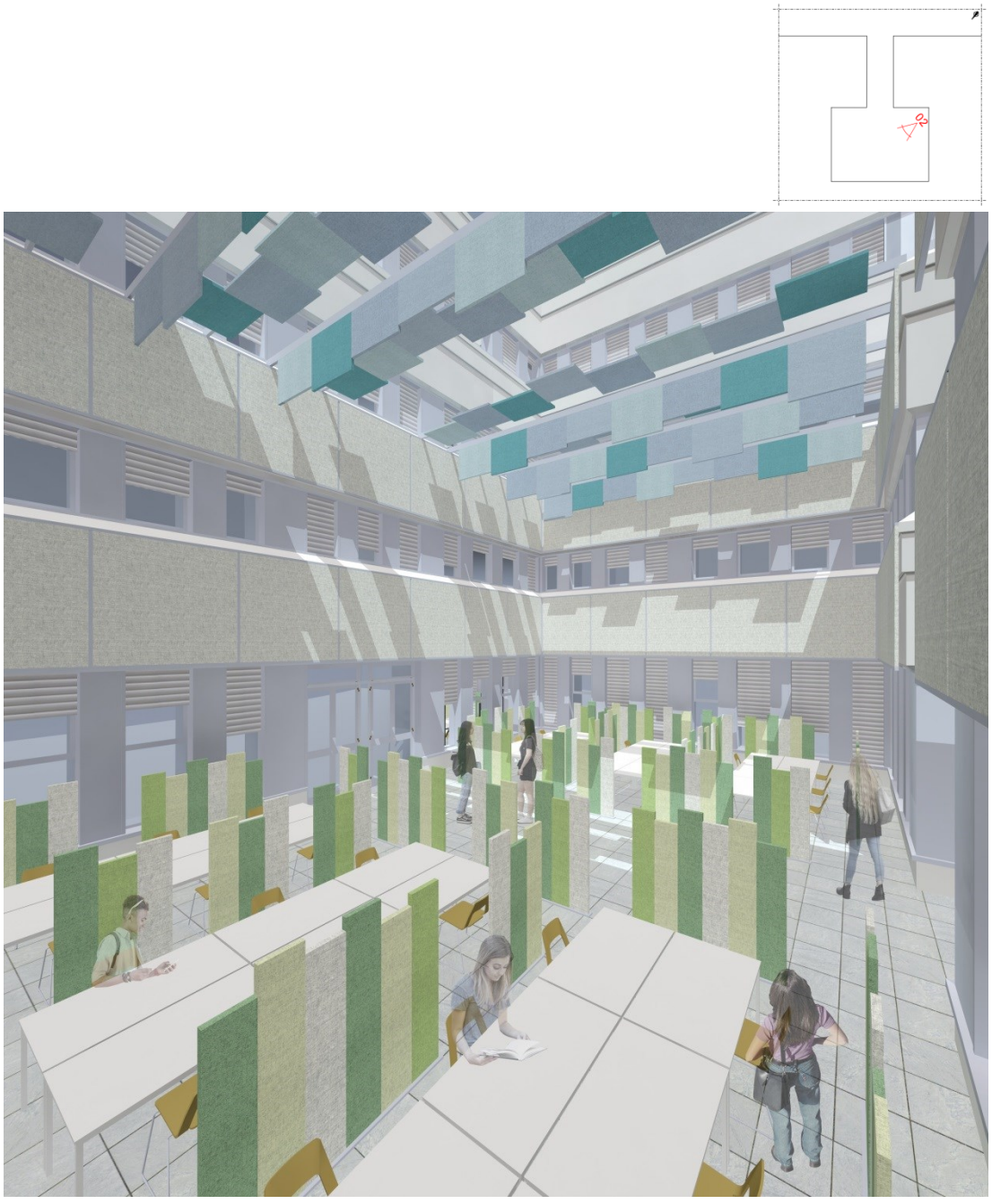

Figure 8.14. Rendering of the atrium: view 02.

Figure 8.15. Rendering of the atrium: view 03.

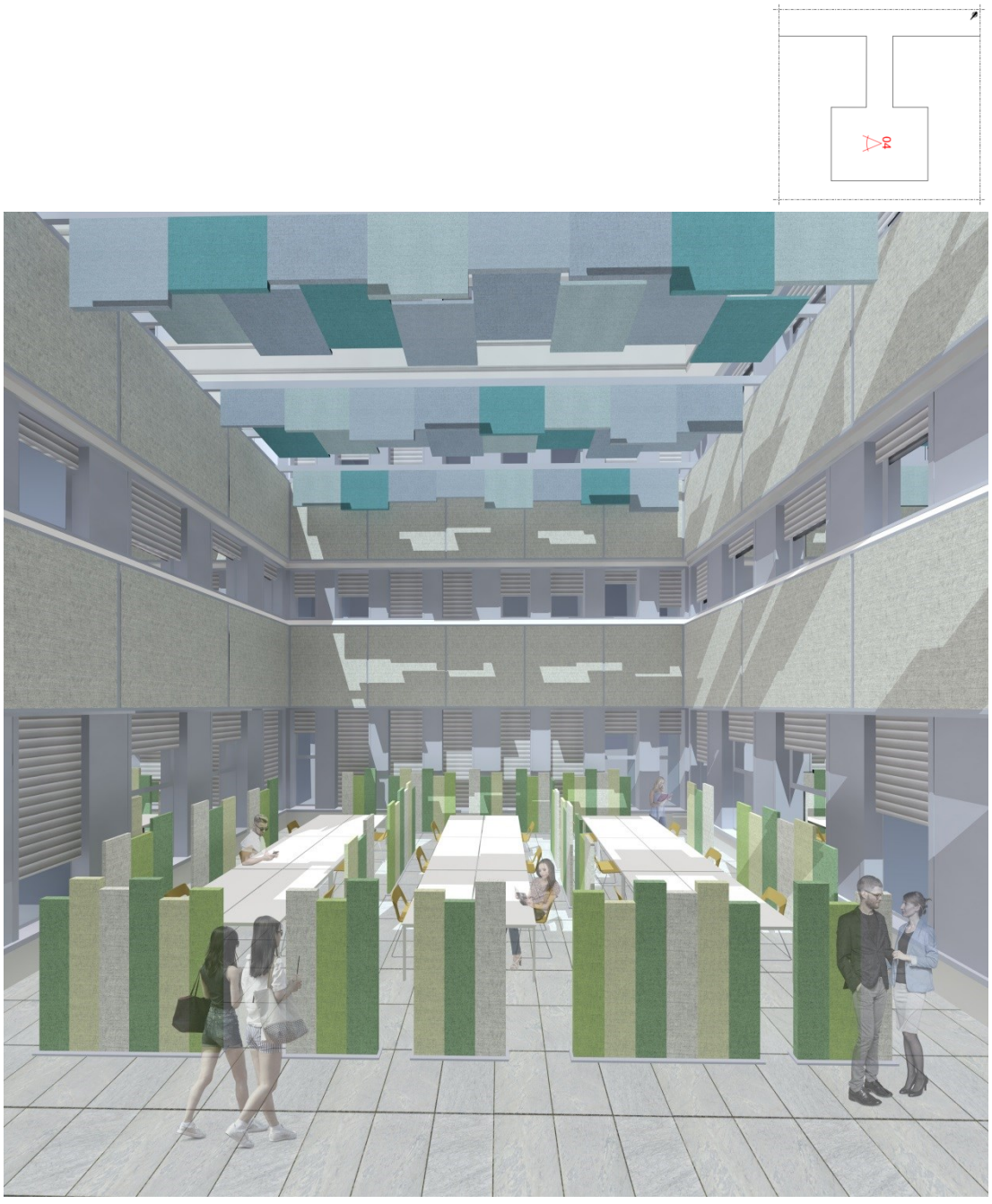

Figure 8.16. Rendering of the atrium: view 04.

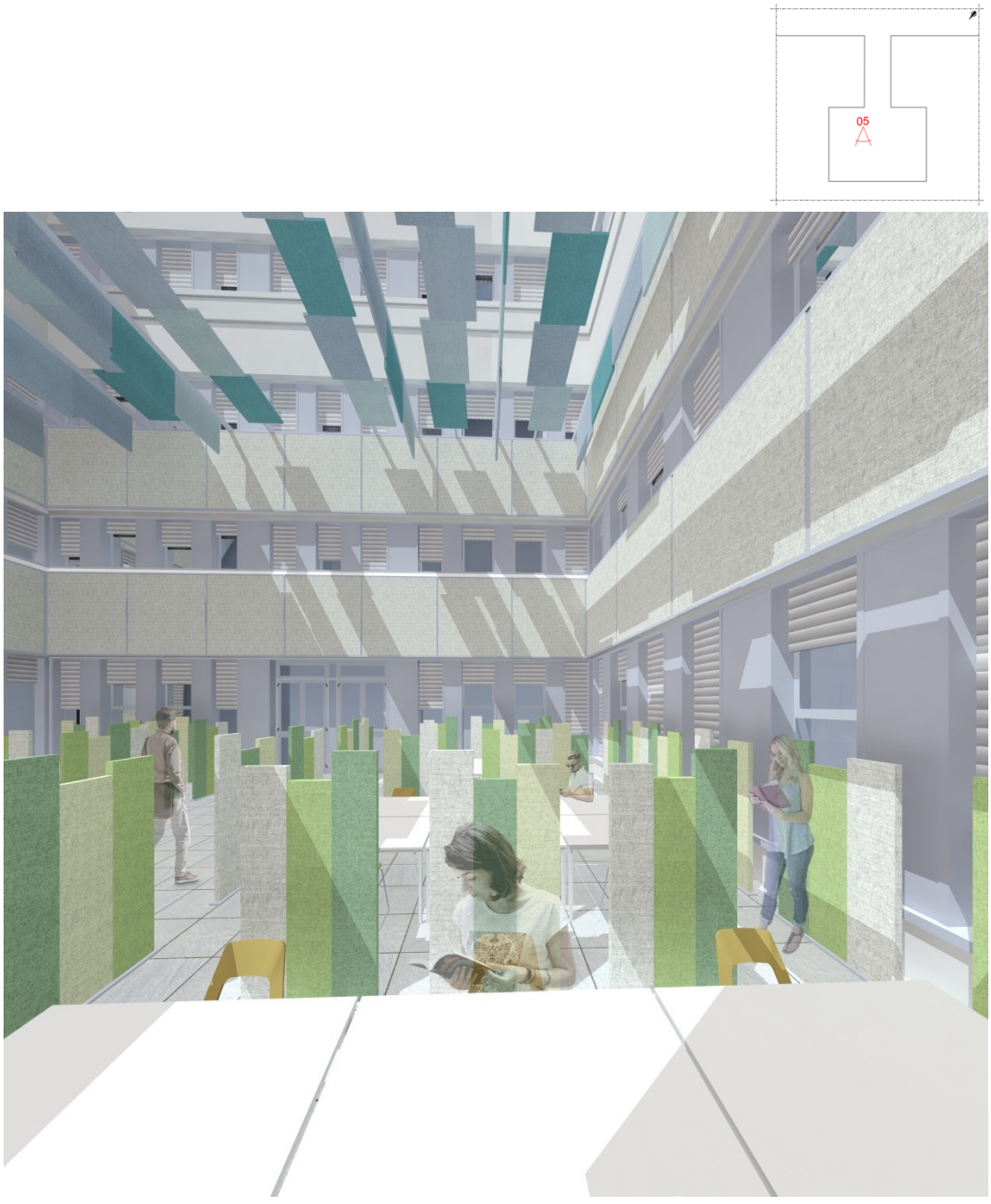

Figure 8.17. Rendering of the atrium: view 05.

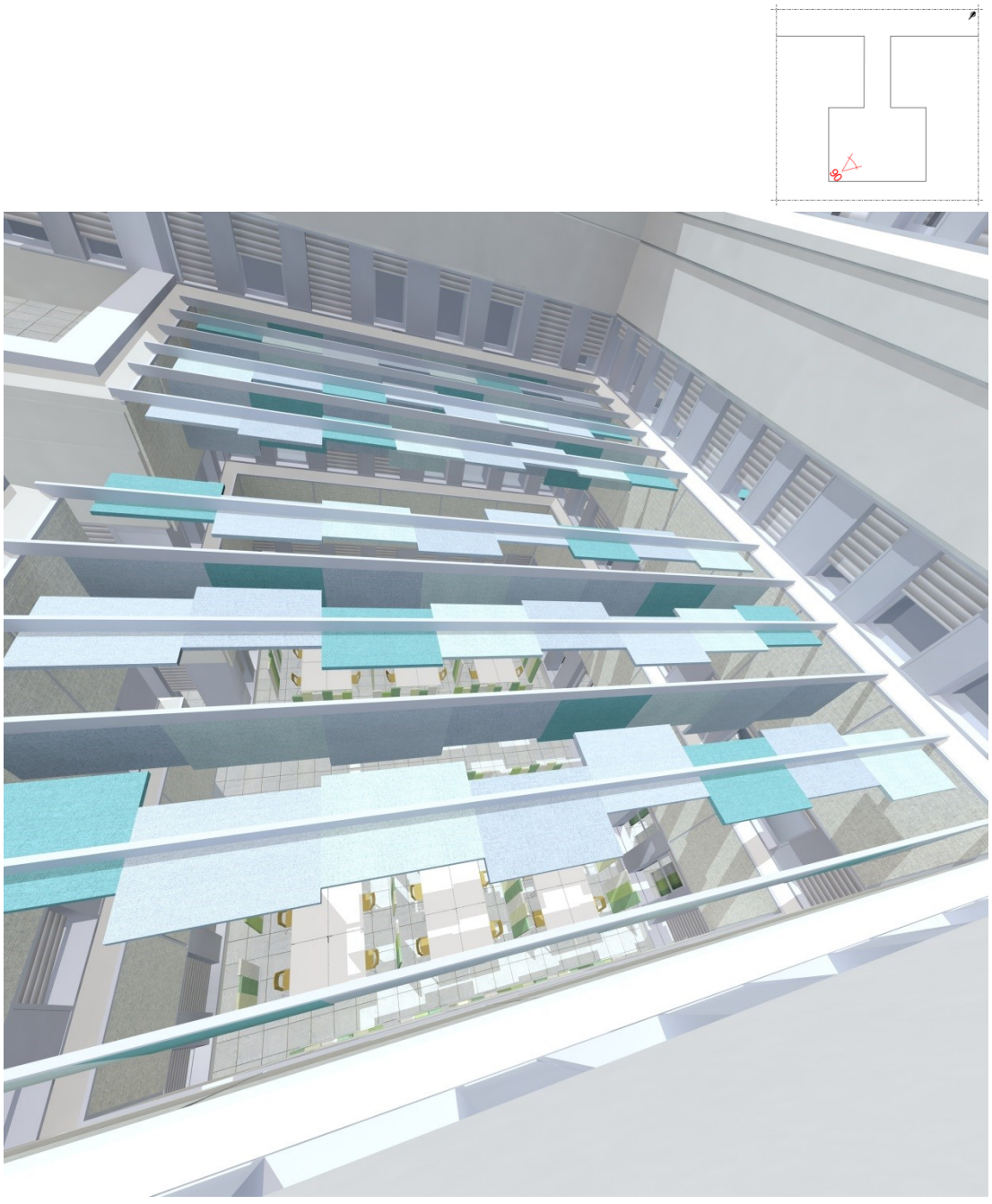

Figure 8.18. Rendering of the atrium: view 06.

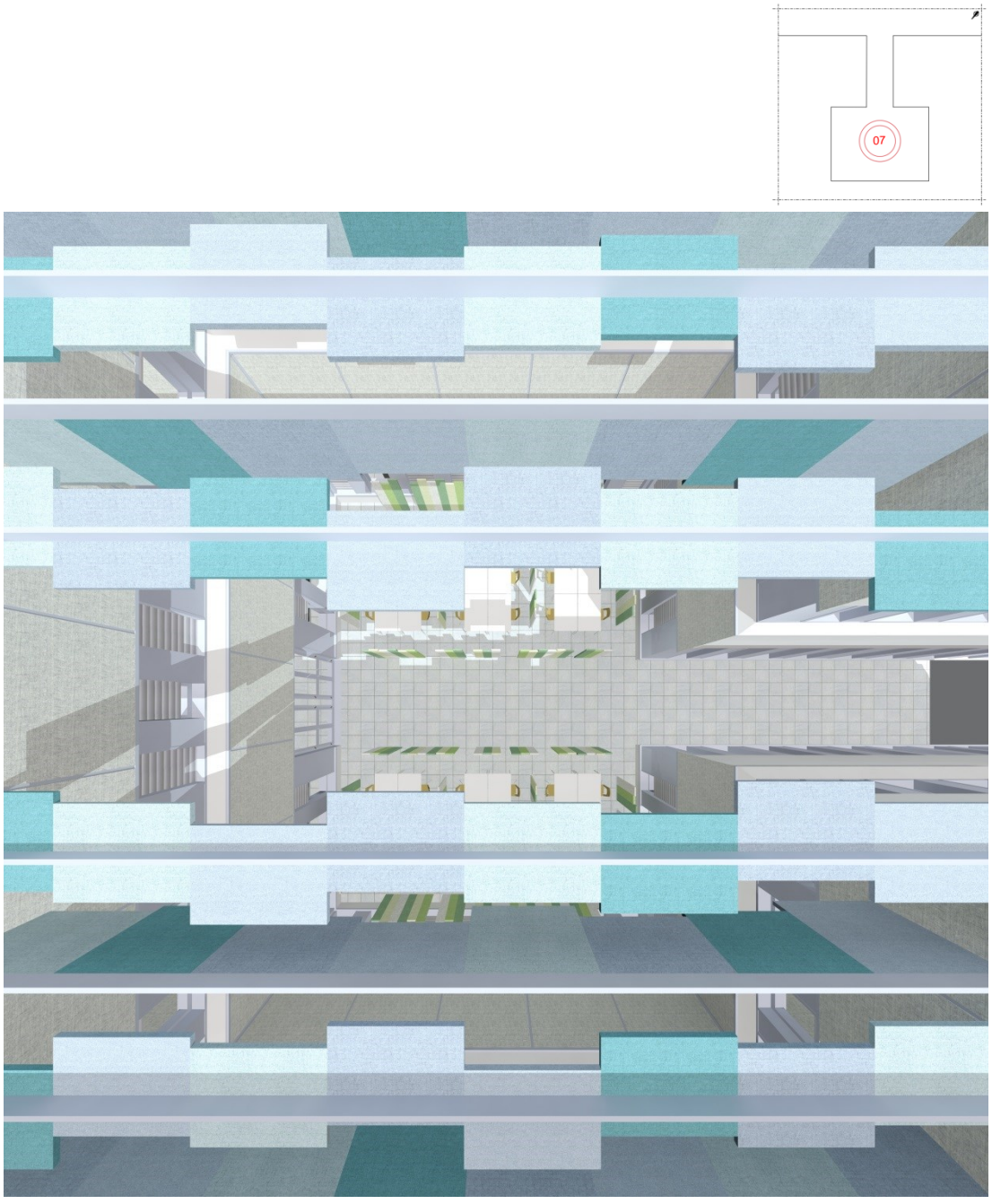

Figure 8.19. Rendering of the atrium: view 07.

References

Alvarez-Morales, L., Martellotta, F., 2015. A geometrical acoustic simulation of the effect of occupancy and source position in historical churches. Appl. Acoust. 91, 47-58. http://dx.doi.org/10.1016/j.apacoust.2014.12.004.

Alberdi, E., Galindo, M., León-Rodríguez, A.L., León, J., 2021. Acoustic behaviour of polychoirs in the Baroque church of Santa María Magdalena, Seville. Appl. Acoust. 175, 107814. https://doi.org/10.1016/j.apacoust.2020.107814.

ANSI S3.79, Draft V3.1 1993. American national standard method for the calculation of the Speech Intelligibility Index.

ASHRAE. Standard 55-2017, Thermal environmental conditions for human occupancy. American Society of Heating, Refrigerating and Air-Conditioning Engineering, Atlanta, GA. 2017.

Cox, T.J., D'Antonio, P.K., 2017. Acoustic Absorbers and Diffusers, Theory, Design and Application; Spon Press: London, UK.

Decree of President of Republic 412,1993. Regolamento recante norme per la progettazione, l'installazione, l'esercizio e la manutenzione degli impianti termici degli edifici ai fini del contenimento dei consumi di energia, in attuazione dell'art. 4, comma 4, della legge 9 gennaio 1991, n. 10. (GU Serie Generale n.242 del 14-10-1993 - Suppl. Ordinario n. 96).

EN 15251, 2008. Indoor environmental input parameters for design and assessment of energy performance of buildings addressing indoor air quality, thermal environment, lighting and acoustics. http://store.uni.com/catalogo/uni-en-15251-2008. (Accessed July 2021).

EN 12086, 2013. Thermal Insulating Products for Building Applications Determination of Long Term Water Absorption by Diffusion. http://store.uni.com/catalogo/uni-en-12088-2013. (Accessed April 2020).

EN 16798, 2019. Energy performance of buildings - Ventilation for buildings - Part 1: Indoor environmental input parameters for design and assessment of energy performance of buildings addressing indoor air quality, thermal environment, lighting and acoustics - Module M1-6. http://store.uni.com/catalogo/uni-en-16798-1-2019. (Accessed July 2021).

Ermann, M., 2015. Architectural acoustic illustrated. John Wiley & Sons Inc, United State, pp.60-66.

Fanger, P.O. Thermal Comfort. Analysis and Applications in Environmental Engineering, Danish Technical Press, Copenhagen, 1970.

Gardner, M.B., 1971. Factors Affecting Individual and Group Levels in Verbal Communication. J. Audio. Eng. Soc. 19, 560-569.

ISO 7730, 2006. Ergonomics of the thermal environment - Analytical determination and interpretation of thermal comfort using calculation of the PMV and PPD indices and local thermal comfort criteria. http://store.uni.com/catalogo/uni-en-iso-9921-2004. (Accessed March 2021).

ISO 9921, 2004. Ergonomics – Assessment of speech communication. http://store.uni.com/catalogo/uni-en-iso-9921-2004. (Accessed March 2021).

ISO 3382-1:2009. Acoustics-measurement of room acoustic parameters. Part 1: performance spaces. https://www.iso.org/standard/40979.html. (Accessed June 2021).

ISO 3382-2:2008. Acoustics-measurement of room acoustic parameters. Part 2: reverberation time in ordinary rooms. http://store.uni.com/catalogo/ec-1-2010-uni-en-

iso-3382-2-2008. (Accessed June 2021).
Katz, B.F.G., Poirier-Quinot, D., Postma, B.N.J., Thery, D., Luizard, P., 2018. Objective and perceptive evaluations of high-resolution room acoustic simulations and auralizations. In: Proceedings of the Euronoise 2018, Crete, Greece, 2107-2114.
Khovalyg, D., Kazanci, O.B., Halvorsen, H., Gundlach, I., Bahnfleth, W.P., Toftum, J., Olesen, B.W., 2020. Critical review of standards for indoor thermal environment and air quality. Energ Buildings 213, 109819. https://doi.org/10.1016/j.enbuild.2020.109819.
Lee K. H. and Schiavon S., 2014. Influence of Three Dynamic Predictive Clothing Insulation Models on Building Energy Use, HVAC Sizing and Thermal Comfort. Energies *7*, 1917-1934. https://doi.org/10.3390/en7041917.
Levy, S.M., 2011. Calculations to determine the effectiveness and control of thermal and sound transmission. In Levy, S.M., (Ed), Construction calculations manual. Butterworth-Heinemann, pp. 504-543.
Marshall, L., 2014. Architectural Acoustics (Second Edition). Academic press.
Meyer, J., 2009. Acoustics and the Performance of Music (Fifth Edition). Springer
Ministerial Decree, 15 July 2015. Requisiti minimi. (GU Serie Generale n.162 del 02-07-2015).
Rindel, J.H., 2010. Verbal communication and noise in eating establishments. Appl. Acoust. 71, 1156–1161. https://doi.org/10.1016/j.apacoust.2010.07.005.
Rindel, J.H., 2012. Acoustical capacity as a means of noise control in eating establishments. In: Proceedings of BNAM 2012, Odense, Denmark.
Schroeder, M.R., 1965. New method of measuring reverberation time. J. Acoust. Soc. Am., 37, 409-412. https://doi.org/10.1121/1.1909343.
Vorländer, M., 2011. Models and algorithms for computer simulations in room acoustics. In: Proceedings of the international seminar on virtual acoustics, Valencia, 72-82.
Webster, J.C. and Klumpp, R.G., 1962. Effects of Ambient Noise and Nearby Talkers on a Face-to-Face Communication Task. J. Acoust. Soc. Am. 34, 936-941. https://doi.org/10.1121/1.191822.

Chapter 9

Conclusions and future directions

The scope of the present research work was that of investigating the performance of innovative materials obtained from the use of fibers derived from recycled textile wastes (100% merino wool), combined with different binders to be used as building materials with sound absorbing and thermal insulating properties. This last Chapter summarizes the results which were illustrated in detail in the previous sections, confirming that the investigated materials have similar or better performance than conventional thermal insulating and sound absorbing products. Thus, in order to understand whether the innovative materials might be actually competitive, worth being used in the real world, some considerations about their circularity and sustainability values are also included.

Eventually, future directions are recommended in order to investigate further aspects especially relating to the industrialization process and its environmental impacts through a Life Cycle Assessment (LCA). In fact, the industrial upscaling of some BICO samples was performed with the aim of comparing the hygrothermal and the acoustic performances of the industrial panels with laboratory scale samples.

9.1 Conclusions

The overall aim of the research work was to investigate the possibility of developing building materials from textile wastes, in response to European and National objectives of circularity and sustainability. Three types of non-woven materials were produced and tested. Two manufacturing techniques and three binders were investigated to prepare samples with different density values. Particularly, "BICO" samples were obtained bonding 100% wool recycled fibers with CoPET/PET bicomponent fibers by means of the thermal bonding technique. Otherwise, chitosan and gum Arabic were investigated as binding agents to produce woolen samples (respectively "CH" and "GA" samples) using the chemical bonding technique. The experimental results were promising both from a thermohygrometric and from acoustic point of view, proving the real possibility of using textile wastes as secondary raw materials in building sector. In this final chapter, a summary of the main findings based on the objectives of this Ph.D. research is presented and considerations on the possible future applications of the obtained outcomes are given.

9.1.1 Review of the state of the art on use of textile waste in building industry

Collecting textile leftovers without recycling them can become a serious environmental problem due to the huge availability of pre-consumer and post-consumer wastes. For this reason, more and more researchers are studying alternative solutions to their disposal. An example is the use of textile wastes as secondary raw resources for developing environmental friendly building materials. An overview of building components produced from textile waste has been compiled through a literature survey up to 2020. All analyzed researches agreed that recycling textile leftovers in construction industry could limit the environmental impact of the building materials, reducing the use of new virgin sources and preserving them for future generations.

Textile waste fibers were mostly used to produce sustainable thermal insulators or sound absorbers in form of mats or panels. In some cases the investigated materials showed much better acoustic and thermal properties than the products currently available in the market. In order to transform textile waste into building components, direct and non-woven methods were proposed. In the latter case, chemically gluing, mechanically

entangling, or thermally bonding techniques were compared. However, there were limited studies about the structure of the textile-based materials, its influence on the insulation and sound absorbing properties, and about the effects of the manufacturing methods on the microstructure of the products.

Furthermore, textile waste fibers were proposed as lightening material for energy efficient lightweight bricks or as reinforcing materials for innovative concretes or plaster mortars with high mechanical resistance performance.

The analysis of the state of the art was useful to have a global idea on the topic and was a starting point to make a responsible choice of the production technologies followed for this research and of the methods used to analyze the experimental data obtained from laboratory tests.

9.1.2 Analysis of different production methods: chemically gluing and thermally bonding techniques

"BICO", "CH" and "GA" materials were produced and tested from various perspectives and their thermal, hygric, acoustic and fire resistance behaviours were analyzed. The experimental results obtained for the three typologies of material were then compared in order to investigate the effects of the two different manufacturing technologies. In fact, testing of the non-acoustic properties (i.e. the porosity, the tortuosity and the air flow resistivity) allowed to analyze how chemical gluing and thermal bonding procedures affected the microstructure of the final products, influencing their hygrothermal and acoustic performances. Conclusions on data collected in the laboratory were drawn, generalizing the information contained in the produced samples using the statistical inference method.

Taking into account the thermal behaviour, all the developed materials exhibited suitable properties (i.e. thermal conductivity less than 0.06 W/(m·K)) to be used as thermal insulation components. Furthermore, the thermal conductivity values were well comparable with literature results and reference values given in national standards.

The statistical analysis proved that changes in the bulk densities of the three different types of material affected their thermal conductivity values in the same way, regardless of the different fabrication techniques. In fact, the slopes of the three regression lines obtained after plotting the thermal conductivity versus the bulk density for BICO, CH and GA

samples were considered comparable when a two tailed hypothesis test with a significance level of 0.05 was carried out. The results of the statistical tests could be expected due to the similar porosity values shown by the compared materials which exhibited a void fraction close 90%.

In light of the high porosity values, the produced materials could be considered a mixture of fibers and air and both of these two phases influenced the thermal behaviour of the whole in terms of effective thermal conductivity. A deeper theoretical analysis showed that the only significant heat transfer mode through tested materials was the conduction of the two phases.

Contrary to what has been observed for thermal conductivity, no significant correlation was found between the bulk density and the water vapour permeability, whatever the material considered.

A two samples Student's *t*-test on the mean values of water vapour permeability of BICO, CH and GA samples showed that the mixes with bicomponent fibers and natural solutions as binder belong to two different groups of materials. This was due to the effect of production techniques used on tortuosity values which resulted to be higher for BICO samples than CH and GA ones. In fact, the thermal bonding technique led to a richly entangled microstructure of the BICO samples which showed a more complex vapour flow path and a consequent lower water vapour permeability than CH and GA ones.

However, the mean values of water vapour permeability resulted to be $2.441 \cdot 10^{-11}$ kg/(m·s·Pa) for samples produced using natural solutions as binding agents, and $2.155 \cdot 10^{-11}$ kg/(m·s·Pa) for samples using bi-component binding fibers. Both results could be considered in agreement with the current construction standards and with literature data on natural insulators.

Porosity and tortuosity variations also affected the air flow resistivity of samples, with consequent implications on their acoustic performance. For each typology of material, more porous samples were characterized by a lower air flow resistivity, showing a better sound absorption in the mid and high frequency ranges. On the contrary, the increased air flow resistivity values of the less porous samples improved sound absorption at low frequencies yielding values as high as 0.5 from 315 Hz on.

The more intricate pores structure of the BICO samples resulted in less air permeability. As a consequence, BICO materials showed acoustic behavior comparable with CH and GA samples despite they exhibited higher values of air flow resistivity, while being less dense.

The non-acoustic properties were useful not only to characterize the microstructure of the materials, but also to predict their acoustic response, in order to validate the experimental data. A comparison between measured and predicted absorption coefficients showed that the phenomenological model developed by Johnson, Champoux and Allard estimated the acoustic behaviour of most samples better than the empirical model proposed by Delany and Bazley. Thus, the importance of the microstructure in altering the sound path was confirmed. However, the empirical model well estimated the behaviour of the samples with lower air flow resistivity values.

The fire resistance behaviour of the tested materials was investigated in relation to a reference sample of pressed wool. Smoke and/or flame spreading on the topmost part of the samples were observed in quantity depending on the type of binder used. Although small carbonized portions of BICO and GA samples kept burning after the burner was retracted, the results could be considered promising for the three typologies of material in light of the possibility of improving their behaviour with additives.

Eventually, part of the research was designated to investigate how the integration of Phase Change Materials (PCMs) in the tested gum Arabic-based samples could improve their thermal performance. Two types of mix, i.e. PCM-26 and PCM-41, respectively containing 26% and 41% of phase change materials were produced. Their thermal properties as a function of temperature were examined in dynamic condition and were compared with results obtained for a reference sample without PCMs (i.e. PCM-00).

It was observed that thermal conductivity increased with increasing temperature and PCM content. Furthermore, the samples containing PCMs showed specific heat capacity values higher than reference sample. However, PCM-00 sample exhibited a specific heat capacity value higher than wool-based samples found in literature, proving a greater thermal storage capacity.

A Hot Box test was carried out in order to better demonstrate the temperature regulation ability of the samples with PCMs. The addition of the microcapsules in the woolen

samples allowed a reduction of the temperature fluctuations on their internal surfaces and shifted temperature peaks on the external ones. The thermal energy storage capacity of the tested samples was further highlighted analyzing the heat flux exchange across the walls of the Hot Box as a function of time and temperature.

9.1.3 Application to a case study

The best performing material among those tested (BICO-5) was selected for a potential application as an acoustic treatment of the internal atrium of the Architecture's Building of the Polytechnic University of Bari in order to improve comfort conditions for the students, while reducing noise exposure in the atrium and save energy thanks to the application of treatments on the walls so to increase their thermal resistance.

The atrium was first modeled with CATT-Acoustic® software and several scenarios characterized by different arrangements of the absorbent material in form of panels were simulated and compared. A total of about 600 m^2 of panels were applied on the opaque walls at the first and the second floors of the buildings surrounding the atrium, partly suspended to the ceiling over the atrium, and as baffles between the worktables usually placed in the atrium. In order to evaluate the acoustic quality of the simulated space, the A-weighted sound pressure level obtained by CATT-Acoustic simulations was compared by the A-weighted sound pressure level calculated taking into account the possible Lombard effect caused by spontaneous increase of people vocal effort due to the high ambient noise level.

Results showed that in the scenario without panels the occupants of the atrium raised their vocal efforts by 4 dB more than the normal vocal spectrum, as a consequence of the Lombard effect. The solutions in which the panels between the worktables didn't create "sound barriers" between the sources and the receivers allowed to reduce the vocal effort of the occupants by at least 4 dB compared to the current situation, while maintaining the normal speech level. When the baffles between the worktables cut the line of sight between the sources and the receivers, acoustic comfort conditions were achieved and the vocal effort of the occupants resulted to be lower than that corresponding to a normal a speech level.

Energy simulations were also carried out using DesignBuilder® software. The aim was to analyze the effects of the panels application on the energy behaviour of the rooms with atrium view, whose opaque walls were treated with the insulating panels.

Results showed that adding the panels allowed to reduce the heating winter loads by 10%; whereas a slight increase of cooling summer loads (i.e. 4%) was observed. In fact, the increase of the insulation allowed to reduce the transmittance value of the external walls of the simulated rooms, reducing their rate of heat loss during the winter seasons. At the same time, heat exchange during the fresh hours of the summer seasons became more difficult, negatively influencing the cooling summer loads.

The application of panels had only negligible effects on the thermal comfort of the occupants of the simulated rooms whose comfort conditions are influenced by environmental factors mainly depended on the HVAC system parameters. Being the HVAC system the same in both solutions with and without BICO panels, the insulating treatment of walls did not have significant effects on the PMV values. However, most of the PMV values resulted distributed around 0.3 during January and around 0.7 during July. Such results meant that acceptable comfort levels were achieved most of the working time during winter seasons, and minimum requirements for thermal comfort were verified most of the time during summer seasons.

9.1.4 Summary of main achievements

The conclusions are summarized in order to highlight the main scientific achievements:

- BICO, CH and GA materials were produced using respectively bi-component fibers, chitosan and gum Arabic as binders, and obtained following two different production processes (thermal and chemical bounding techniques). They were tested from various perspectives and their thermal, hygric, acoustic and fire resistance behaviour was analyzed;
- statistical analysis proved that changes in the bulk densities of the three different types of materials affected in the same way their thermal conductivity values. On the contrary, the technique followed to produce the nonwoven (with or without binders) affected pore microstructure with consequent implications on the sound absorption and water vapour diffusion properties;
- all the materials exhibited suitable thermal properties (i.e. thermal conductivity less

than 0.06 W/(m·K)) to be used as thermal insulation panels;

- deeper theoretical analysis showed that the only significant heat transfer mode through tested materials was the conduction of the two phases (i.e. solid matrix consisting of fibers and a gas phase formed by air);
- the mean values of water vapour permeability which resulted to be $2.441 \cdot 10^{-11}$ kg/(m·s·Pa) for samples produced with natural solutions as binder agents and $2.155 \cdot 10^{-11}$ kg/(m·s·Pa) for samples using bi-component binder fibers, were in agreement with the current construction standards;
- although small carbonized portions of BICO and GA samples kept burning after the burner was retracted, the results of the fire resistance test could be considered promising for the three typologies of material in light of the possibility of improving their behaviour with additives;
- all materials, apart from samples with the highest density, showed good sound absorption coefficients as high as 0.7 at frequencies from 500 Hz on;
- the more intricate pores structure of the BICO samples resulted in less air permeability. Thus, BICO materials showed acoustic behavior comparable with CH and GA samples despite they exhibited higher values of air flow resistivity, while being less dense;
- a comparison between measured and predicted absorption coefficients showed that the phenomenological model developed by Johnson, Champoux and Allard estimated the acoustic behaviour of most samples better than the empirical model proposed by Delany and Bazley;
- the addition of PCMs microcapsules improved the thermal energy storage capacity of the tested samples;
- the simulation of the application of the BICO-5 material for improving the acoustic comfort of the internal atrium of the Architecture's Building of the Polytechnic University of Bari showed a reduction of the vocal effort of the occupants compared to the current situation;
- only negligible effects on the thermal comfort of the rooms interested the application of panels was observed, however acceptable comfort levels were achieved most of the working time during winter seasons, and minimum requirements for thermal comfort were verified most of the time during summer seasons.

9.2 Further considerations

According to the Green Public Procurement (COM 400, 2008), an eco-friendly material is a product having a lesser or reduced effect on human health and the environment when compared with competing product that serve the same purpose. A material can be eco-friendly by itself, or even conventional products can become eco-friendly based on the construction technique that is used. To this purpose, the raw materials used for this research both as matrix and as binder were appropriately selected and thoroughly characterized in order to optimize the manufacturing process.

9.2.1 Environmental advantages of the proposed samples

In terms of the environmental impact of the binders, the actual quantities of materials needed must be taken into account, based on the sample composition.

Taking into account the thermally bonding technique, 200 g of bicomponent fibers were used for 1 kg of material. It might seem a large amount considering the environmental impact of the synthetic fibers production which involves the use of petrochemical materials responsible for carbon dioxide emissions. However, the possibility of using recycled materials offsets the negative effects. Abbasi and Kotek (2019) investigated the potential of producing side-by-side bicomponent fibers from recycled polyester which otherwise become a post-consumer waste in garbage, leading to serious ecology difficulties. In fact, when synthetic fibers are disposed of, do not decompose, becoming source of microplastics and contributing to the environmental pollution (Strähle et al., 2017).

Considering the chemical binding technique, the chitosan solution includes 15 g of chitosan per kg of water, and the amount of binder is 60% the mass of the sample. This results in just 9 g of chitosan per kg of (wet) sample prepared. Thus, the incidence of chitosan production is only marginally reflected on the panel preparation. However, chitosan could be considered an environmentally-friendly choice as its production avoids the composting process of the crab shells, leading to a saving in toxic emissions, especially ammonia (Munõz et al., 2018).

With reference to gum Arabic, the situation is a bit different as the amount of dry product requested to manufacture 1 kg of composite panel is 120 g, which is much higher than chitosan. However, in the light of the positive effects related to Acacia tree cultivation, we might expect a lower overall impact. In fact, gum Arabic is an exudate of

widely distributed Acacia threes, whose cultivation usually involves spontaneously grown plants that do not involve the use of water, fertilizers and pesticides (Mariod, 2018).

The choice of using wool textile leftovers as matrix allowed to implement a circular approach for managing the waste flow. To better appreciate this aspect, it is important to identify the environmental benefits of recycling option compared to the traditional landfill disposal. Recycling activities are promising strategies to lessen the landfill space, reducing the air, earth and water pollution and limiting the harmful effects which a disposal of fibers could have on human health (Yalcin-Enis et al., 2019). In fact, during their decomposition process, organic animal fibers as wool produce ammonia, which is responsible for creating toxicity in land and water (Jayasinghe et al., 2010). Furthermore, when it downpours, water depletes through the solid fibers not yet decomposed, grabbing perilous chemicals. This water is absorbed by earth and feeds the seas and oceans being lethal if ingested in excessive quantities by the marine population (Senthil Kumar and Yaashikaa, 2018).

Using textile wastes as secondary raw materials extended the end-of-life of fibers whose decomposition process, as well as their production represents a risk to the earth and water supplies. Animal fibers like wool, generate environmental pollution due to the large use of land, water, fertilizers and pesticides. Sandin et al. (2019) estimated that the greenhouse gas emissions associated with wool fibers production ranges from 1.7 kg CO_2 to 36.2 kg CO_2 equivalents per kg of fibers. Differences in gas emissions for the production of wool could be affected by geographical location changes (Gowane et al., 2017).

A textile disposal solution different from the landfill involves the use of fibers at the end of their useful life as an alternative fuel source. Muthu et al. (2012a) demonstrated the environmental advantages of recycling practices versus incineration in terms of energy conserved versus the energy generated by incineration, estimating a saving of 16,389 kWh/ton of energy.

In the light of the promising experimental results, the tested materials could be used as alternative to traditional thermal insulators and sound absorbing materials. In this way, the ecological effects of using new virgin sources could be reduced. In fact, materials obtained from mineral wool fibers are the most used for thermal insulation and sound absorption, because of their good performances and low cost. Normally, mineral wool materials are made from molten glass, rock or slag, using a manufacturing process extremely energy-

intensive which involves not-recyclable raw materials. Furthermore, the manufacturing process of mineral wool requires high melting temperatures of 1400/1500 °C; whereas the working temperature used to produce the tested samples was 100 °C.

9.2.2 Economic advantages of the proposed samples

Recycling textiles yielded not only environmental benefits, but also economic advantages due to the decrease in the cost of acquiring new materials, expanding profit efficiency. Muthu et al. (2012a), introduced an Economic Gain Index (EGI) obtained from the ratio of the price of the recycled fibers versus that of virgin ones. An EGI of 0.17 and 0.82 was found respectively for wool and polyester, proving the economic advantages of using recycled materials.

Although the cost of recycled fibers is less than the virgin ones, one of the barriers which complicates the transition from a linear to a circular textile/clothing model is represented by the economic viability. As anticipated in the Introduction Section, the present study was carried out in collaboration with a private company for which the cost of pre-consumer textile disposal (which is considered a special waste) was 70% higher than that of ordinary municipal waste.

Therefore, it is recommended that the textile special waste management system be modified and improved to make it compatible with the requirements of the textile/clothing companies as they can maximize their efforts to actively contribute to converting the waste from their production activities into new sources.

9.2.3 The end-of-life of the proposed materials

Another issue that might raise some concerns is the end-of-life behaviour of the proposed non-wovens. Although the disposal of samples made with bicomponent fibers as binders may seem more problematic than that of the samples made with sustainable solutions of chitosan and gum Arabic, the treatment of mixed fibers is not a new issue. Nowadays, most of the fabrics are blends of synthetic and natural fibers. The presence of non-biodegradable synthetic materials makes the decomposition of natural fibers more difficult, favoring landfilling or incineration of the textile waste (Pensupa, 2020). However, the possible reuse of textile waste made of mixed fibers to produce industrial wipes or filling materials may represent a significant advantage in terms of use of virgin

materials and environmental impact, even if compared to incineration (Schmidt et al., 2016). Obviously, to make the recovery of textile waste really effective, it would be necessary to recycle the fibers separately (Östlund et al., 2017). From this point of view Yousef et al. (2020), tested an ecofriendly hydrophilicity solvent to separate polyester from cotton in jeans fabrics, proving a significant reduction of 1,448 kg CO_2 equivalents per ton of waste than usual approaches (i.e. landfilling and incineration).

9.2.4 Industrial upscaling of the tested materials

As the aim of this research was to investigate and propose solutions that could be applied in practice, a final effort was made to outline the main steps of an industrial production process and actually realize them. As it will be seen, at the present stage, the main steps had to be carried out by different specialized companies. Thus, transportation played a significant role at this early stage, but shortening the distances and clustering the different manufacturing activities would be an obvious requirement of any real-world application.

First, a total of 450 kg of tailored cuttings supplied by Gordon Confezioni s.r.l. were packed to be sent to ZO-MA srl company (Vicenza, Italy) (Figure 9.1(a)). This is a national company with a solid experience in marketing of staples and wastes for operations in textiles, apparel and geotextiles which was commissioned to convert the wastes in a suitable form to became base materials for the non-wovens.

As observed in Figure 9.1 (b), the textile wastes used as raw materials consisted not only in yarns, but also in fabric remnants. Thus, they have been subjected to a “rag grinding” process by a garnett technique able to transform them by first cutting and then tearing pieces in an extremely robust machine. Being feed materials above about 50 mm in length, they needed to be further cut prior to the garnett process.

(a) (b)

Figure 9.1. Textile wastes packaged to be sent to ZO-MA srl. company (a) and their detail (b).

Then, the conversion of textile batts in building panels was commissioned to Cormatex srl (Prato, Italy), a textile machinery manufacturer working worldwide since 1938. It also supplied the bicomponent fibers used as binder. The panels were produced following an airlaying process which involved the uniformly dispersion of wool and bicomponent fibers in an airstream, after blending them in suitable proportions. The aim was to obtain a mix of fibers which did not interact each other mechanically or by friction. This fibers mixture was led towards a permeable conveyor where they were randomly deposited in the form of a web. During the last step, a web with the 5 cm tick was molded in an oven and several panels (120 cm×60 cm) were cut from the web. Figure 9.2 shows some important steps of the airlaying process.

Three different types of materials were commissioned with density values of 50, 90 and 120 kg/m^3, respectively similar to BICO-5, BICO-4 and BICO-3 laboratory scale samples. Binding fibers and working temperature similar to those of the laboratory scale process were used; but slightly different base fibers were considered. In fact, during laboratory tests 100% wool wastes were used in order to better analyze the effects of the synthetic fibers, identifying the minimum content able to guarantee the adequate cohesion of the final product. The wastes used for the industrial process were selected among tailoring of the autumn-winter company collection, resulting mainly of wool, but including small percentages of synthetic material. In this way the upscaling process was more coherent with real-world conditions, considering the difficulty of selecting a large amount of 100%

wool residues among the production wastes of a tailoring company. Being the synthetic content unknown, two different binding fibers contents were investigated: 20% b.w. and 10% b.w. The first percentage was selected in order to reproduce a process with the same boundary condition of the laboratory, while the lower percentage was selected in order to take into account the additional synthetic fibers found in the the waste used as base raw materials.

(a) (b)

(c) (d)

Figure 9.2. Raw materials: textile batts and bicomponent fibers (a), mix of base and binder materials (b), fibers deposited in form of web before (c) and after (d) their treatment in the oven.

9.2.5 Further investigations

The upscaling process was useful to collect data about the energy and gas consumptions with the aim to analyze the environmental impacts of the industrial production process. The capacity of the production line of Cormetex srl is 1000 kg/h of wastes converted into web, with an energy demand of 140 kWh for all the production steps, from the mix of base and binder fibers to cutting the panels. The gas demand is about 70 m^3/h. These data, in addition to more detailed information which will be required to the companies charged in the industrial transformation will be useful to assess the environmental aspects associated with the industrial production process of the investigated materials through a Life Cycle Assessment (LCA).

Thanks to the full-size of the panels obtained with the industrial process compared to the samples produced in laboratory, their random incidence sound absorption coefficients could be measured in the reverberation chamber, following the standard procedure (ISO 354, 2003). Furthermore, a test room could be also developed in order to test and compare the data collected by the experimental campaign, with the results achieved on fields testing the hygrothermal behaviour of the building envelope under dynamic conditions.

Further research is recommended to develop an experimental investigation of the thermal and hygric properties of the panels produced following the industrial process, paying attention to their microstructure. In fact, a different fiber orientation could be observed due to the industrial method, with consequent effects on the porosity and the tortuosity of the materials and hence on the performances depending on them.

Although wool is known to have a very good capacity for storing water vapour, further investigation could be carried out with reference to aging and resistance to external attacks.

References

Abbasi, M., Kotek, R., 2019. Effects of drawing process on crimp formation-ability of side-by-side bicomponent filament yarns produced from recycled, fiber-grade and bottle-grade PET. J. Text. I., 110(10), 1439-1444, https://doi.org/10.1080/00405000.2019.1611523.

COM 400, 2008. Communication from the Commission to the Council, the European Parliament, the European Economic and Social Committee and The Committee of the Regions - Public procurement for a better environment. https://eur-lex.europa.eu/legal-content/EN/TXT/?uri=CELEX:52008DC0400. (Accessed April 2021).

Gowane, G.R., Gadekar, Y.P., Prakash, V., Kadam, V., Chopra, A., Prince, L.L.L., 2017. Climate change impact on sheep production: growth, milk, wool, and meat. In: Sejian, V., Bhatta, R., Gaughan, J., Malik, P., Naqvi, S., Lal, R. (Eds.), Sheep Production Adapting to Climate Change. Springer, Singapore, pp. 31-69.

ISO 354, 2003. Acoustics: Measurements of Sound Absorption in Reverberation Chamber. http://store.uni.com/catalogo/iso-354-2003. (Accessed April 2020).

Jayasinghe, I.H., Basnayake, B.F.A., Amarathunga, K.S.P., Dissanayake, P.B.R., 2010. Environmental conservation efforts in developing textile waste incorporated cement blocks. Trop. Agric. Res. 21, 126-133.

Mariod A.A., 2018. Chemical Properties of Gum Arabic in: Mariod A.A. (Ed), Gum Arabic_Structure, Properties, Application and Economics. Academic press, United Kingdom, pp. 113-123.

Muthu, S.S., Li, Y., Hu, J.Y., Mok, P.-Y., 2012a. Recyclability Potential Index (RPI): the concept and quantification of RPI for textile fibers. Ecol. Indicat. 18, 58e62. https://doi.org/10.1016/j.ecolind.2011.10.003.

Muñoz, I., Rodríguez, C., Gillet, D., Moerschbacher, B.M., 2018. Life cycle assessment of chitosan production in India and Europe. Int. J. Life Cycle Assess.23, 1151-1160. https://doi.org/ 10.1007/s11367-017-1290-2.

Östlund, A., Syrén, P.O., Jönsson, C., Ribitsch, D., Syrén, M., 2017. Re:MixeSeparation and Recycling of Textile Waste Fiber Blends. MISTRA Future Fashion report, Rise: Borås, Sweden.

Pensupa, N., 2020. Recycling of end-of-life clothes. In: Rajkishore, N. (Ed.), Sustainable Technologies for Fashion and Textiles. Woodhead Publishing Series in Textiles, United Kingdom, pp. 251-309.

Sandin, G., Roos, S., Johansson, M., 2019. Environmental Impact of Textile Fibers- What We Know and what We Don't Know, MISTRA Future Fashion Report: 03 Part 2. Rise AB: Goteborg, Sweden.

Schmidt, A., Watson, D., Roos, S., Askham, C., Brunn Poulsen, P., 2016. Mixed Fibres in: Gaining Benefits from Discarded Textiles. Rosendahls-Schultz Grafisk, Hillerød, Denmark, pp. 112-116.

Senthil Kumar, P., Yaashikaa, P.R., 2018. Recycled Fibres. In: Muthu, S.S. (Ed.), Sustainable Innovations in Recycled Textiles. Springer, Hong Kong, pp. 1-17.

Strähle, J., Hauk, K., 2017. Impact on sustainability: production versus consumption, in: Strähle, J., (Ed.) Green fashion retail. Springer, Singapore, pp. 49-76.

Yalcin-Enis, I., Kucukali-Ozturk, M., Sezgin, H., 2019. Risks and Management of Textile Waste, in: Gothandam K., Ranjan S., Dasgupta N., Lichtfouse E. (Eds.), Nanoscience

and Biotechnology for Environmental Applications. Springer, Cham, pp. 29-53.
Yousef, S., Tatariants, M., Tichonovas, M., Kliucininkas, L., Lukoŝitũe, S.I., Yan, L., 2020. Sustainable green technology for recovery of cotton fibers and polyester from textile waste. J. Clean. Prod. 254, 120078 https://doi.org/10.1016/j.jclepro.2020.120078.

List of publications

As a result of the research that has been carried out within these three years of Ph.D., the following publications on international scientific journals were produced:

- Rubino, C., Bonet-Aracil, M., Gisbert-Payá, J., Liuzzi, S., Zamorano Cantó, M., Martellotta, F., Stefanizzi, P. 2016. Composite eco-friendly sound absorbing materials made of recycled textile waste and biopolymers. Materials 12, 4020. https://doi.org/10.3390/ma12234020.

- Rubino, C., Liuzzi, S., Martellotta, F., Stefanizzi, P., Straziota, P., 2021. Nonwoven textile waste added with pcm for building applications. Appl. Sci. 11, 1262. https://doi.org/10.3390/app11031262.

- Rubino, C., Bonet-Aracil, M., Liuzzi, S., Stefanizzi, P., Martellotta, F., 2021 Wool waste used as sustainable nonwoven for building applications. J. Clean. Prod. 278, 123905. https://doi.org/10.1016/j.jclepro.2020.123905.

- Rubino, C., Liuzzi, S., Martellotta, F., Stefanizzi, P., 2018. Textile wastes in building sector: A review. M.M.C. B 87(3),172-179. https://doi.org/10.18280/mmc_b.870309.

Other works were presented at national and international conferences:

- Rubino, C., Bonet-Aracil, M., Liuzzi, S., Martellotta, F. Preliminary investigation on the acoustic properties of absorbers made of recycled textile fibers. 23° International Congress on Acoustics (ICA) Aachen, Germany, 9-13 September 2019.

- Rubino, C., Bonet-Aracil, M.A., Liuzzi, S., Martellotta, F. Indagine preliminare sull'uso degli scarti tessili per la realizzazione di materiali fonoassorbenti, 46° Convegno Nazionale Associazione Italiana di Acustica, Pesaro, 29-31 Maggio 2019

- Rubino, C., Bonet-Aracil, M., Liuzzi, S., Martellotta, F., Stefanizzi, P.,2019. Thermal characterization of innovative sustainable building materials from wool textile fibers waste. Italian journal of engineering science 63(2-4): 277-283, published by 4° AIGE/IIETA International Conference e 13° AIGE Conference, Matera, 13-14 Giugno 2019.

I also have had the opportunity to collaborate on research work about sustainable building materials, which led to the following publications:

- Liuzzi, S., Rubino, C., Martellotta, F., Stefanizzi, P., Casavola, C., Pappalettera , G., 2020. Characterization of biomass-based materials for building applications: The case of straw and olive tree waste. Ind. Crop. Prod. 147, 112229. https://doi.org/10.1016/j.indcrop.2020.112229.

- Liuzzi, S., Rubino, C., Martellotta, F., 2020. Properties of clayey plasters with olive fibers in: F. Pacheco-Torgal, V. Ivanov, D. Tsang (Eds), Bio-based materials and biotechnologies for eco-efficient construction. Woodhead Publishing in Civil and Structural Engineering, United Kingdom, pp. 171-184.

- Liuzzi, S., Rubino, C., Stefanizzi, P., Martellotta, F., 2020. Performance characterization of broad band sustainable sound absorbers made of almond skins. Materials 13, 5474. https://doi.org/10.3390/ma13235474.

I also collaborated on the following studies:

- Liuzzi, S., Di Chio, P., Rubino, C., Stefanizzi, P.,2019. Thermal characterization of innovative sustainable building materials from wool textile fibers waste. Italian journal of engineering science 63(2-4): 431-436, published by 4° AIGE/IIETA International Conference e 13° AIGE Conference, Matera, 13-14 Giugno 2019.

- Martellotta, F., Ayr, U., Rubino, C., On the Use of Geometrical Acoustic Models of a Reverberant Chamber to Improve the Reliability of Sound Absorption Measurements, 23° International Congress on Acoustics (ICA) Aachen, Germany, 9-13 Settembre 2019.

- Cannavale, A., Martellotta, F., Berardi, U., Rubino, C., Liuzzi, S., De Carlo. V., Ayr, U., 2020. Modeling of an aerogel-based “thermal break” for super-insulated window frames. Buildings 10, 60. https://doi.org/10.3390/buildings10030060.

La borsa di dottorato è stata cofinanziata con risorse del
Programma Operativo Nazionale Ricerca e Innovazione 2014-2020 (CCI 2014IT16M2OP005),
Fondo Sociale Europeo, Azione I.1 "Dottorati Innovativi con caratterizzazione Industriale"

UNIONE EUROPEA
Fondo Sociale Europeo

Ministero dell'Istruzione, dell'Università e della Ricerca